PUBLICATIONS OF
THE UNIVERSITY OF EASTERN FINLAND


**Dissertations in Health Sciences**

**AMIR SADEGHI BOROUJENI**

# CHARACTERIZING INTRAVITREAL PHARMACOKINETICS OF MACROMOLECULES AND NANOPARTICULATE SYSTEMS USING NON-INVASIVE FLUORESCENCE AND OPTICAL TECHNIQUES

# CHARACTERIZING INTRAVITREAL PHARMACOKINETICS OF MACROMOLECULES AND NANOPARTICULATE SYSTEMS USING NON-INVASIVE FLUORESCENCE AND OPTICAL TECHNIQUES

Amir Sadeghi Boroujeni

# CHARACTERIZING INTRAVITREAL PHARMACOKINETICS OF MACROMOLECULES AND NANOPARTICULATE SYSTEMS USING NON-INVASIVE FLUORESCENCE AND OPTICAL TECHNIQUES

To be presented by permission of the Faculty of Health Sciences, University of Eastern Finland for public examination in MS301 Auditorium, Kuopio on September 12th, 2022, at 15:00 o'clock

Publications of the University of Eastern Finland
Dissertations in Health Sciences
No 693

School of Pharmacy
University of Eastern Finland, Kuopio
2022

Punamusta Oy
Joensuu, 2022
Distributor: University of Eastern Finland
Kuopio Campus Library

ISBN: 978-952-61-4591-4 (print/nid.)
ISBN: 978-952-61-4592-1 (PDF)
ISSNL: 1798-5706
ISSN: 1798-5706
ISSN: 1798-5714 (PDF)

Author's address: School of Pharmacy
University of Eastern Finland
KUOPIO
FINLAND

Doctoral program: Doctoral Program in Drug Research

Supervisors: Professor Arto Urtti, Ph.D.
School of Pharmacy
University of Eastern Finland
KUOPIO, FINLAND

Lecturer Veli-Pekka Ranta, Ph.D.
School of Pharmacy
University of Eastern Finland
KUOPIO, FINLAND

Lecturer Marika Ruponen, Ph.D.
School of Pharmacy
University of Eastern Finland
KUOPIO, FINLAND

Elisa Toropainen, Ph.D.
School of Pharmacy
University of Eastern Finland
KUOPIO, FINLAND

Reviewers:

Professor Elias Fattal, Ph.D.
Institut Galien Paris-Saclay,
Université Paris-Saclay, CNRS
Paris, France

Principal Scientist Robert F. Kelley, Ph.D.
Genentech, Inc.
San Francisco, USA

Opponent:

Professor Francine Behar-Cohen, MD, Ph.D.
Department of Ophthalmology,
Université de Paris
Paris, France

SADEGHI BOROUJENI, AMIR
CHARACTERIZING INTRAVITREAL PHARMACOKINETICS OF MACROMOLECULES AND NANOPARTICULATE SYSTEMS USING NON-INVASIVE FLUORESCENCE AND OPTICAL TECHNIQUES
KUOPIO: UNIVERSITY OF EASTERN FINLAND
PUBLICATIONS OF THE UNIVERSITY OF EASTERN FINLAND
DISSERTATIONS IN HEALTH SCIENCES 693. 2022, 99 P.
ISBN: 978-952-61-4591-4 (print)
ISSNL: 1798-5706
ISSN: 1798-5706
ISBN: 978-952-61-4592-1 (PDF)
ISSN: 1798-5714 (PDF)

## ABSTRACT

Pharmacokinetics is one of the main features to be assessed in the development of effective and safe therapeutics and drug delivery systems. Pharmacokinetics is especially important in the case of intravitreal drug administration that is used in the drug treatment of retinal diseases. We utilized non-invasive optical techniques to assess the vitreal pharmacokinetics of labeled compounds and nanomaterials in preclinical animal models. The kinetics of different labeled macromolecules and nanoparticles were studied after intravitreal injection into the eyes of rats and rabbits. *In vivo* luminescence imaging revealed the suitability of phosphorescence dyes in monitoring the pharmacokinetics of labeled liposomes in the eyes. Furthermore, new dyes can improve the signal-to-noise ratio in autofluorescent tissues. *In vivo* ocular fluorophotometry was used to monitor the kinetics of intravitreally injected fluorescently labeled dextran in rats and rabbits. Based on this comparison, the same drug exposure is achieved at 2-5 times higher doses in rabbits than in the rats. The intravitreal pharmacokinetics of fluorescently labeled peptide conjugates in the rabbit eye were also studied using fluorophotometry. These peptides bind to the components of the vitreous and this may lead to nonlinear pharmacokinetics, in which the half-life of the peptide in the vitreous is dependent on its concentration, being longer at low concentrations. The intravitreal distribution and elimination of fluorescently

labeled nanomaterials, such as liposomes, polymeric micelles, polymersomes and pullulan-dexamethasone conjugates, were explored with ocular fluorophotometry, fundus photography and optical coherence tomography. Pullulan-dexamethasone conjugates and small liposomes (diameter of ≈50 nm) were mainly eliminated via the anterior route. The results also revealed that the intravitreal retention was not simply dependent on particle size. For example, polymeric micelles were eliminated from the vitreous much slower than liposomes of similar particle sizes. Simulations of drug concentrations after injection of intravitreal particles with different release rates highlighted the importance of synchronizing the particle retention and drug release rate to optimize retinal drug bioavailability. In addition, we observed that material contamination with endotoxin significantly accelerated elimination of nanomaterials from the vitreous. The measurement of endotoxin levels in intravitreal nanomaterials was a critical factor which has been almost completely disregarded in the published studies. In conclusion, we provide kinetic insights into intravitreally administered nanoparticles and macromolecules that can be used in future in the development of novel retinal drug delivery applications.

**Keywords**: intravitreal injections, ocular fluorophotometry, intravitreal pharmacokinetics, fundus imaging, optical coherence tomography, nanoparticle, macromolecule.

SADEGHI BOROUJENI, AMIR
Lasiaiseen annettujen makromolekyylien ja nanopartikkelisysteemien karakterisointi kajoamattomilla, fluoresenssiin ja optiikkaan perustuvilla menetelmillä
Kuopio: Itä-Suomen yliopisto
Publications of the University of Eastern Finland
Dissertations in Health Sciences 693. 2022, 99 s.
ISBN: 978-952-61-4591-4 (print)
ISSNL: 1798-5706
ISSN: 1798-5706
ISBN: 978-952-61-4592-1 (PDF)
ISSN: 1798-5714 (PDF)

## TIIVISTELMÄ

Farmakokinetiikka on yksi tärkeimmistä asioista tehokkaiden ja turvallisten lääkkeiden ja lääkkeiden saattomenetelmien kehittämisessä. Näin on myös verkkokalvon lääkkeiden tapauksessa. Nämä lääkkeet annetaan intravitreaalisina injektioina. Käytimme tässä tutkimuksessa ei-invasiivisia optisia menetelmiä leimattujen makromolekyylien ja nanomateriaalien farmakokinetiikan arvioimiseksi prekliinisissä eläinmalleissa. Fluoresoivasti leimattujen makromolekyylien ja nanopartikkelien kinetiikkaa silmässä tutkittiin lasiaisinjektioiden jälkeen rotissa ja kaneissa. *In vivo* -luminesenssikuvaus paljasti fosforesenssivärien käyttökelpoisuuden leimattujen liposomien farmakokinetiikan seurannassa. Uudet merkkiaineet voivat parantaa signaali-kohinasuhdetta autofluoresoivissa kudoksissa. *In vivo* silmän fluorofotometriaa käytettiin fluoresoivasti leimatun dekstraanin kinetiikan seuraamiseen rotilla ja kaniineilla intravitreaalisen injektion jälkeen. Tämän vertailun perusteella sama lääkealtistus saavutetaan kaniineilla 2-5 kertaa suuremmilla annoksilla kuin rotilla. Myös fluoresoivasti leimattujen peptidikonjugaattien intravitreaalista farmakokinetiikkaa kanin silmässä tutkittiin fluorofotometrialla. Nämä peptidit sitoutuvat lasiaisen komponentteihin, mikä voi johtaa epälineaariseen farmakokinetiikkaan, jossa peptidin puoliintumisaika lasiaisessa riippuu sen pitoisuudesta ja on pidempi pienillä pitoisuuksilla. Fluoresoivasti leimattujen nanomateriaalien, kuten

liposomien, polymeeristen misellien, polymersomien ja pullulaani-deksametasonikonjugaattien intravitreaalista jakautumista ja eliminaatiota tutkittiin silmän fluorofotometrialla, funduskameralla ja optisella koherenssitomografialla. Pullulaani-deksametasoni-konjugaatit ja pienet liposomit (halkaisija ≈50 nm) eliminoituivat lasiaisesta pääasiassa silmän etuosan kautta. Tulokset osoittivat, että lasiaisen sisäinen retentio ei ole riippuvainen vain hiukkaskoosta. Esimerkiksi polymeeriset misellit eliminoituivat lasiaisesta paljon hitaammin kuin liposomit, vaikka niillä on samanlainen hiukkaskoko. Lääkeainepitoisuuksia simuloitiin lasiaisensisäisten hiukkasten annon jälkeen. Simulaatiot osoittivat, että lääkeaineen vapautumisnopeus on synkronoitava hiukkasten laiaisretention kanssa, jotta saavutetaan hyvä lääkeaineen biologinen hyötyosuus verkkokalvossa. Havaitsimme myös, että materiaalien endotoksiinikontaminaatio nopeuttaa merkittävästi niiden eliminaatiota lasiaisesta. Intravitreaalisten nanomateriaalien endotoksiinitasojen mittaaminen on kriittinen tekijä, joka puuttuu lähes kokonaan julkaistuista tutkimuksista. Tämä tutkimus antaa systemaattista tietoa silmän farmakokinetiikasta ja edesauttaa uusien silmälääkkeiden kehitystyötä.

**Avainsanat**: lasiaisinjektiot, silmän fluorofotometria, silmänpohjan kuvantaminen, optinen koherenssitomografia, nanopartikkeli, makromolekyyli

# ACKNOWLEDGEMENTS

This thesis project was carried out in the School of Pharmacy, the University of Eastern Finland from 2017 to 2022. The work was financially supported by the European Union's Horizon 2020 research and innovation program Marie Sklodowska-Curie Innovative Training Networks (OcuTher project). The UEF doctoral school and Gene Cell Nano flagship are gratefully acknowledged for financial support.

Completion of this Ph.D. journey was not possible without the support of different people and colleagues. I am grateful to my God for enabling me to accomplish this highest degree of my career. Foremost, I warmly thank my supervisors: Professor Arto Urtti, who provided me a great opportunity to be his student and perform lots of research in his group. His supervision and innovative view toward scientific experiments helped me to improve my skills and scientific background. University lecturer Veli-Pekka Ranta, from whom I have learned the most of my pharmacokinetic skills. His extensive knowledge and deep scientific insight helped me to perform better experiments and interpret the results. University lecturer Marika Ruponen continuously helped and supported me during this journey. She helped me from the first days during university registration and later in doing research and writing manuscripts and thesis. I want to thank Dr. Elisa Toropainen who trained me for ocular *in vivo* works. Working with her was a unique opportunity since we spent many days doing lab work together, and I had the chance to learn from her extensive *in vivo* experience.

I wish to thank my collaborators and co-authors (whose names can be found in the original publications) for their valuable contribution to this work. Without their great work in preparing nanomaterials and formulations, this work was not possible. In addition, special thanks to Professor Sergey P. Tunik and Julia R. Shakirova from St. Petersburg State University, Russia; Madhushree Bhattacharya, Shirin Tavakoli and Tatu Lajunen from the University of Helsinki and Eastern Finland; Professor Jan van Hest, Shoupeng Cao and Roxane Ridolfo from the Eindhoven University of Technology, the Netherlands; Professor Stefano Salmaso, Professor Paolo Caliceti, and Eva Kicková from the University of Padova, Italy.

I thank the reviewers, Professor Elias Fattal and Principal Scientist Dr. Robert Kelley for their valuable time and brilliant suggestions to improve my thesis. I thank Dr. Ewen McDonald for language editing of my thesis. My sincere appreciation to Professor Francine Behar-Cohen for accepting to act as an opponent at the public examination.

I warmly thank my colleagues at the University of Eastern Finland and the Ocular Drug Delivery (ODD) group for their support and contribution to research. I want to thank Jooseppi Puranen who helped me a lot during my experiments and for all the nice discussions that we had together. I thank Annika Valtari for her efforts and collaborations during the optimization of the various studies at the animal lab center. I thank Anam Hammid for sharing the office and the endless support she provided during tough and good times. I am thankful to my colleagues Anusha Balla, Marko Lamminsalo, Mika Reinisalo, Emma Heikkinen, Laura Hellinen, Astrid Subrizi, Eva del Amo Páez, Kati-Sisko Vellonen, Stanislav Kalinin, Sina Bahrpeyma, Raja Sridevi Gurubaran, Joni Ruotsalainen, Maija Heiskanen, Jaana Leskinen, Lea

Pirskanen, Giuseppe D'Amico Ricci, Jussi Paterno, Toni Tamminen, Melina Malinen, Vijayabhaskarreddy Junnuthula, Unni Tengvall-Unadike, Sonja Korhonen, Marko Antikainen and Markku Taskinen for their support, help and friendly attitude to make my working environment healthy. I also want to thank staff members of the Laboratory Animal Centre at the University of Eastern Finland where I spent most of my time conducting experimental work.

My special thanks also to the OcuTher management team, Professor Paavo Honkakoski, Professor Kai Kaarniranta and Karin Koivisto for providing many opportunities for training, learning and collaborations throughout this project. I thank all the partners in the OcuTher project for providing fruitful collaborations and training. I thank Dr. Achim Sauer and the Department of Drug Discovery Sciences in Boehringer Ingelheim Pharma GmbH for providing a valuable industrial secondment. I appreciate the opportunity to perform secondment also in the laboratory of Professors Wim Hennink and Tina Vermonden at Utrecht University. During these years, many of the OcuTher researchers had visited UEF where we had scientific collaborations and nice time; I thank Merve Sen, Charis Rousou, Ada Annala, Md AL-Amin, Daniel Ajoy Moreno, Marco Bassetto, Chiarra Pretto, Blessing Ilochonwu, Anam Fayyaz, Miao Tang, Stephen Marry and Mike Wels (from NanoMed project).

I warmly thank all my friends for their kind and nice attuite towards me. One of the main factors for choosing research as a career was my friendship with Javad. Thank you for two decades of unbreakable friendship since the summer of 2003. Kourosh, I feel extremely delighted to have a friend like you in my life. I appreciate the friendship with Yahya Nowrouzi, Mohammad Hossein Ebrahimi, Ali Tavakoli, Ali Mohammadi, Ali Ashraf, Ehsan Shad, Vandad Imani, Ali Abdollah-Zadeh, Amir Esrafilian, Ehsan Daneshvar, Iman Kafian Attari, Seyed Hamed Maljaei and many others with whom we spent a nice time during these years together.

I owe my special thanks to my parents; my mother Shahnaz, for always being there and listening to my all problems and providing her wise guidance throughout my life. My father Sirous, for raising me as a strong and independent man. I also thank my family members; my brothers Nima and Iman, their families (Farnoosh, Amir Reza, Zahra, Sofia and Selena) and my sister Gelareh for making my beautiful memories and supporting me unconditionally during my life.

Amir Sadeghi
June 2022
Kuopio

# LIST OF ORIGINAL PUBLICATIONS

This dissertation is based on the following original publications:

**I** Shakirova, Julia R, **Amir Sadeghi**, Alla A Koblova, Pavel S Chelushkin, Elisa Toropainen, Shirin Tavakoli, Leena-Stiina Kontturi, Tatu Lajunen, Sergey P Tunik, and Arto Urtti. 2020. "Design and Synthesis of Lipid-Mimetic Cationic Iridium Complexes and Their Liposomal Formulation for in Vitro and in Vivo Application in Luminescent Bioimaging." RSC Advances 10 (24): 14431-40.

**II** **Amir Sadeghi*****, Jooseppi Puranen*, Marika Ruponen, Annika Valtari, Astrid Subrizi, Veli-Pekka Ranta, Elisa Toropainen, and Arto Urtti. 2021. "Pharmacokinetics of Intravitreal Macromolecules: Scaling between Rats and Rabbits." European Journal of Pharmaceutical Sciences, 105720.

**III** Madhushree Bhattacharya, **Amir Sadeghi**, Sanjay Sarkhel, Marja Hagström, Sina Bahrpeyma, Elisa Toropainen, Seppo Auriola, and Arto Urtti. 2020. "Release of Functional Dexamethasone by Intracellular Enzymes: A Modular Peptide-Based Strategy for Ocular Drug Delivery." Journal of Controlled Release 327: 584-94.

**IV** **Amir Sadeghi,** Marika Ruponen, Jooseppi Puranen, Shoupeng Cao, Roxane Ridolfo, Shirin Tavakoli, Elisa Toropainen, Tatu Lajunen, Veli-Pekka Ranta, Jan van Hest, Arto Urtti. "Imaging, quantitation and kinetic modelling of intravitreal nanomaterials." International Journal of Pharmaceutics (2022): 121800.

**V** Eva Kicková*, **Amir Sadeghi***, Jooseppi Puranen, Shirin Tavakoli, Merve Sen, Veli-Pekka Ranta, Blanca Arango-Gonzalez, Sylvia Bolz, Marius Ueffing, Stefano Salmaso, Paolo Caliceti, Elisa Toropainen, Marika Ruponen, Arto Urtti. Pharmacokinetics of Pullulan–Dexamethasone Conjugates in Retinal Drug Delivery. Pharmaceutics 14, no. 1 (2022): 12

*Equal Contribution. The publications were adapted with the permission of the copyright owners.

# AUTHOR'S CONTRIBUTION

**I)** Author designed and performed the *in vivo* experiment, eye imaging and results analysis and participated in manuscript preparation.

**II)** Author designed and performed the *in vivo* experiment, analysis of results, pharmacokinetics modelling and participated in manuscript preparation.

**III)** Author designed and performed the *in vivo* experiment, analysis of results and pharmacokinetic modelling and participated in manuscript preparation.

**IV)** Author designed and performed the *in vivo* experiment, analysis of results, pharmacokinetics modelling and participated in manuscript preparation.

**V)** Author designed and performed the *in vivo* experiment, pharmacokinetics simulations and participated in manuscript preparation.

# CONTENTS

# Appendix

# ABBREVIATIONS

| | |
|---|---|
| AMD | Age related macular degeneration |
| AUC | Area under the curve |
| $C_a$ | Concentration in aqueous humor |
| cryo-TEM | Cryogenic transmission electron microscopy |
| $C_v$ | Concentration in vitreous |
| DPPC | Dipalmitoylphosphatidylcholine |
| DSPE-PEG | 1,2-distearoyl-sn-glycero-3-phosphoethanolamine-N-[methoxy(polyethylene glycol)-2000 |
| FITC | Fluorescein isothiocyanate |
| GCL | Ganglion cell layers |
| ILM | Inner limiting membrane |
| INL | Inner nuclear layers |
| IPL | Plexiform layers |
| IS | Inner segment |
| Kd | Equilibrium dissociation constant |
| MST | Microscale thermophoresis |
| NFL | Nerve fiber layer |
| OCT | Optical coherence tomography |
| ONL | Outer nuclear layer |
| OPL | Outer plexiform layer |
| OS | Outer segment |
| PBS | Phosphate-buffered saline |
| RPE | Retinal pigmented epithelium |
| SPECT/CT | Single-photon emission computed tomography/computed tomography |
| VEGF | Vascular endothelial growth factor |

# 1. INTRODUCTION

The development of ocular medications has a long history. One of the oldest historical documents is a piece of papyrus that was discovered by the Egyptologist Ebers from a common mummy. The document was written around 1650 B.C. and it describes different diseases and Egyptian remedies in 110 pages with eight pages describing ocular diseases and their treatments (Wheeler, 1946). The diseases were defined as pain in the eye, tera in the eye, pus in the eye, blood in eye, turning in the eye, and dimness of sight. The medications included onion, leeks, beans, castor oil, pomegranate, copper salt, oxymel of squill, hemlock and opium.

Thanks to the developments in the fields of ocular biology and pharmacology, there are numerous diagnostic methods and effective therapeutics that are available for today's ophthalmological patients. Depending on the disease pathology, the target tissues are located in either the anterior or posterior part of the eye. For the anterior targets, topical administration is the preferred route of drug administration. Many ocular drugs are administered as topical eye drops or ointments (Yellepeddi and Palakurthi, 2016). The ocular bioavailability of topical drugs is low as less than 5% of the instilled dose reaches the anterior chamber (Järvinen, Järvinen and Urtti, 1995). Nonetheless, topical drug treatment is still effective in the anterior segment of the eye but for posterior targets, the topical ocular route is not efficient, because too low and thus ineffective drug concentrations are reached in the posterior eye segment (Maurice, 2002). Therefore, for posterior targets in the eye, intravitreal injection is the preferred technique for drug administration (Peyman, Lad and Moshfeghi, 2009).

About 15 years ago, new therapeutics were launched for the treatment of the neovascular form of age-related macular degeneration. These protein drugs, for example, bevacizumab, ranibizumab, aflibercept, and brolucizumab, act as inhibitors of vascular endothelial growth factor (VEGF).

They need to be administered as intravitreal injections (Nicholson and Schachat, 2010) at 1-2 month intervals. Typically, their intravitreal half-life of elimination is a few days (Del Amo *et al.*, 2015). The vitreal elimination half-life of small molecules is much shorter, only a few hours. The number of annual intravitreal anti-VEGF injections in the United States increased from 4 million in 2013 to 5.9 million per year in 2016 and this trend continues upwards (East and Group, 2012; Grzybowski *et al.*, 2018).

Although intravitreal injections are widely used, they are invasive and may occasionally cause unwanted ocular effects, such as inflammation, cataract, and pain; consequently reducing patient compliance (Jager *et al.*, 2004; Sampat and Garg, 2010; Fagan and Al-Qureshi, 2013). One approach to improve patient compliance is to prolong the intervals between the injections with intravitreal sustained release formulations; these include implants (Lee *et al.*, 2010), hydrogels (Ilochonwu *et al.*, 2020), microparticles and nanoparticles (Herrero-Vanrell, 2011; Kompella *et al.*, 2013). Although there are numerous publications and research projects examining these formulations, the implants are the only drug delivery systems available on the market. For example, an intravitreal dexamethasone implant (Ozurdex) has been on the market for several years (Saincher and Gottlieb, 2020).

In order to design efficient vitreal drugs and delivery systems, we need to study their pharmacokinetic behavior *in vivo*. Since many ocular compartments are transparent, optical techniques could be applied to measure a drug's pharmacokinetics in the eye. These techniques include fluorescence based methods like fundus imaging (Yannuzzi *et al.*, 2004), fluorophotometry (Dickmann *et al.*, 2015) and near infrared techniques like optical coherence tomography (OCT) (Hee *et al.*, 1995). These non-invasive techniques make it possible to study a drug's kinetics in a lower number of animals. In contrast, with traditional pharmacokinetic experiments with invasive techniques, several animals must be euthanized at each time point. Furthermore, these non-invasive techniques decrease data variability in the experiments, because measurements at multiple time points can be performed in the same animal. The main topic of this thesis was to examine

how these non-invasive techniques could be best applied to assess the intravitreal pharmacokinetics of macromolecules and nanoparticles in preclinical animal models.

# 2. REVIEW OF THE LITERATURE

## 2.1 Ocular anatomy and routes of drug administration

An overview of ocular anatomy is shown in Figure.1. The eye consists of different anatomical compartments e.g. anterior chamber, lens and vitreous which are protected by different barriers like cornea, blood-aqueous and blood-retinal barriers that limit the efficacy of drug delivery after topical and systemic administration (Urtti, 2006). The main ocular fluids are lacrimal fluid, aqueous humor and vitreous humor. Tear film covers the surface of the cornea and it consists of lipids, proteins and mucin (Yazdani *et al.*, 2019). Aqueous humor has a very low protein concentration and it fills the anterior chamber of the eye (Figure 1). It is produced in the ciliary body and is eliminated through the trabecular meshwork and inner wall of Schlemm's canal or via the uveo-scleral route. Water is the main component of aqueous humor, but the humor also contains organic and inorganic ions, carbohydrates, glutathione, urea, amino acids, proteins, oxygen and carbon dioxide (Goel *et al.*, 2010).

The transparent vitreous humor is the largest compartment in the human eye (Figure 1). The main component of the vitreous is water (98-99%). The solid components are mainly collagen fibers and glycosaminoglycans, in particular hyaluronic acid. The collagen fibrils form a network in the vitreous (Le Goff and Bishop, 2008). A mesh size of 500 nm has been reported for bovine vitreous (Xu *et al.*, 2013). It is this mesh size that can potentially affect the movements of nanoparticulate systems in the vitreous. It should be noted that the vitreous in the aging human eye becomes more liquid-like (Sebag, 1987) and presumably the mesh size becomes enlarged. The binding of small molecule drugs to the vitreal components is modest and does not correlate with plasma protein binding (Rimpelä *et al.*, 2018). The interaction of most macromolecules with vitreous is weak and their diffusion coefficients in vitreous are almost the same as in water (Missel, 2012).

The anterior part of the eye is typically treated with topically applied eye drops. However, this approach is limited to small drug molecules with adequate corneal permeability (Maurice, 1987). The bioavailability of topically applied drugs is limited by their permeability in the cornea, rapid systemic absorption via conjunctiva as well as the fast drainage of instilled eye drops from the ocular surface (Ramsay *et al.*, 2018). Moreover, the reflective lacrimation after administration of an eye drop can dilute the drug solution immediately after its application (Mishima *et al.*, 1966). Ocular injections to the anterior chamber (intracameral) and subconjunctival space are sometimes used in the case of drugs with inadequate corneal permeabilities (Short, 2008).

In order to achieve efficient drug delivery to the posterior ocular tissues, intraocular routes like intravitreal injections (injection to the vitreous) are in use (Maurice, 2003; Lee and Robinson, 2004). The retina is the main target tissue for most intravitreal drug administrations; it consists of several distinct cellular layers (Figure 1). The retinal pigment epithelium forms the main barrier for permeation of drugs from the systemic blood circulation. The inner limiting membrane has been reported as a potential barrier inhibiting the permeation of nanoparticles from the vitreal side to the retina (Tavakoli, Peynshaert, *et al.*, 2020).

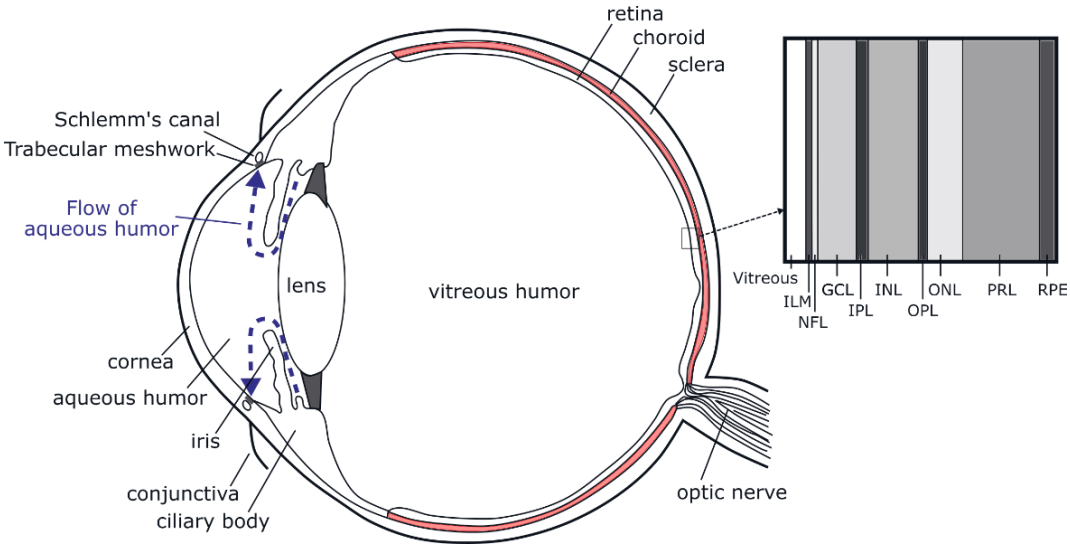


**Figure 1.** Anatomy of the eye. Choroidal blood, vitreous and aqueous humor are the main ocular fluids which affect the intravitreal ocular pharmacokinetics. Aqueous humor flows from the ciliary body to the anterior chamber and is eliminated via the trabecular meshwork. The retinal layers are inner limiting membrane (ILM), nerve fiber layer (NFL), ganglion cell layers (GCL), inner plexiform layer (IPL), inner nuclear layer (INL), outer plexiform layer (OPL), outer nuclear layer (ONL), photoreceptors layers (PRL) and retinal pigment epithelium (RPE).

### 2.1.1 Intravitreal pharmacokinetics

Because of the negligible retinal bioavailability of topically applied drugs, the intravitreal route is extensively used for drug delivery to the posterior part of the eye. Both small drugs and protein drugs are given intravitreally. The application of intravitreal drugs started mostly with small molecule drugs, such as penicillin or streptomycin in the treatment of intraocular infections (LEOPOLD, 1945; SHOEMAKER, 1949). In the last decades, most intravitreally administered drugs were antibiotics, antivirals and anti-inflammatory compounds (Polansky and Weinreb, 1984; Ussery III *et al.*, 1988; Snyder and Glasser, 1994) but about 15 years ago, protein drugs were launched to treat retinal diseases. These therapeutics can be divided into anti-VEGF antibodies, soluble receptors and aptamers and they are used to treat the neovascular form of age-related macular degeneration. Examples of intravitreal drugs and their elimination half-lives in humans and rabbits are shown in Table.1.

The vitreal elimination half-lives of small drug molecules lie in a range of a few to several hours (Eva *et al.*, 2015). Injections of small molecule solutions is not an attractive option in chronic treatment, because maintenance of effective drug concentrations in the retina would require frequent intravitreal injections, even every few days. In the case of macromolecules, the elimination half-lives are in the order of several days (Crowell *et al.*, 2019; García-Quintanilla *et al.*, 2019) and therefore an interval of 1-2 months is needed. The intravitreal injections are invasive and may lead to ocular side effects, including inflammation, cataract, and pain which consequently reduce patient compliance (Jager *et al.*, 2004; Sampat and Garg, 2010; Fagan and Al-Qureshi, 2013). This highlights the importance of designing novel sustained release formulations for intravitreal drugs to prolong the time between injections.

**Table.1** Examples of intravitreal therapeutics and their elimination half-lives in human and rabbit vitreous.

| Drug compound | Class of drugs | Human vitreal half-life (day) | Rabbit vitreal half-life (day) |
|---|---|---|---|
| Dexamethasone phosphate | Glucocorticoid | 0.23 (Gan *et al.*, 2005) | 0.14 (Kwak and D'Amico, 1992) |
| Ranibizumab | Anti-VEGF antibody | 7.19 (Krohne *et al.*, 2012) | 2.88 (Bakri *et al.*, 2007b) |
| Bevacizumab | Anti-VEGF antibody | 9.82 (Krohne *et al.*, 2008) | 4.88 (Bakri *et al.*, 2007a) |
| Aflibercept | Anti-VEGF antibody | 11.00 (Do, Rhoades and Nguyen, 2020) | 3.92 (Park *et al.*, 2016) |
| Pegaptanib | Anti-VEGF aptamer | Not reported | 3.46 (Group, 2002) |

Vitreal distribution studies started mainly to resolve physiological questions in the late 1880's (Smith, 1889). In those studies, different materials, like Indian ink or cinnabar, were injected to the vitreous of rabbits and they were monitored qualitatively by ophthalmoscopy or microscopy. Those historical reports revealed that there was a qualitative distribution of some particles to the ocular tissues like the optic nerve.

Much later, in 1959, David Maurice (Maurice, 1959) published the first quantitative vitreal kinetic study. He injected radioactive albumin into rabbit vitreous and identified two potential routes of elimination of the compound from the vitreous: transretinal and anterior routes. He concluded that macromolecules, like albumin, would be mainly eliminated anteriorly. This is due to the limited permeability of macromolecules through retina into the systemic bloodstream. Likewise, the modern therapeutic antibodies are mainly (even as much as 90%) eliminated via the anterior route (Gadkar *et al.*, 2015; Hutton-Smith *et al.*, 2016, 2017; Schmitt, 2017; Rimpelä *et al.*, 2019). For molecules that permeate across the blood retina barrier (composed of

retinal capillary endothelium and RPE), there is a substantial contribution made by the posterior route to their elimination (Maurice and Mishima, 1984; Durairaj, 2017; Schmitt, 2017). It has been estimated that in the case of small drugs with good permeability through the blood retina barrier, up to 75 percent of the drug may be eliminated transretinally (Rimpelä, Cui and Sauer, 2021).

### 2.1.2 Intravitreal interspecies scaling

The anatomical dimensions and physiological factors of the eye are different in animals and humans (Table 2), and this affects also the ocular pharmacokinetics. For example, the size of vitreous has a direct effect on the vitreal elimination half-life of compounds. The diffusion time in the vitreous is the main factor underlying the elimination rate of intravitreally injected macromolecules (Hutton-Smith *et al.*, 2016; Shatz *et al.*, 2016; Crowell *et al.*, 2019). Therefore, it would be expected that the elimination half-life in the vitreous is longer in the larger human eyes than in smaller animal eyes (Hutton-Smith *et al.*, 2016).

**Table 2.** Physiological and anatomical parameters of rat, rabbit and human eyes.

| Parameter | Rat | Rabbit | Human | References |
|---|---|---|---|---|
| Retinal surface area ($mm^2$) | 80 | 520 | 1204 | (Panda-Jonas *et al.*, 1994; Reichenbach *et al.*, 1994; Mayhew and Astle, 1997) |
| Choroidal blood flow (ml/h) | 3.9 | 62 | 43 | (Sebag *et al.*, 1994; Nilsson and Alm, 2012; Shih *et al.*, 2013) |
| Retinal blood flow (ml/h) | nr | 0.66 | 0.26 | (Nilsson and Alm, 2012; Shih *et al.*, 2013) |
| Ciliary body blood flow (ml/h) | nr | 4.91 | 5.34[a] | (Alm and Bill, 1973; Nilsson and Alm, 2012) |
| Iridial blood flow | nr | 3.72 | 1.02[a] | (Alm and Bill, 1973; Nilsson and Alm, 2012) |
| Anterior chamber volume (µl) | 18 | 300 | 250 | (Conrad and Robinsonx, 1977; Mermoud *et al.*, 1996; Civan, 1997) |
| Aqueous humor flow rate (µl/h) | 21 | 180 | 165 | (Brubaker, 1991; Mermoud *et al.*, 1996; Missel, Horner and Muralikrishnan, 2010) |
| Vitreous volume (µl) | 50 | 1500 | 4500 | (Friedrich, Cheng and Saville, 1997; Sha and Kwong, 2006; Krohne *et al.*, 2008; Zhu *et al.*, 2008). |

a: Since the data was not available, the values of monkey were used. nr: not reported.

Both the flow rate and the volume of aqueous humor affect the pharmacokinetics in the anterior segment of the eye (Table 2). For intravitreal macromolecules that are eliminated via the anterior route, the aqueous humor flow rate is the main mechanism of drug clearance in the anterior chamber. Small lipophilic molecules may be eliminated from the anterior chamber also by iridial blood flow (Fayyaz *et al.*, 2019). Evidently,

both species-related differences in aqueous humor dynamics and iris blood flow may influence the rate of elimination (Table 2).

Rodents are widely used in preclinical ocular pharmacology and toxicology (Chang *et al.*, 2005; Krebs *et al.*, 2017; Shah *et al.*, 2019) e.g. there are several established rodent models available for retinal neovascularization and glaucoma (Morrison, Johnson and Cepurna, 2008; Grossniklaus, Kang and Berglin, 2010). Despite the widespread exploitation of rodents in ocular drug development, their ocular pharmacokinetics is largely unknown. The small volume of ocular tissues in rats and mice make tissue dissection challenging (Table 2). For example, the average volume of vitreous in a rat is about 50 µl and ten time less in a mouse (5 µl) (Remtulla and Hallett, 1985; Sha and Kwong, 2006). For this reason, most of the published ocular pharmacokinetic studies have been carried out in rabbits or monkeys. This highlights the benefits of adopting noninvasive quantitation methods in monitoring the compounds in the ocular compartments since with this approach euthanizing animals and tissue dissections can be avoided.

In the design of pharmacological or toxicological studies, it is useful to know the interspecies dose scaling factors, since these factors can be applied to estimate the required doses when translating from rodents to rabbits or humans (Nair and Jacob, 2016). In intravitreal pharmacokinetics, the scaling factors for translation from mouse to human and rabbit to human have been published (del Amo *et al.*, 2015; Schmitt *et al.*, 2019). Intravitreal doses in humans should be about 40% higher than in the rabbits to obtain the same drug exposure as the average clearance of hydrophilic intravitreal drugs were 1.4 times faster in rabbits than in humans. The intravitreal elimination of three radiolabeled compounds (molecular weights 0.51 - 66.5 kDa) were studied using non-invasive Single-photon Emission Computed Tomography/Computed Tomography (SPECT/CT) imaging in mice. In that study, the elimination rate in mice was much faster than in rabbits or humans (Schmitt *et al.*, 2019). Based on the derived pharmacokinetic parameters, the intravitreal doses in rabbits and humans

should be 27-90 and 38-126 times higher than in mice, respectively (Schmitt *et al.*, 2019).

In the case of rats, intravitreal pharmacokinetics has not been studied. It has been reported that the collection of rat vitreous without cross-contamination from adjacent tissues is very difficult (Kottegoda *et al.*, 2007). For this reason, many kinetic studies in rats use whole eye homogenates, instead of individual tissues (Robinson *et al.*, 2002; Fuchs and Igney, 2017). Since rats are used as animal models for retinal diseases (Montezuma, Vavvas and Miller, 2009), it would be advantageous if the vitreal kinetics could be assessed in these animals in order to estimate a suitable dose when designing *in vivo* experiments.

## 2.2 Drug delivery system for intravitreal injections

The current retinal drug treatments are administered as repeated intravitreal injections. The intravitreal injections are invasive and in some cases, may lead to unwanted ocular effects, including inflammation, cataract, and pain which tend to reduce patient compliance (Sampat and Garg, 2010; Fagan and Al-Qureshi, 2013). Since the vitreal elimination half-lives of small drug molecules are only hours and macromolecules, while longer, are still measured in days (del Amo *et al.*, 2017), one approach to improve patient compliance would be to prolong the time intervals between injections by administering sustained release formulations.

Different formulation approaches for intravitreal sustained drug release have been investigated. Many formulations are still in the research phase or in preclinical development (e.g. nanoparticles), although intravitreal implants are in clinical use (Vieira, Sousa-Pinto and Figueira, 2020). The implant products are used to deliver small drug molecules, like corticosteroids (dexamethasone, fluocinolone acetonide ) (Sanford, 2013; Boyer *et al.*, 2014). A biodegradable dexamethasone implant (Ozurdex, based on polylactic-co-glycolic acid) has a duration of action of several months, while non-degradable implants (e.g. Iluvien) release fluocinolone acetonide for even longer, 18 - 30 months. The administration of these

implants requires surgery or the use of a large needle size (Christoforidis *et al.*, 2012).

Intravitreal nanomaterials can be used for two main purposes: 1) sustained drug release in the vitreous or 2) targeted drug or gene delivery to the retinal cells. Intravitreal liposomes were studied already in the 1980's (Barza *et al.*, 1985; Tremblay *et al.*, 1985). Later, polymeric nanoparticles were tested as intravitreal delivery systems of drugs (Mezei and Meisner, 1993; Zimmer *et al.*, 1994; Blazaki *et al.*, 2020; Delrish *et al.*, 2021; Zhou *et al.*, 2021) and nucleic acid based therapeutics (siRNA, DNA) were examined in experimental animals (Bochot and Fattal, 2012; del Pozo-Rodríguez *et al.*, 2013; Huang and Chau, 2019a). Preclinical success has been achieved i.e. the prolongation of retention and activity of drugs either as small molecules or macromolecules within liposomes (Bochot and Fattal, 2012) and polymeric nanoparticles (Huang and Chau, 2019a), but many aspects of their pharmacokinetics remain largely unknown. For example, some properties which are related to *in vivo* behavior such as the intravitreal kinetics of nanoparticles, drug release, stability and safety have not been studied in a systematic manner.

## 2.3 Methods for non-invasive monitoring of ocular pharmacokinetics

### 2.3.1 Optical coherence tomography

Optical Coherence Tomography (OCT) was introduced in biological imaging in the early 1990s (Huang *et al.*, 1991). Shortly after that, OCT was applied in evaluation of the retinal layers and morphology *in vivo* (Fercher *et al.*, 1993; Puliafito *et al.*, 1995). Application of OCT in clinical ophthalmology led to a dramatic increase in the precision and quality of diagnoses (Gabriele *et al.*, 2011).

The main application of ocular OCT is monitoring of the dimensions and morphology of tissues, for example retina and cornea. An OCT image of

rat retina is shown in Figure 3. OCT contrast mechanisms are based on absorption or back-scattering of near infra-red light (Schmitt, 1999). Therefore, the presence of molecules that can absorb or emit near infra-red light can improve contrast in OCT images. Melanin (Lee *et al.*, 2003) is an endogenous whereas indocyanine green (Ehlers *et al.*, 2014) is an exogenous example of these two kinds of contrast agents.

In some studies, the OCT technique has been used to estimate the corneal permeability of compounds based on their optical clearing effect (Larin *et al.*, 2011). Thus the diffusion rates of metronidazole, dexamethasone or glucose have been estimated indirectly by their effects on different optical properties (like the refractive index) of cornea and sclera (Ghosn, Tuchin and Larin, 2007; Ghosn *et al.*, 2008). This method is semi-quantitative, but the derived values were close to published ones obtained using quantitative methods.

Since micro- or nanoparticles may scatter light, there are publications describing the detection and imaging particulate systems. For example, microspheres were detected *in vivo* in liver with OCT (Lee *et al.*, 2003). Also metal nanoparticles have been detected by OCT qualitatively based on back-scattering of light (Xu *et al.*, 2020; Keahey *et al.*, 2021). The application of OCT for nanomaterial imaging in the eye is a new application of this technique. For example, OCT was used to detect gold nanoparticles (Song *et al.*, 2017) and cells with gold nanoparticles (Chemla *et al.*, 2019) in the rat vitreous.

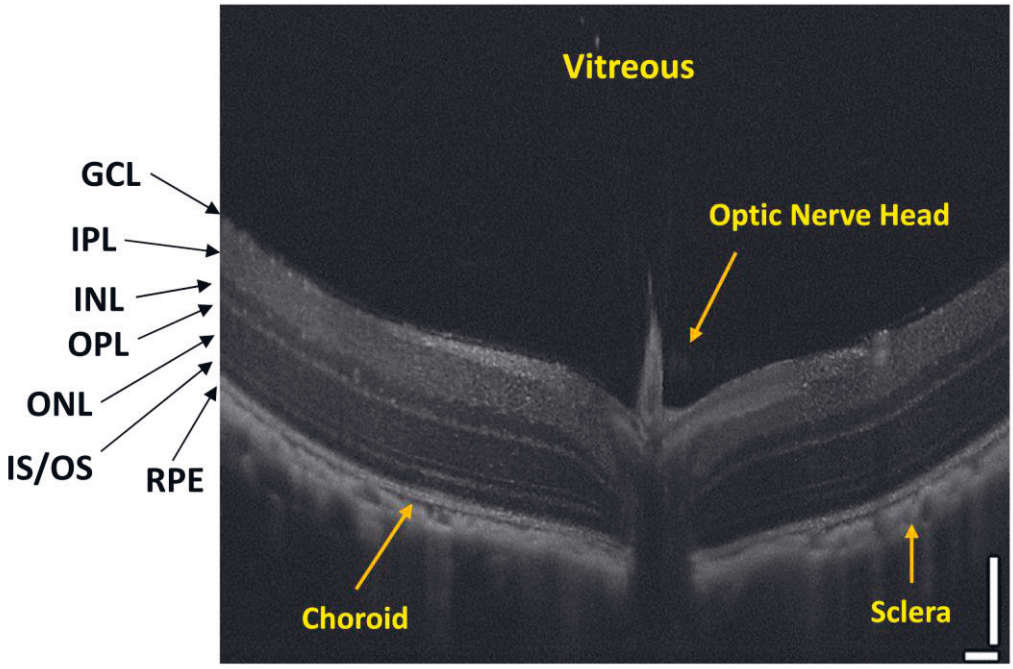


**Figure 3**. Retinal OCT image of a pigmented rat. Retinal layers are shown in the figure. GCL: ganglion cell layers, IPL: inner plexiform layers, INL: inner nuclear layers, OPL: outer plexiform layer, ONL: outer nuclear layer, IS: inner segment, OS: outer segment, RPE: retinal pigmented epithelium.

### 2.3.2 Fundus imaging

Fundus imaging is a non-invasive ocular imaging technique that allows visualization of the retinal surface through cornea and lens (Yannuzzi *et al.*, 2004); usually the pupil must be dilated with mydriatic eye drops before fundus imaging (Agarwal, 2008). With fundus imaging, it is possible to visualize the retinal vessels and optic nerve (Figure 4A). Moreover, fluorescence filters enable the application of fundus photography for retinal angiography and autofluorescence imaging. For example, after systemic injection of green (Ffytche *et al.*, 1980), red (Hochheimer and D'Anna, 1978) or near infrared (Hochheimer, 1971) fluorescent dyes, retinal angiography can be performed with a fundus camera. The aim of retinal angiography is to evaluate the morphology and permeability of retinal vessels which are important features in the evaluation of retinal pathologies associated with

uveitis and AMD (Olsen *et al.*, 2004). Figure 4B shows a retinal fluorescein angiogram of a pigmented rat.

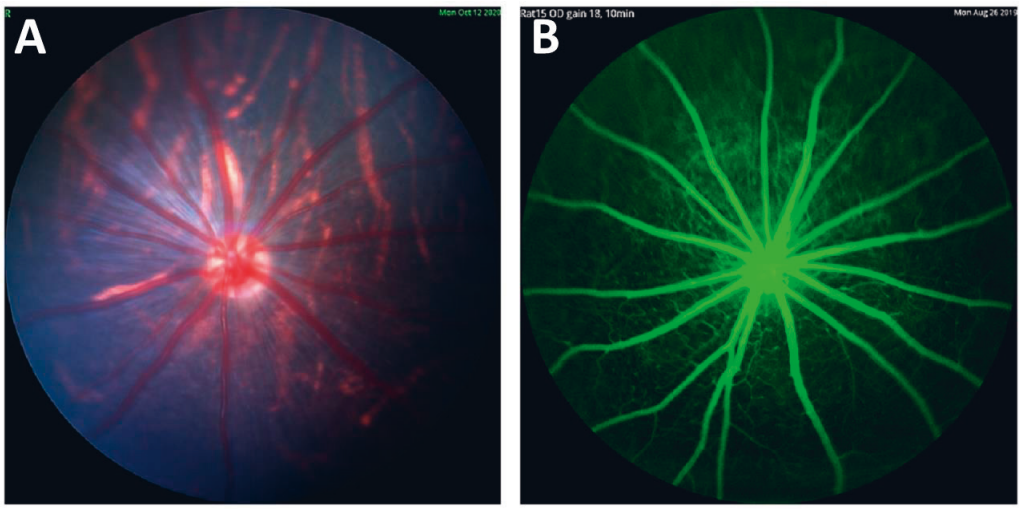


**Figure 4**. A) Fundus color image and B) Retinal fluorescein angiogram of a pigmented rat.

The main application of fundus imaging is in the diagnosis of diseases and retinal abnormalities. However, full color or fluorescence filter based images could be used to follow the distribution of labeled macromolecules and ocular drug delivery systems (Chang-Lin *et al.*, 2011; Cheng *et al.*, 2011; Chemla *et al.*, 2019; Eblimit *et al.*, 2021). Since this is a noninvasive technique, it can follow one subject at multiple times. Therefore, it is possible to monitor both the pharmacokinetics and safety of the injected materials at the same time. For example, the fluorescence signal of sunitinib loaded liposomes in the mice vitreous has been measured semi quantitatively via fundus imaging (Tavakoli *et al.*, 2022).

### 2.3.3 Ocular fluorophotometry

Ocular fluorophotometry is a noninvasive technique which can be used to quantify the concentrations of fluorescent compounds in the transparent ocular compartments, such as tear film, cornea, aqueous humor, lens and

vitreous. This technique was introduced in 1954 (Langham and Wybar, 1954) and later it was improved and used by different groups in the field of ocular physiology (Maurice, 1963; Waltman and Kaufman, 1970; Jones *et al.*, 1979; Munnerlyn, Gray and Hennings, 1985). The quantification of fluorescence signals in the ocular compartments enables measurements of several physiological factors, such as tear turnover, aqueous humor flow and permeability of both blood-aqueous and blood-retinal barriers (Lund-Andersen *et al.*, 1985; Raines, 1988; Docchio, 1989; Maurice *et al.*, 1990; Zeimer, 1990). An example of a fluorophotometric scan is illustrated in Figure 5.

Ocular fluorophotometry is an ideal technique for non-invasive quantification of labeled compounds in the vitreous and aqueous humor. In most intravitreal pharmacokinetic studies, large numbers of test animals, usually rabbits, are needed to monitor drug concentrations at different time points. This is expensive and ethically questionable. Moreover, this approach does not provide information about the inter-subject variability since only a single measurement is obtained from each animal. Fluorophotometry detects fluorescent compounds, enabling ocular pharmacokinetic studies with labeled macromolecules and drug delivery systems, like nanoparticles. However, this technique is only suitable for intrinsically fluorescent small molecules, because fluorescent labeling of small molecules causes dramatic changes in the molecular features that will result in misleading data.

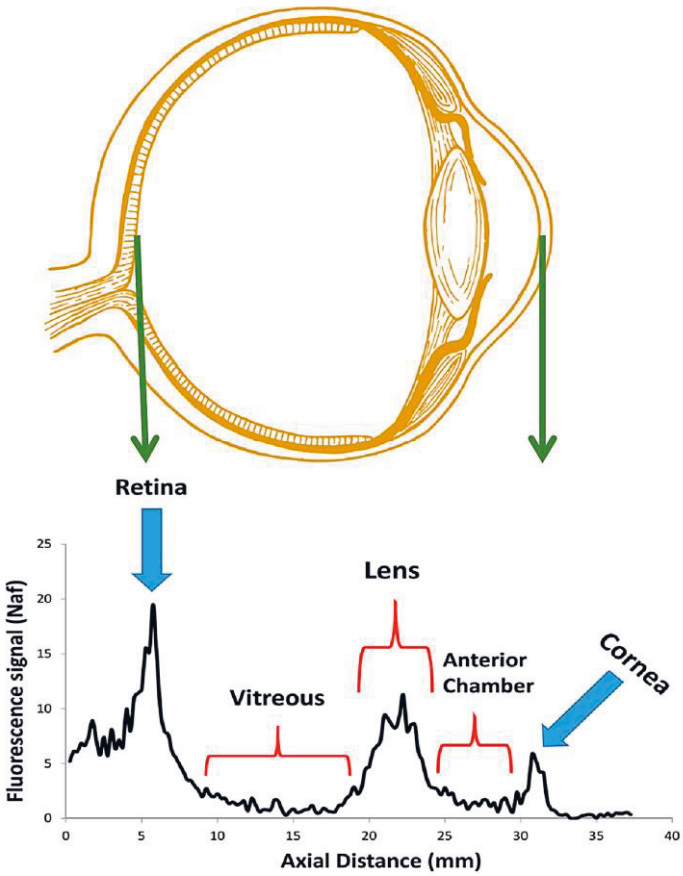


**Figure 5**. An example of fluorophotometric scan of a rabbit eye. This technique measures the fluorescence signal in the axis of the eye from retina to cornea. Autofluorescence is used to locate the different ocular compartments. The observed axial distance is larger than the actual anatomical values due to refractive index of the ocular medium.

Fluorophotometry facilitates the rational use of laboratory animals in accordance with the 3R principles (replacement, reduction, refinement). Fluorophotometry has been used in pharmacokinetic experiments with fluorescently labeled macromolecules in rabbits (Johnson and Maurice, 1984; Araie and Maurice, 1991). Recently, Dickmann and colleagues obtained similar pharmacokinetic results for intravitreally administered

ranibizumab using fluorophotometry and a conventional invasive method (Dickmann *et al.*, 2015).

## 2.4 Autofluorescence of the eye and fluorescent dyes

Ocular tissues can absorb and emit light at different wavelengths (Schmitz-Valckenberg *et al.*, 2008). The fluorescence of the tissues in the anterior part of the eye, like cornea and lens, are mostly in the ultraviolet and green wavelength range due to the protein content in these tissues (Van Best *et al.*, 1985; Holz *et al.*, 2007) (Table 3). The level of green autofluorescence in these tissues tends to increase with aging and in some pathological conditions like diabetes (Bleeker *et al.*, 1986). The range of fluorescence in the posterior tissues of the eye (e.g. retina) is mainly in the wavelength range of red color (Eldred and Katz, 1988; Delori *et al.*, 1995). With aging and in some retinal diseases like AMD, the retinal autofluorescence may increase due to the accumulation of lipofuscin (Marmorstein *et al.*, 2002). For example, an increase in the blue-green autofluorescence of Bruch's membrane relative to the yellow-orange autofluorescence of RPE-associated lipofuscin was observed in AMD patients.

**Table.3**. Ocular natural fluorophores and their excitation and emission wavelengths (Rovati and Docchio, 2004; Spaide, 2007; Dysli *et al.*, 2017) .

| Tissues | Excitation range (nm) | Emission range (nm) |
|---|---|---|
| Crystalline lens | 295-520 | 329-550 |
| Retinal Lipofuscin | 500-720 | 520-750 |
| Melanin | 300-800 | Broad in near infrared |
| Cornea | 366-450 | 440-550 |

Near infrared light has been used in the evaluation of retinal autofluorescence (Skondra *et al.*, 2012). For example, it is possible to image the melanin distribution in the retina with near infrared imaging (excitation: 787 nm and emission: 800 nm). This may be useful in the diagnosis of age-related retinal diseases (Keilhauer and Delori, 2006; Kellner, Kellner and Weinitz, 2010).

Natural autofluorescence of ocular tissues is valuable in diagnosis. The natural luminescence may affect the signals of exogenous probes that are used for angiography and as labels in preclinical studies. The signals of red dyes can interfere with retinal autofluorescence. In addition, green and near infrared fluorescent dyes are widely used in ophthalmology; but for green dyes, the overlap with autofluorescence is significant in anterior tissues, whereas retinal melanin could cause a significant degree of autofluorescence in near infrared imaging.

In order to avoid problems with autofluorescence (Table 3), new luminescent dyes have been designed and synthesized (del Rosal and Benayas, 2018; Jiang and Pu, 2021). For example, the luminescence properties of phosphorescence dyes can be adjusted by chemical modifications. Phosphorescence is another type of photoluminescence; it is similar to fluorescence but with a much longer emission half-life. The emission half-life can be used as a reporter of the chemical and thermal environment of molecules (Chelushkin *et al.*, 2022). This feature makes it possible to utilize these molecules as biological sensors.

Fluorescent dyes display a high emission intensity and they are commercially available. However, these dyes show small Stokes shifts, short lifetimes and may suffer from photobleaching. These deficiencies may result in lower image resolution in luminescent imaging and limit the use of fluorophores in long-term experiments. On the contrary, phosphorescent emitters, based on transition metal complexes, display large Stokes shifts, possess long life-times and are subjected to insignificant photobleaching. The Stokes shift is the difference between the emission and excitation

wavelengths of the dye. A large Stokes shift is useful in avoiding the overlapping of the excitation and emission signals, thus improving the detection limit and image quality. Moreover, dyes with large Stokes shifts should be capable of circumventing natural autofluorescence. Another property, photostability, is important when following the distribution of labeled materials for longer time periods.

Phosphorescence labels are an attractive alternative to be adopted when imaging diagnostic and therapeutic nanocarriers. Moreover, it is possible to use phosphorescence dyes which are sensitive to the chemical environment. For example, the oxygen concentration in biological environments has been quantified in a non-invasive manner (Papkovsky and Dmitriev, 2013), and this has also been achieved in the rodent retina (Wilson *et al.*, 2006; Shahidi *et al.*, 2010).

# 3. AIMS OF THE STUDY

The main goal of this thesis was to study how non-invasive optical techniques could be utilized to assess the vitreal kinetics of macromolecules and nanomaterials in rat and rabbits.

The specific aims of this study are as follows:

1. Imaging of phosphorescence dyes in intravitreal liposomes to avoid ocular autofluorescence problems.

2. Comparing the vitreal kinetics of macromolecules in rats and rabbits by using *in vivo* fluorophotometry and deriving inter-species scaling factors for intravitreal dosing.

3. Applying non-invasive optical techniques to assess both ocular pharmacokinetics and the safety of labeled liposomes, polymeric nanoparticles and peptide conjugates in rat and rabbits

4. Applying pharmacokinetic modelling for the prediction and quantitative understanding of ocular pharmacokinetics nanoparticles, peptide conjugates, and released drug after an intravitreal administration.

# 4. METHODS

| Method | Overview | Publications |
|---|---|---|
| **Anesthesia** | For intravitreal injections, inhalational and subcutaneous injection-based anesthetics were used in rat and rabbits, respectively. *In vivo* fluorophotometry and eye imaging was performed under inhalation anesthesia and a subcutaneous sedative in rat and rabbits, respectively. | **I, II, III, IV, V** |
| **Optical coherence tomography** | OCT was used to monitor the quality of injections and the safety of the materials in rats. The state of the retina was visualized and qualitative imaging of nanomaterials in the vitreous was performed. | **I, II, III, IV, V** |
| **Fundus Imaging** | Fundus imaging was performed with and without a fluorescent filter to follow the labeled materials in the rat and rabbit eyes. | **I, II, IV, V** |
| ***In vivo* ocular fluorophotometry** | Concentrations of the fluorescently labeled compounds were determined in rat and rabbit eyes. | **II, III, IV, V** |
| **Pharmacokinetic calculations and modeling** | Calculation of pharmacokinetic parameters from experimental data was accomplished. Simulation models were built for intravitreally injected materials in rat and rabbit eyes. | **II, III, IV, V** |
| **Liposome preparations** | The lipids were dissolved in chloroform prior to the liposome preparation. The liposomes were formed by a thin film hydration method followed by extrusion through a polycarbonate membrane to produce different particle sizes. | **V** |
| **Polymeric micelles** | Poly(ethylene glycol)- (trimethylene carbonate-g-ε-caprolatcone) block copolymers were synthesized. Polymeric micelles were synthesized by hydration of synthesized polymer in PBS. | **V** |
| **Polymersome** | Poly(ethylene glycol)-b-poly-(D,L-lactide) copolymer were synthesized by dissolving the polymers in organic solvents and then dispersion by addition of water. After dialysis against hyperosmotic solutions, particles with different morphologies were produced. | **V** |
| **Pullulan - dexamethasone nanoparticles** | Dispersion of synthesized polymer in PBS buffer. | **IV** |
| **Peptide conjugates** | The peptide–dexamethasone conjugates consist of a cell penetrating peptide, an enzyme cleavable linker and dexamethasone that is conjugated with a hydrazone bond. | **III** |
| **Particle size** | Differential light scattering was used for particle size and charge analysis | **I, IV, V** |
| **Endotoxin test** | The endotoxin level was evaluated by using the Limulus Amebocyte Lysate gel-clot endotoxin assessment kit. | **IV, V** |
| **Synthesis and characterization of iridium probes** | Iridium (III) lipid-mimetic complexes were synthesized by addition a $C_{16}$ aliphatic chain. The synthesized probes were characterized using nuclear magnetic resonance. | **I** |

| | | |
|---|---|---|
| **Stability and biological interaction of peptide conjugate** | The *ex vivo* stability of peptide conjugates in porcine vitreous were determined by using ultra-performance liquid chromatography tandem mass spectrometry. The interaction of peptide conjugates with vitreous and glucocorticoids was evaluated using Microscale Thermophoresis. | **III** |

# 5. RESULTS

## 5.1 Retinal autofluorescence and luminescent bioimaging

The fluorescence properties of ocular tissues are different (Table 3). Eye imaging using different excitation and emission wavelengths is useful in observing the natural autofluorescence. For example, in Figure 6, the fundus images of a rat at three different wavelengths are shown. Depending on the wavelength, the background intensity is different. In Figure 6B, less autofluorescence is visible than in 6C. Endogenous fluorescence is important since it can affect the signal-to-noise ratio of labelled materials after intravitreal injections.


**Figure 6.** Fundus images of a pigmented rat. A) Full color image, B) filter set of emission (504.7-900 nm) and excitation (451.1- 486.5 nm), C) filter set of emission (610.6-900 nm) and excitation (full color).

In order to design suitable dyes for ocular imaging, two phosphorescence probes (Ir-1 and Ir-2) were synthesized. Because these probes are hydrophobic and not water-soluble, they were formulated into liposomes to allow measurements of the fluorescence spectra in aqueous medium and this made it possible to perform *in vivo* experiments. The structure of the dyes was modified by addition of an aliphatic chain with a length of 16 carbon (Figure 7) to facilitate liposomal incorporation. After this modification, the probes were loaded into a liposomal formulation

(DPPC/DSPE-PEG2000/Ir1 or Ir2) at molar ratios of (94/4.5/1) at a total concentration of 3 μmol/ml. The average sizes of the Ir1 and Ir2 labeled liposomes were 118 ± 24 nm and 106 ± 23 nm, respectively. For these probes, three excitation wavelengths of 290, 335 and 450 nm could be used with the emission wavelength being in the red region (about 650 nm).

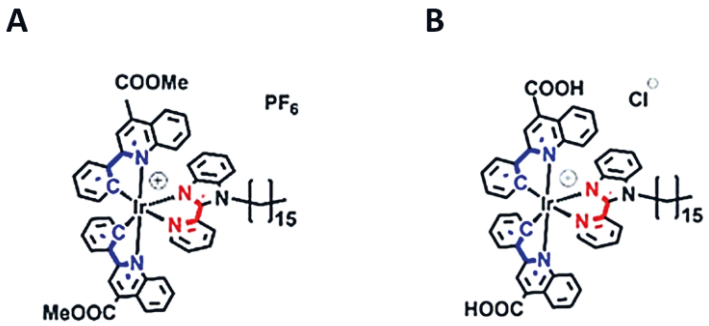


**Figure.7.** Chemical structure of A) Ir-1 and B) Ir-2 compounds.

To evaluate the applicability of phosphorescent liposomes in the *in vivo* imaging, we performed OCT and full color fundoscopy in pigmented rats after intravitreal injection of the labeled liposomes. Ir-1 and Ir-2 complexes are clearly visible not only due to their luminescence in funduscopy, but they also generate OCT contrast (a comparison of OCT images before and after injection as shown in Figure 8). The luminescence and OCT signals are overlapping thereby revealing the colocalization of the signals. In the fundus images (excitation: 451.1-486.5 nm, emission 504.7-900 nm), we could observe the labeled liposomes without any significant autofluorescence background.

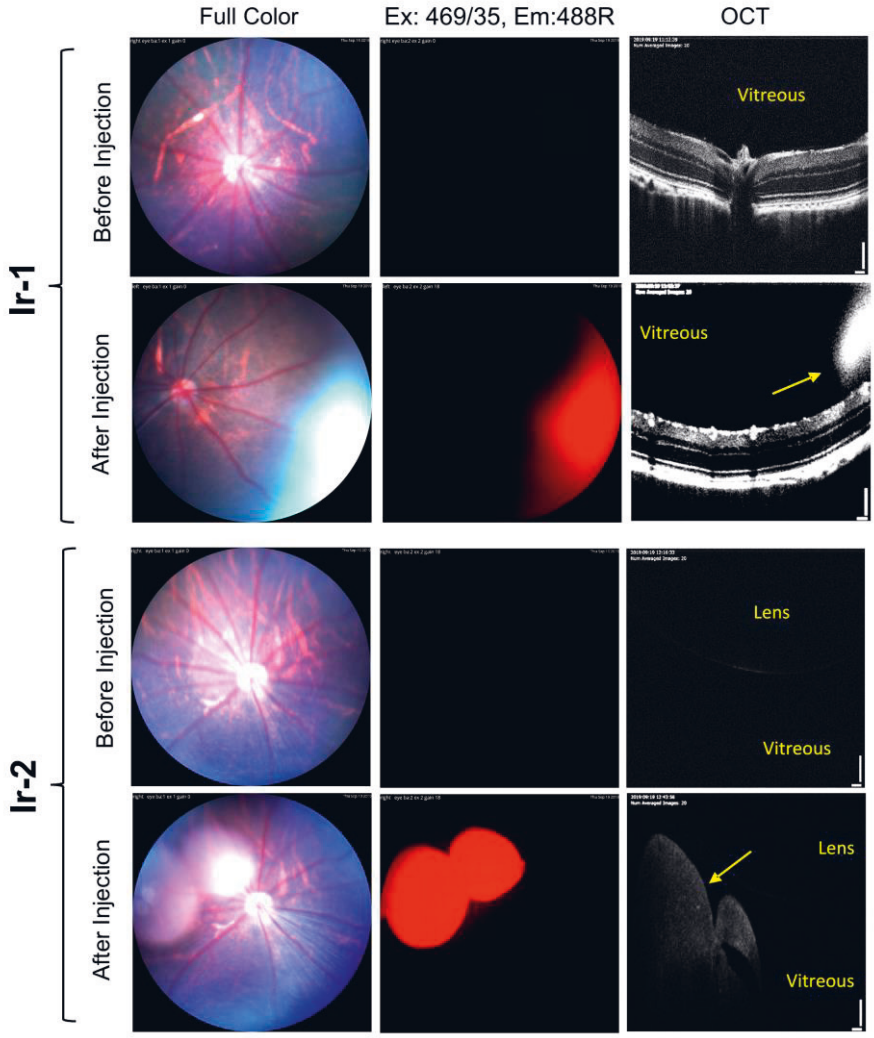


**Figure 8.** Fundus and OCT images in rat eyes before and after intravitreal injection of liposomes labeled with Ir-1 and Ir-2. Fundus image are full color and with filter combination (excitation: Semrock FF01-469/35 and barrier: Semrock BLP01-488R). The labeled liposomes are visible as red color. The right column is the OCT images before and after intravitreal injections. The liposomes are visible in the vitreous after the injection (yellow arrow).

## 5.2 Rat-to-rabbit scaling of intravitreal pharmacokinetics

Intravitreal injections of FITC-dextrans and fluorescein into the rat and rabbit eyes were used to compare the ocular pharmacokinetics in these two species. Ocular fluorophotometry was used to determine the concentration of compounds in the vitreous. The concentrations at different time points were fitted into a one compartment model with a first order elimination rate constant and kinetic parameters were obtained (Table 4). The elimination half-life of a small molecule, fluorescein, is about three times shorter in rats than in rabbits. In the case of FITC-dextrans, the elimination half-lives for molecular weights of 10, 150 and 500 kDa were about 5-6 times longer in rabbits than in rats. The apparent volume of distribution was in the range of the anatomical volume of the vitreal cavity in both species. In both species, the clearance of fluorescein was much faster than the clearance of FITC-dextrans, demonstrating the importance of molecular size in the vitreal clearance.

**Table 4.** Kinetic parameters of intravitreally injected compounds in rats and rabbits (average ± SD).

| Compound | Species | Apparent volume of distribution (µl) | Elimination half-life (h) | Clearance (µl /h) | Number of eyes |
|---|---|---|---|---|---|
| Fluorescein[a] | Rat | 50 | 1.05 ± 0.07 | 33 ± 2.2 | 20 |
| FITC-dextran 10 kDa | Rat | 88 ± 22 | 13.5 ± 1.6 | 4.5 ± 0.8 | 6 |
| FITC-dextran 150 kDa | Rat | 186 ± 57 | 34.1 ± 1.4 | 3.8 ± 1.2 | 6 |
| FITC-dextran 500 kDa | Rat | 73 ± 17 | 26.6 ± 5.4 | 2.1 ± 0.9 | 6 |
| Fluorescein | Rabbit | 1200 ± 970 | 3.0 ± 2.2 | 273 ± 69 | 3 |
| FITC-dextran 10 kDa | Rabbit | 2600 ± 350 | 83 ± 3 | 21.6 ± 2.4 | 4 |
| FITC-dextran 157 kDa[b] | Rabbit | 1700 | 166.3 ± 16.8 | 7.1 ± 0.7 | 14 |
| FITC-dextran 500 kDa | Rabbit | 1300 ± 180 | 152 ± 13 | 5.9 ± 0.7 | 6 |

[a] The values are from the literature (Krupin *et al.*, 1982) which they reported the vitreal elimination half-life of fluorescein in pigmented rats after intravitreal injection. The clearance was calculated by using the average of the anatomical volume of vitreous (50 µl) (Sha and Kwong, 2006). [b] The values are from the literature (Johnson and Maurice, 1984), which they reported the vitreal elimination half-life of FITC-dextran of 157 kDa in pigmented rabbits after intravitreal injection. The anatomical volume of rabbit vitreous (1700 µl) (Missel, Horner and Muralikrishnan, 2010) was used to estimate the clearance (i.e. clearance = vitreous volume × elimination rate constant).

The kinetic parameters of rats and rabbits are compared in Table 5. If we aim at an equal area under the curve (AUC) in rats and rabbits, the ratios of clearance values could be used to estimate the scaling factors for dosing (AUC= Dose/CL). For fluorescein, the scaling factor between rats and rabbits is about 8; for macromolecules, it is in a range 2-5. Thus, similar vitreal drug exposure (AUC) in rabbits is reached at 2-5 time higher doses than in rats

**Table 5.** Relative differences (rabbit/rat values) for intravitreal volume of distribution, clearance and half-life. Dose scaling factor was calculated as $CL_{rabbit}/CL_{rat}$.

| Compound | Apparent volume of distribution | Clearance | Elimination half-life | Dose scaling factor for equal AUC |
|---|---|---|---|---|
| Fluorescein | 24 | 8.3 | 2.9 | 8.3 |
| FITC-dextran 10 kDa | 29 | 4.8 | 6.1 | 4.8 |
| FITC-dextran 150 kDa | 9.1 | 1.9 | 4.9 | 1.9 |
| FITC-dextran 500 kDa | 18 | 2.8 | 5.7 | 2.8 |

## 5.3 Pharmacokinetics of intravitreal peptide conjugates

The intravitreal pharmacokinetics of two peptide conjugates (Dex-1 and Dex-2) were evaluated (Figure 9). The peptide conjugates consist of three components: 1) a cell penetrating sequence for intracellular entry, 2) an enzyme cleavable peptide-based linker and 3) dexamethasone attached to c terminal of peptide-based linker via a hydrazone linkage. The peptides sequences were stable in the isolated vitreous for 6 weeks, whereas they were taken up and cleaved in the RPE cells efficiently (Bhattacharya et al. 2017). The peptide conjugates released dexamethasone with the Arg

residue, and this molecule was able to bind well to the human glucocorticoid receptor as shown in microscale thermophoresis (MST) experiments.

Binding of Alexa Fluor 488 labeled peptides to the vitreous was measured using MST. One of the peptides (Dex-2) had high affinity for binding to the porcine vitreous ($K_d$ =13.5 nM) and the maximum binding capacity was reached at 100 nM. It was not possible to measure the affinity of Dex-1 peptide because of its adherence to the capillary walls of the device.


**Figure 9**. Sequence and structure of dexamethasone conjugate peptides (Dex-1 and Dex-2). CPP stands for cell penetrating peptide and DEX for dexamethasone.

The peptides were injected in the rabbit vitreous and the fluorescence signals were measured at different time points using ocular fluorophotometry (Figure 10). The elimination half-lives of the peptides in the rabbit vitreous were about one day (Table 6). Concentration ratios of the peptides between aqueous humor and vitreous were about 0.3 (Figure 10, Table 6).

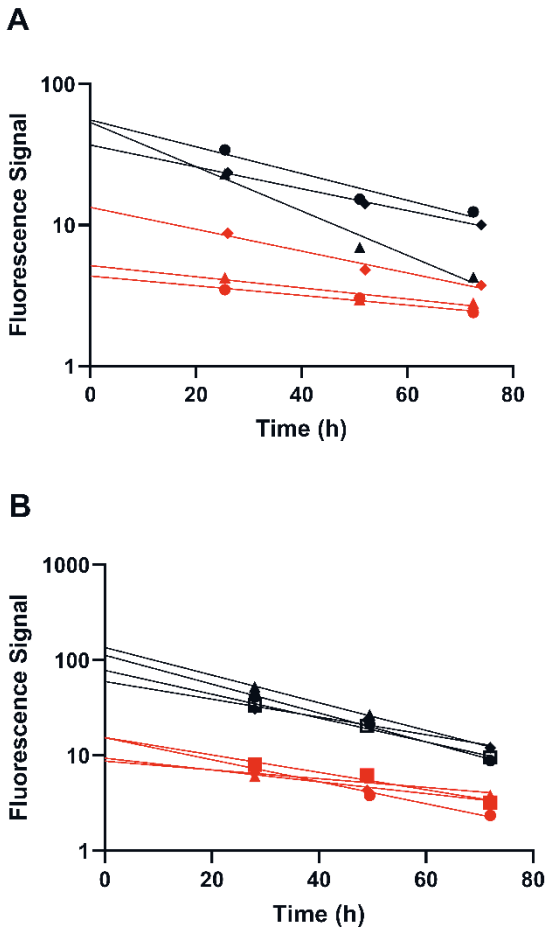


**Figure 10.** The fluorescence signal in the rabbit vitreous (black colour) and aqueous humour (red colour) after intravitreal injection of peptides into the rabbit eye. A) Dex1 and B) Dex2.

**Table 6**. The pharmacokinetics parameters of intravitreal Dex-1 and Dex-2 in rabbit eyes.

| Compound | Number of eyes | Volume of distribution (µl) | Clearance (µl/h) | Elimination half-life (h) | $C_a/C_v$ ratio[b] |
|---|---|---|---|---|---|
| Dex-1 | 3 | 1700 [a] | 41.9 ± 17.0 | 29.9 ± 10.0 | 0.31 ± 0.14 |
| Dex-2 | 4 | 1700 [a] | 49.3 ± 10.1 | 24.3 ± 5.7 | 0.23 ± 0.04 |

[a] Anatomical volume were assumed as vitreal volume of distribution (Missel, 2012). [b] the ratio of signals in aqueous humour ($C_a$) and vitreous ($C_v$).

## 5.3 Pharmacokinetics of intravitreal nanomaterials

Different nanomaterials were used to study their intravitreal kinetics and distribution (Table 7). These formulations included liposomes, polymeric micelles, polymersomes and polymeric conjugates with particle sizes ranging from ≈ 50 nm to > 1000 nm. Polymeric micelles and polymersomes were made both as spherical and longitudinal particles (Table 7). Even though pullulan conjugates are single polymeric chains, they can self-assemble and form nanoparticles (about 200 nm in diameter). The endotoxin tests of the formulation revealed that two of the materials had endotoxin contamination (vesicle ≈300 nm; tube ≈180 nm).

**Table 7.** Nanomaterial properties.

| Formulation | Hydrodynamic diameter (nm) | Polydispersity index | Shape | Endotoxin |
|---|---|---|---|---|
| Liposome ≈ 50 nm | 48.6 ± 3.9 | 0.148 | Spherical | - |
| Liposome ≈ 100 nm | 94. 6 ± 5.7 | 0.054 | Spherical | - |
| Liposome ≈ 250 nm | 231.7 ± 44.8 | 0.029 | Spherical | - |
| Liposome > 1000 nm | 1160.9 ± 234.1 | 0.494 | Spherical | - |
| Micelle≈ 40 nm | 37.5 ± 0.3 | 0.061 | Spherical | - |
| Worm ≈90 nm [b] | 91.8 ± 1.2 | 0.294 | Worm shape | - |
| Vesicle ≈300 nm | 303.0 ± 23.0 | 0.101 | Spherical | + |
| Tube ≈180 nm [b] | 183.5 ± 4.1 | 0.055 | Tubular | + |
| BDP-pullulan-DEX | 219 ± 15 | 0.25 | Spherical | - |

The lowest dilution of the injected solution (1 to 64 times dilution) which contained more than 0.03 EU/ml of endotoxin was indicated as positive. [b] The reported sizes are based on the DLS method. The shape of the particles was not considered in this size measurement. The width and length of the particles (tubes and worms) based on cryo-TEM are more than 1 µm and the width is about 100 to 50 nm (Ridolfo *et al.*, 2020).

***Vitreal distribution of nanomaterials by using fundus imaging.***

The vitreal distribution of nanomaterials was studied in rats after intravitreal injection by means of fundus imaging and OCT. Fluorescently labelled materials were used for fundus imaging. In fundus images, the fluorescence signal was detectable up to 20 days after the intravitreal injection of large liposomes (> 1000 nm in diameter). The signal for ≈50 nm liposomes was detectable still at 10 days, but not after injection of ≈100 nm and ≈250 nm liposomes (Figure 11).

The vitreal distribution of polymeric micelles (micelles ≈40 nm and worms ≈90 nm) revealed the retention in the vitreous for at least 65 days, mostly close to site of injection (Figure 12). Polymersomes (vesicles ≈300 nm, tubes ≈180 nm) were eliminated from the vitreous in about 8 days (Figure 13). The polymersomes contained endotoxin which may lead to faster elimination (Table 7).

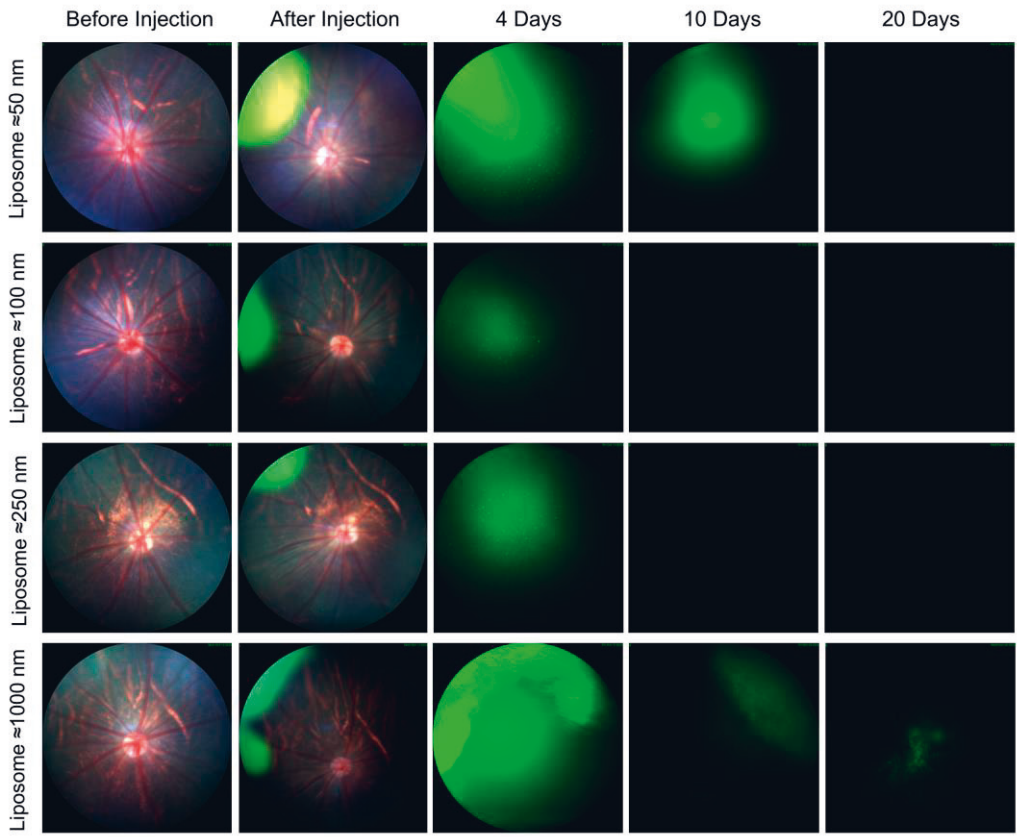


**Figure 11** Fundus images showing the distribution of labeled liposomes with average size of ≈50 nm, ≈100 nm, ≈250 nm and ≈1000 nm in the rat vitreous after intravitreal injection. Two eyes were injected and both eyes showed similar distribution patterns. The imaged time points are immediately after injection and then 4 days, 10 days and 20 days post-injection.

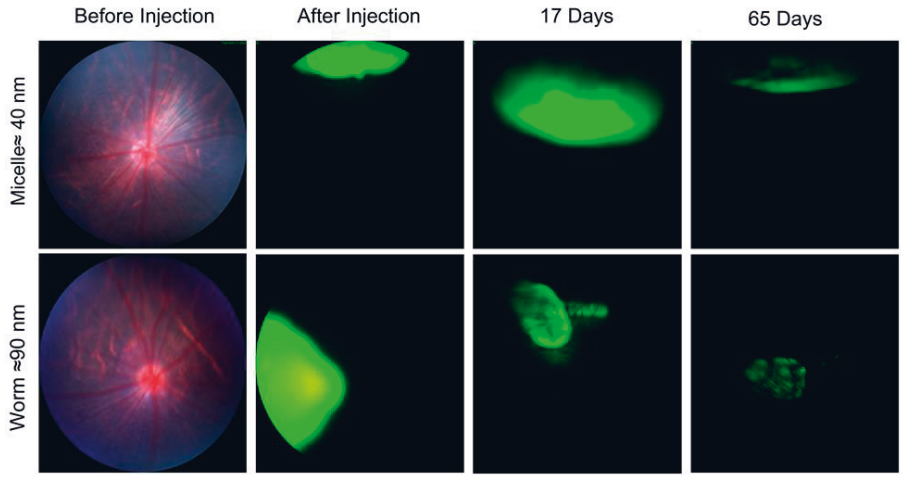


**Figure 12** Fundus images showing the distribution of intravitreally injected polymeric micelles with spherical (micelles ≈40 nm) and worm shapes (worm ≈90 nm) in the rat vitreous. The time points for imaging are shown above the images.

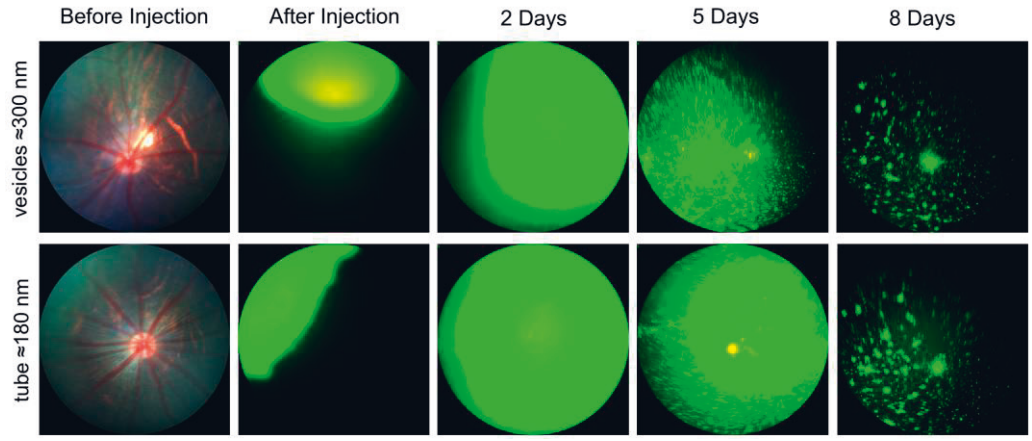


**Figure 13.** Fundus images showing the distribution of intravitreally injected polymersomes with spherical (vesicle ≈300 nm) and tubular (tube ≈180 nm) shape. The time points for imaging are shown in the columns.

***Pharmacokinetics of intravitreal nanoparticles with fluorophotometry:***

The vitreal kinetics of fluorescently labeled liposomes and pullulan conjugates were assessed with *in vivo* fluorophotometry. One compartment

model with a first order elimination rate constant was applicable in all cases. The apparent volumes of distribution of all formulations were close to the anatomical volume of the vitreous in rats and rabbits (Table 8).

Intravitreal half-life of BDP-pullulan in rats was about 17 hours (Table 8) and conjugation of dexamethasone to BDP-pullulan did not change the half-life. The elimination half-life of BDP-pullulan-DEX in rabbits was about 60 hours.

Pharmacokinetics of labeled liposomes (≈50 nm in diameter) was evaluated in rabbits with fluorophotometry. The retention time of the liposomes was much longer than the retention of pullulan derivatives (half-life about 200 hours) (Table 8).

**Table.8.** Kinetic parameters of nanomaterial after intravitreal injections to rat and rabbit eyes.

| Compound | Species | Apparent volume of distribution (µl) | Elimination half-life (h) | Clearance (µl /h) | Number of eyes |
|---|---|---|---|---|---|
| BDP-pullulan | rat | 42 ± 12 | 17.4 ± 3.9 | 1.8 ± 0.7 | 6 |
| BDP-pullulan-DEX | rat | 84 ± 30 | 16.7 ± 0.8 | 3.5 ± 1.2 | 5 |
| BDP-pullulan-DEX | rabbit | 932 ± 72 | 60.3 ± 4. 9 | 11 ± 0.4 | 6 |
| liposome≈50 nm | rabbit | 954 ± 478 | 202.1 ± 91.2 | 3.4 ± 1.4 | 6 |

We performed kinetic simulations in order to estimate the elimination routes of BDP-pullulan-DEX and liposomes (≈50 nm) in rabbit eyes. In these simulations, the concentration of compounds was simulated in vitreous and aqueous humor by assuming the anterior route as the only elimination pathway. The clearance from aqueous humor was assumed to be equal with the aqueous humor flow rate. The simulated concentrations matched with

the experimental values from vitreous and aqueous humor (Figure 14), suggesting that these nanomaterials are eliminated via the anterior route.

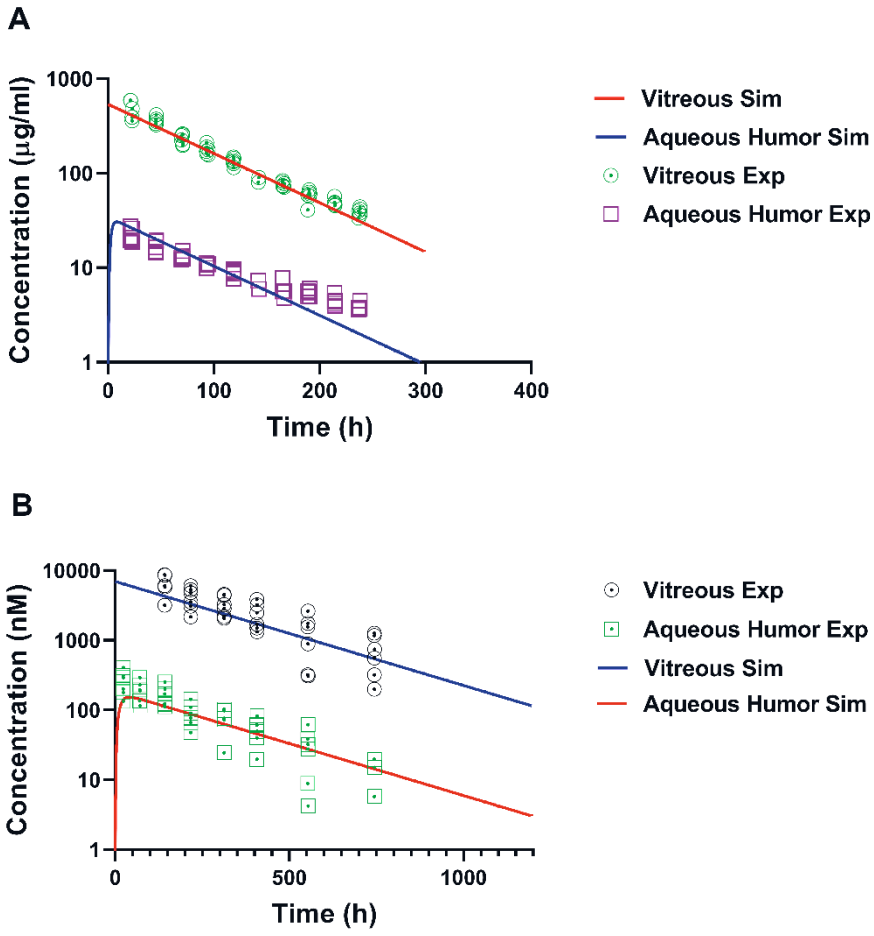


**Figure 14.** Experimental and simulated concentrations of A) BDP-pullulan-DEX conjugates (vitreal elimination half-life of about 60 h) and B) liposomes (≈ 50 nm in diameter; vitreal elimination half-life of about 200 h) in the vitreous and aqueous humor of rabbits after intravitreal injections.

The kinetics of the peptide conjugates, liposomes and BDP-pullulan-DEX were compared with anteriorly eliminating sucrose and FITC-dextrans in Maurice plot (Figure 15). The Maurice equation (Eq.1) (Maurice and Mishima, 1984) assumes that vitreal elimination takes place only via anterior route:

Eq.1 $$\frac{Ca}{Cv} = k_v \frac{V_v}{f}$$

in which $C_a$ and $C_v$ are compound concentrations in aqueous humor and vitreous, respectively. $K_v$, $V_v$ and $f$ are the vitreal elimination rate constant, and the volumes of vitreous and aqueous humor flow rates in rabbits, respectively. In Figure 15, both the anatomical and the average of intravitreal volume of distribution were used (red and green line) (Missel, 2012; Del Amo *et al.*, 2015) The values of liposomes and BDP-pullulan-DEX are close to the Maurice line and in agreement with sucrose and FITC-dextran data, indicating that the anterior route is the main elimination route for these materials.

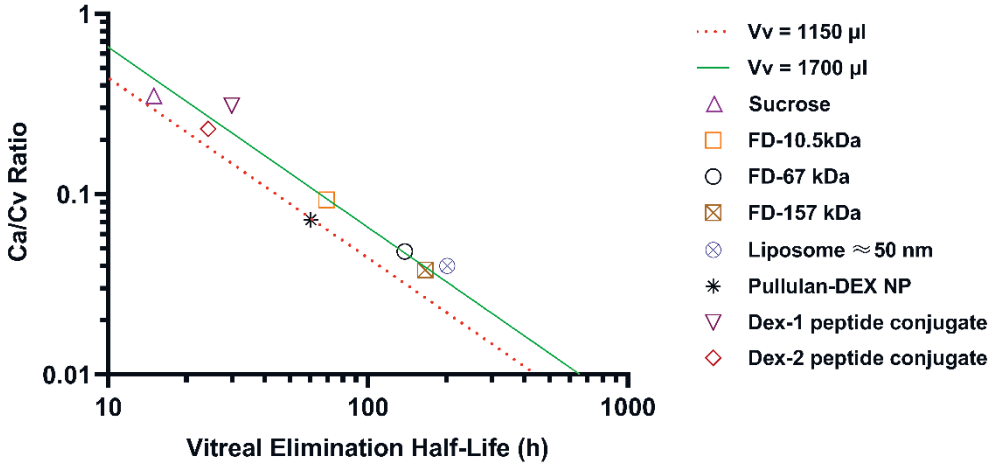


**Figure 15.** Maurice plot of intravitreally administered compounds in the eyes of rabbits. The plot shows anteriorly eliminating compounds based on literature data: sucrose (0.342 kDa ) (Bito and Salvador, 1972), FITC-dextran (FD-10.5, FD-67, FD-157 kDa) (Johnson and Maurice, 1984; Missel, 2012). The green and red (dotted) lines are derived from the Maurice equation by assuming 1150 and 1700 µl as the vitreal volume of distribution (Missel, 2012; Del Amo *et al.*, 2015). Positions of BDP-pullulan-DEX (~75 kDa),

liposome and peptide conjugate (Dex-1, Dex-2) data close to the straight lines indicate the anterior route of elimination in the rabbit eyes.

In compartmental kinetics and simulations, a homogenous distribution of nanoparticles in the vitreous was assumed. However, the results of fluorophotometry and fundus imaging show an intravitreal concentration gradient and liposome accumulation near to the optic nerve head (Figure 16). No such gradient was observed for BDP-pullulan-DEX.

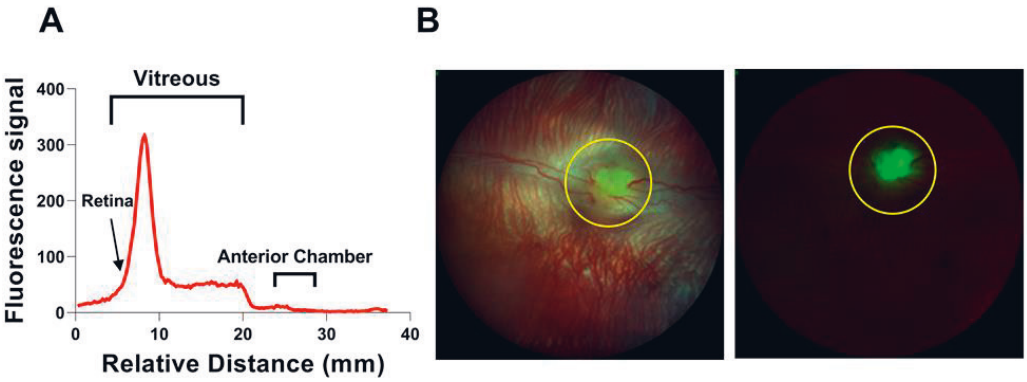


**Figure 16.** A) Fluorophotometric scan of a rabbit eye one month after intravitreal liposome (≈ 50 nm size) injection. B) Fundus images of the same eye with full color (left) and green filter (right) settings. The yellow circle shows the accumulation of liposomes in the optic nerve head.

***Importance of synchronizing drug release and nanoparticle elimination***

We showed that vitreal kinetics of nanomaterials can be well described with a one compartment model and first-order elimination. The elimination of the particles and drug release affect the drug response after intravitreal injection, but their inter-relationship has not been explored. In order to investigate this phenomenon, we simulated pharmacokinetics of intravitreal liposomes by using experimental rate constants of liposomes (≈50 nm) from rabbit eyes and assumed different first-order drug release rates. With

respect to the released drug, we used kinetic parameters of dexamethasone.

The simulations demonstrate the importance of synchronizing ocular retention and drug release from nanoparticles. Figure 17 shows the dependence of ocular bioavailability (ocular exposure to released drug) on the release half-life. Increasing the release half-life prolongs the expected duration of action (exposure period), but it plateaus after ≈ 15 days. On the other hand, bioavailability will decrease with a slower drug release rate, since more drug will be eliminated from the eye in a liposome encapsulated form. Thus, the design of efficient long-acting nanoparticles must involve both a prolongation of particle elimination and controlled drug release.

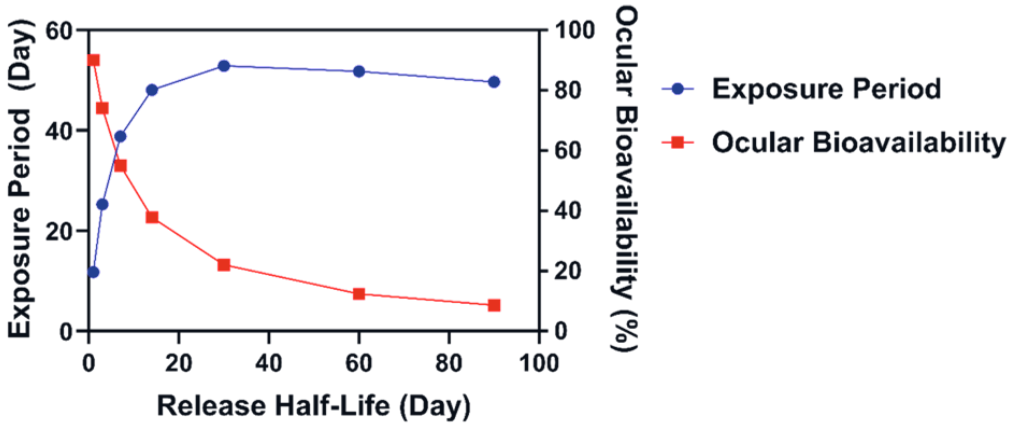


**Figure.17.** Relationship between ocular drug bioavailability (percentage of dexamethasone release in the vitreous and aqueous humor) and drug release rate (half-life of release) from intravitreally injected liposomes. The simulation was performed using liposomal kinetic parameters from Table 8. The effective exposure period of free dexamethasone in the vitreous is shown as a function of the drug release rate. The exposure period is defined as the time period for dexamethasone concentrations staying above 1 nM in the vitreous.

# 6. DISCUSSION

## 6.1 Ocular autofluorescence and eye imaging

Ocular tissues show emission wavelengths when subjected to excitation beams leading to different background signals in ocular tissues. In this study, we imaged the retina and vitreous of pigmented rats after intravitreal injections. Autofluorescence may affect the quality of imaging when investigating labeled molecules or particles. For example, Marmorstein et al. (Marmorstein *et al.*, 2002) elucidated the spectral profile of natural autofluorescence in the human retina. They studied the retinas of healthy and diseased AMD human subjects using different excitation and emission wavelengths. When excitation was performed at 488 nm, the emitted signal at 655 nm wavelength was minimal.

In our study, two phosphorescence probes (Ir-1 and Ir-2) were synthesized and formulated into liposomes that were injected intravitreally into the rat eye. These two dyes are iridium complexes with excitation wavelengths in ultraviolet (290 to 330 nm) or blue light (430 to 470 nm) and emission wavelengths range from the red to the near infrared range (650-800 nm). For *in vivo* imaging, we used excitation wavelength 488 nm and monitored the IR-1 and IR-2 dyes in a range of 500 to 700 nm. The maximum emission of these dyes in aqueous media is reached at about 650 nm. Therefore, the background noise from the retinal autofluorescence should be minimal for these dyes. As we have shown with the fluorescent fundus imaging of IR-1 and IR-2 labeled liposomes, these dyes improve both the quality and sensitivity of the imaging procedure.

Another potential application of these dyes could be their simultaneous detection with green dyes, like fluorescein, in a single image. This is feasible because by using filter sets in fluorescein angiography, the retinal vessels are visible in green color and the IR-1 and IR-2 are in red color. For example, when we injected intravitreally compounds or formulations with IR-1 or IR-2

labels, and perform fluorescein based retinal angiography, we could detect the intravitreally injected materials with the same set of filters in a single image. Retinal angiography is a valuable tool in the evaluation of retinal vessels, an important part in preclinical safety and drug efficacy studies (Littlewood *et al.*, 2019). These labels potentially broaden the information which can be gained in such investigations. Compared to fluorescent labels, the phosphorescent labels are expected to display an improved signal-to-noise ratio due to the large Stokes shift and negligible quenching in long-term experiments with ocular drug delivery systems capable of prolonged action.

In this study, we observed the injected liposomes in the vitreous by OCT. To the best of our knowledge, this is the first report on the applicability of phosphorescent dyes for simultaneous use with *in vivo* funduscopy and OCT. The wavelength in ocular OCT imaging was in the near infra-red region. Thus, the molecules that are capable of absorbing or emitting light at a range of around 800 nm or higher can generate a contrast in the OCT images. Previously, OCT-based detection of unlabeled microspheres *in vivo* in liver was demonstrated (Lee *et al.*, 2003). The contrast mechanisms of OCT are based on the absorption or back-scattering of light. Endogenous melanin (Lee *et al.*, 2003) and exogenous indocyanine green (Ehlers *et al.*, 2014) are examples of contrast agents which can be detected by OCT. Since the detected wavelength in OCT is in the near infrared region, and IR-1 and IR-2 do not have strong emission in this range, it is likely that the OCT signals of the Ir-labeled liposomes originate mostly from physical light scattering. Interestingly, the signals of fluorescence fundus images and OCT overlap. This shows that the liposomes are detectable by both OCT and fluorescence imaging. Colocalization of the signals also indicates that the labels are stably embedded in the liposomes after intravitreal injections.

The combination of OCT and fluorescence imaging simultaneously may provide a means to monitor simultaneously tissue microstructures (OCT) and molecular processes (fluorescence signals) (Yuan *et al.*, 2009). Such an approach may be interesting in the experiments of ocular drug safety and

pharmacodynamics *in vivo*. Fluorescence signals may demonstrate the distribution of compound or drug delivery system, while OCT could reveal the distribution of materials and ocular microstructures, such as retinal layers (Yang, 2005).

The ocular safety of Ir-complexes is still unknown. We encountered occasional toxic responses, and thus the overall the safety status of these materials is unclear.

## 6.2 Dose scaling for intravitreal drug delivery

Rats are widely used in efficacy and safety studies of intravitreally injected compounds (Grossniklaus, Kang and Berglin, 2010), but data on intravitreal pharmacokinetics in rats have not been available. Non-invasive fluorophotometry was used to evaluate the effect of molecular weight on vitreal pharmacokinetics in rats and rabbits. Although vitreal pharmacokinetics in rabbits has been investigated in many studies (del Amo *et al.*, 2015) ), drug concentrations have not been monitored in the rat eyes after intravitreal injections. In conventional pharmacokinetic studies, the vitreous is isolated from the eyes of sacrificed rabbits and drug concentrations are analyzed with LC/MS, radiochemical or ELISA methods (Laurent and Fraser, 1983; Kwak and D'Amico, 1992; Sinapis *et al.*, 2011). In such studies, intravitreal clearance for molecular weights of 7-149 kDa were in the range of 11-71 µl/h (del Amo *et al.*, 2015). In our study, similar values have been obtained (5.9-21.6 µl/h) at mean molecular weights of 10-500 kDa. This is in line with a previous study (Dickmann *et al.*, 2015) that utilized non-invasive fluorophotometry to examine the vitreal pharmacokinetics of ranibizumab. Fluorescent labeling changes the properties of small molecules dramatically and for this reason this technique can be applied only for macromolecules, nanoparticles or small molecules with intrinsic fluorescence (e.g. fluorescein sodium).

To the best of our knowledge, this is the first quantitative study on vitreal pharmacokinetics in rats. Our main findings are as follows: 1) the intravitreal elimination of macromolecules is faster in rats than in rabbits; vitreal half-lives in the rabbits are 5-6 times longer than in the rats. 2) Intravitreal clearance values of macromolecules in the rabbits are 2-5 times higher than in rats, suggesting that the average intravitreal daily doses should be 2-5 times higher in rabbits than in rats. 3) Increasing the molecular weight decreased the rate of vitreal elimination in both species, presumably due to the slower diffusion in the vitreous and different retinal permeability.

Like in rabbits (Rimpelä *et al.*, 2018), the intravitreal clearance of macromolecules in the rats (≈ 2-5 µl/h) is slower than the rate of aqueous humor outflow (18 µl/h) (Mermoud *et al.*, 1996; Toris, 2008). This suggests that these compounds are mainly eliminated via the anterior route, but access of the compounds to the aqueous humor is limited by the vitreous, iris-ciliary body and lens. Small molecules, capable of permeating through the blood retina barrier, are eliminated posteriorly (Hosoya *et al.*, 2010). For example, the clearance of fluorescein was faster than the aqueous humor outflow in rats (CL=33 µl/h; outflow 18 µl/h) and rabbits (CL=273 µl/h; outflow 180 µl/h) indicating significant transretinal clearance.

Based on our results, the apparent volume of distribution was in the range of anatomical values in both rats and rabbits. The shorter vitreal residence time in the rats, as compared to the rabbits, could be explained based on a smaller vitreal volume in rats (≈ 0.05 ml) than in rabbits (≈ 1.7 ml). A larger apparent volume of distribution prolongs the half-life of elimination ($t_{1/2}$ = ln 2 x V/CL). On the other hand, vitreal clearance of rabbits is higher than in rats, because rabbits have a larger surface area of blood-ocular barriers, higher diffusional area in the vitreous and faster aqueous humor outflow than the corresponding value in rats. Similar trends were seen in a SPECT/CT imaging study investigating intravitreal elimination in mice; these animals had shorter half-lives and smaller clearance values than rabbits (del Amo *et al.*, 2015; Schmitt *et al.*, 2019).

We report here the first scaling factors for rat-to-rabbit translation. The dose-scaling factors indicate that 2-5 times higher doses of macromolecules (mw. ≈ 10 to 1000 kDa) should be used in rabbits to achieve similar vitreal drug exposure (AUC). For small drug-like molecules, the scaling factor is about 8. A scaling factor of 1.4 has been reported for rabbit-to-man translation (del Amo *et al.*, 2015). Thus, we estimate that the scaling factor of dose for rat-to-man translation is in a range of 3-7. Due to the size difference between the eyes, the scaling factors for rat-to-rabbit translation are smaller than those for the following translations mouse-to-rabbit (≈ 84) and mouse-to-man (≈ 118) (Schmitt *et al.*, 2019).

## 6.3 Drug-peptide conjugates and nonlinear vitreal pharmacokinetics

Intravitreal kinetics of two fluorescently labeled peptides were evaluated by means of fluorophotometry. These two peptides were conjugated to dexamethasone via an acid-sensitive hydrazone bond that is expected to release dexamethasone in the intracellular space. The peptides contained cell penetrating sequences which increase their permeability to the retinal cells. Previously, it was shown that these peptides can release drug cargo in the RPE cells (Bhattacharya *et al.*, 2017). The peptides have cationic residues in their sequence to increase binding to hyaluronic acid, which is an anionic polymer and the main component in the vitreous (Kleinberg *et al.*, 2011). Both peptides with molecular weights of around 4 kDa had almost similar elimination half-lives which is around one day. If we compare the kinetics of these two peptides conjugates in the Maurice graph (Figure 15), we can see that both of the peptides had values close to the line which supports the anterior elimination route from the rabbit eyes. Moreover, it seems that the vitreal elimination of Dex-1 and Dex-2 was similar to that of macromolecules like dextran, which has almost the same diffusion constant in water and vitreous (Missel, Horner and Muralikrishnan, 2010). This will raise one question i.e. Dex-2 shows high affinity for binding to vitreous, but the *in vivo*

kinetics by using *in vivo* fluorophotometry reveals that there is a lack of effective vitreal affinity.

Based on in vitro binding to porcine vitreous with MST, it is possible to estimate peptide pharmacokinetics for bound and free peptide fractions. The free fraction can be estimated with the following equation (Talevi and Quiroga, 2018):

Eq.2 $$C_{tot} = C_{free} + \frac{B_m \times C_{free}}{K_d + C_{free}}$$

In the equation, $C_{tot}$ and $C_{free}$ are total and free peptide concentrations, respectively. $B_m$ is the maximum capacity of the tissue for peptide binding and $K_d$ is equilibrium dissociation constant. Based on the MST results, $B_m$ of porcine vitreous for Dex-2 peptide is 100 nM and $K_d$ is 13.5 nM.

When the drug concentration is much higher than the maximum binding capacity of the tissue, most of the binding sites are saturated and nonlinear pharmacokinetics will become possible. In this case, the elimination rate constant and half-life will be concentration dependent. Coffey et al. (Coffey, Bullock and Schoenemann, 1971; Coffey, 1972) introduced an apparent elimination constant for such a case (Eq.3).

Eq.3 $$K_{app} = \frac{K_f \, C_{free}}{C_{tot}}$$

They assumed that the elimination process operated only on the free fraction of drug. In equation 3, $K_{app}$ is the apparent elimination constant. $K_f$ is the elimination rate constant for free drug fraction, whereas $C_{tot}$ and $C_{free}$ are the bound and free concentrations of the drug, respectively. This equation reveals that the elimination rate constant and elimination half-life for a compound with significant binding affinity will become dose dependent.

Since the amount of peptide was not enough to perform a concentration-signal calibration, we had to estimate the concentrations of Dex2 peptide in

the vitreous based on some assumptions. If we consider the average anatomical volume of rabbit vitreous (1700 µl (Missel, 2012) ), after intravitreal injection of 40 µl of peptide solution, about a 42.5 times dilution would take place in the vitreous. Considering the concentration of injected Dex-2 solution (0.125 mM), we then estimated the initial concentration of peptide ($C_0$) as 3000 nM. During the follow-up time of 3 days post-injection, the range of peptide concentration in the vitreous should be 700-3000 nM, when its half-life of elimination is about one day. Thus, these levels are much higher than the maximum binding capacity of porcine vitreous (100 nM). Moreover, as the elimination of Dex-2 from rabbit vitreous displays a dependency on molecular size (Maurice plot, Figure 15), the elimination seems to be governed by the unbound peptide fraction.

At lower concentrations, the fraction of bound peptide will increase substantially (Figure 18A). For example, at a total peptide concentration of 100 nM in the vitreous, about 62 % of the drug would be in the bound form, leading to an elimination half-life of ≈60 hours (Figure 18C). When the total concentration is much higher than the saturation concentration (100 nM), the half-life of elimination will be ≈24 hours; this matches the experimental value *in vivo*. Thus, we conclude that the observed elimination half-life in the rabbit vitreous originate mostly from unbound Dex-2 peptide. In principle, the elimination half-life of the bound fraction could be longer and non-linear kinetics would be detected at low concentrations.

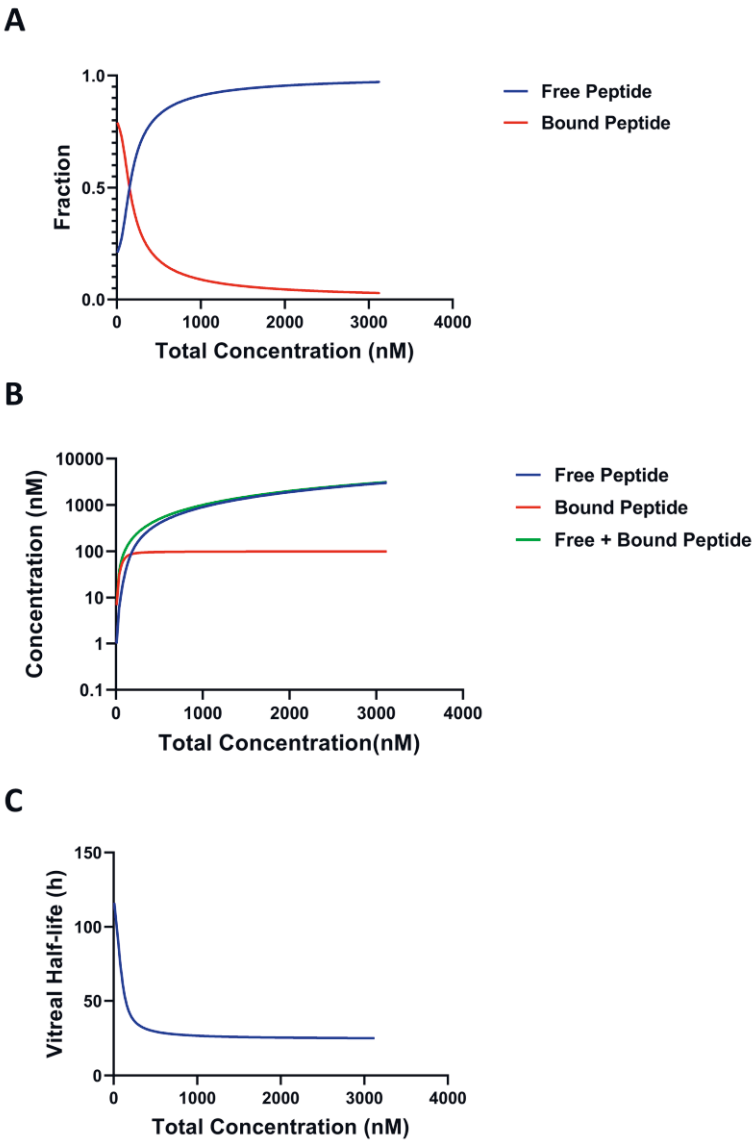


**Figure 18.** A) Bound and free fraction of peptides Dex-2 to hyaluronic acid versus different concentration. B) Free, bound and total concentration of peptides vs total peptide concentration. C) Theoretical vitreal elimination half-life of Dex-2 considering the vitreal affinity and apparent elimination rate constant.

## 6.4 Intravitreal kinetics of nanomaterials

### *Factors affecting vitreal kinetics of nanomaterials*

In this study, we evaluated intravitreal kinetics of nanomaterials. We demonstrated long intravitreal retention of >10 days and 65 days for small liposomes (≈ 50 nm) and polymeric micelles (spherical ≈ 40 nm; longitudinal ≈ 90 nm), respectively, in the rat eyes. Unexpectedly, larger liposomes (≈ 100 and 250 nm) and polymersomes (spherical 300 nm; tubular 180 nm) had shorter retention times in the rats' eyes (< 10 days), even though another polymersome formulation had a half-life of ≈ 30 days in rabbits' eyes (Junnuthula *et al.*, 2021). Since large liposomes (> 1 µm) remained for >20 days in the rats' eyes, we conclude that small nanoparticles (< 100 nm) and large ones (> 1 µm) are preferred for prolonged vitreal retention. However, the relationship between particle size and vitreal retention is complicated due to confounding variables, such as charge interactions, particle disintegration and aggregation (Pitkänen *et al.*, 2003; Bochot and Fattal, 2012; Huang and Chau, 2019a). In previous reports, similar (Sakurai *et al.*, 2001) and opposite (Kim *et al.*, 2020) trends have been presented for the relationship between particle size and vitreal retention.

Vitreal retention of 50 nm liposomes was longer in rabbits (> 30 days) than in rats (> 10 days), which is in line with studies with intravitreal soluble molecules in mice (Schmitt *et al.*, 2019) and rats (chapter 5.2). The literature on vitreal retention of intravitreally injected nanoparticle embedded drugs shows a wide range of values in the rat and rabbit eyes as the half-lives range from 0.25 to 78 days (Peyman *et al.*, 1987; Alghadyan *et al.*, 1988; Mezei and Meisner, 1993; Zeng *et al.*, 1993; Sakurai *et al.*, 2001; Claro *et al.*, 2009; Kim *et al.*, 2020). This reflects differences in the size, charge, drug release as well as other possible factors. We detected the presence of the particles, not the drug that may have been released before the particles were eliminated from the vitreous. In addition, the use of covalently bound fluorescent labels in the polymeric nanoparticles and fluorescent lipids in the liposomes minimized the risk of non-covalent release of the labels.

The shape of fluorophotometric scans showed a gradient of concentrations with higher values close to retina. This may be due to anterior elimination of liposomes and convective flow (Araie and Maurice, 1991; Smith, Lee and Gardiner, 2020). The anterior route of elimination can lead to the kinds of concentration gradients in the vitreous demonstrated by Araie et al. (Araie and Maurice, 1991), who showed that there were vitreal gradients for eliminating dextrans through the anterior pathway.

***Retinal permeability of nanomaterials***

Small particles (≈ 50 nm) may permeate to the retina across the inner limiting membrane (ILM), whereas particles of 100 nm and larger diameters do not permeate to the retina in bovine eyes with proper ILM barrier (Tavakoli, Peynshaert, *et al.*, 2020). Potentially misleading and easier retinal permeation of particles has been seen in the rodent eyes with thinner and leaky ILM (Lee *et al.*, 2017). A prolonged vitreal retention of small liposomes and polymeric micelles will improve the chances of retinal permeation as they are capable of diffusing both in the vitreous and ILM (Lee *et al.*, 2017; Tavakoli, Kari, *et al.*, 2020; Tavakoli, Peynshaert, *et al.*, 2020). Such formulations may be optimized for retinal drug targeting. On the other hand, very large liposomes are larger than the mesh size of the vitreous (≈ 550 nm) (Peeters *et al.*, 2005; Xu *et al.*, 2013). These kinds of particles are retained for a long time at the injection site and could be suitable for the controlled release of the drugs to the vitreous, but not for particle mediated delivery into the retina.

Pullulan-dexamethasone nanoparticles (mean diameter 219 nm) showed an accumulation on the surface of ILM. The size distribution is also an important factor, since in the case of average particle size with a large polydispersity, the fraction of smaller particles could permeate into the retina. Interestingly, some of the pullulan conjugate seemed to be taken up into the Müller cells in the retinal explant cultures and transported within these cells deeper into the retina. However, it is still unclear if the particles

can escape from the cells into other parts of the retina. This phenomenon was not seen in the isolated bovine retinas, where pullulan conjugates localized to the ILM and some ganglion cells. It may be possible to target some nanomaterials to certain retinal cell types, but this aspect needs further investigation.

***Accumulation of particles in optics nerve head***

Based on the fundus images, we observed an accumulation of 50 nm liposomes in the optic nerve head region of the rabbits' eyes. Smith et al (Smith, Lee and Gardiner, 2020) recently published a review article on the possible fluid flow from the anterior chamber to the posterior part of the eye. They estimated that a considerable fraction of the aqueous humor may flow to the vitreous and subsequently being eliminated via the transretinal route. This flow may contribute to the higher levels of liposomes in the posterior vitreous and at the optic nerve head in the rabbit eyes. Accumulation in the optic nerve head is in line with our previous report (Junnuthula *et al.*, 2021). Interestingly, this kind of accumulation was not seen in healthy rat eyes, but some optic nerve accumulation was detected in the case of the polymersomes containing endotoxin. In the case of pullulan-Dex particles, we did not observe a gradient of concentration in the vitreous or accumulation in the optic nerve of rats or rabbits. The data suggests that optic nerve accumulation depends on the type of nanomaterial administered.

Optic nerve accumulation may be useful for therapeutic targeting to the optic nerve (e.g. in glaucoma) (Lavik, Kuehn and Kwon, 2011; DeBusk and Moster, 2018), but it may potentially lead also to unwanted effects or toxicity. It has been claimed that optic nerve accumulation is less significant in monkeys and humans than in rabbits (Hayreh, 1965), but this hypothesis has not been proven in humans.

### *Elimination route of intravitreal nanomaterials*

It has been proposed that there is anterior elimination of intravitreally injected materials (via aqueous humor outflow to the Schlemm's canal), and elimination to the conjunctival lymphatics as well as posterior elimination across the blood retina barrier (Camelo *et al.*, 2007; del Amo *et al.*, 2017). The anterior route is considered to be more likely than the posterior route, because the posterior pathway is quantitatively significant only in the elimination of small soluble molecules, capable of permeating across the retinal pigment epithelium and the endothelial of the retinal capillaries (Del Amo *et al.*, 2015). The diffusion in the vitreous has been established as the critical factor in the anterior elimination of intravitreal biologicals (Hutton-Smith *et al.*, 2016) and simulations based on this assumption predict perfectly their vitreal and aqueous humor concentration profiles (Rimpelä *et al.*, 2018). Hutton-Smith et al. (Hutton-Smith *et al.*, 2016) used the same principles and stated that the vitreal elimination of large protein molecules depended on anatomical factors and the diffusion coefficient of drug in the vitreous.

Although the anterior elimination of intravitreal liposomes has been suggested previously (Barza *et al.*, 1987), we quantitatively prove here for the first time that intravitreal liposomes are removed mainly (or only) via the anterior route in rabbits. This conclusion was reached by using a combination of *in vivo* experiments and kinetic simulations. We determined vitreal clearance of liposomes and then assumed that the entire clearance would represent anterior elimination, and furthermore that liposomes were eliminated from anterior chamber solely at a known rate of aqueous humor outflow. The simulated liposome concentrations in the aqueous humor matched the experimental values demonstrating anterior elimination of intravitreal liposomes. This result does not provide any support for the proposal that either posterior or conjunctival elimination routes would be important. Moreover, a comparison of the kinetic parameters of liposomes with dextran in the Maurice plot provides support for the predominant role of the anterior elimination route. We performed similar simulations and

comparisons for pullulan-Dex nanoparticles. Again, it does seem that most of the elimination took place anteriorly.

***Pharmacokinetic considerations for designing intravitreal drug designing nanomaterials***

Unfortunately, there are no published studies investigating the free drug concentrations in the vitreous after intravitreal delivery of particulate drug delivery systems. Furthermore, no publications have reported the simultaneous residence of both particle material and drug in the vitreous. Most publications show levels of total drug in the vitreous (Alghadyan *et al.*, 1988; Assil *et al.*, 1991; Bourlaist *et al.*, 1996; Gupta *et al.*, 2000), even though only released drug is active pharmacologically. In order to estimate the interplay of the drug release rate and ocular residence of nanoparticles, we performed simulations at three hypothetical rates of dexamethasone release and one drug loading level in liposomes. We demonstrated that the ideal drug delivery requires the synchronization of drug release and vitreal retention of the nanoparticles. Too slow drug release may lead to the ocular elimination of a major part of the drug dose in an encapsulated form, resulting in sub-optimal ocular bioavailability of free drug, whereas too fast release may lead to premature drug release, short action and the non-productive residence of empty nanoparticles in the eye. Our simulation models provide tools for drug development, since *in vitro* drug release rates, pharmacokinetics of free drug and retention of the particles can be incorporated into the model as parameters.

A similar simulation for pullulan nanoparticles was performed using the in vitro drug release rate and *in vivo* kinetics of labeled particles. In the simulations, *in vivo* dexamethasone release was assumed to be similar as in the experimentally determined in vitro release. Of course, *in vitro*/*in vivo* correlations are not simple and in many cases there are biological factors that might affect drug release *in vivo*. In the case of pullulan-Dex, the elimination rate of particles from vitreous (half-life ≈ 60 h) was much faster than the drug release rate (half-life ≈ 500 h). In this case, most of

dexamethasone dose would be eliminated from the eye before being released from the particles. This formulation is a good example which shows the importance of synchronizing the drug release and particle elimination in order to have efficient and prolonged drug retinal drug delivery. Basically, vitreal retention of pullulan-Dex formulation should be clearly longer to match its slow drug release kinetics otherwise, the full benefit from the injected drug dose would not be achieved.

***Role of endotoxin***

Unlike liposomes and polymeric micelles, the polymersome (spherical and tubular) samples contained endotoxin levels that were above the limits set by FDA for intraocular formulations (U.S. Food and Drug Administration, 2015). Intravitreal endotoxins may cause inflammation in the eye (Bantseev *et al.*, 2018). Despite the importance of endotoxins, most of the published literature on intravitreal nanomaterials have not described the performance of any endotoxin tests (Fishman, Peyman and Lesar, 1986; Peyman *et al.*, 1987, 1988; Zeng *et al.*, 1993; Gupta *et al.*, 2000; Bochot *et al.*, 2002; Merodio *et al.*, 2002; Kawakami *et al.*, 2004; Xu *et al.*, 2007; Zhang *et al.*, 2009; Honda *et al.*, 2011; Koo *et al.*, 2012; Lu *et al.*, 2014; Huang and Chau, 2019b; Delrish *et al.*, 2021). Therefore, the validity of those studies could be questioned. Our results indicate that endotoxin contamination may accelerate the removal of polymersomes from the rat vitreous: retention of polymersomes in this study was ≈ 8 days in rat vitreous, whereas another polymersome formulation with a similar particle size was retained in rabbit vitreous for as long as 4 months (Junnuthula *et al.*, 2021). Apparently, the increased rate of nanoparticle elimination may be due to the infiltration of phagocytic cells. For example, McGahan et.al (McGahan and Fleisher, 1992) detected a high level of vitreal neutrophilic activity 24 hours after intravitreal injection of endotoxin in the eyes of rabbits. Furthermore, the elimination of endotoxin contaminated nanoparticles might be increased due to the induced inflammation as shown previously (Barza *et al.*, 1987). Our data addresses the importance of including endotoxin controls in the preclinical pharmacokinetic studies of intravitreal drug formulations. Thus, testing for

the presence of endotoxin in the trial formulations is essential to guarantee the reliability of the results.

# 7. CONCLUSIONS

Non-invasive techniques were useful in preclinical intravitreal pharmacokinetic studies. They made it possible for the following conclusions to be drawn:

1. Phosphorescence dyes with a minimal overlap with the natural ocular autofluorescence and large Stoke shift improve the quality of the *in vivo* luminescent imaging of labelled compounds.

2. Intravitreal retention of macromolecules is shorter in rats than in rabbits. In order to achieve a similar drug exposure, 2-5 times higher intravitreal doses are needed in rabbits than in rats.

3. Vitreous binding of compounds may lead to non-linear intravitreal pharmacokinetics. Thus, the elimination rate constant in the vitreous may be affected by the number of binding sites, affinity for binding to vitreal components and the concentration of the test compound.

4. Increasing particle size does not always prolong the retention of nanomaterials in the vitreous.

5. In rabbits, intravitreally injected dexamethasone pullulan conjugates and liposomes are mainly eliminated through the anterior chamber.

6. Endotoxin contamination significantly accelerates vitreal elimination of nanomaterials. Most of the publications regarding intravitreal nanoformulations lack the endotoxin assessments prior to *in vivo* experiments.

7. Intravitreal nanoparticles show uneven distribution patterns, with higher values occurring posteriorly near the retina.

8. Intravitreally injected nanomaterials accumulate at detectable levels in the region of the optic nerve head in rabbit eyes.

9. In order to achieve effective drug delivery and good bioavailability in the retina, drug release and particle elimination should be synchronized.

# 8. FUTURE PERSPECTIVES

In this study, we showed potential applicability of phosphorescence dyes in following and monitoring vitreal distribution and retention of liposomes. Duration of this study was short, just demonstrating the concept. In the future, it would be useful to follow pharmacokinetics of the labelled liposomes and morphology of retina for longer times to better understand usefulness of phosphorescence labels as reporters of vitreal pharmacokinetics. Also, it is important to study the safety aspects of these labels in longer experiments. Moreover, by using suitable instrument and phosphorescent lifetime measurements it should be possible to quantify additional *in vivo* parameters, such as vitreal oxygen levels and pH, with phosphorescence probes. Thus, these dyes might be useful compounds for non-invasive monitoring of ocular physiology and pathology.

In the current study on intravitreal pharmacokinetics, we investigated dose scaling between rats and rabbits by using FITC-dextran and fluorescein as model substances for small and large molecules. Although the molecular size is a main factor that determines the vitreal elimination half-life of macromolecules, labelled antibodies (e.g bevacizumab), Fab-fragments (e.g. ranibizumab) or soluble receptors (e.g., aflibercept) could also be investigated with this approach in rats and rabbits. For the measurements, the protein drugs should be labelled with a fluorescent probe at suitable levels that will provide adequate signals for *in vivo* fluorophotometry, but not changing significantly the physico-chemical properties of the compounds. Such studies would be an interesting part in building understanding between pharmacokinetics and pharmacodynamics of anti-VEGF biologicals.

In order to understand the observed *in vivo* retention time of the studied peptide in the rabbit vitreous, we introduced a kinetic model for non-linear vitreal pharmacokinetics. Vitreal binding affinity was a key factor in the model. *In vitro* binding studies were done with porcine vitreous that differs from rabbit vitreous in terms of hyaluronic acid content. Determination of binding affinity to rabbit vitreous would provide valuable data for *in vitro* to

*in vivo* translation. Moreover, it will be interesting to study compounds with different vitreal binding affinities to validate the model. Binding studies and modelling may be useful tools in the development of molecular conjugates with controlled vitreal retention.

During our projects, we have occasionally obtained nanomaterials with endotoxin trace contamination. Such contamination may originate from the starting materials or from the manufacturing processes (incl. production, purification). Published literature on intravitreal drug administration either lacks endotoxin tests or they are not mentioned in the reports. However, this is an important issue, because endotoxin traces may induct inflammation and alter pharmacokinetics of injected materials. Improved understanding on the biological mechanisms of pharmacokinetic alteration is needed. Also, this aspect should be strongly presented in the scientific literature so that endotoxins would be monitored properly in the investigations.

Our pharmacokinetic modelling of free drug concentrations in the eye was based on the rates of *in vitro* drug release. Assumption of identical drug release rates *in vitro* and *in vivo* may not be valid. Different *in vitro* and *in vivo* release rates have been observed in some unpublished experiments of our laboratory. Differences between *in vitro* and *in vivo* release rates may be due to different interactions of nanomaterials with *in vivo* vitreous and *in vitro* release medium. Differences in mixing conditions and clearance of released drug may also cause deviations in drug release. Thus, improved *in vitro* release methods and *in vivo* data on drug release are needed. Determination of *in vivo* release rate of drug from intravitreal nanomaterials is challenging. Released drug should be analysed separately from the drug that is still incorporated to the nanomaterial. *In vivo* intravitreal microdialysis may be applicable technique that would allow estimation of the free drug concentration in the vitreous. Thereafter, assuming that clearance of free drug from vitreous has been determined, modelling would allow determination of *in vivo* release rate from the nanomaterials. More invasive approach of obtain vitreous at different times post-injection, separate the fractions of free and encapsulated drug, and determine drug contents in these fractions. Currently, there are hardly any published experimental data

on intravitreal drug release *in vivo.* Although such experiments can be technically challenging, the obtained data would be beneficial for scientific understanding and ocular drug development.

# REFERENCES


Agarwal, A. (2008) *Fundus fluorescein and indocyanine green angiography: a textbook and atlas*. SLACK incorporated.

Alghadyan, A. A. *et al.* (1988) 'Liposome-bound cyclosporine: clearance after intravitreal injection', *International ophthalmology*. Springer, 12(2), pp. 109–112.

Alm, A. and Bill, A. (1973) 'Ocular and optic nerve blood flow at normal and increased intraocular pressures in monkeys (Macaca irus): a study with radioactively labelled microspheres including flow determinations in brain and some other tissues', *Experimental eye research*. Elsevier, 15(1), pp. 15–29.

del Amo, E. M. *et al.* (2015) 'Rabbit as an animal model for intravitreal pharmacokinetics: Clinical predictability and quality of the published data', *Experimental Eye Research*. Elsevier, 137(February), pp. 111–124. doi: 10.1016/j.exer.2015.05.003.

del Amo, E. M. *et al.* (2017) 'Pharmacokinetic aspects of retinal drug delivery', *Progress in Retinal and Eye Research*. Elsevier, 57(2017), pp. 134–185. doi: 10.1016/j.preteyeres.2016.12.001.

Del Amo, E. M. *et al.* (2015) 'Intravitreal clearance and volume of distribution of compounds in rabbits: In silico prediction and pharmacokinetic simulations for drug development', *European Journal of Pharmaceutics and Biopharmaceutics*. Elsevier, 95(Pt B), pp. 215–226. doi: 10.1016/j.ejpb.2015.01.003.

Araie, M. and Maurice, D. M. (1991) 'The loss of fluorescein, fluorescein glucuronide and fluorescein isothiocyanate dextran from the vitreous by the anterior and retinal pathways', *Experimental eye research*. Elsevier, 52(1), pp. 27–39.

Assil, K. K. *et al.* (1991) 'Liposome suppression of proliferative vitreoretinopathy. Rabbit model using antimetabolite encapsulated liposomes.', *Investigative ophthalmology & visual science*. The Association for Research in Vision and Ophthalmology, 32(11), pp. 2891–2897.

Bakri, S. J. *et al.* (2007a) 'Pharmacokinetics of Intravitreal Bevacizumab ( Avastin )', pp. 855–859. doi: 10.1016/j.ophtha.2007.01.017.

Bakri, S. J. *et al.* (2007b) 'Pharmacokinetics of Intravitreal Ranibizumab ( Lucentis )', pp. 2179–2182. doi: 10.1016/j.ophtha.2007.09.012.

Bantseev, V. *et al.* (2018) 'Determination of a No-Observable Effect Level for Endotoxin Following a Single Intravitreal Administration to Dutch Belted Rabbits', *Investigative ophthalmology & visual science*. The Association for Research in Vision and Ophthalmology, 58(3), pp. 1545–1552. doi: 10.1167/iovs.16-21356.

Barza, M. *et al.* (1985) 'Ocular toxicity of intravitreally injected liposomal amphotericin B in rhesus monkeys', *American journal of ophthalmology*. Elsevier, 100(2), pp. 259–263.

Barza, M. *et al.* (1987) 'Effect of size and lipid composition on the pharmacokinetics of intravitreal liposomes.', *Investigative ophthalmology & visual*

*science*. The Association for Research in Vision and Ophthalmology, 28(5), pp. 893–900.

Van Best, J. A. *et al.* (1985) 'In vivo assessment of lens transmission for blue-green light by autofluorescence measurement', *Ophthalmic research*. Karger Publishers, 17(2), pp. 90–95.

Bhattacharya, M. *et al.* (2017) 'Differentially cleaving peptides as a strategy for controlled drug release in human retinal pigment epithelial cells', *Journal of Controlled Release*, 251, pp. 37–48.

Bito, L. Z. and Salvador, E. V. (1972) 'Intraocular fluid dynamics. III. The site and mechanism of prostaglandin transfer across the blood intraocular fluid barriers', *Experimental eye research*. Elsevier, 14(3), pp. 233–241. doi: 10.1016/0014-4835(72)90008-5.

Blazaki, S. *et al.* (2020) 'Novel Liposome Aggregate Platform (LAP) system for sustained retention of drugs in the posterior ocular segment following intravitreal injection', *International journal of pharmaceutics*. Elsevier, 576, p. 118987.

Bleeker, J. C. *et al.* (1986) 'Autofluorescence of the lens in diabetic and healthy subjects by fluorophotometry.', *Investigative ophthalmology & visual science*. The Association for Research in Vision and Ophthalmology, 27(5), pp. 791–794.

Bochot, A. *et al.* (2002) 'Intravitreal delivery of oligonucleotides by sterically stabilized liposomes', *Investigative ophthalmology & visual science*. The Association for Research in Vision and Ophthalmology, 43(1), pp. 253–259.

Bochot, A. and Fattal, E. (2012) 'Liposomes for intravitreal drug delivery: a state of the art', *Journal of Controlled Release*. Elsevier, 161(2), pp. 628–634. doi: 10.1016/j.jconrel.2012.01.019.

Bourlaist, C. Le *et al.* (1996) 'Release kinetics of liposome-encapsulated ganciclovir after intravitreal injection in rabbits', *Journal of microencapsulation*. Taylor & Francis, 13(4), pp. 473–480.

Boyer, D. S. *et al.* (2014) 'Three-year, randomized, sham-controlled trial of dexamethasone intravitreal implant in patients with diabetic macular edema', *Ophthalmology*. Elsevier, 121(10), pp. 1904–1914.

Brubaker, R. F. (1991) 'Flow of aqueous humor in humans [The Friedenwald Lecture].', *Investigative ophthalmology & visual science*, 32(13), pp. 3145–66. Available at: http://www.ncbi.nlm.nih.gov/pubmed/1748546.

Camelo, S. *et al.* (2007) 'Ocular and systemic bio-distribution of rhodamine-conjugated liposomes loaded with VIP injected into the vitreous of Lewis rats', *Molecular vision*. Emory University, 13, p. 2263.

Chang-Lin, J.-E. *et al.* (2011) 'Pharmacokinetics and pharmacodynamics of a sustained-release dexamethasone intravitreal implant', *Investigative ophthalmology & visual science*. The Association for Research in Vision and Ophthalmology, 52(1), pp. 80–86. doi: 10.1167/iovs.10-5285.

Chang, B. *et al.* (2005) 'Mouse models of ocular diseases', *Visual neuroscience*. Cambridge University Press, 22(5), pp. 587–593.

Chelushkin, P. S. *et al.* (2022) 'Phosphorescent NIR emitters for biomedicine:

applications, advances and challenges', *Dalton Transactions*. Royal Society of Chemistry.

Chemla, Y. *et al.* (2019) 'Gold nanoparticles for multimodal high-resolution imaging of transplanted cells for retinal replacement therapy', *Nanomedicine*. Future Medicine, 14(14), pp. 1857–1871.

Cheng, L. *et al.* (2011) 'Intraocular pharmacokinetics of a crystalline lipid prodrug, octadecyloxyethyl-cyclic-cidofovir, for cytomegalovirus retinitis', *Journal of ocular pharmacology and therapeutics*. Mary Ann Liebert, Inc. 140 Huguenot Street, 3rd Floor New Rochelle, NY 10801 USA, 27(2), pp. 157–162.

Christoforidis, J. B. *et al.* (2012) 'Intravitreal devices for the treatment of vitreous inflammation', *Mediators of inflammation*. Hindawi, 2012.

Civan, M. M. (1997) 'Transport components of net secretion of the aqueous humor and their integrated regulation', in *Current topics in membranes*. Elsevier, pp. 1–24.

Claro, C. *et al.* (2009) 'Determination and pharmacokinetic profile of liposomal foscarnet in rabbit ocular tissues after intravitreal administration', 88, pp. 528–534. doi: 10.1016/j.exer.2008.11.015.

Coffey, J. J. (1972) 'Effects of protein binding of drugs on areas under plasma concentration—time curves', *Journal of pharmaceutical sciences*. Elsevier, 61(1), pp. 138–139.

Coffey, J. J., Bullock, F. J. and Schoenemann, P. T. (1971) 'Numerical solution of nonlinear pharmacokinetic equations: effects of plasma protein binding on drug distribution and elimination', *Journal of pharmaceutical sciences*. Elsevier, 60(11), pp. 1623–1628.

Conrad, J. M. and Robinsonx, J. R. (1977) 'Aqueous Chamber Drug Distribution Volume Measurement in Rabbits', 66(2).

Crowell, S. R. *et al.* (2019) 'Influence of charge, hydrophobicity, and size on vitreous pharmacokinetics of large molecules', *Translational vision science & technology*. The Association for Research in Vision and Ophthalmology, 8(6), p. 1.

DeBusk, A. and Moster, M. L. (2018) 'Gene therapy in optic nerve disease', *Current opinion in ophthalmology*. Wolters Kluwer, 29(3), pp. 234–238.

Delori, F. C. *et al.* (1995) 'In vivo fluorescence of the ocular fundus exhibits retinal pigment epithelium lipofuscin characteristics.', *Investigative ophthalmology & visual science*. The Association for Research in Vision and Ophthalmology, 36(3), pp. 718–729.

Delrish, E. *et al.* (2021) 'Efficacy of topotecan nanoparticles for intravitreal chemotherapy of retinoblastoma', *Experimental Eye Research*. Elsevier, 204, p. 108423.

Dickmann, L. J. *et al.* (2015) 'Evaluation of fluorophotometry to assess the vitreal pharmacokinetics of protein therapeutics', *Investigative Ophthalmology and Visual Science*. The Association for Research in Vision and Ophthalmology, 56(11), pp. 6991–6999. doi: 10.1167/iovs.15-17457.

Do, D. V, Rhoades, W. and Nguyen, Q. D. (2020) 'Pharmacokinetic study of

intravitreal aflibercept in humans with neovascular age-related macular degeneration', *Retina*. LWW, 40(4), pp. 643–647.

Docchio, F. (1989) 'Ocular fluorometry: principles, fluorophores, instrumentation, and clinical applications', *Lasers in surgery and medicine*. Wiley Online Library, 9(6), pp. 515–532.

Durairaj, C. (2017) 'Ocular pharmacokinetics', in *Handbook of Experimental Pharmacology*. Springer, pp. 31–55. doi: 10.1007/164_2016_32.

Dysli, C. *et al.* (2017) 'Fluorescence lifetime imaging ophthalmoscopy', *Progress in retinal and eye research*. Elsevier, 60, pp. 120–143.

East, N. and Group, R. (2012) 'Treatment protocol for the use of Ozurdex ® ( dexamethasone intravitreal implant ) in the management of uveitis', (February), pp. 1–2.

Eblimit, A. *et al.* (2021) 'Co-Injection of Sulfotyrosine Facilitates Retinal Uptake of Hyaluronic Acid Nanospheres Following Intravitreal Injection', *Pharmaceutics*. Multidisciplinary Digital Publishing Institute, 13(9), p. 1510.

Ehlers, J. P. *et al.* (2014) 'Visualisation of contrast-enhanced intraoperative optical coherence tomography with indocyanine green', *British journal of ophthalmology*. BMJ Publishing Group Ltd, 98(11), pp. 1588–1591. doi: 10.1136/bjophthalmol-2014-305295.

Eldred, G. E. and Katz, M. L. (1988) 'Fluorophores of the human retinal pigment epithelium: separation and spectral characterization', *Experimental eye research*. Elsevier, 47(1), pp. 71–86.

Eva, M. *et al.* (2015) 'European Journal of Pharmaceutics and Biopharmaceutics Intravitreal clearance and volume of distribution of compounds in rabbits : In silico prediction and pharmacokinetic simulations for drug development', *European Journal of Pharmaceutics and Biopharmaceutics*. Elsevier B.V., 95(January), pp. 215–226. doi: 10.1016/j.ejpb.2015.01.003.

Fagan, X. J. and Al-Qureshi, S. (2013) 'Intravitreal injections: a review of the evidence for best practice', *Clinical & experimental ophthalmology*. Wiley Online Library, 41(5), pp. 500–507.

Fayyaz, A. *et al.* (2019) 'Ocular intracameral pharmacokinetics for a cocktail of timolol, betaxolol, and atenolol in rabbits', *Molecular pharmaceutics*. ACS Publications, 17(2), pp. 588–594.

Fercher, A. F. *et al.* (1993) 'In vivo optical coherence tomography', *American journal of ophthalmology*, 116(1), pp. 113–114.

Ffytche, T. J. *et al.* (1980) 'Indications for fluorescein angiography in disease of the ocular fundus: a review', *Journal of the Royal Society of Medicine*. SAGE Publications Sage UK: London, England, 73(5), pp. 362–365.

Fishman, P. H., Peyman, G. A. and Lesar, T. (1986) 'Intravitreal liposome-encapsulated gentamicin in a rabbit model. Prolonged therapeutic levels.', *Investigative ophthalmology & visual science*. The Association for Research in Vision and Ophthalmology, 27(7), pp. 1103–1106.

Friedrich, S., Cheng, Y.-L. and Saville, B. (1997) 'Drug distribution in the vitreous

humor of the human eye: the effects of intravitreal injection position and volume', *Current eye research*. Taylor & Francis, 16(7), pp. 663–669.

Fuchs, H. and Igney, F. (2017) 'Binding to ocular albumin as a half-life extension principle for intravitreally injected drugs: evidence from mechanistic rat and rabbit studies', *Journal of Ocular Pharmacology and Therapeutics*. Mary Ann Liebert, Inc. 140 Huguenot Street, 3rd Floor New Rochelle, NY 10801 USA, 33(2), pp. 115–122. doi: 10.1089/jop.2016.0083.

Gabriele, M. L. *et al.* (2011) 'Optical coherence tomography: history, current status, and laboratory work', *Investigative ophthalmology & visual science*. The Association for Research in Vision and Ophthalmology, 52(5), pp. 2425–2436.

Gadkar, K. *et al.* (2015) 'Design and pharmacokinetic characterization of novel antibody formats for ocular therapeutics', *Investigative ophthalmology & visual science*. The Association for Research in Vision and Ophthalmology, 56(9), pp. 5390–5400.

Gan, I. M. *et al.* (2005) 'Effect of intravitreal dexamethasone on vitreous vancomycin concentrations in patients with suspected postoperative bacterial endophthalmitis', *Graefe's Archive for Clinical and Experimental Ophthalmology*. Springer, 243(11), pp. 1186–1189.

García-Quintanilla, L. *et al.* (2019) 'Pharmacokinetics of intravitreal anti-VEGF drugs in age-related macular degeneration', *Pharmaceutics*. Multidisciplinary Digital Publishing Institute, 11(8), p. 365.

Ghosn, M. G. *et al.* (2008) 'Differential permeability rate and percent clearing of glucose in different regions in rabbit sclera', *Journal of biomedical optics*. International Society for Optics and Photonics, 13(2), p. 21110.

Ghosn, M. G., Tuchin, V. V. and Larin, K. V. (2007) 'Nondestructive quantification of analyte diffusion in cornea and sclera using optical coherence tomography', *Investigative Ophthalmology and Visual Science*, 48(6), pp. 2726–2733. doi: 10.1167/iovs.06-1331.

Goel, M. *et al.* (2010) 'Aqueous humor dynamics: a review', *The open ophthalmology journal*. Bentham Science Publishers, 4, p. 52.

Le Goff, M. M. and Bishop, P. N. (2008) 'Adult vitreous structure and postnatal changes', *Eye*. Nature Publishing Group, 22(10), pp. 1214–1222.

Grossniklaus, H. E., Kang, S. J. and Berglin, L. (2010) 'Animal models of choroidal and retinal neovascularization', *Progress in retinal and eye research*. Elsevier, 29(6), pp. 500–519.

Group, E. S. (2002) 'Preclinical and phase 1A clinical evaluation of an anti-VEGF pegylated aptamer (EYE001) for the treatment of exudative age-related macular degeneration', *Retina*. LWW, 22(2), pp. 143–152.

Grzybowski, A. *et al.* (2018) '2018 update on intravitreal injections: Euretina expert consensus recommendations', *Ophthalmologica*. Karger Publishers, 239(4), pp. 181–193.

Gupta, S. K. *et al.* (2000) 'Intravitreal pharmacokinetics of plain and liposome-entrapped fluconazole in rabbit eyes', *Journal of ocular pharmacology and*

*therapeutics*, 16(6), pp. 511–518.

Hayreh, S. S. (1965) 'Pathogenesis of Oedema of the Optic Disc (papilloedema).' University College London (University of London).

Hee, M. R. *et al.* (1995) 'Optical coherence tomography of the human retina', *Archives of ophthalmology*. American Medical Association, 113(3), pp. 325–332.

Herrero-Vanrell, R. (2011) 'Microparticles as drug delivery systems for the back of the eye', in *Drug product development for the back of the eye*. Springer, pp. 231–259.

Hochheimer, B. F. (1971) 'Angiography of the retina with indocyanine green', *Archives of ophthalmology*. American Medical Association, 86(5), pp. 564–565.

Hochheimer, B. F. and D'Anna, S. A. (1978) 'Angiography with new dyes', *Experimental eye research*. Elsevier, 27(1), pp. 1–16.

Holz, F. *et al.* (2007) *Atlas of fundus autofluorscence imaging*. Springer.

Honda, M. *et al.* (2011) 'Suppression of choroidal neovascularization by intravitreal injection of liposomal SU5416', *Archives of Ophthalmology*. American Medical Association, 129(3), pp. 317–321.

Hosoya, K. *et al.* (2010) 'Lipophilicity and transporter influence on blood-retinal barrier permeability: a comparison with blood-brain barrier permeability', *Pharmaceutical research*. Springer, 27(12), pp. 2715–2724.

Huang, D. *et al.* (1991) 'Optical coherence tomography', *science*. American Association for the Advancement of Science, 254(5035), pp. 1178–1181.

Huang, X. and Chau, Y. (2019a) 'Intravitreal nanoparticles for retinal delivery', *Drug Discovery Today*. doi: 10.1016/j.drudis.2019.05.005.

Huang, X. and Chau, Y. (2019b) 'Investigating impacts of surface charge on intraocular distribution of intravitreal lipid nanoparticles', *Experimental eye research*. Elsevier, 186, p. 107711.

Hutton-Smith, L. A. *et al.* (2016) 'A mechanistic model of the intravitreal pharmacokinetics of large molecules and the pharmacodynamic suppression of ocular vascular endothelial growth factor levels by ranibizumab in patients with neovascular age-related macular degeneration', *Molecular Pharmaceutics*. ACS Publications, 13(9), pp. 2941–2950. doi: 10.1021/acs.molpharmaceut.5b00849.

Hutton-Smith, L. A. *et al.* (2017) 'Ocular pharmacokinetics of therapeutic antibodies given by intravitreal injection: estimation of retinal permeabilities using a 3-compartment semi-mechanistic model', *Molecular pharmaceutics*. ACS Publications, 14(8), pp. 2690–2696. doi: 10.1021/acs.molpharmaceut.7b00164.

Ilochonwu, B. C. *et al.* (2020) 'Intravitreal hydrogels for sustained release of therapeutic proteins', *Journal of Controlled Release*. Elsevier.

Jager, R. D. *et al.* (2004) 'Risks of intravitreous injection: a comprehensive review', *Retina*. LWW, 24(5), pp. 676–698.

Järvinen, K., Järvinen, T. and Urtti, A. (1995) 'Ocular absorption following topical delivery', *Advanced drug delivery reviews*. Elsevier, 16(1), pp. 3–19.

Jiang, Y. and Pu, K. (2021) 'Molecular Probes for Autofluorescence-Free Optical Imaging', *Chemical Reviews*. ACS Publications.

Johnson, F. and Maurice, D. (1984) 'A simple method of measuring aqueous

humor flow with intravitreal fluoresceinated dextrans', *Experimental eye research*. Elsevier, 39(6), pp. 791–805.

Jones, D. P. *et al.* (1979) 'Ophthalmic fluorophotometry: an improved slit-lamp fluorophotometer', *Medical and Biological Engineering and Computing*. Springer, 17(3), pp. 365–370.

Junnuthula, V. *et al.* (2021) 'Intravitreal Polymeric Nanocarriers with Long Ocular Retention and Targeted Delivery to the Retina and Optic Nerve Head Region', *Pharmaceutics*. Multidisciplinary Digital Publishing Institute, 13(4), p. 445.

Kawakami, S. *et al.* (2004) 'In vivo gene transfection via intravitreal injection of cationic liposome/plasmid DNA complexes in rabbits', *International Journal of Pharmaceutics*, 278(2), pp. 255–262. doi: 10.1016/j.ijpharm.2004.03.013.

Keahey, P. *et al.* (2021) 'Spectral-and Polarization-Dependent Scattering of Gold Nanobipyramids for Exogenous Contrast in Optical Coherence Tomography', *Nano Letters*. ACS Publications.

Keilhauer, C. N. and Delori, F. C. (2006) 'Near-infrared autofluorescence imaging of the fundus: visualization of ocular melanin', *Investigative ophthalmology & visual science*. The Association for Research in Vision and Ophthalmology, 47(8), pp. 3556–3564.

Kellner, U., Kellner, S. and Weinitz, S. (2010) 'Fundus autofluorescence (488 NM) and near-infrared autofluorescence (787 NM) visualize different retinal pigment epithelium alterations in patients with age-related macular degeneration', *Retina*. LWW, 30(1), pp. 6–15.

Kim, H. M. *et al.* (2020) 'Intraocular distribution and kinetics of intravitreally injected antibodies and nanoparticles in rabbit eyes', *Translational vision science & technology*. The Association for Research in Vision and Ophthalmology, 9(6), p. 20.

Kleinberg, T. T. *et al.* (2011) 'Vitreous substitutes: a comprehensive review', *Survey of ophthalmology*. Elsevier, 56(4), pp. 300–323.

Kompella, U. B. *et al.* (2013) 'Nanomedicines for back of the eye drug delivery, gene delivery, and imaging', *Progress in Retinal and Eye Research*. Pergamon, 36, pp. 172–198. doi: 10.1016/J.PRETEYERES.2013.04.001.

Koo, H. *et al.* (2012) 'The movement of self-assembled amphiphilic polymeric nanoparticles in the vitreous and retina after intravitreal injection', *Biomaterials*. Elsevier, 33(12), pp. 3485–3493. doi: 10.1016/j.biomaterials.2012.01.030.

Kottegoda, S. *et al.* (2007) 'Demonstration and use of nanoliter sampling of in vivo rat vitreous and vitreoretinal interface', *Mol Vis*, 13, pp. 2073–2082.

Krebs, M. P. *et al.* (2017) 'Mouse models of human ocular disease for translational research', *PLoS One*. Public Library of Science San Francisco, CA USA, 12(8), p. e0183837.

Krohne, T. I. M. U. *et al.* (2008) 'Intraocular pharmacokinetics of bevacizumab after a single intravitreal injection in humans', *American journal of ophthalmology*. Elsevier, 146(4), pp. 508–512. doi: 10.1016/j.ajo.2008.05.036.

Krohne, T. U. *et al.* (2012) 'Intraocular pharmacokinetics of ranibizumab following a single intravitreal injection in humans', *American journal of ophthalmology*. Elsevier,

154(4), pp. 682–686.

Krupin, T. *et al.* (1982) 'Fluorometric Studies on the Blood-Retinal Barrier in Experimental Animals', *Archives of Ophthalmology*, 100(4), pp. 631–634. doi: 10.1001/archopht.1982.01030030633021.

Kwak, H. W. and D'Amico, D. J. (1992) 'Evaluation of the Retinal Toxicity and Pharmacokinetics of Dexamethasone After Intravitreal Injection', *Archives of Ophthalmology*. American Medical Association, 110(2), p. 259. doi: 10.1001/archopht.1992.01080140115038.

Langham, M. and Wybar, K. C. (1954) 'FLUOROPHOTOMETRIC APPARATUS FOR TIE OBJECTIVE DETERMINATION OF FLUORESCENCE IN TIE ANTERIOR CHAMBER OF THE LIVING EYE *', pp. 52–57.

Larin, K. V *et al.* (2011) 'Optical clearing for OCT image enhancement and in-depth monitoring of molecular diffusion', *IEEE journal of selected topics in quantum electronics*. IEEE, 18(3), pp. 1244–1259.

Laurent, U. B. G. and Fraser, J. R. E. (1983) 'Turnover of hyaluronate in the aqueous humour and vitreous body of the rabbit', *Experimental eye research*. Elsevier, 36(4), pp. 493–503.

Lavik, E., Kuehn, M. H. and Kwon, Y. H. (2011) 'Novel drug delivery systems for glaucoma', *Eye*. Nature Publishing Group, 25(5), pp. 578–586.

Lee, J. *et al.* (2017) 'Effective retinal penetration of lipophilic and lipid-conjugated hydrophilic agents delivered by engineered liposomes', *Molecular pharmaceutics*. ACS Publications, 14(2), pp. 423–430.

Lee, S. S. *et al.* (2010) 'Biodegradable implants for sustained drug release in the eye', *Pharmaceutical research*. Springer, 27(10), pp. 2043–2053. doi: 10.1007/s11095-010-0159-x.

Lee, T. M. *et al.* (2003) 'Engineered microsphere contrast agents for optical coherence tomography', *Optics letters*. Optical Society of America, 28(17), pp. 1546–1548. doi: 10.1364/ol.28.001546.

Lee, T. W.-Y. and Robinson, J. R. (2004) 'Drug delivery to the posterior segment of the eye II: development and validation of a simple pharmacokinetic model for subconjunctival injection', *Journal of ocular pharmacology and therapeutics*. Mary Ann Liebert, Inc., 20(1), pp. 43–53.

LEOPOLD, I. H. (1945) 'Intravitreal penetration of penicillin and penicillin therapy of infections of the vitreous', *Archives of Ophthalmology*. American Medical Association, 33(3), pp. 211–216.

Littlewood, R. *et al.* (2019) 'The utility of fundus fluorescein angiography in neuro-ophthalmology', *Neuro-Ophthalmology*. Taylor & Francis, 43(4), pp. 217–234.

Lu, Y. *et al.* (2014) 'Effect of intravitreal injection of bevacizumab-chitosan nanoparticles on retina of diabetic rats', *International journal of ophthalmology*. Press of International Journal of Ophthalmology, 7(1), p. 1.

Lund-Andersen, H. *et al.* (1985) 'Quantitative vitreous fluorophotometry applying a mathematical model of the eye', *Investigative Ophthalmology and Visual Science*, 26(5), pp. 698–710.

Marmorstein, A. D. *et al.* (2002) 'Spectral profiling of autofluorescence associated with lipofuscin, Bruch's membrane, and sub-RPE deposits in normal and AMD eyes', *Investigative ophthalmology & visual science*. The Association for Research in Vision and Ophthalmology, 43(7), pp. 2435–2441.

Maurice, D. (2003) 'Review: Practical Issues in Intravitreal Drug Delivery', *Journal of Ocular Pharmacology and Therapeutics*, 17(4), pp. 393–401. doi: 10.1089/108076801753162807.

Maurice, D. M. (1959) 'Protein dynamics in the eye studied with labelled proteins', *American journal of ophthalmology*. Elsevier, 47(1), pp. 361–368.

Maurice, D. M. (1963) 'A new objective fluorophotometer', *Experimental eye research*. Elsevier, 2(1), pp. 33-IN5.

Maurice, D. M. (1987) 'Kinetics of topically applied ophthalmic drugs', in *Ophthalmic Drug Delivery*. Springer, pp. 19–26.

Maurice, D. M. *et al.* (1990) 'Fluorometry of the anterior segment', in *Noninvasive diagnostic techniques in ophthalmology*. Springer, pp. 248–280.

Maurice, D. M. (2002) 'Drug delivery to the posterior segment from drops', *Survey of ophthalmology*. Elsevier, 47, pp. S41–S52.

Maurice, D. M. and Mishima, S. (1984) 'Ocular pharmacokinetics', in *Pharmacology of the Eye*. Springer, pp. 19–116.

Mayhew, T. M. and Astle, D. (1997) 'Photoreceptor number and outer segment disk membrane surface area in the retina of the rat: stereological data for whole organ and average photoreceptor cell', *Journal of neurocytology*. Springer, 26(1), pp. 53–61.

McGahan, M. C. and Fleisher, L. N. (1992) 'Cellular response to intravitreal injection of endotoxin and xanthine oxidase in rabbits', *Graefe's archive for clinical and experimental ophthalmology*. Springer, 230(5), pp. 463–467.

Mermoud, A. *et al.* (1996) 'Aqueous humor dynamics in rats', pp. 198–203.

Merodio, M. *et al.* (2002) 'Ocular disposition and tolerance of ganciclovir-loaded albumin nanoparticles after intravitreal injection in rats', 23, pp. 1587–1594.

Mezei, M. and Meisner, D. (1993) 'Liposomes and nanoparticles as ocular drug delivery systems', *Biopharmaceutics of Ocular Drug Delivery*. CRC Press Boca Raton, FL, pp. 91–101.

Mishima, S. *et al.* (1966) 'Determination of tear volume and tear flow', *Investigative Ophthalmology & Visual Science*. The Association for Research in Vision and Ophthalmology, 5(3), pp. 264–276.

Missel, P. J. (2012) 'Simulating intravitreal injections in anatomically accurate models for rabbit, monkey, and human eyes', *Pharmaceutical research*. Springer, 29(12), pp. 3251–3272. doi: 10.1007/s11095-012-0721-9.

Missel, P. J., Horner, M. and Muralikrishnan, R. (2010) 'Simulating dissolution of intravitreal triamcinolone acetonide suspensions in an anatomically accurate rabbit eye model', *Pharmaceutical research*. Springer, 27(8), pp. 1530–1546.

Montezuma, S. R., Vavvas, D. and Miller, J. W. (2009) 'Review of the ocular angiogenesis animal models', in *Seminars in ophthalmology*. Taylor & Francis, pp. 52–

61.

Morrison, J. C., Johnson, E. and Cepurna, W. O. (2008) 'Rat models for glaucoma research', *Progress in brain research*. Elsevier, 173, pp. 285–301.

Munnerlyn, C. R., Gray, J. R. and Hennings, D. R. (1985) 'Design considerations for a fluorophotometer for ocular research', *Graefe's Archive for Clinical and Experimental Ophthalmology*. Springer, 222(4), pp. 209–211.

Nair, A. B. and Jacob, S. (2016) 'A simple practice guide for dose conversion between animals and human', *Journal of basic and clinical pharmacy*. Wolters Kluwer--Medknow Publications, 7(2), p. 27.

Nicholson, B. P. and Schachat, A. P. (2010) 'A review of clinical trials of anti-VEGF agents for diabetic retinopathy', *Graefe's Archive for Clinical and Experimental Ophthalmology*. Springer, 248(7), pp. 915–930.

Nilsson, S. F. E. and Alm, A. (2012) 'Determination of ocular blood flows with the microsphere method', in *Ocular blood flow*. Springer, pp. 25–47.

Olsen, T. W. *et al.* (2004) 'Fluorescein angiographic lesion type frequency in neovascular age-related macular degeneration', *Ophthalmology*. Elsevier, 111(2), pp. 250–255.

Panda-Jonas, S. *et al.* (1994) 'Retinal photoreceptor count, retinal surface area, and optic disc size in normal human eyes', *Ophthalmology*. Elsevier, 101(3), pp. 519–523.

Papkovsky, D. B. and Dmitriev, R. I. (2013) 'Biological detection by optical oxygen sensing', *Chemical Society Reviews*. Royal Society of Chemistry, 42(22), pp. 8700–8732.

Park, S. J. *et al.* (2016) 'Intraocular pharmacokinetics of intravitreal aflibercept (Eylea) in a rabbit model', *Investigative ophthalmology & visual science*. The Association for Research in Vision and Ophthalmology, 57(6), pp. 2612–2617.

Peeters, L. *et al.* (2005) 'Vitreous: A barrier to nonviral ocular gene therapy', *Investigative Ophthalmology and Visual Science*, 46(10), pp. 3553–3561. doi: 10.1167/iovs.05-0165.

Peyman, G. A. *et al.* (1987) 'Intravitreal injection of liposome-encapsulated ganciclovir in a rabbit model.', *Retina (Philadelphia, Pa.)*, 7(4), pp. 227–229.

Peyman, G. A. *et al.* (1988) 'Intravitreal liposome-encapsulated drugs: a preliminary human report', *International ophthalmology*. Springer, 12(3), pp. 175–182.

Peyman, G. A., Lad, E. M. and Moshfeghi, D. M. (2009) 'Intravitreal injection of therapeutic agents', *Retina*. LWW, 29(7), pp. 875–912.

Pitkänen, L. *et al.* (2003) 'Vitreous is a barrier in nonviral gene transfer by cationic lipids and polymers', *Pharmaceutical research*. Springer, 20(4), pp. 576–583.

Polansky, J. R. and Weinreb, R. N. (1984) 'Anti-inflammatory agents', in *Pharmacology of the Eye*. Springer, pp. 459–538.

del Pozo-Rodríguez, A. *et al.* (2013) 'Lipid nanoparticles as drug/gene delivery systems to the retina', *Journal of ocular pharmacology and therapeutics*. Mary Ann Liebert, Inc. 140 Huguenot Street, 3rd Floor New Rochelle, NY 10801 USA, 29(2), pp. 173–188.

Puliafito, C. A. *et al.* (1995) 'Imaging of macular diseases with optical coherence tomography', *Ophthalmology*. Elsevier, 102(2), pp. 217–229.

Raines, M. F. (1988) 'Vitreous fluorophotometry: a review', *Journal of the Royal Society of Medicine*. SAGE Publications Sage UK: London, England, 81(7), pp. 403–406.

Ramsay, E. *et al.* (2018) 'Corneal and conjunctival drug permeability: Systematic comparison and pharmacokinetic impact in the eye', *European Journal of Pharmaceutical Sciences*. Elsevier, 119, pp. 83–89.

Reichenbach, A. *et al.* (1994) 'Development of the rabbit retina. V. The question of "columnar units"', *Developmental brain research*. Elsevier, 79(1), pp. 72–84.

Remtulla, S. and Hallett, P. E. (1985) 'A schematic eye for the mouse, and comparisons with the rat', *Vision Research*, 25(1), pp. 21–31. doi: 10.1016/0042-6989(85)90076-8.

Ridolfo, R. *et al.* (2020) 'Exploring the impact of morphology on the properties of biodegradable nanoparticles and their diffusion in complex biological medium', *Biomacromolecules*. ACS Publications.

Rimpelä, A.-K. *et al.* (2018) 'Binding of small molecule drugs to porcine vitreous humor', *Molecular pharmaceutics*. ACS Publications, 15(6), pp. 2174–2179.

Rimpelä, A.-K., Cui, Y. and Sauer, A. (2021) 'Mechanistic Model for the Prediction of Small-Molecule Vitreal Clearance Combining Diffusion-Limited and Permeability-Limited Clearance', *Molecular Pharmaceutics*. ACS Publications.

Rimpelä, A. *et al.* (2018) 'Pharmacokinetic Simulations of Intravitreal Biologicals : Aspects of Drug Delivery to the Posterior and Anterior Segments', pp. 9–11. doi: 10.3390/pharmaceutics11010009.

Rimpelä, A. *et al.* (2019) 'Pharmacokinetic simulations of intravitreal biologicals: aspects of drug delivery to the posterior and anterior segments', *Pharmaceutics*. Multidisciplinary Digital Publishing Institute, 11(1), p. 9. doi: 10.3390/pharmaceutics11010009.

Robinson, M. R. *et al.* (2002) 'Safety and pharmacokinetics of intravitreal 2-methoxyestradiol implants in normal rabbit and pharmacodynamics in a rat model of choroidal neovascularization', *Experimental eye research*. Elsevier, 74(2), pp. 309–317. doi: 10.1006/exer.2001.1132.

del Rosal, B. and Benayas, A. (2018) 'Strategies to overcome autofluorescence in nanoprobe-driven in vivo fluorescence imaging', *Small Methods*. Wiley Online Library, 2(9), p. 1800075.

Rovati, L. L. and Docchio, F. (2004) 'Autofluorescence methods in ophthalmology', *Journal of Biomedical Optics*. International Society for Optics and Photonics, 9(1), pp. 9–22.

Saincher, S. S. and Gottlieb, C. (2020) 'Ozurdex (dexamethasone intravitreal implant) for the treatment of intermediate, posterior, and panuveitis: a systematic review of the current evidence', *Journal of ophthalmic inflammation and infection*. Springer, 10(1), pp. 1–10.

Sakurai, E. *et al.* (2001) 'Effect of particle size of polymeric nanospheres on intravitreal kinetics', *Ophthalmic research*. Karger Publishers, 33(1), pp. 31–36.

Sampat, K. M. and Garg, S. J. (2010) 'Complications of intravitreal injections', *Current opinion in ophthalmology*. LWW, 21(3), pp. 178–183. doi: 10.1097/ICU.0b013e328338679a.

Sanford, M. (2013) 'Fluocinolone acetonide intravitreal implant (Iluvien®)', *Drugs*. Springer, 73(2), pp. 187–193.

Schmitt, J. M. (1999) 'Optical coherence tomography (OCT): a review', *IEEE Journal of selected topics in quantum electronics*. IEEE, 5(4), pp. 1205–1215.

Schmitt, M. *et al.* (2019) 'Intravitreal Pharmacokinetics in Mice: SPECT/CT Imaging and Scaling to Rabbits and Humans', *Molecular pharmaceutics*. ACS Publications, 16(10), pp. 4399–4404.

Schmitt, W. (2017) 'Estimation of Intra-vitreal Half-Lifes in the Rabbit Eye with Semi-mechanistic Equations', *Pharmaceutical Research*. Pharmaceutical Research, pp. 49–57. doi: 10.1007/s11095-016-2037-7.

Schmitz-Valckenberg, S. *et al.* (2008) 'Fundus autofluorescence imaging: review and perspectives', *Retina*. LWW, 28(3), pp. 385–409.

Sebag, J. (1987) 'Ageing of the vitreous', *Eye*. Nature Publishing Group, 1(2), pp. 254–262.

Sebag, J. *et al.* (1994) 'Effects of pentoxifylline on choroidal blood flow in nonproliferative diabetic retinopathy', *Angiology*. Sage Publications Sage CA: Thousand Oaks, CA, 45(6), pp. 429–433.

Sha, O. and Kwong, W. H. (2006) 'Postnatal developmental changes of vitreous and lens volumes in Sprague-Dawley rats', *Neuroembryology and Aging*. Karger Publishers, 4(4), pp. 183–188.

Shah, M. *et al.* (2019) 'Translational Preclinical Pharmacologic Disease Models for Ophthalmic Drug Development', *Pharmaceutical research*. Springer, 36(4), p. 58.

Shahidi, M. *et al.* (2010) 'Retinal tissue oxygen tension imaging in the rat', *Investigative ophthalmology & visual science*. The Association for Research in Vision and Ophthalmology, 51(9), pp. 4766–4770.

Shatz, W. *et al.* (2016) 'Contribution of Antibody Hydrodynamic Size to Vitreal Clearance Revealed through Rabbit Studies Using a Species-Matched Fab'. doi: 10.1021/acs.molpharmaceut.6b00345.

Shih, Y.-Y. I. *et al.* (2013) 'Quantitative retinal and choroidal blood flow during light, dark adaptation and flicker light stimulation in rats using fluorescent microspheres', *Current eye research*. Taylor & Francis, 38(2), pp. 292–298.

SHOEMAKER, R. E. (1949) 'Intravitreal use of streptomycin', *Archives of Ophthalmology*. American Medical Association, 41(5), pp. 629–632.

Short, B. G. (2008) 'Safety evaluation of ocular drug delivery formulations: techniques and practical considerations', *Toxicologic pathology*. Sage Publications, 36(1), pp. 49–62.

Sinapis, C. I. *et al.* (2011) 'Pharmacokinetics of intravitreal bevacizumab (Avastin®) in rabbits', *Clinical Ophthalmology (Auckland, NZ)*. Dove Press, 5, p. 697.

Skondra, D. *et al.* (2012) 'Near infrared autofluorescence imaging of retinal diseases', in *Seminars in ophthalmology*. Taylor & Francis, pp. 202–208.

Smith, D. W., Lee, C.-J. and Gardiner, B. S. (2020) 'No flow through the vitreous humor: How strong is the evidence?', *Progress in retinal and eye research*. Elsevier, p. 100845.

Smith, P. (1889) 'Erasmus Wilson Lectures on the Pathology of Glaucoma', *British medical journal*. BMJ Publishing Group, 1(1475), p. 759.

Snyder, R. W. and Glasser, D. B. (1994) 'Antibiotic therapy for ocular infection.', *Western journal of medicine*. BMJ Publishing Group, 161(6), p. 579.

Song, H. B. *et al.* (2017) 'Intraocular application of gold nanodisks optically tuned for optical coherence tomography: inhibitory effect on retinal neovascularization without unbearable toxicity', *Nanomedicine: Nanotechnology, Biology, and Medicine*. Elsevier Inc., 13(6), pp. 1901–1911. doi: 10.1016/j.nano.2017.03.016.

Spaide, R. F. (2007) 'Autofluorescence from the outer retina and subretinal space', *Atlas of fundus autofluorescence imaging*. Springer, pp. 241–311.

Talevi, A. and Quiroga, P. A. M. (2018) *ADME Processes in Pharmaceutical Sciences: Dosage, Design, and Pharmacotherapy Success*. Springer.

Tavakoli, S., Kari, O. K., *et al.* (2020) 'Diffusion and Protein Corona Formation of Lipid-Based Nanoparticles in the Vitreous Humor: Profiling and Pharmacokinetic Considerations', *Molecular Pharmaceutics*. ACS Publications.

Tavakoli, S., Peynshaert, K., *et al.* (2020) 'Ocular barriers to retinal delivery of intravitreal liposomes: Impact of vitreoretinal interface', *Journal of Controlled Release*. Elsevier.

Tavakoli, S. *et al.* (2022) 'Liposomal sunitinib for ocular drug delivery: A potential treatment for choroidal neovascularization', *International Journal of Pharmaceutics*. Elsevier, 620, p. 121725.

Toris, C. B. (2008) 'Aqueous humor dynamics I: measurement methods and animal studies', *Current Topics in Membranes*. Elsevier, 62(08), pp. 193–229. doi: 10.1016/S1063-5823(08)00407-9.

Tremblay, C. *et al.* (1985) 'Reduced toxicity of liposome-associated amphotericin B injected intravitreally in rabbits.', *Investigative ophthalmology & visual science*. The Association for Research in Vision and Ophthalmology, 26(5), pp. 711–718.

U.S. Food and Drug Administration (2015) 'Endotoxin testing recommendations for single-use intraocular ophthalmic devices - Guidance for industry and Food and Drug Administration staff'.

Urtti, A. (2006) 'Challenges and obstacles of ocular pharmacokinetics and drug delivery', *Advanced Drug Delivery Reviews*, 58(11), pp. 1131–1135. doi: 10.1016/j.addr.2006.07.027.

Ussery III, F. M. *et al.* (1988) 'Intravitreal ganciclovir in the treatment of AIDS-associated cytomegalovirus retinitis', *Ophthalmology*. Elsevier, 95(5), pp. 640–648.

Vieira, R., Sousa-Pinto, B. and Figueira, L. (2020) 'Efficacy and safety of corticosteroid implants in non-infectious uveitis: a systematic review with network meta-analysis', *Ocular Immunology and Inflammation*. Taylor & Francis, pp. 1–8.

Waltman, S. R. and Kaufman, H. E. (1970) 'A new objective slit lamp fluorophotometer', *Investigative Ophthalmology & Visual Science*. The Association for

Research in Vision and Ophthalmology, 9(4), pp. 247–249.

Wheeler, J. R. (1946) 'History of ophthalmology through the ages', *The British journal of ophthalmology*. BMJ Publishing Group, 30(5), p. 264.

Wilson, D. F. *et al.* (2006) 'Imaging oxygen pressure in the rodent retina by phosphorescence lifetime', in *Oxygen transport to tissue XXVII*. Springer, pp. 119–124.

Xu, J. *et al.* (2007) 'Inhibitory efficacy of intravitreal dexamethasone acetate-loaded PLGA nanoparticles on choroidal neovascularization in a laser-induced rat model', *Journal of ocular pharmacology and therapeutics*. Mary Ann Liebert, Inc. 2 Madison Avenue Larchmont, NY 10538 USA, 23(6), pp. 527–540.

Xu, Q. *et al.* (2013) 'Nanoparticle diffusion in, and microrheology of, the bovine vitreous ex vivo', *Journal of controlled release*. Elsevier, 167(1), pp. 76–84.

Xu, Q. *et al.* (2020) 'Monitoring the topical delivery of ultrasmall gold nanoparticles using optical coherence tomography', *Skin Research and Technology*. Wiley Online Library, 26(2), pp. 263–268.

Yang, C. (2005) 'Molecular Contrast Optical Coherence Tomography: A Review¶', *Photochemistry and Photobiology*. Wiley Online Library, 81(2), pp. 215–237.

Yannuzzi, L. A. *et al.* (2004) 'Ophthalmic fundus imaging: today and beyond', *American journal of ophthalmology*. Elsevier, 137(3), pp. 511–524.

Yazdani, M. *et al.* (2019) 'Tear metabolomics in dry eye disease: a review', *International journal of molecular sciences*. Multidisciplinary Digital Publishing Institute, 20(15), p. 3755.

Yellepeddi, V. K. and Palakurthi, S. (2016) 'Recent advances in topical ocular drug delivery', *Journal of Ocular Pharmacology and Therapeutics*. Mary Ann Liebert, Inc. 140 Huguenot Street, 3rd Floor New Rochelle, NY 10801 USA, 32(2), pp. 67–82.

Yuan, S. *et al.* (2009) 'Co-registered optical coherence tomography and fluorescence molecular imaging for simultaneous morphological and molecular imaging', *Physics in Medicine & Biology*. IOP Publishing, 55(1), p. 191.

Zeimer, R. C. (1990) 'Assessment of Posterior Segment Transport by Vitreous Fluorophotometry', in *Noninvasive Diagnostic Techniques in Ophthalmology*. Springer, pp. 366–389.

Zeng, S. *et al.* (1993) 'Intravitreal pharmacokinetics of liposome-encapsulated amikacin in a rabbit model', *Ophthalmology*. Elsevier, 100(11), pp. 1640–1644. doi: 10.1016/S0161-6420(93)31423-5.

Zhang, L. *et al.* (2009) 'Pharmacokinetics and tolerance study of intravitreal injection of dexamethasone-loaded nanoparticles in rabbits', pp. 175–183.

Zhou, X. *et al.* (2021) 'Rescue the retina after the ischemic injury by polymer-mediated intracellular superoxide dismutase delivery', *Biomaterials*. Elsevier, 268, p. 120600.

Zhu, Q. *et al.* (2008) 'Vitreous levels of bevacizumab and vascular endothelial growth factor-A in patients with choroidal neovascularization', *Ophthalmology*. Elsevier, 115(10), pp. 1750–1755.

Zimmer, A. K. *et al.* (1994) 'Hydrocortisone delivery to healthy and inflamed eyes using a micellar polysorbate 80 solution or albumin nanoparticles', *International*

*journal of pharmaceutics*. Elsevier, 110(3), pp. 211–222.

# Appendix

# Publication I

RSC Advances

PAPER

View Article Online
View Journal | View Issue



Cite this: *RSC Adv.*, 2020, **10**, 14431

# Design and synthesis of lipid-mimetic cationic iridium complexes and their liposomal formulation for *in vitro* and *in vivo* application in luminescent bioimaging†

Julia R. Shakirova,[a] Amir Sadeghi,[b] Alla A. Koblova,[a] Pavel S. Chelushkin,[a] Elisa Toropainen,[b] Shirin Tavakoli,[c] Leena-Stiina Kontturi,[c] Tatu Lajunen,[cd] Sergey P. Tunik*[a] and Arto Urtti*[abc]

Two iridium $[Ir(N^C)_2(N^N)]^+$ complexes with the diimine N^N ligand containing a long polymethylene hydrophobic chain were synthesized and characterized by using NMR and ESI mass-spectrometry: N^N – 2-(1-hexadecyl-1*H*-imidazol-2-yl)pyridine, N^C – methyl-2-phenylquinoline-4-carboxylate (**Ir1**) and 2-phenylquinoline-4-carboxylic acid (**Ir2**). These complexes were used to prepare the luminescent PEGylated DPPC liposomes (DPPC/DSPE-PEG2000/Ir-complex = 95/4.5/1 mol%) using a thin film hydration method. The narrowly dispersed liposomes had diameters of about 110 nm. The photophysics of the complexes and labeled liposomes were carefully studied. **Ir1** and **Ir2** give red emission ($\lambda_{em}$ = 667 and 605 nm) with a lifetime in the microsecond domain and quantum yields of 4.8% and 10.0% in degassed solution. Incorporation of the complexes into the liposome lipid bilayer results in shielding of the emitters from interaction with molecular oxygen and partial suppression of excited state nonradiative relaxation due to the effect of the relatively rigid bilayer matrix. Delivery of labeled liposomes to the cultured ARPE-19 cells demonstrated the usefulness of **Ir1** and **Ir2** in cellular imaging. Labeled liposomes were then injected intravitreally into rat eyes and imaged successfully with optical coherence tomography and funduscopy. In conclusion, iridium complexes enabled the successful labeling and imaging of liposomes in cells and animals.

Received 5th February 2020
Accepted 30th March 2020

DOI: 10.1039/d0ra01114b

rsc.li/rsc-advances

## Introduction

During the last decades liposomes have been actively studied as basic models of lipid bilayers and as carrier structures in diagnostics and drug delivery.[1] Liposomes are versatile nanostructures that can be prepared with different sizes (from 40 nm to micrometer scale), lipid wall properties (rigid or fluid state) and surface functionalities (*e.g.* PEGylation for prolonged circulation times, antibodies for targeting).[2–8] Liposomal delivery of small molecule and biomacromolecule drugs has been widely studied for many medical applications. The advantages of liposomes include their safety profile, solubility in physiological media, possibilities for controlled and induced drug release, and relatively easy surface vectorization for targeted delivery of encapsulated drug molecules.[9,10]

Targeting of drug carrier into the target cells and tissues can be visualized non-invasively with luminescent labels and radioactive probes. In most imaging experiments, the liposomes were labelled with fluorescent dyes.[11–16] The fluorescent markers display high emission intensity and they are commercially available, but these emitters show small Stokes shifts, short lifetimes and often suffer of photobleaching. These deficiencies may result in lower image resolution in luminescent microscopy and also limit the use of fluorophores in long-term experiments. On the contrary, phosphorescent emitters based on transition metal complexes display large Stokes shifts, long life-times and negligible photobleaching. Thus, phosphorescence labels are an attractive, but not widely studied, alternative to imaging of diagnostic and therapeutic nanocarriers.

Previously, phosphorescent polypyridyl ruthenium[17–20] and orthometalated iridium[17,21–25] complexes have been used for labeling of liposomes. Incorporation of the phosphorescent labels into liposomes can be carried out using intrinsic hydrophobicity of the ligand,[17–19,21,24,25] thereby targeting the label into

[a]*St. Petersburg State University, Institute of Chemistry, Universitetskii pr., 26, 198504 St. Petersburg, Russia. E-mail: sergey.tunik@spbu.ru*

[b]*School of Pharmacy, Faculty of Health Sciences, University of Eastern Finland, Yliopistonranta 1C, 70211 Kuopio, Finland. E-mail: arto.urtti@uef.fi*

[c]*Drug Research Program, Faculty of Pharmacy, University of Helsinki, Viikinkaari 5 E, 00710 Helsinki, Finland*

[d]*Laboratory of Pharmaceutical Technology, Department of Pharmaceutical Science, Tokyo University of Pharmacy & Life Sciences, 1432-1 Hachioji 192-0392, Tokyo, Japan*

† Electronic supplementary information (ESI) available. See DOI: 10.1039/d0ra01114b

inner lipid layer of the liposome membrane. Alternatively, the ligand can be designed as amphiphilic moiety resembling the components of the target membrane.[17,19,21,23] The first approach is based on the affinity of the labels to hydrophobic tails of the phospholipids, whereas the latter approach mimics the structural patterns of phospholipids allowing predictable localization to the liposomal membrane.

Two recent publications[24,25] introduce liposome based drug delivery systems with loaded iridium complexes. These liposome formulations included iridium compounds as active components for cancer therapy and PEGylated long circulating liposomes were used for iridium complex delivery.[26–29] In addition, the luminescent iridium complexes enabled visualization of the liposome localization *in vitro* in the cells. The results prompted us to investigate similar systems for potential applicability in ophthalmology as there is a need for long acting and targeted delivery of drugs for retinal treatment.[30,31]

In the present communication we describe synthesis of amphiphilic luminescent iridium complexes, which contain hydrophobic aliphatic tails and relatively hydrophilic (polar and charged) metal containing head group. These compounds were incorporated into PEGylated liposomes and the formulations were tested in *in vitro* and *in vivo*. We demonstrate the usefulness of these phosphorescent labels in imaging of liposomes in the cells and in the eye *in vivo*. The structure and photophysical properties of the complexes and labeled liposomes are presented and discussed.

## Experimental

### General comments

Solvents were used as received. Solution $^1$H, $^1$H–$^1$H COSY, NOESY NMR spectra were recorded using a Bruker Avance 400 and AMX-400 spectrometers. Mass spectra were measured on a Bruker maXis II ESI-QTOF instrument in the ESI$^+$ mode. Microanalyses were carried out in the analytical laboratory of the University of Eastern Finland. The bis(μ-chlorido) bridged dimeric precursor {(**N^C–COOMe**)$_2$IrCl}$_2$ (N^C–COOMe = methyl 2-phenylquinoline-4-carboxylate) were synthesized according to published procedures.[32] Methyl 2-phenylquinoline-4-carboxylate, 1,2-dipalmitoyl-*sn*-glycero-3-phosphocholine (DPPC) and 1,2-distearoyl-*sn*-glycero-3-phosphoethanolamine-*N*-[methoxy(polyethylene glycol)-2000] (DSPE-PEG2000) were purchased from Sigma-Aldrich (St. Louis, MO, USA). HEPES buffer solution contained 20 mM HEPES and 140 mM NaCl in MilliQ purified water and the pH was adjusted to 7.4 with NaOH. Calcein solution had 60 mM of calcein and 29 mM of NaCl in MilliQ purified water and the pH was set to 7.4 with NaOH.

### Synthesis of the diimine N^N ligand

Diimine ligand was synthesized with a slightly modified literature procedure.[33] KO$^t$Bu (0.57 g, 5.12 mmol) was added to a solution of 2-(pyridin-2-yl)-1*H*-benzo[*d*]imidazole (1 g, 5.12 mmol) in 12 mL of DMF. The resulting mixture was stirred at room temperature for 30 min, and then 1-bromohexadecane (6.14 mmol) was added with constant stirring for 12 h. The reaction mixture was subsequently extracted with water and ether to remove DMF and excess KO$^t$Bu. The organic layer was isolated, dried over anhydrous $Na_2SO_4$, and filtered. The solvent was then removed under reduced pressure. The purification of the crude product was carried out by column chromatography on silica gel with hexane/DCM (9 : 1) as the eluent to yield light-yellow oil that crystallized into a light-yellow solid after a week of standing into the fridge, 75%. $^1$H NMR (400 MHz, acetone-d$_6$, 298 K) *d* 8.75 (ddd, $J$ = 4.8, 1.7, 0.9 Hz, 1H), 8.45 (ddd, 1H), 8.00 (dd, $J$ = 7.8, 1.7 Hz, 1H), 7.74 (d, $J$ = 7.7 Hz, 1H), 7.63 (d, $J$ = 7.7 Hz, 1H), 7.49 (ddd, $J$ = 7.7, 4.8, 1.1 Hz, 1H), 7.37–7.31 (m, 1H), 7.30–7.25 (m, 1H), 4.98–4.85 (m, 2H), 1.49–1.22 (m, 31H). HR ESI$^+$-MS: found 420.3376 [M + H$^+$]; calcd. 420.3374.

### Synthesis of iridium complexes

The synthesis of heteroleptic biscyclometallated Ir(III) complexes containing diimine ligands was slightly modified compared to the standard procedure.[34]

**(N^C–COOMe)$_2$Ir(N^N)]PF$_6$, Ir1.** A solution of N^N ligand (0.2 mmol) in dichloromethane (DCM) (10 mL) was added to the corresponding bis(μ-chlorido) bridged dimeric precursor (0.1 mmol) suspended in DCM/MeOH 1 : 1 mixture (20 mL). The reaction mixture was refluxed for 3 h. The resulting clear red solution was cooled down to room temperature, followed by the addition of excess of $KPF_6$ and the mixture was stirred for additional 30 minutes. The reaction mixture was evaporated to dryness, dissolved in DCM, filtered and evaporated once more. The obtained crude product was purified by flash column chromatography on silica with DCM as eluent. The pure compound was obtained as red solid (85%).

$^1$H NMR (400 MHz, acetone-d$_6$, 298 K) *d* 8.91 (s, 1H), 8.60 (s, 1H), 8.55 (d, $J$ = 8.5 Hz, 1H), 8.50 (d, $J$ = 8.6 Hz, 1H), 8.47–8.42 (m, 2H), 8.35 (d, $J$ = 8.0 Hz, 1H), 8.30–8.18 (m, 3H), 7.80 (d, $J$ = 8.4 Hz, 1H), 7.78–7.71 (m, 1H), 7.55 (d, $J$ = 8.0 Hz, 1H), 7.53–7.45 (m, 3H), 7.33–7.27 (m, 1H), 7.27–7.24 (m, 1H), 7.24–7.19 (m, 1H), 7.19–7.12 (m, 1H), 6.99–6.86 (m, 3H), 6.72 (d, $J$ = 4.3 Hz, 1H), 6.70 (d, $J$ = 4.4 Hz, 1H), 6.58 (d, $J$ = 8.3 Hz, 1H), 4.88–4.75 (m, 1H), 4.75–4.60 (m, 1H), 4.15 (s, 3H), 4.06 (s, 3H), 1.49–1.36 (m, 2H), 1.31 (br. s, 29H). Anal. calculated for $C_{62}H_{65}F_6IrN_5O_4P$: C, 58.11; H, 5.11; N, 5.47; found: C, 58.06; H, 5.26; N, 5.36 HR ESI$^+$-MS: found 1136.4758 [M$^+$]; calcd. 1136.4666.

**[(N^C–COOH)$_2$Ir(N^N)]Cl, Ir2.** The complex **Ir2** was obtained by hydrolysis of **Ir1** according to the following procedure: 60 mg (0.049 mmol) of **Ir1** was suspended in 20 mL of MeOH and excess of KOH (0.07 mmol) was added. The resulting mixture was refluxed overnight, evaporated to dryness and redissolved in water. A clear orange solution was acidified by diluted hydrochloric acid until pH 6, to give resulting complex as an orange solid, which was separated by centrifugation, washed with water a few times and dried in air (yield 78%).

$^1$H NMR (400 MHz, DMSO-d$_6$, 298 K) $\delta$ 8.50 (s, 1H), 8.48–8.34 (m, 3H), 8.26 (s, 1H), 8.26–8.21 (m, 2H), 8.21–8.09 (m, 2H), 7.94 (d, $J$ = 9.0 Hz, 1H), 7.81 (d, $J$ = 8.5 Hz, 1H), 7.77–7.69 (m, 1H), 7.43 (t, $J$ = 7.5 Hz, 1H), 7.35 (t, $J$ = 7.6 Hz, 1H), 7.30 (t, $J$ = 7.6 Hz, 1H), 7.24 (d, $J$ = 8.8 Hz, 1H), 7.21–7.09 (m, 3H), 6.99 (t, $J$ = 7.7 Hz, 1H), 6.87 (t, $J$ = 7.7 Hz, 1H), 6.82 (t, $J$ = 7.8 Hz, 1H), 6.72

(t, $J$ = 7.8 Hz, 1H), 6.55 (d, $J$ = 7.8 Hz, 1H), 6.48 (d, $J$ = 7.8 Hz, 1H), 6.45 (d, $J$ = 8.3 Hz, 1H), 4.85–4.69 (m, 1H), 4.67–4.53 (m, 1H), 1.24 (s, 31H). Anal. calculated for $C_{60}H_{61}ClIrN_5O_4$: C, 63.00; H, 5.38; N, 6.12; found: C, 62.89; H, 5.62; N, 6.05. HR ESI$^+$-MS: found 1108.4347 [M$^+$]; calcd 1108.4369.

### Liposome preparation

Liposomes were prepared by thin film hydration method followed by an extrusion and purification.[35] Briefly, the phospholipids in choloroform and the synthesized phosphorescent complexes (**Ir1**, **Ir2**) in MeOH were mixed together (DPPC/DSPE-PEG2000/**Ir#**) with molar ratios of 95/4.5/1, respectively. The organic solvent was evaporated in a rotary evaporator forming a thin film at the bottom of a glass test tube. The lipids were hydrated with 500 μL of HEPES buffer solution (+60 °C) and extruded 11 times at +60 °C through a polycarbonate membrane (100 nm pore size) with a syringe-type extrusion device (Avanti Polar Lipids). Thereafter, the liposomes were quickly cooled and stored in a refrigerator for the further use. The liposomes were purified by gel filtration through a Sephadex G-50 (Sigma-Aldrich) column with HEPES buffer elution. The final total lipid concentration of the samples was 3 μmol mL$^{-1}$.

### Size and ζ-potential measurements

The size and ζ-potential of the liposomes were analyzed with a Zetasizer APS dynamic light scattering automated plate sampler (Malvern Instruments, Malvern, United Kingdom) and reported as hydrodynamic diameters ($D_h$) and polydispersity index (PDI). $D_h$, PDI and ζ-potentials were averaged and corresponding standard deviations (SD) were calculated based on data obtained from at least three independent liposomal formulations.

### Photophysical experiments

All photophysical measurements in solution were carried out in freshly distilled solvents; when appropriate the solutions were degassed by freeze–pump–thaw cycles. UV/Vis spectra were recorded using a Shimadzu UV-1800 spectrophotometer. The emission and excitation spectra in solution were measured with a Fluorolog-3 (JY Horiba Inc.) spectrofluorometer. The emission quantum yields in solution were determined by a comparative method using LED 365 nm pumping and Ru(bipy)$_3$Cl$_2$ in aerated water ($\Phi_r$ = 0.04) as the reference with the refraction coefficients of methanol and water equal to 1.331 and 1.333, respectively.[36] The following equation:

$$\Phi_s = \Phi_r \frac{\eta_s^2 A_r I_s}{\eta_r^2 A_s I_r}$$

was used to calculate the quantum yield, where $\Phi_s$ is the quantum yield of the sample, $\Phi_r$ is the quantum yield of the reference, $\eta$ is the refractive index of the solvent, $A_s$ and $A_r$ are the absorbance of the sample and the reference at the wavelength of excitation, respectively, $I_s$ and $I_r$ are the integrated areas of emission bands. Pulse laser TECH-263 Basic (263 nm), a Tektronix (DPO2012B, band width 100 MHz) oscilloscope, Ocean Optics (Monoscan-2000, interval of wavelengths 1 nm) scanning monochromator, FASTComTec (MCS6A1T4) multiple-event time digitizer and Hamamatsu (H10682-01) Photon counting head were used for lifetime measurements.

### Cell uptake studies

The cell uptake to retinal pigment epithelium cell line (ARPE-19) was imaged with Cytation 5 cell imaging multi-mode reader (BioTek Instruments, Inc., Winooski, VT, USA). The ARPE-19 cells (CRL-2302, American Type Culture Collection, ATCC, Manassas, VA, USA) were cultured in DMEM:F12 medium (Gibco 31330–038) supplemented with 10% fetal bovine serum, 2 mM L-glutamine, 100 U mL$^{-1}$ penicillin and 100 μg mL$^{-1}$ streptomycin at +37 °C, 5% $CO_2$. 50 000 cells per well were seeded on a 24-well thin glass bottom Sensoplate (Greiner Bio-One GmbH, Kremsmünster, Austria) one day before exposing them to the liposomes. The cells were incubated for 3 h with liposomes at lipid concentrations of 1.5 μmol mL$^{-1}$ (high concentration) or 0.3 μmol mL$^{-1}$ (low concentration) in serum-free medium. After the incubation, the cells were washed with phosphate buffered saline (PBS) and incubated 10 min at 37 °C in 5 μg mL$^{-1}$ of Hoechst 33342 label (Thermo Fisher Scientific) for cell nuclei. The cells were washed with PBS and imaged using Cytation 5 with ex/em 445 nm/685 nm for the phosphorescent liposomes and with ex/em 377 nm/447 nm for the nuclear stain.

### Imaging experiments *in vivo*

Pigmented rats (HsdOla:LH; age 4 months; weight ~450 g) were anesthetized with medetomidine (0.4 mg kg$^{-1}$):ketamine (60 mg kg$^{-1}$) mixture. The pupils were dilated with tropicamide (Oftan Tropicamid 5 mg mL$^{-1}$, Santen, Finland) and the eyes were locally anaesthetized with oxybuprocaine hydrochloride (Oftan Obucain 4 mg mL$^{-1}$, Santen, Finland). The intravitreal injections were performed into both eyes of the animals under direct ophthalmoscopic control through an operating microscope. The needle (34 G) was inserted, about 1 mm from the limbus, through the sclera into the vitreous, and 3 μl of the solution was injected per eye. Four eyes were used for each formulation. A topical carbomer hydrogel (Viscotears) was applied to prevent dryness of the cornea. Prior and 30 min after the intravitreal injection, imaging of each eye was performed using optical coherence tomography (OCT), and full color funduscopy (Phoenix MICRON™ MICRON IV/OCT, CA, USA) without and with the filter combination of excitation: Semrock FF01-469/35 and barrier: Semrock BLP01-488R. The transmission bands for the filters were as follows: (i) Semrock FF01-469/35: 451.5 nm to 486.5 nm; (ii) Semrock BLP01-488R: 504.7 nm to 900 nm. Due to the sensitivity limitations of the camera at near infrared region, we the maximal wavelength of detection was about 700 nm for fundus imaging.

## Results and discussion

### Design and characterization of Ir(III) lipid–mimetic complexes

Pyridine-benzimidazole with inserted $C_{16}$ aliphatic chain was chosen as diimine ligand (N^N) in the synthesis of iridium

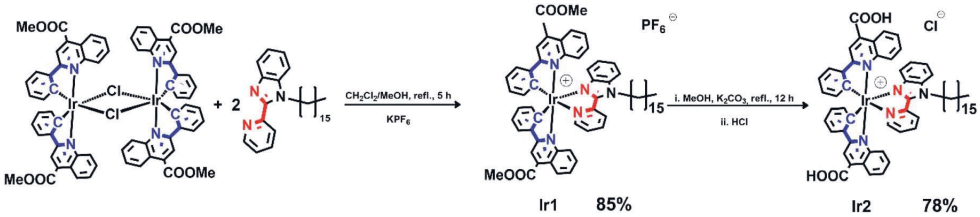


Scheme 1 Synthesis of iridium complexes.

complexes to increase affinity of resulting compounds to phospholipid membrane. The N^N ligand has been synthesized according to Scheme S1 (see ESI†). The heteroleptic cationic iridium complexes of the $[(N^C)_2Ir(N^N)]PF_6$ type were synthesized according to the reaction sequence shown below in high yields (Scheme 1). The aromatic system of the N^C ligand has been modified by insertion of the ester function, which was carefully hydrolyzed at the last stage of the synthesis to increase hydrophilicity of the "head" in this amphiphilic molecule. Moreover, the presence of the electron withdrawing groups (C(O)OMe in **Ir1** and C(O)OH in **Ir2**) gives red shift of excitation and emission bands that is useful for *in vivo* visualization experiments. At the last stage the ester groups of the metalating ligands in **Ir1** were hydrolyzed to increase hydrophilicity of the "head" in this amphiphilic molecule.

The complexes obtained were carefully characterized using appropriate spectroscopic techniques. The HR-ESI$^+$ mass spectra (Fig. S1 and S2†) demonstrate the dominant signals of singly charged molecular cations with *m/z* values equal to 1136.4758 (**Ir1**) and 1108.4347 (**Ir2**), the isotopic patterns of the corresponding signals match well the calculated ones. The $^1$H NMR spectra of all the complexes display three sets of signals corresponding to the N^N-ligand protons and the protons of inequivalent N^C ligands (Fig. 1 and S4†). Assignment of the signals observed in the $^1$H NMR spectra was done using the $^1$H–$^1$H COSY, NOESY spectra (Fig. S3 and S5†). Relative intensity and multiplicity of the signals in the proton spectra fit well the suggested structures (Scheme 1).

Normalized electronic absorption spectra of the both complexes in methanol at 298 K are shown in Fig. S6.† Similar to the interpretation given in earlier publications[32,34,37–42] for this type of iridium complexes the intense absorption bands in the 250–320 nm range could be assigned to spin allowed $^1\pi$–$\pi^*$ ligand centered (LC) transitions located at the cyclometalated and diimine ligands. The longer wavelength absorption bands and shoulders with lower extinction coefficients evidently originate from the mixture of metal-to-ligand ($^1$MLCT) and ligand-to-ligand ($^1$LLCT) charge transfer.[32,42] The absorption spectra of **Ir1** and **Ir2** have similar features except the blue shift of the low energy absorption ($^1$MLCT + $^1$LLCT transitions) in the latter complex for *ca.* 30 nm, which can be assigned to stronger electron withdrawing effect of carboxylic group in the metalating ligands.

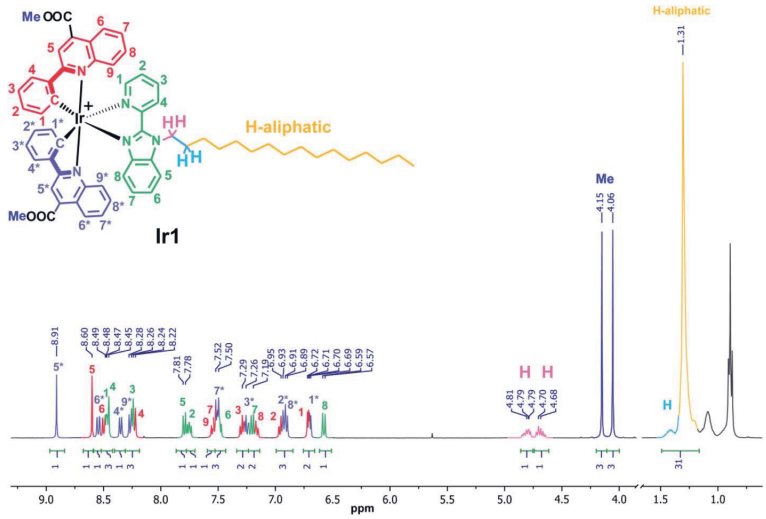


Fig. 1 $^1$H NMR spectrum of **Ir1**, acetone-$d_6$, 298 K.

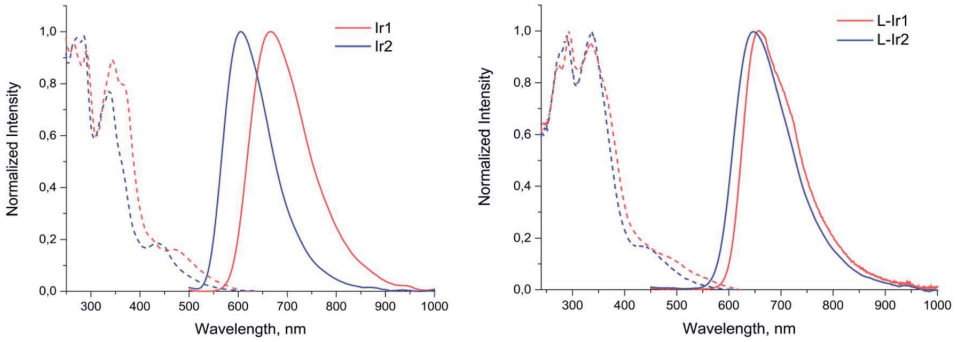


Fig. 2 Excitation (dotted lines) and emission (solid lines) spectra of **Ir1**, **Ir2** (methanol solution) and **L-Ir1**, **L-Ir2** (aqueous solution).

Both complexes display broad and featureless emission bands (Fig. 2, Table 1), which resemble the luminescence profiles of the previously reported complexes[32] with the similar cyclometalating ligand. The lifetimes in microsecond domain and a considerable quenching of emission in aerated solution clearly indicate the triplet origin of the emission observed, *i.e.* phosphorescence. According to the results of theoretical analysis made for the closely related heteroleptic $[(N^C)_2Ir(N^N)]^+$ complexes,[32] the observed emission bands can be tentatively assigned to the mixture of $^3$MLCT and $^3$LLCT transitions with dominating contribution of the N^C ligand orbitals into the triplet excited state. The **Ir2** complex containing carboxylic group in the N^C ligand displays a considerable blue shift of emission band compared to **Ir1** with non-hydrolyzed ester function. This trend is essentially similar to the behavior of analogous pair of iridium complexes upon hydrolysis of ester group in the pyridyl-benzimidazole metalating ligands.[18]

## Preparation and photophysical characterization of liposomes labelled with Ir(III) complexes

Both Ir(III) complexes were then embedded into lipid bilayers of the PEGylated DPPC liposomes (DPPC/DSPE-PEG2000/**Ir#** = 95/4.5/1 mol%) by thin film hydration method. The formed liposomes were of *ca.* 110 nm in diameter and narrowly dispersed (Table 2). They also had slightly negative ζ-potential (Table 2) because of 4.5 mol% of anionic DSPE-PEG2000 added to sterically protect the liposomes by the PEG outer shell.

Photophysical investigation of the liposomes bearing the iridium complexes (**L-Ir1** and **L-Ir2**) revealed that they display luminescence with very similar band profiles (Fig. 2, Table 1). As compared to the starting complex **L-Ir1** demonstrates slight (*ca.* 10 nm) hypsochromic shift, evidently due to variations in polarity of the liposomal microenvironment compared to methanol; on the contrary, **L-Ir2** emission band displays pronounced (*ca.* 32 nm) bathochromic shift, most probably due to (at least, partial) charging of carboxyl groups of the N^C ligand at pH 7.4. The lifetime values of iridium chromophores are more characteristic with respect to microenvironment and may be considered as indirect indications of emitters' location in lipid bilayers of the liposomes. In aerated aqueous solution both **L-Ir1** and **L-Ir2** show longer lifetime compared to the free complexes in methanol that point to isolation of the chromophores from oxygen quenching. However, **L-Ir1** displays much stronger increase in lifetime, which may be considered as deeper immersion of the complex into the liposome bilayer compared to the **L-Ir2** counterpart. However, substantial increase in lifetime (**L-Ir1** *cf.* **Ir1**) in degassed solution also indicates considerable effect of the matrix rigidity (suppression of nonradiative vibrational relaxation), which also plays important role in the observed lifetime variations. Nearly equal lifetime values for **L-Ir2** and **Ir2** in degassed solutions point to the absence of "rigidity effect", whereas relatively small lifetime

Table 1 Photophysical properties of **Ir1** and **Ir2** in methanol and labelled liposomes **L-Ir1**, **L-Ir2** in aqueous solution, $\lambda_{exc}$ = 365 nm, 298 K

| Sample | Absorbance, $\lambda_{max}$, nm ($\varepsilon \times 10^{-4}$, $M^{-1}$ $cm^{-1}$) | Excitation, $\lambda_{max}$, nm | Emission, $\lambda_{max}$, nm | τ, μs (deg/aer) | QY, % deg/aer |
|---|---|---|---|---|---|
| **Methanol solution** | | | | | |
| **Ir1** | 267(*59*), 293(*55*), 342(*49*), 367sh(*34*), 468(*6*) | 250–288, 344, 366, 468 | 667 | 0.19/0.12 | 4.8/2.3 |
| **Ir2** | 267(*57*), 285(*55*), 335(*47*), 435(*6*) | 250–288, 338, 435 | 605 | 0.42/0.26 | 10.0/5.3 |
| **Aqueous solution** | | | | | |
| **L-Ir1** | 332, 437 | 293, 334, 476 | 657 | 0.50/0.46 | [a] |
| **L-Ir2** | [a] | 289, 337, 437 | 647 | 0.41/0.38 | [a] |

[a] These are unavailable due to strong scattering of solutions.

Table 2 Characterization of PEGylated DPPC liposomes labelled with Ir(III) complexes, in aqueous solution

| Sample | $D_h \pm$ SD, nm | PDI |
|---|---|---|
| Neat liposomes | 94 ± 25 | 0.050 |
| **L-Ir1** | 118 ± 24 | 0.075 |
| **L-Ir2** | 106 ± 23 | 0.153 |

growth (**L-Ir2** *vs.* **Ir2**) in aerated solutions indicate ineffective shielding of the chromophore from interaction with molecular oxygen. The both observations are very probably indicative of the iridium emitter location in the "near-surface" area of the liposome that is a natural consequence of hydrophilic character of the carboxylic groups at the N^C ligands.

Both types of phosphorescent liposomes were then evaluated for their application potential in both *in vitro* and *in vivo* imaging.

### Evaluation of phosphorescent liposomes in bioimaging

**Uptake of the liposomes by ARPE-19 cells.** Retinal pigment epithelium cell line (ARPE-19) was chosen for the uptake studies since this line is one of the most appropriate *in vitro* models of retinal pigment epithelium.[43] Incubation of ARPE-19 cells with phosphorescent liposomes resulted in an effective uptake visualized by the appearance of red luminescence in cytoplasm (Fig. 3A and B) compared to control (Fig. 3C). Fig. 3A and B clearly show that though both complexes are reliably visualized to lipid concentrations as low as 0.3 μmol mL$^{-1}$, the **L-Ir2** species provide stronger luminescence signal and better contrast compared to the background (Fig. S7†). Overall, the presented *in vitro* studies clearly show that PEGylated liposomes containing Ir(III) lipid–mimetic complexes readily internalize into cells and provide reliable signal in microscopic experiments.

**Ocular imaging *in vivo*.** To evaluate the applicability of phosphorescent liposomes in *in vivo* imaging, we performed OCT and full color funduscopy on pigmented rats. The labeled liposomes were administered as intravitreal injections. Fig. 4 and 5 show that both Ir(III) complexes are clearly visible not only because of their luminescence in funduscopy, but they also generate OCT contrast (compare OCT images in Fig. 4 and 5 before and after injection). The luminescence and OCT signals are overlapping thereby revealing the colocalization of both signals. Both formulations were detectable in the vitreous for 48 hours post-injection with both fluorescence and OCT imaging. The images show typical localized distribution of intravitreally injected liposomes that were then subject to diffusion and dislocation from the site of injection at different times after injection (Fig. 4 and 5).

Wavelength of the light in ocular OCT imaging is in the near infra-red region. Therefore, the molecules that can absorb or emit light could cause contrast in the OCT images. Previous study has demonstrated OCT-based detection of microspheres *in vivo* in liver tissue.[44] The contrast mechanisms of OCT are based on the absorption or back scattering of light. Endogenous melanin[44] and exogenous indocyanine green[45] are examples of contrast agents in OCT. Since the wavelength of light in OCT is in the near infrared region, and **IR-1** and **IR-2** do not have strong emission in this range, it is expected that the OCT signals of the labeled liposomes stem from physical light scattering. Interestingly, the signals of fluorescence fundus images and OCT overlap. This shows that the liposomes are detectable by both OCT and fluorescence imaging. Colocalization of the signals also indicates that the labels are stably embedded in the liposomes after intravitreal injections.

Combination of OCT and fluorescence imaging simultaneously may provide means to monitor simultaneously tissue microstructures (OCT) and molecular processes (fluorescence signals).[46] Such approach may be interesting in the experiments of ocular drug safety and pharmacodynamics *in vivo*. Fluorescence signals may demonstrate the distribution of compound or drug delivery system, while OCT could reveal the distribution of materials and ocular microstructures, such as retinal layers.[47]

Fig. 6 shows the fundus images of the eyes of a rat at the age of more than one year. The images were captured by BLP01-488R and FF01-469/35 set of filters. Green autofluorescence, mostly originating from anterior ocular tissues (*e.g.* lens), is seen in this old rat. It is known that ocular green autofluorescence increases with aging.[48] The rats in our liposome studies were 4 months old and they showed low natural autofluorescence in the eyes. With **IR-1** and **IR-2** dyes green autofluorescence background of the eyes can be eliminated, because **IR-1** and **IR-2** show red signals with this set of filters.

Endogenous autofluorescence of posterior ocular tissues, like retina, is also an important factor that may affect the quality of fluorescence imaging. Marmorstein *et al.*[49] elucidated the spectral profile of natural autofluorescence of human retina. They

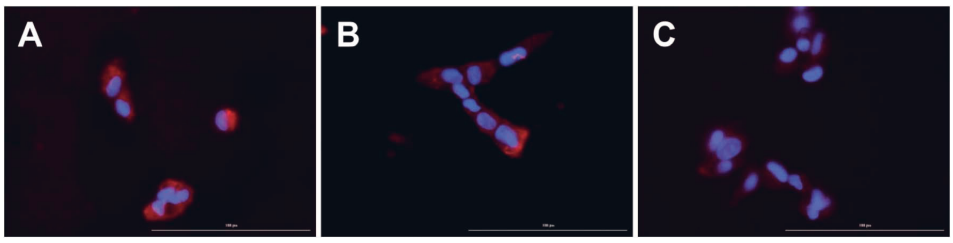


Fig. 3 Uptake of liposomes labeled with **Ir1** (panel A) and **Ir2** (panel B), and unlabeled control liposomes (panel C) into ARPE-19 cells. The **Ir#** labeled liposomes are shown in red and cell nucleic labeled with Hoechst in blue. Images were acquired using the Cytation 5 fluorescence microscope. Lipid concentration: 0.3 μmol mL$^{-1}$. Magnification: 40×. Scale bar: 100 μm.

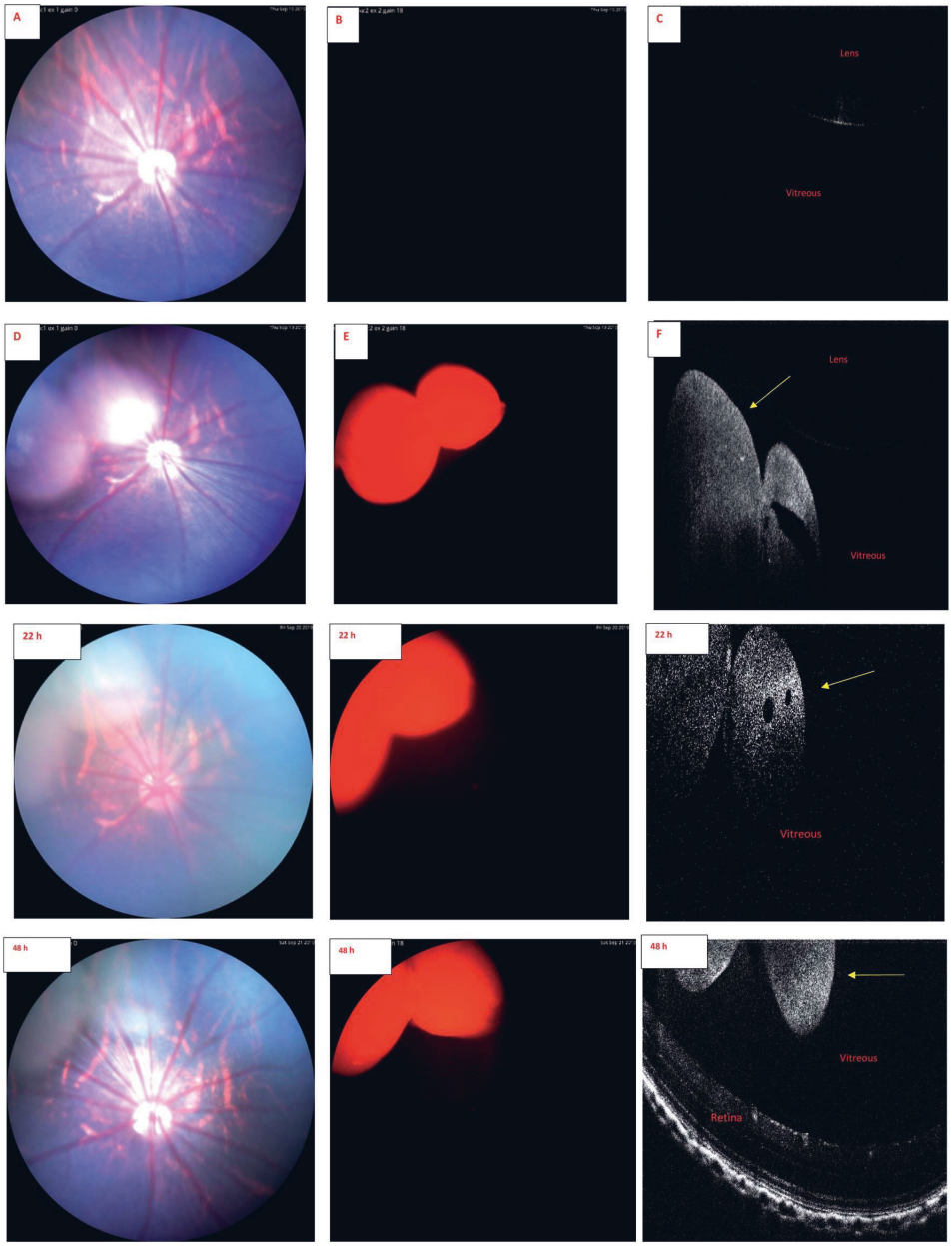


Fig. 4 **IR-2** Fundus and OCT images of rat eye. *Upper panel*. (A) Color fundus image before injection of liposomes containing **IR-2** compound. (B) Fundus image with the filter combination of excitation: Semrock FF01-469/35 and barrier: Semrock BLP01-488R, before injection. (C) OCT image before injection. (D) Color fundus image 30 min after injection of liposomes containing **IR-2** compound. (E) Fundus image 30 min after injection with the filter combination of excitation: Semrock FF01-469/35 and barrier: Semrock BLP01-488R. (F) OCT image 30 min after injection. The liposomes are visible in the vitreous after the injection (yellow arrow). *Lower panel*. Following images are from same eye and same set of filters 22 and 48 h after intravitreal injection.

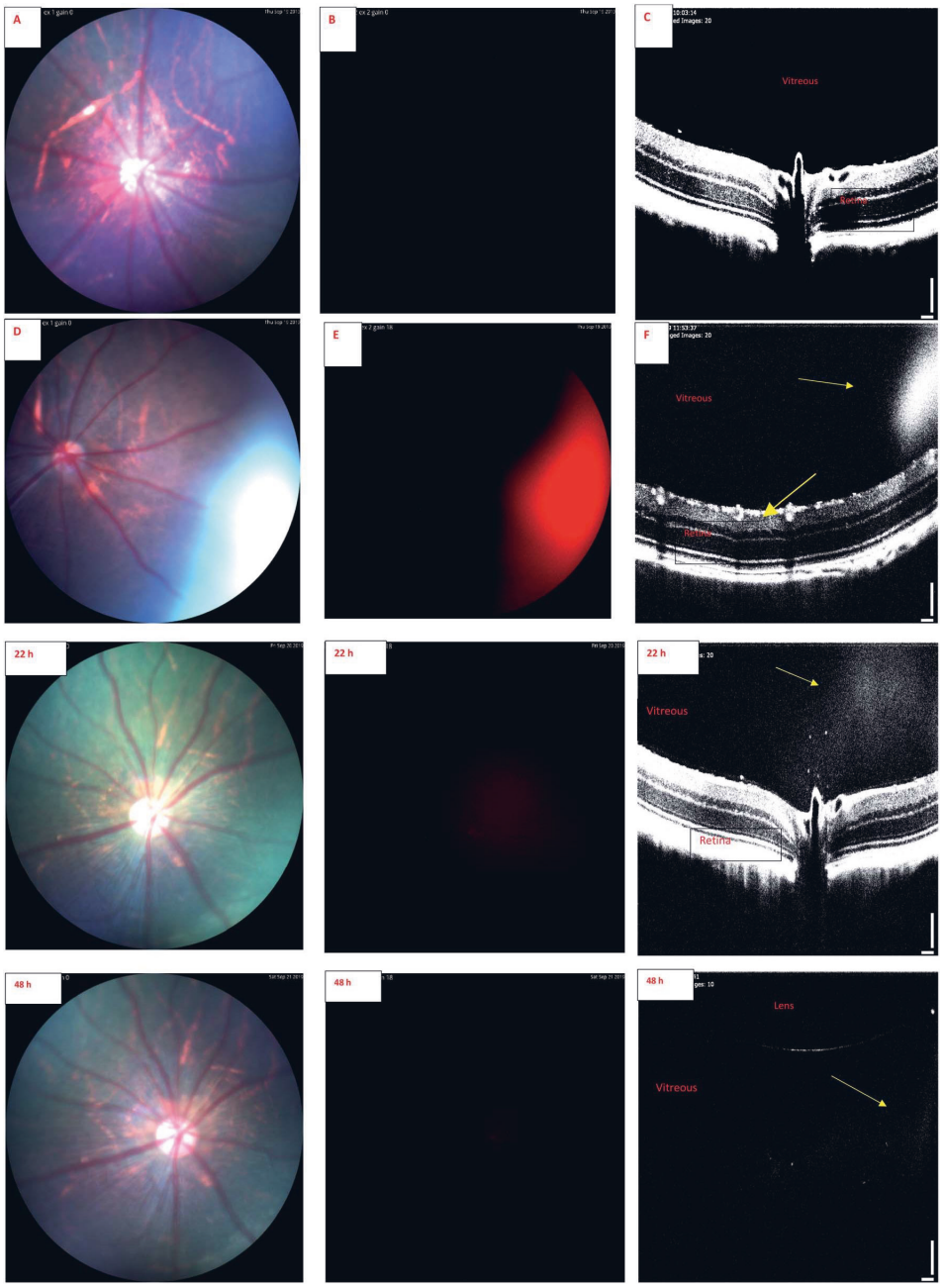


Fig. 5 **IR-1** Fundus and OCT images of rat eye. *Upper panel*. (A) Color fundus image before injection of liposomes containing **IR-1** compound. (B) Fundus image with the filter combination of excitation: Semrock FF01-469/35 and barrier: Semrock BLP01-488R, before injection. (C) OCT image before injection. (D) Color fundus image 30 min after injection of liposomes containing **IR-1** compound. (E) Fundus image with the filter combination: excitation Semrock FF01-469/35 and barrier Semrock BLP01-488R, 30 min after injection. (F) OCT image 30 min after injection. The liposomes are visible in the vitreous after the injection (yellow arrow). *Lower panel*. Following images are from same eye and same set of filters 22 and 48 h after injection.

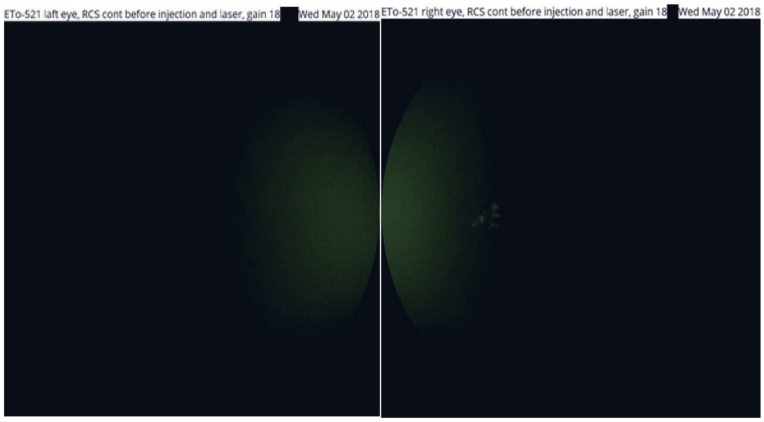


Fig. 6 Fundus image of both eyes of an one-year old rat (excitation: Semrock FF01-469/35 and barrier: Semrock BLP01-488R). Green natural autofluorescence is seen.

studied retinas of healthy and diseased (age-related macular degeneration) human subjects using different excitation and emission wavelengths. When excitation was performed at 488 nm, the emitted signal at 655 nm wavelength was minimal. It is noteworthy that we used excitation wavelength of 488 nm and monitored the **IR-1** and **IR-2** dyes at 657 nm and 647 nm, respectively. Therefore, the background noise from the retinal autofluorescence should be minimal for these dyes. This may open potential applications of these dyes in retinal research.

Another potential application of these dyes involves their simultaneous detection with green dyes, like fluorescein, in a single image. This is feasible, because BLP01-488R and FF01-469/35 filter sets are ideal for fluorescein angiography of the retina. For example, if we inject intravitreally compounds or formulations labeled with **IR-1** or **IR-2**, and perform retinal angiography by systemic administration of fluorescein, we could still detect the intravitreally injected materials with the same set of filters in a single image. Retinal angiography is a valuable tool in the evaluation of retinal vessels, an important part in preclinical safety and drug efficacy studies. These new labels may broaden the information gain in such investigations.

Our results suggest that phosphorescence labeling of drug delivery systems can be used as a tool to follow intracellular and intraocular particle distribution. To the best of our knowledge, this is the first report of the applicability of a phosphorescent sensor for simultaneous use in *in vivo* fundoscopy and OCT. Compared to fluorescent labels, the phosphorescent labels are expected to show improved signal-to-noise ratio and negligible quenching in long-term experiments with prolonged action ocular drug delivery systems. Despite the preliminary character of these *in vivo* results this research allows to conclude that the developed iridium complexes have high potential for *in vitro* and *in vivo* bioimaging applications. Wider *in vivo* use, particularly in clinical settings, would require more thorough exploration of the safety aspects of these materials.

## Conflicts of interest

There are no conflicts of interest to declare.

## Ethical statement

The animal experiments were approved by the national Animal Experiment Board (ELLA, Regional State Administrative Agency for Southern Finland). The experiments were performed under project license (ESAVI/8621/04.10.07/2017) and in compliance with 3Rs principle (replacement, reduction, refinement). The animal-welfare body of University of Eastern Finland Lab Animal Center (UEF LAC) monitored the use of the animals and followed the development and outcome of the project.

## Acknowledgements

Grant support from Russian Government Mega-Grant 14.W03.031.0025 "Biohybrid technologies for modern biomedicine" is acknowledged. The NMR, photophysical and analytical measurements were performed using the following core facilities at St. Petersburg State University Research Park: Centre for Magnetic Resonance and Centre for Chemical Analysis and Materials Research. We would like to thank the Bioactivity Screening core facility of HI-LIFE, University of Helsinki (Dr Polina Ilina) for enabling the use of Cytation 5 instrument.

## References

1 H. Daraee, A. Etemadi, M. Kouhi, S. Alimirzalu and A. Akbarzadeh, *Artif. Cells, Nanomed., Biotechnol.*, 2016, **44**, 381–391.
2 Z. Amoozgar and Y. Yeo, *Wiley Interdiscip. Rev.: Nanomed. Nanobiotechnol.*, 2012, **4**, 219–233.
3 T. Lajunen, K. Hisazumi, T. Kanazawa, H. Okada, Y. Seta, M. Yliperttula, A. Urtti and Y. Takashima, *Eur. J. Pharm. Sci.*, 2014, **62**, 23–32.

4 H. Talsma, A. Y. Özer, L. van Bloois and D. J. A. Crommelin, *Drug Dev. Ind. Pharm.*, 1989, **15**, 197–207.
5 P. L. Felgner, T. R. Gadek, M. Holm, R. Roman, H. W. Chan, M. Wenz, J. P. Northrop, G. M. Ringold and M. Danielsen, *Proc. Natl. Acad. Sci. U. S. A.*, 1987, **84**, 7413–7417.
6 O. Meyer, D. Kirpotin, K. Hong, B. Sternberg, J. W. Park, M. C. Woodle and D. Papahadjopoulos, *J. Biol. Chem.*, 1998, **273**, 15621–15627.
7 K. Maruyama, T. Takizawa, N. Takahashi, T. Tagawa, K. Nagaike and M. Iwatsuru, *Adv. Drug Delivery Rev.*, 1997, **24**, 235–242.
8 F. Szoka and D. Papahadjopoulos, *Annu. Rev. Biophys. Bioeng.*, 1980, **9**, 467–508.
9 A. Gomez-Hens and J. Fernandez-Romero, *TrAC, Trends Anal. Chem.*, 2006, **25**, 167–178.
10 T. Lajunen, R. Nurmi, L. Kontturi, L. Viitala, M. Yliperttula, L. Murtomäki and A. Urtti, *J. Controlled Release*, 2016, **244**, 157–166.
11 P. S. Uster and R. E. Pagano, in *Methods in Enzymology*, 1989, pp. 850–857.
12 V. Torchilin and T. Levchenko, *Curr. Protein Pept. Sci.*, 2003, **4**, 133–140.
13 V. P. Torchilin, *Adv. Drug Delivery Rev.*, 2005, **57**, 95–109.
14 G. J. Strijkers, E. Kluza, G. A. F. Van Tilborg, D. W. J. van der Schaft, A. W. Griffioen, W. J. M. Mulder and K. Nicolay, *Angiogenesis*, 2010, **13**, 161–173.
15 B. C. Roy, R. Peterson, S. Mallik and A. D. Campiglia, *J. Org. Chem.*, 2000, **65**, 3644–3651.
16 X. Yue and Z. Dai, *Curr. Med. Chem.*, 2018, **25**, 1397–1408.
17 A. Mechler, B. D. Stringer, M. S. H. Mubin, E. H. Doeven, N. W. Phillips, J. Rudd-Schmidt and C. F. Hogan, *Biochim. Biophys. Acta, Biomembr.*, 2014, **1838**, 2939–2946.
18 M. R. Gill, D. Cecchin, M. G. Walker, R. S. Mulla, G. Battaglia, C. Smythe and J. A. Thomas, *Chem. Sci.*, 2013, **4**, 4512–4519.
19 F. R. Svensson, M. Li, B. Nordén and P. Lincoln, *J. Phys. Chem. B*, 2008, **112**, 10969–10975.
20 S. Bonnet, B. Limburg, J. D. Meeldijk, R. J. M. Klein Gebbink and J. A. Killian, *J. Am. Chem. Soc.*, 2011, **133**, 252–261.
21 Y. Hisamatsu, A. Shibuya, N. Suzuki, T. Suzuki, R. Abe and S. Aoki, *Bioconjugate Chem.*, 2015, **26**, 857–879.
22 W. Jiang, Y. Gao, Y. Sun, F. Ding, Y. Xu, Z. Bian, F. Li, J. Bian and C. Huang, *Inorg. Chem.*, 2010, **49**, 3252–3260.
23 K. K.-W. Lo, P.-K. Lee and J. S.-Y. Lau, *Organometallics*, 2008, **27**, 2998–3006.
24 C. Liao, D. Xu, X. Liu, Y. Fang, J. Yi, X. Li and B. Guo, *Int. J. Nanomed.*, 2018, **13**, 4417–4431.
25 W.-Y. Zhang, F. Du, M. He, L. Bai, Y.-Y. Gu, L.-L. Yang and Y.-J. Liu, *Eur. J. Med. Chem.*, 2019, **178**, 390–400.
26 T. M. Allen, *Adv. Drug Delivery Rev.*, 1994, **13**, 285–309.
27 A. Kolate, D. Baradia, S. Patil, I. Vhora, G. Kore and A. Misra, *J. Controlled Release*, 2014, **192**, 67–81.
28 A. G. Kohli, P. H. Kierstead, V. J. Venditto, C. L. Walsh and F. C. Szoka, *J. Controlled Release*, 2014, **190**, 274–287.
29 V. P. Torchilin, *Nat. Rev. Drug Discovery*, 2005, **4**, 145–160.
30 A. Urtti, *Adv. Drug Delivery Rev.*, 2006, **58**, 1131–1135.
31 E. M. del Amo, A. K. Rimpelä, E. Heikkinen, O. K. Kari, E. Ramsay, T. Lajunen, M. Schmitt, L. Pelkonen, M. Bhattacharya, D. Richardson, A. Subrizi, T. Turunen, M. Reinisalo, J. Itkonen, E. Toropainen, M. Casteleijn, H. Kidron, M. Antopolsky, K. S. Vellonen, M. Ruponen and A. Urtti, *Prog. Retinal Eye Res.*, 2017, **57**, 134–185.
32 R. A. Smith, E. C. Stokes, E. E. Langdon-Jones, J. A. Platts, B. M. Kariuki, A. J. Hallett and S. J. A. Pope, *Dalton Trans.*, 2013, **42**, 10347–10357.
33 C. D. Sunesh, G. Mathai and Y. Choe, *ACS Appl. Mater. Interfaces*, 2014, **6**, 17416–17425.
34 K. K. W. Lo, C. K. Chung, T. K. M. Lee, L. H. Lui, K. H. K. Tsang and N. Zhu, *Inorg. Chem.*, 2003, **42**, 6886–6897.
35 T. Lajunen, L. S. Kontturi, L. Viitala, M. Manna, O. Cramariuc, T. Róg, A. Bunker, T. Laaksonen, T. Viitala, L. Murtomäki and A. Urtti, *Mol. Pharm.*, 2016, **13**, 2095–2107.
36 K. Suzuki, A. Kobayashi, S. Kaneko, K. Takehira, T. Yoshihara, H. Ishida, Y. Shiina, S. Oishi and S. Tobita, *Phys. Chem. Chem. Phys.*, 2009, **11**, 9850–9860.
37 K. J. Lee, W.-K. Oh, J. Song, S. Kim, J. Lee and J. Jang, *Chem. Commun.*, 2010, **46**, 5229–5231.
38 K. Hasan, L. Donato, Y. Shen, J. D. Slinker and E. Zysman-Colman, *Dalton Trans.*, 2014, **43**, 13672–13682.
39 B. Tong, P. Ma, Q. Mei and Z. Hua, *Inorg. Chim. Acta.*, 2014, **421**, 405–409.
40 B. Tong, J. Qiang, Q. Mei, H. Wang, Q. Zhang and Z. Han, *Z. Naturforsch., B: J. Chem. Sci.*, 2012, **67**, 213–218.
41 Q. Zhao, M. Yu, L. Shi, S. Liu, C. Li, M. Shi, Z. Zhou, C. Huang and F. Li, *Organometallics*, 2010, **29**, 1085–1091.
42 J. R. Shakirova, O. A. Tomashenko, E. E. Galenko, A. F. Khlebnikov, P. Hirva, G. L. Starova, S.-H. Su, P.-T. Chou and S. P. Tunik, *Inorg. Chem.*, 2018, **57**, 6853–6864.
43 K. C. Dunn, A. E. Aotaki-Keen, F. R. Putkey and L. M. Hjelmeland, *Exp. Eye Res.*, 1996, **62**, 155–170.
44 T. M. Lee, A. L. Oldenburg, S. Sitafalwalla, D. L. Marks, W. Luo, F. J.-J. Toublan, K. S. Suslick and S. A. Boppart, *Opt. Lett.*, 2003, **28**, 1546–1548.
45 J. P. Ehlers, S. McNutt, S. Dar, Y. K. Tao and S. K. Srivastava, *Br. J. Ophthalmol.*, 2014, **98**, 1588–1591.
46 S. Yuan, C. A. Roney, J. Wierwille, C.-W. Chen, B. Xu, G. Griffiths, J. Jiang, H. Ma, A. Cable and R. M. Summers, *Phys. Med. Biol.*, 2009, **55**, 191.
47 C. Yang, *Photochem. Photobiol.*, 2005, **81**, 215–237.
48 F. Holz, A. C. Bird, S. Schmitz-Valckenberg and R. Spaide, *Atlas of Fundus Autofluorscence Imaging*, Springer, 2007, vol. 1.
49 A. D. Marmorstein, L. Y. Marmorstein, H. Sakaguchi and J. G. Hollyfield, *Invest. Ophthalmol. Visual Sci.*, 2002, **43**, 2435–2441.

# Publication II

European Journal of Pharmaceutical Sciences 159 (2021) 105720

Contents lists available at ScienceDirect

European Journal of Pharmaceutical Sciences

journal homepage: www.elsevier.com/locate/ejps

# Pharmacokinetics of intravitreal macromolecules: Scaling between rats and rabbits

Amir Sadeghi [a,1,*], Jooseppi Puranen [a,1], Marika Ruponen [a], Annika Valtari [a], Astrid Subrizi [a], Veli-Pekka Ranta [a], Elisa Toropainen [a], Arto Urtti [a,b,c]

[a] School of Pharmacy, University of Eastern Finland, Yliopistonranta 1 C, 70210 Kuopio, Finland
[b] Institute of Chemistry, Saint Petersburg State University, Universitetskii pr. 26, 198584 Saint Petersburg, Russia
[c] Faculty of Pharmacy, University of Helsinki, Viikinkaari 5 E, 00790 Helsinki, Finland

ARTICLE INFO

*Keywords:*
Intravitreal
Ocular fluorophotometry
Pharmacokinetics
Interspecies translation
Dose scaling

ABSTRACT

Rats are widely used to study ocular drug responses, whereas rabbits are the most widely used preclinical model of ocular pharmacokinetics. Despite their wide use in evaluation of intravitreally injected drugs, translational information about pharmacokinetics and dose scaling between rats and rabbits is missing. In this study, we investigated intravitreal pharmacokinetics in rats and rabbits using non-invasive ocular fluorophotometry. Fluorescein and fluorescently labeled molecules (dextrans) with different molecular weights (376 Da, 10, 150 and 500 kDa), were injected into the vitreous of rabbits and rats. Intravitreal concentrations of the compounds were determined and pharmacokinetic parameters were calculated. Overall, the elimination half-lives of the macromolecules in rat vitreous were 5–6 times shorter than in rabbits, and the half-lives were prolonged at increasing molecular weights. The apparent volumes of distribution for tested compounds in rats and rabbits were in the range of the anatomical vitreal volumes. In both species, anterior route of elimination was predominant for the dextrans, whereas fluorescein was mainly eliminated via posterior route. Rabbit-to-rat ratios for intravitreal clearance were in the range of 2 to 5 for dextrans. Therefore, 2–5 times higher doses are needed for similar drug exposure in rabbits than in rats. Also, the shorter half-lives of macromolecules in the rat vitreous must be taken into account in translation to rabbit and human studies. The scaling factors presented herein will augment translational drug development for eye diseases.

## 1. Introduction

Drug delivery to the posterior eye segment is important, because large number of patients suffer from the retinal diseases. Currently, intravitreal injections are clinically established procedure in the treatment of posterior eye segment. Intravitreal injections of anti-VEGF antibody (bevacizumab), Fab-fragment (ranibizumab) and soluble receptor (aflibercept) are widely used in the treatment of wet age-related macular degeneration (Lanzetta et al., 2013). These biologics have vitreal half-lives of about 4–5 days in rabbits (Bakri et al., 2007), whereas small molecule drugs have typically elimination half-lives less than 10 h (Kidron et al., 2012).

In most intravitreal pharmacokinetic studies, large number of test animals, usually rabbits, are sacrificed at different times for monitoring drug concentrations in ocular tissues. This is ethically questionable, expensive, laborious and this approach does not provide adequate information about the inter-subject variability. Ocular fluorophotometry is a non-invasive optical *in vivo* technique that measures the emitted light from fluorescently labeled molecules in transparent ocular compartments; for example, cornea, aqueous humor, lens and vitreous (Raines, 1988). Fluorophotometry enables quantitation of fluorescent compounds, enabling ocular pharmacokinetic studies of labeled macromolecules and drug delivery systems. Fluorophotometry facilitates rational use of animals in accordance with the 3R principles (replacement, reduction, refinement) of laboratory animal use. Fluorophotometry has been used in pharmacokinetic experiments with fluorescently labeled macromolecules in rabbits (Araie and Maurice, 1991; Johnson and Maurice, 1984). Recently, Dickmann and colleagues (Dickmann et al., 2015) obtained similar pharmacokinetic results for intravitreal ranibizumab using fluorophotometry and conventional

* Corresponding author.
*E-mail address:* amir.sadeghi@uef.fi (A. Sadeghi).
[1] Equal contribution

https://doi.org/10.1016/j.ejps.2021.105720
Received 18 September 2020; Received in revised form 10 January 2021; Accepted 12 January 2021
Available online 16 January 2021

invasive method.

Even though rats are widely used in preclinical ocular pharmacology and toxicology (Shah et al., 2019), pharmacokinetics of intravitreal macromolecules in rats has not been reported. Furthermore, there are no data to support rat-to-rabbit dose scaling in intravitreal drug development. Lack of rat studies is due to the difficult dissection and collection of rat vitreous, since average volume of the rat vitreous is about 50 μl (Sha and Kwong, 2006). Collection of rat vitreous without cross contamination from adjacent tissues is very difficult (Kottegoda et al., 2007). For this reason, many kinetic studies in rats use whole eye homogenates, instead of individual tissues (Fuchs and Igney, 2017; Robinson et al., 2002).

Recently, we showed that intravitreal elimination of three compounds (molecular weight range 0.51 - 66.5 kDa) in mice was much faster than in the rabbits or humans (Schmitt et al., 2019). Based on the pharmacokinetic parameters, the intravitreal doses in rabbits and humans should be 27–90 and 38- 126 higher than in mice, respectively (Schmitt et al., 2019). This study was performed with non-invasive SPECT/CT imaging, thereby avoiding dissection and cross-contamination. We published previously also scaling factors for rabbit-to-human translation using kinetic analysis of 12 intravitreal drugs (del Amo et al., 2015). Intravitreal drug doses in humans should be about 40% higher than in the rabbits.

In this study, we studied four intravitreal compounds with molecular weights of 376 – 500,000 Da in rat and rabbit eyes. Pharmacokinetic parameters were calculated from the results of ocular fluorophotometry and were further used to estimate scaling factors for rat-to-rabbit and rat-to-human translation. The parameters, scaling factors and kinetic simulations were used to generate dosing guidance for inter-species translation.

## 2. Materials and methods

### 2.1. Materials

Fluorescein isothiocyanate (FITC)-dextrans (Sigma Aldrich) with the average molecular weights of 10 kDa, 150 kDa and 500 kDa were dissolved in sterile saline. In rat experiments, the concentration of intravitreal FITC-dextran injectable was 5 mg/ml (500 kDa) or 10 mg/ml (10 and 150 kDa). In rabbit studies, FITC-dextran concentration was of 5 mg/ml and 10 mg/ml for the molecular weight of 10 and 500 kDa, respectively. Fluorescein sodium (2 μg/ml) was diluted from Fluorescite 100 mg/ml (Alcon Nordic A7S, Denmark) with sterile 0.9% sodium chloride. All the solutions were prepared fresh prior to their use in the animal experiments. The solutions were filtered using syringe filter with pore size of 0.2 μm (Fisher Scientific, USA). Viscotears was obtained from Dr. Winzer Pharma (Germany). Ketamine was the product of Pfizer (Ketalar®/Ketaminol® 50 mg/ml, Pfizer Oy Animal Health, Espoo, Finland) and medetomidine was obtained from Orion Pharma (Domitor® vet 1 mg/ml, Orion Pharma, Espoo, Finland). Tropicamide (Oftan Tropicamid 5 mg/ml), obucaine (Oftan Obucain 4 mg/ml) and phenylephrine (Oftan Metaoksedrin 100 mg/ml) were obtained from Santen Pharmaceutical Co., Ltd. (Tampere, Finland).

### 2.2. Animals

Lister hooded outbred male rats of 300–400 gr and age of 2–6 months were used. Dutch-belted rabbits (average age of 6 months, weight 2.7 - 4.0 kg) were used for fluorescein injections. Albino rabbits (average age of 6 months and weight of 3.0 - 3.5 kg) were used for FITC-dextran injections. The animals were handled in accordance with ARVO statement for the use of animals in ophthalmic research. All animal experiments were approved by the national Animal Experiment Board of Finland.

### 2.3. Fluorophotometry in rats

Intravitreal injections to the rat eyes were performed under isoflurane anesthesia. Anesthesia was induced with combination of 4% isoflurane and 500 ml/min air flow. The anesthesia was maintained with 2% isoflurane and 250/min air flow. Topical phenylephrine (100 mg/ml) and tropicamide (5 mg/ml) were for maximal pupillary dilation (Murata et al., 1998). Topical oxybuprocaine hydrochloride (4 mg/ml) was applied topically to anaesthetize the ocular surface just before the intravitreal injections. Possible eye movements, induced by isoflurane anesthesia (Nair et al., 2011), were suppressed with topical medetomidine (10 μl; 1 mg/ml) (Potter and Ogidigben, 1991) before the intravitreal injections.

The intravitreal injections were monitored and controlled with an ophthalmoscopic operating microscope. The needle (34 G) was inserted through the sclera (about 1 mm from the limbus) into the vitreous, and 3 μl of the solution was injected per eye. Both eyes in each animal were injected. After injection, a topical hydrogel (Viscotears) was applied to prevent corneal dryness. After injection the eyes were checked with optical coherence tomography and fundus camera (Phoenix MICRON™ MICRON IV/OCT, CA, USA) for any damage to the lens and the retina. Damaged eyes were excluded from the kinetic measurements.

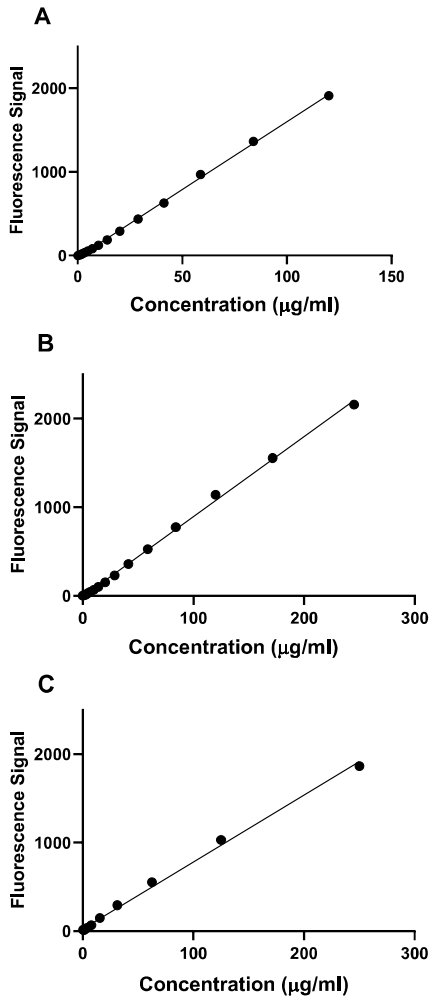


**Fig. 1.** Linear ranges of concentration vs fluorescence signals of the fluorescent compounds. A) FITC-dextran 10 kDa ($y = 16.24x - 22.55$, $R^2 = 0.999$), B) FITC-dextran 150 kDa ($y = 9.05x - 11.85$, $R^2 = 0.998$), C) FITC-dextran 500 kDa ($y = 7.56x + 23.27$, $R^2 = 0.996$).

Fluorophotometry was performed using a Fluorotron Master fluorophotometer (Ocumetrics, Mountain View, CA) under isoflurane anesthesia. The pupil was dilated about 10 min before each scan with a combination of topical phenylephrine and tropicamide. Also, 10 μl of topical medetomidine was used as a local muscle relaxant to avoid any eye movements during fluorophotometric measurements. The anterior chamber lens of Fluorotron Master was used in the measurements. The injected doses of all test compounds were designed so that all measured signals were within the linear range of detection.

### 2.4. Fluorophotometry in rabbits

Rabbits were anaesthetized with a cocktail of ketamine (25 mg/kg) and medetomidine (0.5 mg/kg). The pupil was dilated with topical 5 mg/ml tropicamide solution. Topical oxybuprocaine hydrochloride (4 mg/ml) was applied for local anesthesia of the ocular surface. The intravitreal injections (40 μl per eye) were performed to the supertemporal quadrant (4.5 mm behind the surgical limbus) using a 31 G needle and a 100 μl Hamilton syringe perpendicularly to the scleral surface. After the injections, topical hydrogel (Viscotear) was applied to prevent corneal dryness. In the case of macromolecules, both eyes were injected in each animal. For fluorescein, only one eye was injected to minimize systemic exposure (Knudsen, 2002).

For each fluorophotometric measurement, the rabbits were lightly sedated by subcutaneous medetomidine (0.5 mg/kg). The pupil was dilated by topical tropicamide eye drop 20 min before the measurements. In the case of FITC-dextrans with slow elimination, the rabbits were woken up with subcutaneous atipamezole (1 mg/kg). In fluorescein experiments, the rabbits were kept under continuous anesthesia with a combination of medetomidine (0.5 mg/kg) and ketamine (25 mg/kg) (Kitano et al., 1988). Isotonic 0.9% saline solution was injected subcutaneously to prevent dehydration of the anaesthetized rabbits. The vitreous adapter of Fluorotron Master (axial resolution of 0.25 mm) was used in the rabbit studies.

### 2.5. Analysis of the fluorescent signals

A baseline measurement was performed before the intravitreal injections to determine the levels of autofluorescence. The autofluorescence was subtracted from the measured fluorescence to obtain the net signals of the intravitreally injected fluorescent compounds. The signals were measured over the anterior-to posterior axis of the vitreous. For rabbits, The average signal in the rabbit vitreous was obtained 3 mm anteriorly (Zeimer et al., 1983) from the retina. In the case of rats, with vitreal diameter of ≈ 1.4 mm (Hughes, 1979), the maximum signal intensity in the middle of the vitreous was used.

The net signals at each time point were converted to the intravitreal concentrations. Calibration solutions of each fluorescent compound were prepared in phosphate buffer at pH 7.3 to mimic the vitreal pH (Lorget et al., 2015). The solutions were placed in cuvettes and the signals were recorded with Fluorotron. The signal vs concentration relationship was used to derive the calibration equations. In the case of fluorescein, the pre-calibrated instrument reports the actual concentrations and there was no need for calibration solutions.

The vitreal concentrations of the compounds as a function of time were obtained and used for kinetic calculations. PKSolver (Zhang et al., 2010) software was used to estimate pharmacokinetic parameters (apparent volume of distribution, elimination half-life and and clearance) using one compartment model with first order elimination kinetics. Weighting (1/(observed concentration)) was used to obtain reliable fitting even at low concentrations

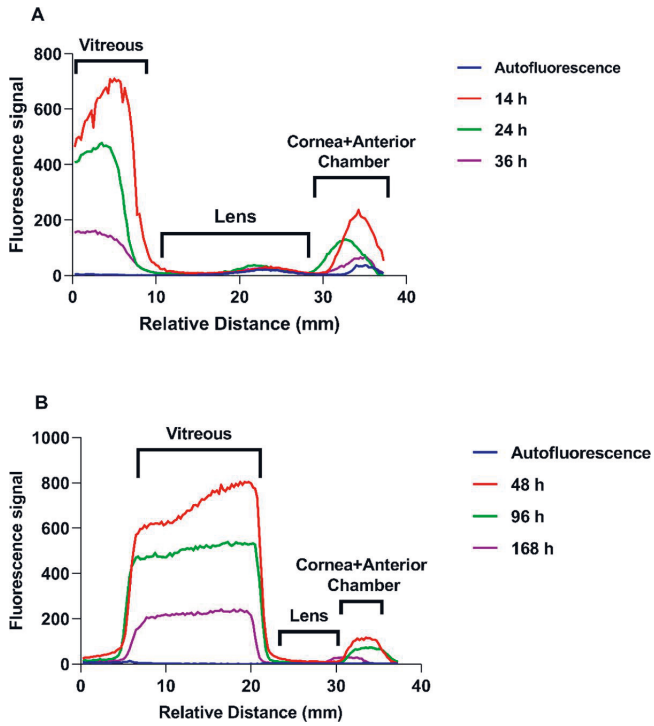


**Fig. 2.** Example of fluorophotometric scans before (autofluorescence) and after intravitreal injections of FITC-dextran 10 kDa to a rat (A) and a rabbit (B). The colours indicate different times of scanning post-injection.

## 3. Results

### 3.1. Calibration and fluorophotometry scans in rats and rabbits

The relationships between fluorescence signals and concentrations of the compounds show linearity ($R^2 = 0.996–0.999$) over broad range of concentrations (Fig. 1). As examples, the fluorophotometric scans of one rat and one rabbit eye after injections of FITC-dextran 10 kDa at different time points are shown in Fig. 2. The figure illustrates the decline of fluorescence levels in the vitreous and anterior part (cornea and anterior chamber) with time in the rat and rabbit eyes.

### 3.2. Intravitreal pharmacokinetics in rat

The log-linear concentration vs time profiles of intravitreal FITC-dextrans (10, 150 and 500 kDa) in rats are shown in Fig. 3. Each fitted line shows the first-order elimination profile of one eye. The kinetic parameters are compiled in Table 1. The apparent volumes of distribution are moderately higher (averages 73–186 μl) than the anatomical volume of rat vitreous (≈ 50 μl) (Sha and Kwong, 2006). The average half-lives of elimination are 13–34 h and the clearances are 2.1–4.5 μl/h. Clearance decreased with increasing average molecular weight of the polymers (Fig. 5). The short elimination half-life of fluorescein (1 h; from the literature) is explained by its low molecular weight and active transport across the retinal pigment epithelium.

### 3.3. Intravitreal pharmacokinetics in rabbit

The log-linear graphs (Fig. 4) show that elimination of the intravitreal compounds followed first-order kinetics in the rabbit vitreous. Each fitted line shows the elimination profile of one eye. The range of the elimination half-lives are from a few hours (fluorescein) to about one week (FITC-dextrans 157 and 500 kDa) (Table 2). The apparent volumes of distribution (1.2–2.6 ml) are in the range of anatomical volume of the rabbit vitreous (≈ 1.7 ml) (Missel et al., 2010). The average elimination half-life and clearance of FITC-dextran 500 kDa were 183% and 27% of those for FITC-dextran 10 kDa, respectively. The elimination half-life of FITC-dextran 157 kDa (166 h) obtained from literature was similar to FITC-dextran 500 kDa (152 h) in our study. The results of Tables 1 and 2 are valid under the assumption that the regression lines of Figs. 3 and 4 are linear.

### 3.4. Rat-to-rabbit scaling factors

Half-life and clearance (Fig. 5) of intravitreal compounds changed with increasing molecular size of the compounds in both rats and rabbits.

The relative differences in the values of rat and rabbit pharmacokinetic parameters are shown in Table 3. The area under the curve (AUC) in the vitreous describes the total drug exposure, and it is inversely related to the intravitreal clearance (AUC = Dose/CL). Thus, the dose scaling factor for equal drug exposure (AUC) in rabbits and in rats is defined as $D_{rabbit}/D_{rat} = (CL_{rabbit}/CL_{rat})$. The rat-to-rabbit scaling factor for fluorescein is 8.3, whereas the range of the scaling factors of FITC-dextrans is 1.9–4.9 for the macromolecules.

The scaling of doses for 10 kDa macromolecule based on different exposure targets were simulated (Fig. 6). The simulations are based on pharmacokinetic parameters of intravitreal FITC-dextran 10 kDa. In Fig. 6A, intravitreal dose of 260 μg is given to rabbit, resulting in initial concentration of 100 μg/ml. The same initial concentration is obtained in the rat with the dose of 8.8 μg, but AUC and drug retention time (the time to reach 10 μg/ml that is 10% of the initial concentration) are much lower in the rat than in rabbit. When the intravitreal dose to rat is increased to 54.2 μg to get the same AUC as in rabbit, the initial concentration in rat becomes 6 times higher, but the retention time is still much shorter than in rabbit. At the same dose in both species (260 μg),

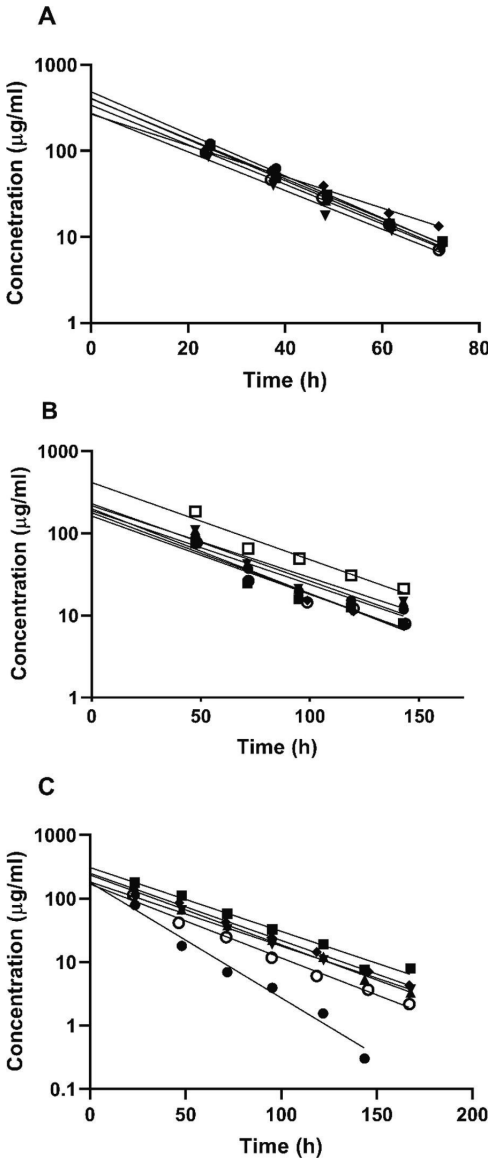


**Fig. 3.** Concentration-time profiles of individual injections in rat vitreous after intravitreal injections. A) FITC-dextran 10 kDa, B) FITC-dextran 150 kDa and C) FITC-dextran 500 kDa.

the initial concentration in rat becomes about 30 times higher than in rabbit, potentially causing toxicity, but yet concentration of 10 μg/ml is reached faster in rat. When the same retention time is targeted, the dose in rat becomes unrealistic, as the initial concentration is more than 100,000 times higher than in the rabbit (Fig. 6A). Fig. 6B shows similar scenarios using rat as the reference (dose 8.8 μg). For example, when the doses in rabbits are 42.5 μg and 37.8 μg, the AUC and retention time, respectively, are similar in both species, but the initial concentration in the rabbit is 15% of the rat value. The simulations based on the kinetic parameters of FITC-dextran 500 kDa are shown in the supplement (Supplement, chapter A, Fig. S1).

**Table 1**
Kinetic parameters of intravitreally injected compounds in rats (average ± SD). The values for fluorescein are from Krupin et al., (1982). $C_{max}$ was derived from the y-intercept of Figs. 3A, 3B and 3C.

| Compound | Number of eyes | Dose per eye (μg) | Apparent volume of distribution (μl) | Elimination half-life (h) | $C_{max}$ (μg/ml) | Clearance (μl/h) |
|---|---|---|---|---|---|---|
| Fluorescein [a] | 20 | 5 | 50 | 1.05 ± 0.07 | n.r[b] | 33 ± 2.2 |
| FITC-dextran 10 kDa | 6 | 30 | 88 ± 22 | 13.5 ± 1.6 | 359 ± 86 | 4.5 ± 0.8 |
| FITC-dextran 150 kDa | 6 | 30 | 186 ± 57 | 34.1 ± 1.4 | 180 ± 78 | 3.8 ± 1.2 |
| FITC-dextran 500 kDa | 6 | 15 | 73 ± 17 | 26.6 ± 5.4 | 215 ± 52 | 2.1 ± 0.9 |

[a] The values are from literature (Krupin et al., 1982), where they reported the vitreal elimination half-life of fluorescein in pigmented rats after intravitreal injection. The clearance was calculated by using the average of anatomical volume of vitreous (50 μl) (Sha and Kwong, 2006).
[b] Not reported.

## 4. Discussion

We utilized non-invasive fluorophotometry to evaluate the effect of molecular weight on intravitreal pharmacokinetics in rats and rabbits. Drug concentrations have not been monitored in the rats after intravitreal injections, but intravitreal pharmacokinetics in rabbits has been investigated in many studies (for see ref. (del Amo et al. (2015)). In those invasive studies vitreous was isolated from the eyes of sacrificed rabbits and drug concentrations were analyzed using LC/MS, radiochemical methods or ELISA (Kwak and D'Amico, 1992; Laurent and Fraser, 1983; Sinapis et al., 2011). In such studies, intravitreal clearance at molecular weights of 7–149 kDa were in the range of 11–71 μl/h (del Amo et al., 2015). We obtained similar values (5.9–21.6 μl/h) at mean molecular weights of 10–500 kDa (Table 2), which supports previous suggestion (Dickmann et al., 2015) about the utility of non-invasive fluorophotometry in vitreal pharmacokinetic studies of macromolecules. However, the method is not useful in the pharmacokinetic assays of small molecule drugs, because fluorescent labeling would change the molecular properties and pharmacokinetics of such compounds.

To the best of our knowledge this is the first study on intravitreal pharmacokinetics in rats. Our main findings are the following: 1) Intravitreally injected macromolecules are retained longer in the vitreous of the rabbits than in the rats. The vitreal half-lives in the rabbit eyes are 5–6 times longer than in the rats (Fig. 5). 2) Intravitreal clearance values of macromolecules in the rabbits are 2–5 times higher than in the rats, suggesting that average intravitreal doses per day should be 2–5 times higher in the rabbits than in the rats (Table 3). 3) Increasing molecular weight decreased the rate of vitreal elimination in both species.

Like in the rabbits (Rimpelä et al., 2018), the intravitreal clearance (≈ 2–5 μl/h) of macromolecules in the rats is clearly slower than the rate of aqueous humor outflow (18 μl/h) (Mermoud et al., 1996; Toris, 2008), suggesting that the same mechanisms, dominant anterior elimination and limited posterior elimination (Maurice and Mishima, 1984), regulate vitreal pharmacokinetics of macromolecules in rats and rabbits. Clearance is smaller than aqueous humor outflow, because the access of the intravitreal compounds to the anterior chamber is limited by the lens and iris-ciliary body. Hutton-smith et al. (2016) propose that the vitreal elimination of macromolecules to the anterior chamber is controlled by their diffusion in the vitreous (Supplement, chapter B). Fluorescein clearance was faster than the aqueous humor outflow in rats (CL = 33 μl/h; outflow 18 μl/h) and rabbits (CL = 273 μl/h; outflow 180 μl/h) indicating significant posterior clearance via blood-retina barrier.

Shorter vitreal residence time in the rats, as compared to the rabbits, may be explained based on smaller vitreal volume in rats (≈ 0.05 ml) than in rabbits (≈ 1.7 ml). Larger apparent volume of distribution prolongs the half-life of elimination ($t_{1/2} = ln\ 2 \times V/CL$). On the other hand, vitreal clearance of rabbits is higher than in rats (Fig. 5). This is due to the larger surface area of blood-ocular barriers, higher diffusional area in the vitreous and faster aqueous humor outflow in rabbits. Similar trends were seen in a SPECT/CT imaging study on intravitreal elimination in mouse, i.e. mice data showed shorter half-lives and smaller clearance values than the values in the rabbits (del Amo et al., 2015; Schmitt et al., 2019).

Rats are widely used in efficacy and safety studies of intravitreally injected compounds (Grossniklaus et al., 2010), but data on intravitreal pharmacokinetics in rats is not available. Herein, we publish the first scaling factors for rat-to-rabbit translation. The dose scaling factors indicate that 2–5 times higher doses of macromolecules (mw. ≈ $10^4$–$10^6$ Da) should be used in rabbits to achieve similar drug exposure (AUC) in the posterior eye segment, whereas a larger scaling factor (≈ 8) may be necessary for smaller molecule (Table 3). As a scaling factor of 1.4 has been reported for rabbit-to-man translation (del Amo et al., 2015), we estimate that the dose scaling factor for rat-to-man translation is about 3–7. The rat scaling factors are obviously smaller than the estimated scaling factors for mouse-to-rabbit (≈ 84) and mouse-to-man (≈ 118) (Schmitt et al., 2019).

The species differences in intravitreal pharmacokinetics are of practical significance. Short drug retention in the rat vitreous leads to short drug exposure, possibly causing misleading conclusions on drug response or toxicity (Iriyama et al., 2007; Kim and Csaky, 2010; Sakai et al., 2007; Thaler et al., 2010). Average daily doses of drugs during multiple or constant dosing regimen are inversely related to the intravitreal clearance, i.e. 2–5 times higher daily doses of macromolecules are needed in rabbits than in rats. For example, drug release rate from an ocular controlled release system should be 2–5 times higher in the rabbits than in the rats (Supplement, chapter C). Since repeated intravitreal injections are problematic in small rat eyes (Sakai et al., 2007), single dose experiments are frequently used in drug testing. Depending on the pharmacological features and study goals, the investigator must select the criterion of translation, e.g. the same average drug exposure over time (AUC based approach), time period above threshold drug concentration, or the same initial concentration.

Pharmacokinetic differences between rat and rabbit eyes complicate drug dosing issues in translational studies. The same principles operate in rat-to-human translation, but in that case the differences are even more pronounced. Overall, the scaling factors are recommended in the dose selection, but the duration of drug retention in the rat eye anyway tends to be shorter than in the rabbit or human eyes. On the other hand, the peak concentrations in the rat eyes will be much higher than in the rabbit eyes, and potentially toxic, if similar doses are used in both species.

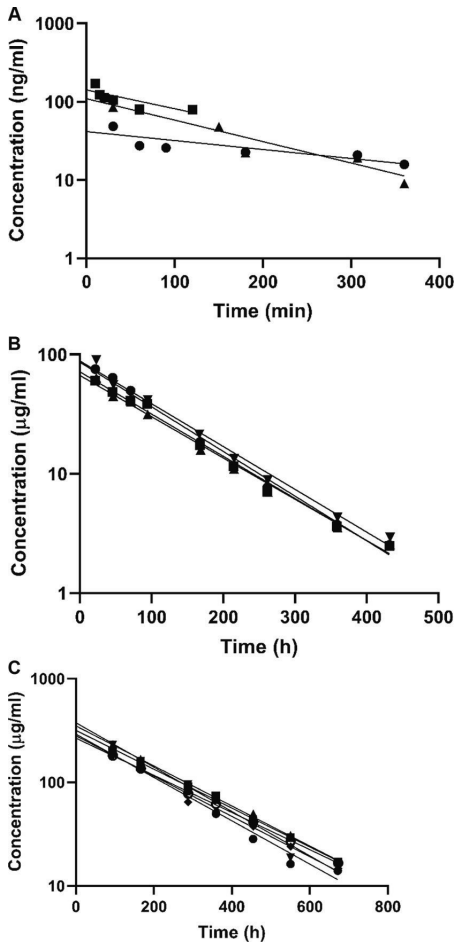


**Fig. 4.** Concentration-time profiles of intravitreally injected A) fluorescein, B) FITC-dextran 10 kDa and C) FITC-dextran 500 kDa in the rabbit vitreous.

**Table 2**
Kinetic parameters of the intravitreally injected compounds in the rabbit vitreous (average ± SD). The values for FITC-dextran 157 kDa are from Johnson and Maurice (Johnson and Maurice, 1984). $C_{max}$ was derived from the y-intercept of Fig. 4A, 4B and 4C.

| Compound | Number of eyes | Dose per eye (μg) | Apparent volume of distribution (ml) | Elimination half-life (h) | $C_{max}$ (μg/ml) | Clearance (μl/h) |
|---|---|---|---|---|---|---|
| Fluorescein | 3 | 0.08 | 1.2 ± 0.97 | 3.0 ± 2.2 | 0.09 ± 0.05 | 273 ± 69 |
| FITC-dextran 10 kDa | 4 | 200 | 2.6 ± 0.35 | 83 ± 3 | 77.8 ± 10.3 | 21.6 ± 2.4 |
| FITC-dextran 157 kDa [a] | 14 | 1000 to 2000 | 1.7 | 166.3 ± 16.8 | n.r[b] | 7.1 ± 0.7 |
| FITC-dextran 500 kDa | 6 | 400 | 1.3 ± 0.18 | 152 ± 13 | 314 ± 45 | 5.9 ± 0.7 |

[a] The values are from literature (Johnson and Maurice, 1984), where they reported the vitreal elimination half-life of FITC-dextran of 157 kDa in pigmented rabbits after intravitreal injection. Anatomical volume of rabbit vitreous (1700 μl) (Missel et al., 2010) was used to estimate the clearance (ie. clearance = vitreous volume × elimination rate constant).
[b] Not reported.

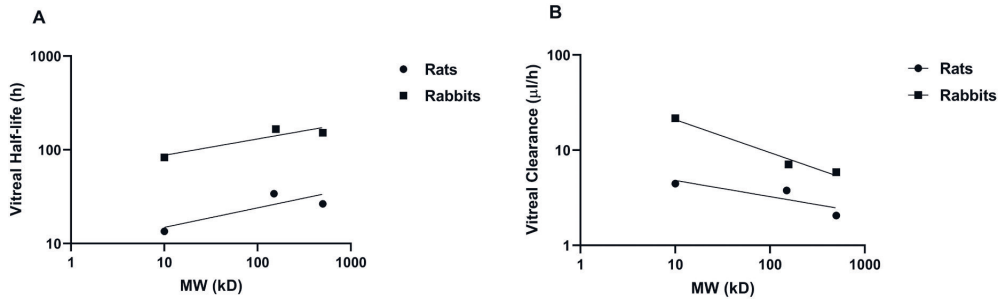


**Fig. 5.** Intravitreal half-life (A) and clearance (B) in rat and rabbit eyes as a function of average molecular weights of the injected compounds. A) Equations of the fitted lines for half-lives in rats and rabbits are $y = 9.22x^{0.208}$ and $y = 58.55x^{0.174}$, respectively. B) Equations of the fitted lines for clearances in rats and rabbits are $y = 7.1x^{-0.169}$ and $y = 46.41\ x^{-0.345}$, respectively. For nonlinear fitting, 1/^Y weighting method were used.

**Table 3**
Relative differences (rabbit/rat values) for intravitreal volume of distribution, clearance and half-life. Dose scaling factor was calculated as $CL_{rabbit}/CL_{rat}$.

| Compound | Apparent volume of distribution | Clearance | Elimination half-life | Dose scaling factor for equal AUC |
|---|---|---|---|---|
| Fluorescein | 24 | 8.3 | 2.9 | 8.3 |
| FITC-dextran 10 kDa | 29 | 4.8 | 6.1 | 4.8 |
| FITC-dextran 150 kDa | 9.1 | 1.9 | 4.9 | 1.9 |
| FITC-dextran 500 kDa | 18 | 2.8 | 5.7 | 2.8 |

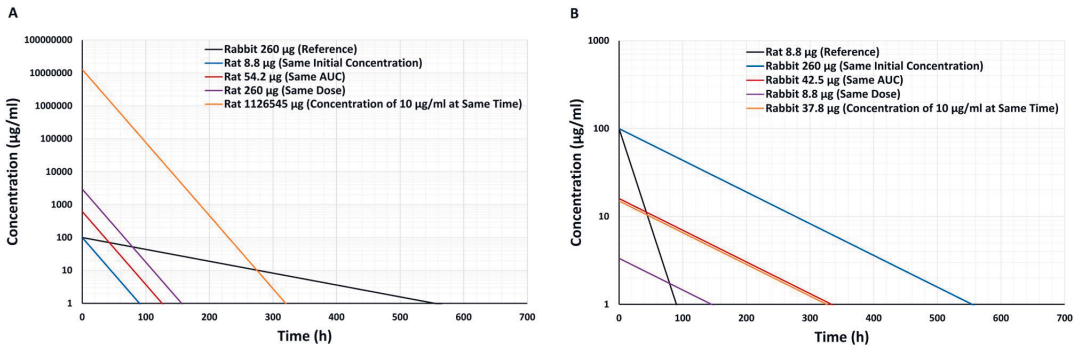


**Fig. 6.** Dose translation for the intravitreal injection of a macromolecule with the molecular weight of 10 kDa. The average pharmacokinetic parameters for FITC-dextran 10 kDa were used in the simulations: clearance (rabbit 21.6 μl/h, rat 4.5 μl/h), apparent volume of distribution (rabbit 2600 μl, rat 88 μl) and elimination half-life (rabbit 83 h, rat 13.5 h). A) Rabbit to rat translation. Rabbit dose was 260 μg to get an initial concentration of 100 μg/ml (black line). The doses in rats were selected to match the following values in the rabbit simulation: initial drug concentration (blue), AUC (red), dose (purple) and concentration of 10 μg/ml at the same time to describe the drug retention time (orange). B) Rat to rabbit translation. Rat dose was 8.8 μg.

## 5. Conclusion

Overall, the results of this study reveal faster rate of vitreal elimination in rats than in rabbits. Drug retention in the rabbit eyes is longer, but clearance values are higher than in the rat eyes. Rat-to-rabbit scaling factor of 2–5 was obtained for intravitreal macromolecules. This comparison provides useful translational information for the design of pharmacological and toxicological studies during ophthalmic drug discovery and development.

## Credit author statement

***Amir Sadeghi:***Experimental work, Writing, Pharmacokinetics modeling. ***Jooseppi Puranen:*** Experimental work, Methodology. ***MarikaRuponen:*** Supervision, Conceptualization, Writing, Editing and Reviewing. ***Annika Valtari:***Experimental work. ***Astrid SubriziSupervision,*** Writing, Editing and Reviewing. ***Veli-Pekka Rana:***Supervision, Conceptualization, Pharmacokinetics Modelling. ***Elisa Toropainen:***Experimental work, Supervision, Methodology. ***Arto Urtti:*** Supervision, Conceptualization, Pharmacokinetics Modelling, Writing, review & editing.

## Acknowledgements

Grant support from EU-ITN project OCUTHER (H2020-MSCA-ITN-2016, 722717) is acknowledged. Arto Urtti acknowledges the support from Russian Government Mega-Grant 14.W03.031.0025 "Biohybrid technologies for modern biomedicine".

## Supplementary materials

Supplementary material associated with this article can be found, in the online version, at doi:10.1016/j.ejps.2021.105720.

## References

Araie, M., Maurice, D.M., 1991. The loss of fluorescein, fluorescein glucuronide and fluorescein isothiocyanate dextran from the vitreous by the anterior and retinal pathways. Exp. Eye Res. 52, 27–39.

Bakri, S.J., Snyder, M.R., Reid, J.M., Pulido, J.S., 2007. Pharmacokinetics of Intravitreal Ranibizumab (Lucentis) 2179–2182. https://doi.org/10.1016/j.ophtha.2007.09.012.

del Amo, E.M., Urtti, A., Eva, M., Urtti, A., del Amo, E.M., Urtti, A., 2015. Rabbit as an animal model for intravitreal pharmacokinetics: clinical predictability and quality of the published data. Exp. Eye Res. 137, 111–124. https://doi.org/10.1016/j.exer.2015.05.003.

Dickmann, L.J., Yip, V., Li, C., Abundes, J., Maia, M., Young, C., Stainton, S., Hass, P.E., Joseph, S.B., Prabhu, S., Andrew Boswell, C., 2015. Evaluation of fluorophotometry to assess the vitreal pharmacokinetics of protein therapeutics. Investig. Ophthalmol. Vis. Sci. 56, 6991–6999. https://doi.org/10.1167/iovs.15-17457.

Fuchs, H., Igney, F., 2017. Binding to ocular albumin as a half-life extension principle for intravitreally injected drugs: evidence from mechanistic rat and rabbit studies. J. Ocul. Pharmacol. Ther. 33, 115–122. https://doi.org/10.1089/jop.2016.0083.

Grossniklaus, H.E., Kang, S.J., Berglin, L., 2010. Animal models of choroidal and retinal neovascularization. Prog. Retin. Eye Res. 29, 500–519.

Hughes, A., 1979. A schematic eye for the rat. Vision Res. 19, 569–588.

Hutton-smith, L.A., Gaffney, E.A., Byrne, H.M., Maini, P.K., Schwab, D., Mazer, N.A., Ga, E.A., Byrne, H.M., Maini, P.K., Schwab, D., Mazer, N.A., 2016. A mechanistic model of the intravitreal pharmacokinetics of large molecules and the pharmacodynamic suppression of ocular vascular endothelial growth factor levels by ranibizumab in patients with neovascular age-related macular degeneration. Mol. Pharm. 13, 2941–2950. https://doi.org/10.1021/acs.molpharmaceut.5b00849.

Iriyama, A., Chen, Y.-N., Tamaki, Y., Yanagi, Y., 2007. Effect of anti-VEGF antibody on retinal ganglion cells in rats. Br. J. Ophthalmol. 91, 1230–1233.

Johnson, F., Maurice, D., 1984. A simple method of measuring aqueous humor flow with intravitreal fluoresceinated dextrans. Exp. Eye Res. 39, 791–805.

Kidron, H., Amo, E.M., Vellonen, K., Urtti, A., 2012. Prediction of the Vitreal Half-Life of Small Molecular Drug-Like Compounds 3302–3311. https://doi.org/10.1007/s11095-012-0822-5.

Kim, H., Csaky, K.G., 2010. Nanoparticle–integrin antagonist C16Y peptide treatment of choroidal neovascularization in rats. J. Control. Release 142, 286–293.

Kitano, S., Hori, S., Nagataki, S., 1988. Transport of Fluoresce in in the Rabbit Eye after Treatment with Sodium Iodate 863–870.

Knudsen, L.L., 2002. Ocular fluorophotometry in human subjects and in swine–with particular reference to long-term pharmacokinetics. Acta Ophthalmol. Scand. 80, 1–24.

Kottegoda, S., Pulido, J.S., Thongkhao-on, K., Shippy, S.A., 2007. Demonstration and use of nanoliter sampling of in vivo rat vitreous and vitreoretinal interface. Mol. Vis. 13, 2073–2082.

Krupin, T., Waltman, S.R., Szewczyk, P., Koloms, B., Farber, M., Silverstein, B., Becker, B., 1982. Fluorometric Studies on the Blood-Retinal Barrier in Experimental Animals. Arch. Ophthalmol. 100, 631–634. https://doi.org/10.1001/archopht.1982.01030030633021.

Kwak, H.W., D'Amico, D.J., 1992. Evaluation of the Retinal Toxicity and Pharmacokinetics of Dexamethasone After Intravitreal Injection. Arch. Ophthalmol. 110, 259. https://doi.org/10.1001/archopht.1992.01080140115038.

Lanzetta, P., Mitchell, P., Wolf, S., Veritti, D., 2013. Different antivascular endothelial growth factor treatments and regimens and their outcomes in neovascular age-related macular degeneration: a literature review. Br. J. Ophthalmol. 97, 1497–1507.

Laurent, U.B.G., Fraser, J.R.E., 1983. Turnover of hyaluronate in the aqueous humour and vitreous body of the rabbit. Exp. Eye Res. 36, 493–503.

Lorget, F., Parenteau, A., Carrier, M., Lambert, D., Gueorguieva, A., Schuetz, C., Bantseev, V., Thackaberry, E., 2015. Characterization of the pH and temperature in the rabbit, pig, and monkey eye: key parameters for the development of long-acting delivery ocular strategies. Mol. Pharm. 13, 2891–2896. https://doi.org/10.1021/acs.molpharmaceut.5b00731.

Maurice, D.M., Mishima, S., 1984. Ocular pharmacokinetics. Pharmacology of the Eye. Springer, pp. 19–116.

Mermoud, A., Baerveldt, G., Minckler, D.S., Prata, J.A., 1996. Aqueous humor dynamics in rats 198–203.

Missel, P.J., Horner, M., Muralikrishnan, R., 2010. Simulating dissolution of intravitreal triamcinolone acetonide suspensions in an anatomically accurate rabbit eye model. Pharm. Res. 27, 1530–1546.

Murata, Y., Kaidoh, T., Inoué, T., 1998. Ultrastructural changes of the myoepithelium of the dilator pupillae during miosis and mydriasis in the rat iris. Arch. Histol. Cytol. 61, 29–36.

Nair, G., Kim, M., Nagaoka, T., Olson, D.E., Thulé, P.M., Pardue, M.T., Duong, T.Q., 2011. Effects of common anesthetics on eye movement and electroretinogram. Doc. Ophthalmol. 122, 163–176.

Potter, D.E., Ogidigben, M.J., 1991. Medetomidine-induced alterations of intraocular pressure and contraction of the nictitating membrane. Invest. Ophthalmol. Vis. Sci. 32, 2799–2805.

Raines, M.F., 1988. Vitreous fluorophotometry: a review. J. R. Soc. Med. 81, 403–406.

Rimpelä, A., Kiiski, I., Deng, F., Kidron, H., Urtti, A., 2018. Pharmacokinetic Simulations of Intravitreal Biologicals : Aspects of Drug Delivery to the Posterior and Anterior Segments 9–11. https://doi.org/10.3390/pharmaceutics11010009.

Robinson, M.R., Baffi, J., Yuan, P., Sung, C., Byrnes, G., Cox, T.A., Csaky, K.G., Fi, J.B.A. F., Division, P.S., 2002. Safety and pharmacokinetics of intravitreal 2-methoxyestradiol implants in normal rabbit and pharmacodynamics in a rat model of choroidal neovascularization. Exp. Eye Res. 74, 309–317. https://doi.org/10.1006/exer.2001.1132.

Sakai, T., Kuno, N., Takamatsu, F., Kimura, E., Kohno, H., Okano, K., Kitahara, K., 2007. Prolonged protective effect of basic fibroblast growth factor–impregnated nanoparticles in royal college of surgeons rats. Invest. Ophthalmol. Vis. Sci. 48, 3381–3387. https://doi.org/10.1167/iovs.06-1242.

Schmitt, M., Hippeläinen, E., Ravina, M., Arango-Gonzalez, B., Antopolsky, M., Vellonen, K.-S., Airaksinen, A.J., Urtti, A., 2019. Intravitreal pharmacokinetics in Mice: SPECT/CT imaging and scaling to rabbits and humans. Mol. Pharm. 16, 4399–4404.

Sha, O., Kwong, W.H., 2006. Postnatal developmental changes of vitreous and lens volumes in Sprague-Dawley rats. Neuroembryol. Aging 4, 183–188.

Shah, M., Cabrera-Ghayouri, S., Christie, L.-A., Held, K.S., Viswanath, V., 2019. Translational preclinical pharmacologic disease models for ophthalmic drug development. Pharm. Res. 36, 58.

Sinapis, C.I., Routsias, J.G., Sinapis, A.I., Sinapis, D.I., Agrogiannis, G.D., Pantopoulou, A., Theocharis, S.E., Baltatzis, S., Patsouris, E., Perrea, D., 2011. Pharmacokinetics of intravitreal bevacizumab (Avastin®) in rabbits. Clin. Ophthalmol. (Auckland, NZ) 5, 697.

Thaler, S., Fiedorowicz, M., Choragiewicz, T.J., Bolz, S., Tura, A., Henke-Fahle, S., Yoeruek, E., Zrenner, E., Bartz-Schmidt, K., Ziemssen, F., 2010. Toxicity testing of the VEGF inhibitors bevacizumab, ranibizumab and pegaptanib in rats both with and without prior retinal ganglion cell damage. Acta Ophthalmol. 88 e170–e176.

Toris, C.B., 2008. Aqueous humor dynamics I. Measurement methods and animal studies. Curr. Top. Membr. 62, 193–229. https://doi.org/10.1016/S1063-5823(08)00407-9.

Zeimer, R.C., Blair, N.P., Cunha-Vaz, J.G., 1983. Vitreous fluorophotometry for clinical research: I. Description and evaluation of a new fluorophotometer. Arch. Ophthalmol. 101, 1753–1756.

Zhang, Y., Huo, M., Zhou, J., Xie, S., 2010. PKSolver: an add-in program for pharmacokinetic and pharmacodynamic data analysis in Microsoft Excel. Comput. Methods Programs Biomed. 99, 306–314.

# Publication III

Journal of Controlled Release 327 (2020) 584–594

Contents lists available at ScienceDirect

Journal of Controlled Release

journal homepage: www.elsevier.com/locate/jconrel

# Release of functional dexamethasone by intracellular enzymes: A modular peptide-based strategy for ocular drug delivery

Madhushree Bhattacharya[a,b,*], Amir Sadeghi[b], Sanjay Sarkhel[a], Marja Hagström[a], Sina Bahrpeyma[a,b], Elisa Toropainen[b], Seppo Auriola[b], Arto Urtti[a,b,c]

[a] Drug Research Programme, Division of Pharmaceutical Biosciences, University of Helsinki, Helsinki, Finland
[b] School of Pharmacy, University of Eastern Finland, Kuopio, Finland
[c] Institute of Chemistry, Saint-Petersburg State University, Peterhoff, Russian Federation

ARTICLE INFO

*Keywords:*
Peptide
Conjugate
Dexamethasone
Drug delivery
Retinal pigment epithelium
Intravitreal
Pharmacokinetics

ABSTRACT

Tissue barriers limit drug delivery in the eye. Therefore, retinal diseases are treated with intravitreal injections. Delivery systems with reduced dosing frequency and/or cellular drug delivery properties are needed. We present here a modular peptide-based delivery system for cell targeted release of dexamethasone in the retinal pigment epithelial cells. The peptide–dexamethasone conjugates consist of cell penetrating peptide, enzyme cleavable linker and dexamethasone that is conjugated with hydrazone bond. The conjugates are chemically stable in the vitreous, internalize into the retinal pigment epithelial cells and release dexamethasone intracellularly by enzymatic action of cathepsin D. *In vitro* binding assay and molecular docking confirm binding of the released dexamethasone fragment to the human glucocorticoid receptor. *In vivo* rabbit studies show increased vitreal retention of dexamethasone with a peptide conjugate. Modular peptide conjugates are a promising approach for drug delivery into the retinal cells.

## 1. Introduction

Ocular drug delivery poses significant challenges due to the unique anatomy and physiology of the eye. Various static and dynamic barriers limit efficient drug delivery, particularly to the posterior segment of the eye [1–3]. Therapeutic intervention of the posterior segment is crucial for many vision-threatening diseases, such as age-related macular degeneration, glaucoma, macular edema, diabetic retinopathy, and uveitis. These diseases cause disorders in the retina and choroid, thereby leading to impaired vision and blindness in millions of patients worldwide.

Topical eye drops are useful in the treatment of anterior segment diseases in the eye but they are ineffective in the treatment of retinal diseases. Several tissue barriers and flow factors limit drug distribution from topical application site to posterior segment tissues [4–6]. Tight tissue barriers between blood stream and ocular compartments (anterior, posterior) prevent drug distribution from the blood circulation into the ocular drug target tissues [7]. Alternative modes of ocular drug administration, such as sub-conjunctival, suprachoroidal, and periocular injections, have only achieved sub-optimal retinal drug delivery [8]. For these reasons, intravitreal injections are widely used even though it is an invasive method of retinal drug delivery. In the case of intravitreal drug delivery, it is important to ascertain delivery to the retinal target cells and adequate duration of drug action. Consequently, novel drug delivery systems are needed for intravitreal drug administration [9].

Current drug delivery systems for clinical treatment of the posterior segment diseases include intravitreal injection of drug solutions and implants [10,11]. For example, Ozurdex is a dexamethasone releasing injectable, degradable implant that is used to treat macular edema and inflammation of the eye [12]. Nonetheless, many implants comprise of non-degradable polymers that are used to control drug release for several months and might require surgical intervention; limiting their wide-spread clinical use [13,14]. Also, particulate based systems for intravitreal administration have been investigated [6]. Both implants and particulate systems might however obstruct vision and possible toxicity arising from polymer degradation products is of concern. Furthermore, their physical size does not allow targeted delivery to the retinal cells [5]. Development of alternative drug delivery systems are thus needed to meet the therapeutic challenges of retinal diseases.

Intravitreally administered small molecules are rapidly eliminated from the vitreous and they distribute non-specifically to ocular tissues and may cause adverse effects, such as increased intraocular pressure and cataract associated with corticosteroid treatment [4,15]. One

* Corresponding author at: Drug Research Programme, Division of Pharmaceutical Biosciences, University of Helsinki, Helsinki, Finland.
*E-mail address:* madhushree.bhattacharya@helsinki.fi (M. Bhattacharya).

https://doi.org/10.1016/j.jconrel.2020.09.005
Received 23 June 2020; Received in revised form 27 August 2020; Accepted 3 September 2020
Available online 08 September 2020

approach to mitigate side effects and rapid elimination of small molecule drugs is to form drug conjugates for targeted delivery and controlled release. Polymeric and antibody drug conjugates have been well investigated in the context of cancer therapy [16], but this concept has not been extensively explored for ocular drug delivery. A recent report introduced hyaluronic acid binding polypeptide chain to successfully prolong the half-life of protein drug [17]. We reported a peptide-based delivery system for controlled release of peptide cargo (D-peptides) within the intra-cellular space of the retinal pigment epithelial cells [18]. The peptide-based strategy utilized linkers that were cleaved by the enzymes present in the RPE cells to release the cargo. Additionally, the peptide-cargo conjugates were stable within the vitreous environment to avoid premature drug release in the vitreous. The modular delivery system consisted of three components: (a) cell penetrating peptide to promote intracellular entry, (b) peptide linker with controlled enzymatic cleavage rate and (c) D-peptide cargo. Notably, the peptide-based delivery system offers advantages of relative ease of synthesis, targeted intracellular delivery and controlled release of cargo exploiting intracellular components (enzyme cathepsin D) of the retinal cells.

In the present study, we demonstrate the potential of the modular peptide-based system for the retinal cellular delivery of dexamethasone. Dexamethasone is used in ophthalmology to treat ocular inflammations and uveitis in both anterior and posterior segments [19], but the use of dexamethasone is associated with side-effects, such as increased intraocular pressure and cataract formation [20]. Consequently, to overcome such effects, alternative delivery systems are desired for controlled or sustained release of dexamethasone at the site of action. We report here targeted and controlled release of dexamethasone from modular peptide-based delivery system within the retinal pigment epithelial cells.

## 2. Materials and methods

### 2.1. Design and synthesis of conjugates

#### 2.1.1. Design of peptide-dexamethasone conjugates

A set of three peptide-dexamethasone conjugates (Scheme 1) were synthesized based on our previous findings [18]. The conjugates consisted of three components: (1) N-terminal cell penetrating peptide (CPP) to promote intracellular entry, (2) an enzyme cleavable peptide-based linker (PCL) and (c) dexamethasone conjugated to the C-terminal of PCL via hydrazone linkage. Fluorescent Alexa 488 dye was covalently attached to the conjugates. The differences between the three conjugates are entirely attributed to the CPPs with varying number of positively charged residues (Arg/Lys) (Scheme 1). Dex-1 contains a cationic CPP (from HIV-1 Tat) with 7 Arg/Lys residues, Dex-2 contains 2 Lys/Arg residues in the CPP sequence and Dex-3 consists of a hydrophobic CPP sequence [21].

#### 2.1.2. Peptide synthesis

The peptide-dexamethasone conjugates (Scheme 1, Table 1) were synthesized by Peptide Synthetics Peptide Protein Research Ltd. (Hampshire, UK). In general, the peptides were synthesized using solid phase peptide synthesis. Chlorotrityl resin (Iris, 300 mg, per sequence, 200 mesh, 1.1 mmol/g chloride loading) was functionalized by mixing the resin in dry dimethyl formamide (DMF) with hydrazine (0.5 equivalents) for 30 min. Un-functionalized sites on the resin were capped with a brief treatment of methanol in DMF containing DIPEA (0.25 ml), to obtain a working substitution level of 0.3–0.5 mmol/g. The hydrazine resin obtained was then employed to generate peptides with the desired sequence via an automated peptide synthesizer (Symphony, Protein Technologies Inc. Arizona) using the Fmoc chemistry method [22] with Fmoc amino acids appropriately side chain protected (Matrix Innovation). After the synthesis, the hydrazide peptides were cleaved from the solid support and their side chain protecting groups were removed with trifluoroacetic acid (TFA) cocktail containing 2% isopropyl silane, 1% phenol and 2% ethane dithiol for 2 h. The TFA solution was filtered from the resin and the crude peptides precipitated by adding diethyl ether. The precipitated peptides were pelleted by centrifugation.

The peptides were purified by RP-HPLC on a Varian system equipped with a C-18 preparative Axia column (Phenomenex) at room temperature, using a Varian 325 UV-detector with a detection wavelength 225 nm, two 210 Varian pumps with flow rate of 20 ml/min and a gradient of 5–55% acetonitrile in 60 min. Peptides were loaded in dimethyl sulfoxide (DMSO) to the column and eluted with increasing gradient between water (with 0.1% TFA) and acetonitrile (with 0.1% TFA). The eluting peptides were visualized with UV absorption and the fractions were collected manually. The purity of the product-containing fractions was confirmed by LC-MS, combined and freeze-dried.

For peptide labeling with Alexa 488 dye, a cysteine residue was incorporated in the linker sequence between the CPP and PCL (Scheme-1). The side chain thiol of the cysteine was used to react with a maleimido-activated form of the Alexa 488 dye (Invitrogen): 5 mg of maleimido dye was added to the peptide (5 mg dissolved in 50:50 DMSO/PBS, pH 7.4, 2 ml). The mixture was stirred until all the peptide has been labeled (checked by mass spectrometry). Then, the peptide was introduced onto an HPLC column and the labeled peptide was eluted as described above. Purified labeled peptide was freeze-dried.

#### 2.1.3. Synthesis of peptide-dexamethasone conjugates

The synthesized Alexa-labeled C-terminal peptide hydrazide was purified and then condensed with the ketone group of dexamethasone to form the hydrazone linked peptide-drug conjugate. In brief, the labeled peptide (2 mg) was dissolved in DMSO (0.5 ml) and sodium

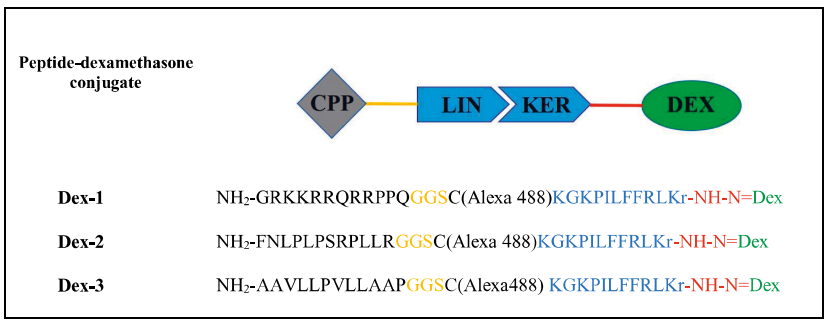


**Scheme 1.** Dexamethasone conjugated to the C-terminus of CPP-PCL chimeras via a hydrazone linkage (red). CPP, PCL sequences and dexamethasone are shown in black, blue and green, respectively. A short flexible linker, Gly-Gly-Ser (shown in yellow) was introduced in between the CPP and PCL sequences. A cysteine residue was introduced after the linker to attach the fluorescent dye Alexa 488 to the side chain thiol of Cys. Lower case single letter amino acid abbreviation refers to a D-amino acid. The D-amino acid enhances the sensitivity and specificity of the linker for cathepsin D mediated cleavage. (For interpretation of the references to color in this figure legend, the reader is referred to the web version of this article.)

**Table 1**
Peptide-dexamethasone conjugates and corresponding fragments after intracellular cleavage.

| Conjugate # | Structure of the conjugates | Released fragment | Fragment mass | |
|---|---|---|---|---|
| | | | Calculated | Detected ($MH^{+1}$ Mono) |
| Dex-1 | $NH_2$-GRKKRRQRRPPQGGSC(Alexa 488)KGKPILFFRLKr-NH-N = Dex | r-NH-N = Dex | 562.6 | 563.6 |
| Dex-2 | $NH_2$-FNLPLPSRPLLRGGSC(Alexa 488)KGKPILFFRLKr-NH-N = Dex | r-NH-N = Dex | 562.6 | 563.6 |
| Dex-3 | $NH_2$-AAVLLPVLLAAPGGSC(Alexa488)KGKPILFFRLKr-NH-N = Dex | r-NH-N = Dex | 562.6 | 563.6 |

Fragments were detected by LC-MS. r denotes D-Arginine residue.

acetate buffer (0.1 M, 0.5 ml) was added. A 10-fold molar excess of dexamethasone, pre-dissolved in DMSO, was added and the solution was stirred at 40 °C for 48 h. A further 10-fold molar excess of dexamethasone was added and mixed for another 48 h in case the reaction was not complete (as followed by LC/MS, Phenomenex C18 kinetex core-shell column, 50 × 4.6 mm, 2.6 μm internal diameter with a 100 Å pore size, step gradient of acetonitrile). When the reaction was completed (confirmed by LC/MS), the product was isolated by RP-HPLC as mentioned above.

### 2.2. In vitro stability and binding studies

#### 2.2.1. Stability of conjugates in porcine vitreous

Stability of the peptide-dexamethasone conjugates against degradation in porcine vitreous was determined. Porcine eyes were procured from a local slaughterhouse and the eyes were kept on ice bath during the isolation of vitreous humor. The eyes were first cleansed of extra-ocular material and dipped in 70% ethanol. The eyes were opened by incision with a dissecting knife and the clear vitreous humor was separated gently from the retina. Isolated vitreous humor was homogenized, centrifuged (3200 ×*g*) for 1 h at +4 °C and the supernatant was sterile-filtered using a 0.22 μm filter to remove cellular debris and possible microbial contamination. The vitreous was stored at −80 °C. For stability studies, 10 μM of the conjugates were mixed with porcine vitreous humor with 1% antibiotics (penicillin/streptomycin; Gibco) in Eppendorff tubes. Each time point had designated separate tube. The tubes were incubated at 37 °C and release of dexamethasone from the conjugate was monitored using ultra-performance liquid chromatography tandem mass spectrometry (UPLC-MS/MS). Before the mass analysis, the mixture was subjected to acetonitrile clean-up. Three volumes of cold acetonitrile were added to each sample, vortexed and stored at room temperature for 1 h. The samples were centrifuged for 10 min at 12,000 ×*g* to remove precipitates. The supernatant was freeze-dried and stored at −20 °C for further UPLC-MS/MS analysis.

Liquid chromatography separation was carried out using Waters Acquity UPLC instrument (Waters, MA, USA) coupled with Waters Acquity UPLC BEH Shield RP18 (2.1 × 100 mm, 1.7 μm) column at 50 °C. The mobile phase consisted of 0.1% of formic acid in ultrapure water (A) and 100% of LC-MS grade acetonitrile (B). Freeze dried samples were diluted with cold 30% LC/MS grade acetonitrile (Chromasolv™, Honeywell, Seelze, Germany) in ultrapure water, and vortexed prior to the analysis. Mass spectrometry measurements were carried out using a Waters Xevo triple quadrupole mass spectrometer (TQ-S) equipped with an electrospray (ESI) source. Samples were analyzed on positive ionization mode and multiple reaction monitoring (MRM) mode was used for quantification. Minimum of five calibration curve points in the range 0.005–250 nM were used for quantification of the dexamethasone. The resulting data were analyzed with Waters MassLynx software V4.1.

#### 2.2.2. Interactions of conjugates with the vitreous humor

Binding of peptide-dexamethasone conjugates to the porcine vitreous was studied by microscale thermophoresis (MST). MST is a biophysical technique used to study the molecular interaction by monitoring the directed movement of fluorescently labeled molecule in a temperature gradient [23–25]. The MST measurements were performed using a Monolith NT.115 instrument from Nanotemper Technologies (München, Germany) with MST grade premium NT.115 capillaries. Literature precedence's suggest that cationic particulate systems interact with hyaluronic acid, HA (anionic hydrophilic polymer), a primary component of the vitreous [26,27]. Consequently, for the positively charged peptide-dexamethasone conjugates, we postulate that they interact with vitreous HA. The concentration of HA in porcine vitreous (stock solution) was considered to be 1600 nM based on estimates from earlier reports [28,29]. The unlabeled vitreous (Section 2.2.1) was serially diluted and mixed with 100 nM fluorescently labeled conjugates in MST optimized buffer (50 mM Tris-HCl pH 7.4, 150 mM NaCl, 10 mM $MgCl_2$, 0.05% Tween-20). HA concentration range in the assay mixture was 0.02–800 nM. All the samples were centrifuged at 14,000 ×*g* for 10 min to remove any aggregates present. The samples were loaded into Monolith NT.115 capillaries after incubation at room temperature for 5 min and MST measurements were performed at 22 °C by using nano-blue excitation with LED excitation power 20% and 80% for Dex-2 and 3 respectively, infrared laser (MST power) was set to medium. Data analyses were performed using Nanotemper analysis software. For determination of the dissociation constant ($K_d$) of the binding interaction, normalized fluorescence values were plotted against log of the estimated hyaluronic acid concentration in the porcine vitreous using GraphPad Prism software (version7.04, San Diego, CA, USA).

#### 2.2.3. Binding of Dexamethasone-Arginine fragment to glucocorticoid receptor

Microscale thermophoresis (MST) technique was used to study the binding interaction of Dexamethasone-Arginine (Dex-Arg) fragment and glucocorticoid receptor. The MST measurements were performed using a Monolith NT.115 instrument from Nanotemper Technologies with MST grade premium NT.115 capillaries. Purified human glucocorticoid receptor (hGR, Abcam) was labeled with Lightning-Link® Rapid Alexa Fluor® 488 kit (Expedeon) following manufacturer's instruction. The labeling kit enables direct conjugation of Alexa Fluor® 488 with the available amine groups in the hGR. Unlabeled Dex-Arg fragment was serially diluted from 0.5 μM to 0.015 nM in MST optimized buffer and titrated into a fixed concentration of labeled hGR (10 nM). All the samples were centrifuged at 14,000 ×*g* for 10 min to remove aggregates. The samples were loaded into Monolith NT.115 premium capillaries after incubation at room temperature for 10 min and MST measurements were performed at 22 °C by using 5% LED power and medium MST power. Data analyses were done using Nanotemper analysis software. Normalized fluorescence values were plotted against the log of Dex-Arg fragment concentration using GraphPad Prism software (version7.04, San Diego, CA, USA).

#### 2.2.4. Molecular docking to glucocorticoid receptor

For computational modeling of the Dex-Arg fragment, we utilized the crystal structure of human glucocorticoid receptor (hGR) in complex with dexamethasone (PDB id: 1M2Z). The protein-ligand complex exists as a dimer in the crystal structure. Only a single chain of the receptor was considered for molecular docking. Dexamethasone and other small molecules (including water) were removed from the ligand-

binding domain to generate the native structural model of the hGR as the target protein. 3D-structural models of dexamethasone and Dex-Arg fragment were built by using MarvinSketch (version 20.11.0; http://www.chemaxon.com). CB-Dock server [30] was used to predict the binding modes of dexamethasone and Dex-Arg fragment with the hGR. The best docking results were then compared with the crystal structure complex and visualized using UCSF Chimera package [31].

### 2.3. Cell culture and cell based assays

ARPE-19 cells (human retinal pigment epithelial cell line, ATCC CRL-2302) were cultured in Dulbecco's Modified Eagle Medium: Nutrient Mixture F-12 (DMEM/F-12) supplemented with 10% fetal bovine serum (Gibco), 100 U/ml penicillin, 100 μg/ml streptomycin and 2 mM L-glutamine (Gibco). The cells were cultured in a T-75 flask at 37 °C in a 7% $CO_2$ atmosphere. The cells were sub-cultured once a week until they reached 80% confluency. The culture media was changed twice a week.

#### 2.3.1. Cytotoxicity

Cytotoxicity of the peptide-dexamethasone conjugates was evaluated using MTT assay as previously described [32]. Briefly, the cells were seeded in 96-well plates at a density of 20,000 cells per well in 150 μl of cell growth medium. After over-night incubation, the cells were washed with PBS. Peptides at various concentrations (0.01–100 μM) in complete cell growth medium (100 μl) were added to each well for incubation (5 h at 37 °C, 7% $CO_2$). Poly-L-lysine (PLL) treated and untreated cells served as negative and positive controls, respectively. After incubation, the medium was aspirated, the cells were washed with PBS and 150 μl of growth medium was added to the cells. Then, the cells were washed with PBS after incubation of 24 h. A mixture of 90 μl of complete growth medium and 10 μl of 5 mg/ml of MTT solution was added to the wells and the plates were incubated for 4 h at 37 °C. After incubation, 100 μl of 10% sodium dodecyl sulfate (Merck) in 0.01 M HCl (Sigma-Aldrich) was added to the wells to solubilize formazan crystals followed by overnight incubation at 37 °C. Formazan was quantified by measuring absorbance at 570 nm using a spectral scanning multimode plate reader (Varioskan Flash, Thermo Scientific). Viability of the treated cells was compared to the untreated control cells.

#### 2.3.2. Cellular uptake

ARPE-19 cells were seeded on a 24-well Sensoplate polystyrene flat glass bottom black plates (Greiner bio-one) at a density of 25,000 cells/well and incubated at 37 °C with 7% $CO_2$ for 24 h. The cells were rinsed twice with 2 ml HBSS buffer (Gibco, supplemented with 10 mM Hepes, pH 7.4) and equilibrated in the same buffer for 30 min at 37 °C. The cells were then treated with labeled peptide-dexamethasone conjugates (5 μM) for 1 h at 37 °C. Afterwards cells were washed thrice with HBSS buffer to remove unbound and surface bound conjugates followed by plasma membrane staining with CellMask™ Deep Red (Invitrogen) for 30 min at room temperature in dark. The nuclei were stained with 1 μg/ml Hoechst 33342 for 10 min at room temperature in dark, washed with HBSS to remove excess stain and live cells were imaged immediately using Cytation 5 cell imaging multimode reader (BioTek). Images were taken using 40× plan fluorite phase objective (1,320,518, Olympus) and processed with Gen5 Image Prime software, version 3.08. All images were obtained under identical conditions; the cell nucleus, the cytoskeleton and the conjugates were visualized in blue, deep red and green, respectively.

#### 2.3.3. Intracellular drug release

Intracellular release of dexamethasone from the peptide-dexamethasone conjugates was studied using sub-confluent ARPE-19 cells that were cultured on 6 well plate. The cells were seeded at a density of 500,000 cells/well and experiments were performed 48 h after the cells had achieved sub-confluent monolayer. The conjugates were dissolved in complete growth medium (DMEM/F-12; supplemented with 100 U/ml streptomycin/penicillin and 2 mM L-glutamine). Prior to the experiment, the cells were washed twice with PBS (Gibco) and incubated with the conjugates (5 μM/well) for 1 h at 37 °C. After 1 h, the cells were washed thrice with PBS to remove unbound and surface bound conjugates. The cells were detached from the bottom of the wells using TrypLE Express enzyme (Gibco) and the number of cells harvested from each well was determined. Lysis buffer (Biovision) was added to the cells collected from each well and the cells were lysed following the manufacturer's instructions. Clear cell lysate from each well was collected into low binding Eppendorf tubes and stored on ice before UPLC-MS analyses.

### 2.4. LC-MS analyses

To identify the molecule released from the conjugates in the cells (Section 2.3.3), three volumes of cold acetonitrile were added to the cell lysate samples, vortexed and stored at room temperature for 1 h. The samples were centrifuged for 10 min at 12,000 ×g to remove precipitates. The supernatant was freeze-dried and stored at −20 °C for further UPLC-MS analysis.

UPLC-MS profiling analyses were carried out with Orbitrap-MS System (Q Exactive Focus, Thermo Fisher, Bremen, Germany) using reversed phase (RP) chromatography with positive mode ESI. The RP separation was performed on a Zorbax Eclipse XDB-C18 column (100 mm × 2.1 mm, 1.8 μm; Agilent Technologies). The flow rate was 0.4 ml/min, and gradient elution of 2–100% was used with water with 0.1% *v*/v of formic acid (eluent A) and methanol (eluent B). The injection volume was 10 μL and the sample tray was maintained at 4 °C. For data acquisition, the mass range was 300–1100 amu and 320–1200 amu with a resolution of 70,000. Data acquisition and analysis was conducted with Xcalibur and Freestyle software.

### 2.5. Intravitreal pharmacokinetics

Pigmented 2.5–3.0 kg female Dutch belted rabbits (Linköping, Sweden) were used in the study. The animals were housed under normal diet at a set temperature of 21 °C, humidity and 12/12 h light-dark cycle. All animal experiments were approved by the national Animal Experiment Board in Finland. Free dexamethasone was not included for *in vivo* PK studies to limit the number of animals used and due to limitations of non-invasive fluorophotometry that was employed in the present study.

#### 2.5.1. Intravitreal injections

The animals were anesthetized with medetomidine (Domitor vet 1 mg/ml; Orion Pharma, Espoo, Finland; dose 0.5 mg/kg) and ketamine (Ketalar/Ketaminol vet 50 mg/ml; Pfizer Oy Animal Health, Espoo, Finland; dose 0.5 ml/kg). Pupils were dilated with tropicamide (Oftan Tropicamid 5 mg/ml, Santen Pharmaceutical Co., Ltd., Tampere, Finland) and eyes were locally anesthetized with oxybuprocaine (Oftan Obucain 4 mg/ml, Santen Pharmaceutical Co., Ltd., Tampere, Finland). Viscotears 2 mg/g (carbomer) was used for ocular surface moistening. The 31G disposable needle was inserted, about 4.5 mm out of limbus, through the sclera into the vitreous and 40 μl of the peptide solution with the concentration 125 μM (dose of 5 nmol per eye) was injected into the vitreous. After withdrawing the needle, the eyes were covered with antibiotic ointment in order to avoid infections (chloramphenicol; Oftan Chlora 10 mg/g). Two rabbits were injected with labeled Dex-1 conjugate and two others with labeled Dex2 conjugate in both eyes ($n$ = 4 eyes/peptide). Dex-3 was not included in the pharmacokinetics study, as this particular conjugate had too low fluorescence intensity for Fluorotron assays. This could be due to internal quenching of the fluorescence signal as a consequence of the solution conformation of the peptide conjugate. Atipamezole (Antisedan vet 5 mg/ml; 0.2 ml/kg),

was used after anesthesia to wake the animals.

#### 2.5.2. Fluorotron measurements

*In vivo* fluorophotometry measurements were performed with ocular fluorophotometer (Fluorotron Master, OcuMetrics, CA, USA). The animals were kept under light sedation (Domitor vet 1 mg/ml; 0.3 ml/kg) during the measurements. Baseline autofluorescence values were measured prior to the intravitreal injections. After the injections, the fluorescence levels in the vitreous and aqueous humor were measured daily for 3 days. Bepanthen Eye (sodium hyaluronate 0.15% and dexpanthenol 2%) was used for eye surface moisturizing during the measurements. The average fluorescence signal of vitreous was calculated by averaging in the axial region of eye starting 3 mm anteriorly from retina to the posterior edge of the lens. The distance of 3 mm from the retina decreases artifacts related to the tailing effect of retinal peak [33]. For aqueous humor values, the average of the signal in the middle of the compartment was used and calculated using the program of Flourotron. GraphPad Prism (version7.04, San Diego, CA, USA) was used for fitting concentration vs time curves and calculation of the pharmacokinetic parameters.

## 3. Results

### 3.1. Stability of the conjugates in the vitreous humor

To investigate the stability of the peptide-dexamethasone conjugates in the vitreal environment, the conjugates were incubated with porcine vitreous at 37 °C. All three conjugates were chemically stable in the vitreous humor. No significant quantities of free dexamethasone were detected during the assay period of 6 weeks (Fig. 1). These results ensure that the dexamethasone release takes place only after internalization within the RPE cells. Small quantity of unreacted dexamethasone (< 5%) as impurity was present in all the conjugates (Fig. 1).

### 3.2. Binding of the conjugates to the vitreous humor

Binding of peptide-dexamethasone conjugates to porcine vitreous was evaluated with microscale thermophoresis. Fig. 2 shows the thermophoresis signal from the binding interaction of Alexa 488 labeled conjugates (Dex-2 and Dex-3) and HA present in the vitreous humor. Normalized fluorescence values (Fnorm) plotted against log of HA concentration in porcine vitreous to obtain the binding affinity. The dissociation constants ($K_d$) for the binding of Dex-2 and Dex-3 conjugates to the vitreal HA were 13.5 nM and 64.3 nM, respectively. Dex-1 conjugate was not included in the study due to its adherence to the capillary walls.

### 3.3. Cellular uptake

Internalization of peptide-dexamethasone conjugates to cultured ARPE-19 cells was investigated. Fluorescence microscope images shows that the conjugates were internalized within the ARPE-19 cells without association at the cell surface (Fig. 3).

### 3.4. Cytotoxicity

Fig. 4 summarizes the results of the cytotoxicity assay. ARPE-19 cells tolerate the conjugates well at the concentration range of 0.01–5 μM without significant differences among the conjugates. The cytotoxicity of free dexamethasone was evaluated and no cell toxicity was seen (Supplementary material, Fig. S1).

### 3.5. Cellular release of dexamethasone from the conjugates

Dexamethasone did not release as pure drug from the conjugates. Instead, a fragment Dexamethasone-Arginine (r-NH-N = Dex: Dex-Arg), with one Arg residue from the PCL was detected linked to the drug. Full sequences of the peptide-dexamethasone conjugates, the fragments detected in the cell lysate and molecular masses of the detected fragments are shown in Table 1.

### 3.6. Binding affinity of Dexamethasone-Arginine fragment to glucocorticoid receptor

Binding of Dex-Arg fragment (0.01 nM to 0.5 μM) to a fixed concentration of labeled hGR (10 nM) was studied with thermophoresis (Fig. 5). The thermophoresis signal indicates binding of Dex-Arg to hGR in a dose dependent manner.

### 3.7. Molecular docking of Dexamethasone-Arginine fragment to glucocorticoid receptor

The application of CB-Dock and Chimera visualization elucidated the binding modes of dexamethasone and the Dex-Arg fragment. Top 5 cavity sizes were identified and Vina scores for binding were obtained for each of the cavities. The largest identified cavity (sized 690) for dexamethasone docking was the same as the LBD in the crystal structure of the hGR-dexamethasone complex. A structural comparison of the docked dexamethasone (best binding score) in the LBD with that over in the crystal structure resulted in a near perfect match as evidenced by the low *r.m.s.d.* value of 0.33 Å. This validated the docking methodology. The Dex-Arg fragment was similarly docked and the best binding orientation (score) in the LBD (cavity sized 690) was considered. Structural comparisons of the docked Dex-Arg fragment in the LBD with dexamethasone bound in the crystal structure complex showed a good-fit between the two ligands. A *r.m.s.d.* value of 1.34 Å

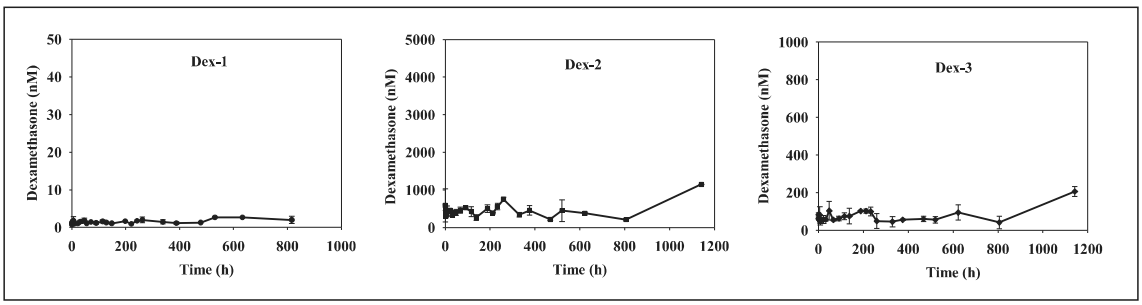


**Fig. 1.** Stability of peptide-dexamethasone conjugates in porcine vitreous. The conjugates were incubated with porcine vitreous and release of dexamethasone upon cleavage of the hydrazone bond in the conjugate was followed.

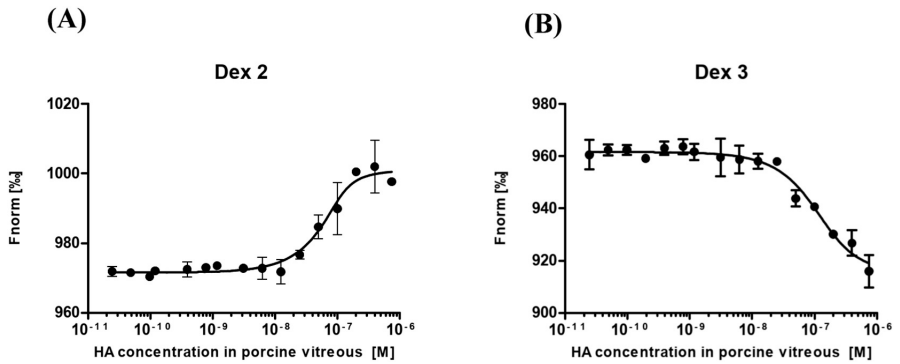


**Fig. 2.** Binding affinities of peptide-dexamethasone conjugates and porcine vitreous. Normalized fluorescence values (Fnorm) plotted against log of HA concentration in porcine vitreous to obtain the binding curves and the data fitted to obtain the $K_d$ values. (A) Binding of fluorescently labeled Dex-2 with porcine vitreous, binding affinity ($K_d$) determined to be 13.5 nM (B) Binding of fluorescently labeled Dex-3 with porcine vitreous with a $K_d$ value of 64.3 nM. Error bars represent standard error of $n = 3$ measurements.

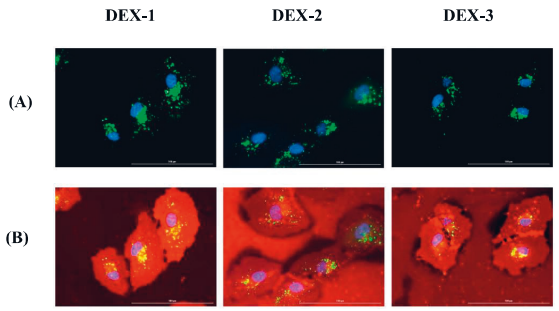


**Fig. 3.** Images of uptake of Alexa 488 labeled peptide-dexamethasone conjugates (5 μM) in living ARPE-19 cells, determined by Cytation 5 automated digital fluorescence imaging system. The peptides were incubated with the cells at 37 °C for 1 h. The cell nuclei and the conjugates (Alexa 488 labeled) were visualized with blue and green fluorescence respectively (A); cytoskeleton was visualized with deep red fluorescence (B). (For interpretation of the references to colour in this figure legend, the reader is referred to the web version of this article.)

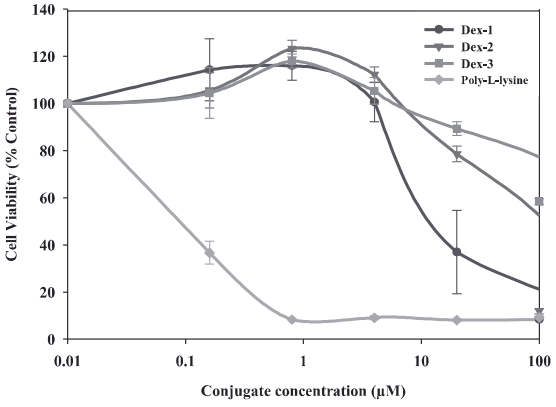


**Fig. 4.** Cytotoxicity of peptide-dexamethasone conjugates in ARPE-19 cells. Cells were treated with conjugates for 5 h and cell viability was evaluated with MTT cytotoxicity assay. The data were normalized based on the viability of untreated cells. Data are represented as mean ± standard deviation ($n = 3$).

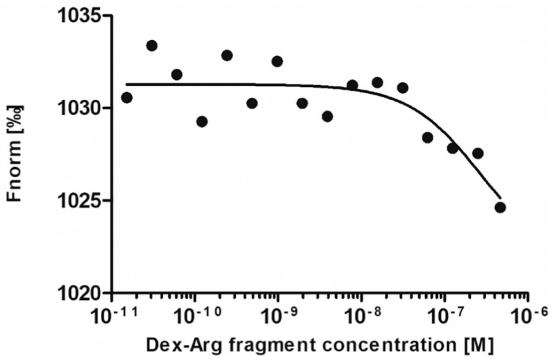


**Fig. 5.** Binding interaction of Dex-Arg fragment to human glucocorticoid receptor. Unlabeled Dex-Arg fragment (0.015 nM to 0.5 μM) was titrated into a fixed concentration of labeled hGR (10 nM). The thermophoretic signal (Fnorm) plotted as a function of log of Dex-Arg fragment concentration is shown.

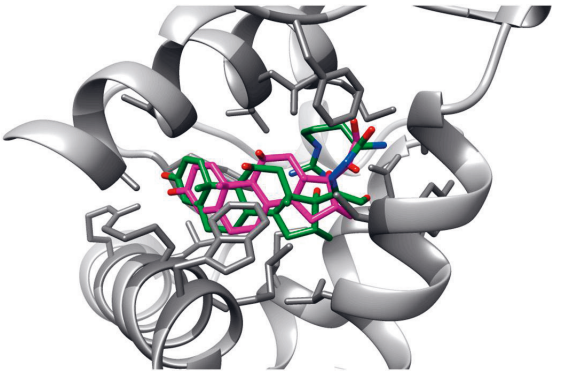

**Fig. 6.** Structural comparison of the docked Dex-Arg fragment (green) with the structural model of dexamethasone (magenta) in complex with hGR (PDB id: 1M2Z). Residues of the ligand-binding domain have been depicted in dark grey. (For interpretation of the references to colour in this figure legend, the reader is referred to the web version of this article.)

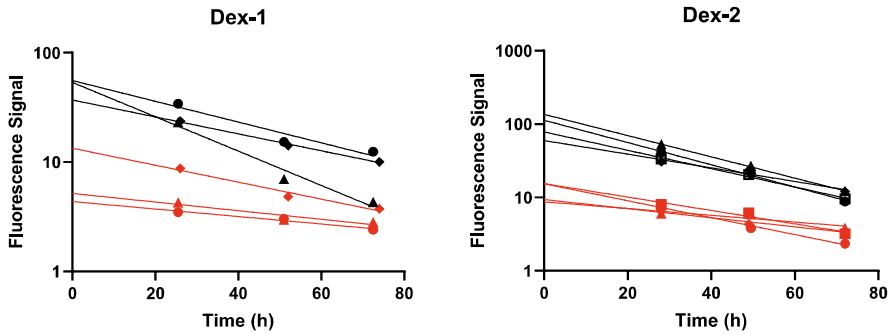


**Fig. 7.** Fluorophotometric signal versus time graphs of peptide-dexamethasone conjugates. Different symbols represent replicates from individual eyes. Black and red symbols correspond to signals from the vitreous and aqueous humor, respectively. (For interpretation of the references to colour in this figure legend, the reader is referred to the web version of this article.)

(matching the corresponding non-H atoms of the dexamethasone part of the molecule) was observed. Fig. 6 depicts the degree of structural superposition of the docked Dex-Arg fragment with that of the structural model of dexamethasone in complex with the hGR (PDB id: 1M2Z). The docking results validated that the Dex-Arg fragment binds at the same site as dexamethasone on the hGR.

### 3.8. In vivo pharmacokinetics

The results from the three rabbit eyes that received Dex-1 and four rabbit eyes that received Dex-2 (Scheme 1) injections intravitreally are shown in Fig. 7. The data from the fourth eye that was injected with Dex-1 is not included because some complications emerged after the injection. Vitreous and aqueous humor fluorescence signals of Dex-2 from a single rabbit eye (Supplementary Material, Fig. S2) shows a concentration gradient at 3 h after intravitreal injection. However, after 24 h, the conjugate was homogenously distributed in the vitreous (the first data point for PK calculations). The concentrations in the vitreous humor were approximately one order of magnitude higher than the concentrations in the aqueous humor. The vitreous and anterior chamber peptide conjugate concentrations were fitted with one-compartment model with first order elimination kinetics resulting in the elimination half-lives of 29.9 ± 10.0 h and 24.3 ± 5.6 h for Dex-1 and Dex-2, respectively. The anatomical vitreous volume was used as volume of drug distribution to calculate drug clearance (Table 2) (for most intravitreal compounds the volume of distribution ($V_d$) is in the range of anatomical vitreal volume [15]):

$$CL = V_d * K_v \quad (1)$$

where CL is the vitreal clearance (μl/h), $V_d$ is the anatomical volume of vitreous in rabbits (1700 μl) [34] and $K_v$ is elimination constant ($h^{-1}$) from vitreous. The average clearance values of the peptide-dexamethasone conjugates from the vitreous were approximately 40–50 μl/h.

To further ascertain the elimination route of the peptide-dexamethasone conjugates (anterior or posterior) after intravitreal injection, a method of Maurice and Mishima was used [35,36]. For anterior elimination pathway, the $C_a/C_v$ ratio and vitreal elimination half-lives of the compounds can be expressed by the following equations:

$$\frac{Ca}{Cv} = \frac{Kv\ Vv}{f} \text{ or } \frac{Ca}{Cv} = \frac{0.693\ Vv}{f\ t1/2} \quad (2)$$

where $C_a$ and $C_v$ are the concentrations of the injected molecule in the anterior segment and the vitreous, respectively; $K_v$ is elimination constant from vitreous; $V_v$ is the average volume of vitreous compartment in rabbit (1700 μl) [34]; $f$ is the aqueous humor flow rate (3 μl/min) [37] and $t_{1/2}$ is elimination half-life of the injected molecule from the vitreous. The calculated pharmacokinetic parameters of the peptide-dexamethasone conjugates (Dex-1, Dex-2) were in the close vicinity of the predicted blue trend line of the relationship in the Eq. (2) (Fig. 8). This suggests that the anterior route dominates in the vitreal elimination of the peptide conjugates. Fig. 8 also suggests that the elimination of Dex-1 and Dex-2 from the vitreous takes place as expected on the basis of their molecular weights. The elimination of the peptide conjugates via the anterior route is in contrast with that of free dexamethasone. Posterior clearance from the vitreous has been reported to be dominant for free dexamethasone [4]. The higher vitreal clearance rate of free dexamethasone (460 μl/h) as compared to the average flow-rate of aqueous humor (180 μl/h) also supports the major contribution of the posterior route of dexamethasone elimination.

## 4. Discussion

Intravitreal administration of small molecule drugs are associated

**Table 2**
Vitreal pharmacokinetic parameters of the conjugates after intravitreal injection.

| | Elimination half-life (h) | Elimination rate constant ($h^{-1}$) | Vitreal clearance (μl/h) | $C_a/C_v$ ratio |
|---|---|---|---|---|
| Dex-1 | | | | |
| Eye-1 | 31.7 | 0.021 | 35.7 | 0.16 |
| Eye-2 | 19.2 | 0.036 | 61.2 | 0.42 |
| Eye-3 | 38.90 | 0.017 | 28.9 | 0.36 |
| Average ± SD | 29.9 ± 10.0 | 0.024 ± 0.010 | 41.9 ± 17.0 | 0.31 ± 0.14 |
| Dex-2 | | | | |
| Eye-1 | 19.9 | 0.034 | 57.8 | 0.20 |
| Eye-2 | 20.8 | 0.033 | 56.1 | 0.21 |
| Eye-3 | 32.3 | 0.021 | 35.7 | 0.22 |
| Eye-4 | 24.1 | 0.028 | 47.6 | 0.29 |
| Average ± SD | 24.3 ± 5.7 | 0.029 ± 0.005 | 49.3 ± 10.1 | 0.23 ± 0.04 |

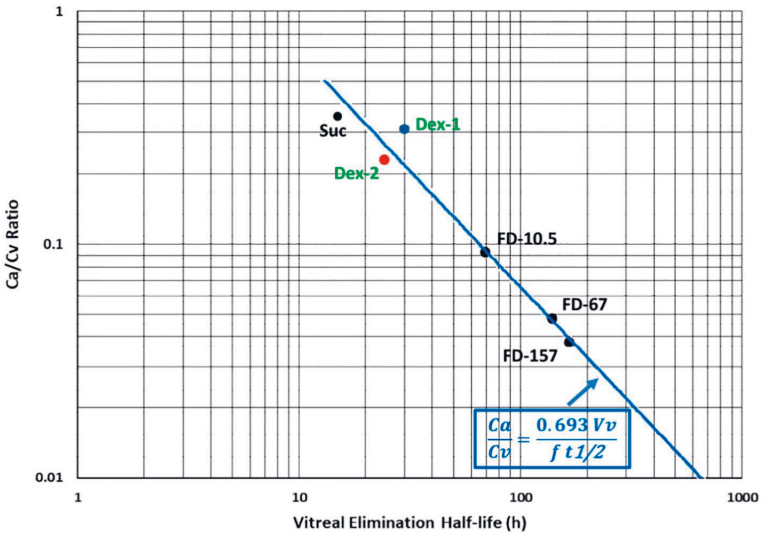


**Fig. 8.** Vitreal elimination half-life vs aqueous/vitreous concentration ratio of the peptide-dexamethasone conjugates following intravitreal injection in rabbit. Dex-1 and Dex-2 parameters falls in the vicinity of the blue trend line and are consistent with the other compounds with different molecular weight suggesting that the anterior pathway is the main route of their elimination. The data sources are as follows: sucrose (Suc) [38], FD-10.5, FD-67 and FD-157 [36]. The mean molecular weights of FITC-dextrans (FD) are 10.5 kD, 67 kD, respectively. The molecular weight of sucrose (Suc) is 0.342 kD. Dex-1 and Dex-2 has molecular weight of 4.43 and 4.29 kD, respectively. (For interpretation of the references to colour in this figure legend, the reader is referred to the web version of this article.)

with disadvantages, such as fast elimination rate, non-specific distribution to various ocular tissues and require frequent dosing [6,15]. Development of long acting and tissue specific drug delivery systems are needed to overcome such challenges. Polymer-drug conjugates (i.e. polymeric prodrugs) offer several potential advantages: increased solubility, prolonged drug retention, and targeted delivery of the therapeutics [39,40]. Although such approaches have been explored in the field of anticancer therapy [16,41]; their utility in the context of ocular drug delivery has been only sparsely investigated [18]. Conjugates are interesting option in intravitreal dug delivery, because they can be administered as clear solutions, and pharmacokinetics can be optimized in terms of cellular drug delivery and duration of action.

Dexamethasone is a corticosteroid that is used to treat inflammatory conditions in the anterior and posterior segments [19,42]. Intravitreal dexamethasone injections have been used to treat posterior segment inflammation, macular edema and neovascular macular degeneration [43] but short half-life of dexamethasone in the vitreous humor ($\approx$ 3 h) suggests that frequent intravitreal injections would be required to maintain levels of therapeutic concentration [44,45]. Therefore, dexamethasone has been delivered to the vitreous as biodegradable implants and coarse suspensions but these modes of drug delivery may interfere with vision and require larger needle or applicator for intravitreal placement. These approaches prolong duration of drug action without improvement in the drug distribution profiles. As such, typical adverse effects of corticosteroids (elevation of intraocular pressure, cataract formation) are unavoidable. In this study, we have explored a modular peptide-based delivery system for prolonged vitreal retention and drug delivery into the retinal pigment epithelial cells.

The modular delivery system is derived from our previous study [18] that demonstrated the release of short model peptides within the retinal pigment epithelial cells. The modular construct consists of the N-terminus segment for cellular delivery (cell penetrating peptide sequence) and a linker peptide that cleaves in intracellular environment. Dexamethasone was attached to the C-terminus of the linker peptide with hydrazone linkage (Scheme 1). Recent reports suggest that polycationic surface charge on particles bind electrostatically to the hyaluronic acid [27]. Li and co-workers reported the use of cationic nanoparticles, coated with L-Arg, as ocular drug delivery system with prolonged vitreal half-life [46]. In the design of our modular delivery system, we hypothesized to exploit this information. The N-terminus sequences were varied to contain differing amounts of positive charge to serve dual purpose: intracellular localization and vitreal retention by interactions with the vitreal components. Binding to hyaluronic acid in the vitreous is expected to slow down the vitreal diffusion of the modular peptide conjugates resulting in increased retention time and low clearance. Indeed, the interaction studies of peptide-dexamethasone conjugates with porcine vitreous revealed that the Dex-2 conjugate with higher number of positive charges has higher binding affinity compared to Dex-3 conjugate (Fig. 2). The apparent $K_d$ values are 13.5 nM and 64.3 nM for Dex-2 and Dex-3 conjugates, respectively.

Plots of vitreal elimination half-life and aqueous/vitreous concentration ratios for the peptide-dexamethasone conjugates [36] (Fig. 8) reveal that the anterior route is their main elimination pathway. Diffusion in the vitreous is a critically important parameter in the anterior elimination of intravitreal compounds [6]. Binding to the hyaluronic acid is expected to prolong intravitreal half-life. A recent study reported 3–4 fold increase in half-life of a protein when hyaluronic acid binding polypeptide sequence of 97 amino acids was fused to the structure [17]. In our study, the peptide-dexamethasone conjugates showed 8–10 fold increase in the vitreal half-life (24–30 h) as compared to the half-life of dexamethasone solution (3 h) [44,47]. This is due to the reduced elimination of dexamethasone across the blood ocular barriers. Fig. 8 demonstrates that the anterior elimination in the rabbit eyes was as expected based just on the molecular weight even though the peptides bind to hyaluronic acid. This may be explained by the binding equilibria. We used Coffey's approach [48,49] to simulate the impact of hyaluronic acid binding on vitreal drug elimination (for details, see Supplementary Material). After an injection of 5 nmol of peptide-dexamethasone conjugate into the vitreous, the initial concentration of the compound in the rabbit vitreous is about 3000 nM (approx. Volume 1.5 ml). Most of the conjugate is in free form after injection until $\approx$80% of the dose has been eliminated from the vitreous (Fig. 9A). The fraction of bound peptide increases at low concentrations ($<$ 600 nM) (Fig. 9A) and half-life will increase significantly only at concentrations below 300 nM (Fig. 9B). These estimates were obtained based on binding profile (MST studies) data with the porcine vitreous. However, the impact of binding of hyaluronic acid on conjugate clearance is expected to be rather small in the rabbit vitreous as it has lower hyaluronic acid concentration than the pig vitreous [50,51]. Apparently, higher affinity and/or smaller doses are required for further prolongation of the vitreal retention.

Stability in the vitreous is one of the key requirements for the

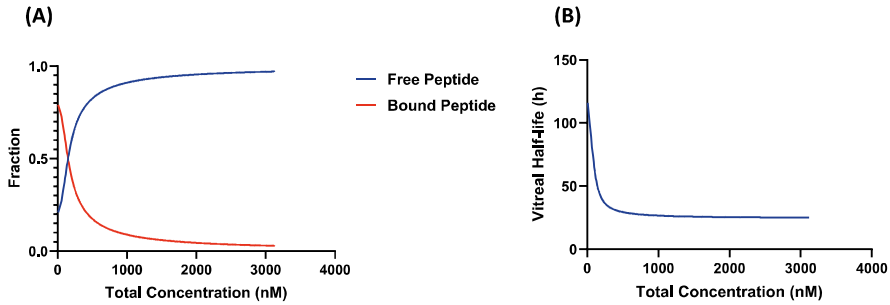


**Fig. 9.** Fraction of bound and free Dex-2 peptide at different concentrations in the porcine vitreous (A). The correlation of vitreal elimination half-life of Dex-2 peptide and total concentration in the vitreous (B).

intravitreal applicability of modular drug delivery systems. Ex vivo stability data reveal that the dexamethasone-peptide conjugates were chemically stable for over 6 weeks in the porcine vitreous, suggesting that no significant enzymatic cleavage by the peptidases takes place in the vitreous humor. Thus, the peptide-dexamethasone conjugates stay intact until delivered to the intracellular environment in the retina. In a recent report, Matter et al. (2019) suggest that dexamethasone is not stable in water solutions [52]. It is noteworthy that only minimal concentrations of free dexamethasone (mostly residual amounts from conjugate synthesis) were seen in the vitreal incubation studies of 6 weeks. Consequently, degradation product levels, if any, is expected to be negligible. Furthermore, the available time for any degradation is only a few days based on *in vivo* kinetics (Fig. 7).

We postulate that the modular delivery system has potential therapeutic benefits, because the drug is released within the cells. Therefore, this may enable effect at lower dose and reduced drug distribution to the off-target cells, which may reduce adverse effects of the corticosteroid. This principle may be applicable also to other drugs. Furthermore, cellular internalization and drug release in the retinal pigment epithelial cells might turn these cells as reservoirs for drug release to the neighboring cells [18]. Many diseases of the posterior segment of the eye, such as age-related macular degeneration and proliferative vitreoretinopathy, have a common therapeutic target cell, the retinal pigment epithelium [53–55]. To this effect, the modular peptide-based delivery system meets the key objective of being able to release dexamethasone within the retinal pigment epithelial cells. Larger sized protein molecules, such as, the ciliary derived neurotropic factor (CNTF; mol wt. 23 kDa) is known to permeate into the retina [56]. We therefore postulate that the smaller sized peptide conjugates (mol wt. 4.5 kDa) will easily permeate across the inner limiting membrane to the retina. The peptide-dexamethasone conjugates demonstrated significant cellular uptake, aided by the N-terminal cell penetrating peptide (Fig. 3) and dexamethasone release by cathepsin D mediated enzymatic cleavage of the peptide linker. The released fragment Dex-Arg is in accordance with results from our previous study on sequence-activity relationship of the peptide based linkers [18]. The fragment Dex-Arg binds to the glucocorticoid receptor as evidenced by computational and experimental approaches.

The focus and scope of the present work was to highlight and demonstrate the utility of our modular peptide-based drug delivery system for application in ocular diseases. Although the fluorescence based technique, Fluorotron, does not monitor the levels of dexamethasone or Dex-Arg fragment in the vitreous or retina *in vivo*; data suggests that Dex-Arg fragment is generated in the retina (RPE cells). Chemical quantitation of all relevant molecular species will be a topic of future studies with promising conjugate(s).

Importantly, modular peptide conjugates are rather small molecules. This is important for retinal permeation across the inner limiting membrane [6] to the retinal layers. Secondly, these are soluble molecules, allowing injection of transparent solutions. Thirdly, the conjugates are based on endogenous components (i.e. amino acids) which reduces the risk of toxicity. In addition, manufacturing of injectable solutions is less complex than production of particle based delivery systems.

## 5. Conclusions

We have shown the potential utility of a modular peptide-based delivery system for the retinal delivery of dexamethasone. The system is stable in the vitreous, internalizes within the retinal pigment epithelial cells and releases the drug after enzymatic cleavage of the peptide based linker. The modular peptide systems are promising candidates for ocular drug delivery and should be further optimized.

## Declaration of competing interest

The authors declare no conflict of interest.

## Acknowledgements

We thank Leena Pietilä for technical support and the Drug Discovery and Chemical Biology core facilities supported by the University of Helsinki and Biocenter Finland for live cell imaging. The Biomolecular Interaction Unitat the Faculty of Biological & Environmental Sciences, University of Helsinki is thanked for providing facilities for MST studies. HI-LIFE and Biocenter Finland infrastructure on Drug Discovery and Chemical Biology, University of Helsinki is acknowledged for mass spectrometry facility. *In vivo* experiments were carried out at the Ocular Drug Development Laboratory infrastructure, University of Eastern Finland. Biocenter Finland and Biocenter Kuopio is acknowledged for supporting Kuopio LC-MS laboratory facility. This work was funded and supported by grants to A.U. from European Union MCSA-ITN programme (OCUTHER project 722717), Business Finland (project 5734/31/2016) and Academy of Finland (project 311122).

## Appendix A. Supplementary data

Supplementary data to this article can be found online at https://doi.org/10.1016/j.jconrel.2020.09.005.

## References

[1] A. Urtti, Challenges and obstacles of ocular pharmacokinetics and drug delivery, Adv. Drug Deliv. Rev. 58 (2006) 1131–1135, https://doi.org/10.1016/j.addr.2006.07.027.

[2] Barriers for posterior segment ocular drug delivery, in: R.J. Gaudana, M. Barot, A. Patel, V. Khurana, A.K. Mitra (Eds.), Treatise Ocul. Drug Deliv. BENTHAM SCIENCE PUBLISHERS, 2013, pp. 68–95, , https://doi.org/10.2174/9781608051755113010007.

[3] V. Gote, S. Sikder, J. Sicotte, D. Pal, Ocular drug delivery: present innovations and future challenges, J. Pharmacol. Exp. Ther. 370 (2019) 602–624, https://doi.org/10.1124/jpet.119.256933.

[4] D.M. Maurice, S. Mishima, Ocular Pharmacokinetics, Springer, Berlin, Heidelberg, 1984, pp. 19–116, https://doi.org/10.1007/978-3-642-69222-2_2.

[5] A. Urtti, J.D. Pipkin, G. Rork, A.J. Repta, Controlled drug delivery devices for experimental ocular studies with timolol 1. In vitro release studies, Int. J. Pharm. 61 (1990) 235–240, https://doi.org/10.1016/0378-5173(90)90214-O.

[6] E.M. del Amo, A.K. Rimpelä, E. Heikkinen, O.K. Kari, E. Ramsay, T. Lajunen, M. Schmitt, L. Pelkonen, M. Bhattacharya, D. Richardson, A. Subrizi, T. Turunen, M. Reinisalo, J. Itkonen, E. Toropainen, M. Casteleijn, H. Kidron, M. Antopolsky, K.S. Vellonen, M. Ruponen, A. Urtti, Pharmacokinetic aspects of retinal drug delivery, Prog. Retin. Eye Res. 57 (2017) 134–185, https://doi.org/10.1016/j.preteyeres.2016.12.001.

[7] K.S. Vellonen, E.M. Soini, E.M. Del Amo, A. Urtti, Prediction of ocular drug distribution from systemic blood circulation, Mol. Pharm. 13 (2016) 2906–2911, https://doi.org/10.1021/acs.molpharmaceut.5b00729.

[8] H.F. Edelhauser, C.L. Rowe-Rendleman, M.R. Robinson, D.G. Dawson, G.J. Chader, H.E. Grossniklaus, K.D. Rittenhouse, C.G. Wilson, D.A. Weber, B.D. Kuppermann, K.G. Csaky, T.W. Olsen, U.B. Kompella, V.M. Holers, G.S. Hageman, B.C. Gilger, P.A. Campochiaro, S.M. Whitcup, W.T. Wong, Ophthalmic drug delivery systems for the treatment of retinal diseases: basic research to clinical applications, Investig. Ophthalmol. Vis. Sci. 51 (2010) 5403–5420, https://doi.org/10.1167/iovs.10-5392.

[9] N. Kuno, S. Fujii, Recent advances in ocular drug delivery systems, Polymers (Basel) 3 (2011) 193–221.

[10] E. Delamo, A. Urtti, Current and future ophthalmic drug delivery systems: a shift to the posterior segment, Drug Discov. Today 13 (2008) 135–143.

[11] R. Nagaraj, D.R. Bijukumar, B. Mathew, E.A. Scott, M.T. Mathew, A review on recent advancements in ophthalmology devices: currently in market and under clinical trials, J. Drug Deliv. Sci. Technol. 52 (2019) 334–345, https://doi.org/10.1016/j.jddst.2019.04.038.

[12] F. Pacella, A.F. Ferraresi, P. Turchetti, T. Lenzi, R. Giustolisi, A. Bottone, V. Fameli, M.R. Romano, E. Pacella, Intravitreal injection of Ozurdex® implant in patients with persistent diabetic macular edema, with six-month follow-up, Ophthalmol. Eye Dis. 8 (2016) OED.S38028, https://doi.org/10.4137/oed.s38028.

[13] T.V. Chirila, D.G. Harkin, Biomaterials and Regenerative Medicine in Ophthalmology: Second Edition, Elsevier Inc, 2016, https://doi.org/10.1016/C2014-0-01443-8.

[14] K. Nayak, M. Misra, A review on recent drug delivery systems for posterior segment of eye, Biomed. Pharmacother. 107 (2018) 1564–1582, https://doi.org/10.1016/j.biopha.2018.08.138.

[15] E.M. Del Amo, K.S. Vellonen, H. Kidron, A. Urtti, Intravitreal clearance and volume of distribution of compounds in rabbits: in silico prediction and pharmacokinetic simulations for drug development, Eur. J. Pharm. Biopharm. 95 (2015) 215–226, https://doi.org/10.1016/j.ejpb.2015.01.003.

[16] J.H. Park, S. Lee, J.H. Kim, K. Park, K. Kim, I.C. Kwon, Polymeric nanomedicine for cancer therapy, Prog. Polym. Sci. (2008), https://doi.org/10.1016/j.progpolymsci.2007.09.003.

[17] J.G. Ghosh, A.A. Nguyen, C.E. Bigelow, S. Poor, Y. Qiu, N. Rangaswamy, R. Ornberg, B. Jackson, H. Mak, T. Ezell, V. Kenanova, E. De La Cruz, A. Carrion, B. Etemad-Gilbertson, R.G. Caro, K. Zhu, V. George, J. Bai, R. Sharma-Nahar, S. Shen, Y. Wang, K.K. Subramanian, E. Fassbender, M. Maker, S. Hanks, J. Vrouvlianis, B. Leehy, D. Long, M. Prentiss, V. Kansara, B. Jaffee, T.P. Dryja, M. Roguska, Long-acting protein drugs for the treatment of ocular diseases, Nat. Commun. 8 (2017) 1–10, https://doi.org/10.1038/ncomms14837.

[18] M. Bhattacharya, S. Sarkhel, J. Peltoniemi, R. Broadbridge, M. Tuomainen, S. Auriola, A. Urtti, Differentially cleaving peptides as a strategy for controlled drug release in human retinal pigment epithelial cells, J. Control. Release 251 (2017) 37–48.

[19] J. Rodríguez Villanueva, L. Rodríguez Villanueva, M. Guzmán Navarro, Pharmaceutical technology can turn a traditional drug, dexamethasone into a first-line ocular medicine. A global perspective and future trends, Int. J. Pharm. 516 (2017) 342–351, https://doi.org/10.1016/j.ijpharm.2016.11.053.

[20] B. Abadia, P. Calvo, A. Ferreras, F. Bartol, G. Verdes, L. Pablo, Clinical applications of dexamethasone for aged eyes, Drugs Aging 33 (2016) 639–646, https://doi.org/10.1007/s40266-016-0392-z.

[21] F. Milletti, Cell-penetrating peptides: classes, origin, and current landscape, Drug Discov. Today 17 (2012) 850–860, https://doi.org/10.1016/j.drudis.2012.03.002.

[22] E. Atherton, R.C. Sheppard, Solid Phase Peptide Synthesis: A Practical Approach, IRL Press at Oxford University Press, 1989.

[23] M. Jerabek-Willemsen, T. André, R. Wanner, H.M. Roth, S. Duhr, P. Baaske, D. Breitsprecher, MicroScale thermophoresis: interaction analysis and beyond, J. Mol. Struct. 1077 (2014) 101–113, https://doi.org/10.1016/j.molstruc.2014.03.009.

[24] C.J. Wienken, P. Baaske, U. Rothbauer, D. Braun, S. Duhr, Protein-binding assays in biological liquids using microscale thermophoresis, Nat. Commun. 1 (2010) 1–7, https://doi.org/10.1038/ncomms1093.

[25] S.A.I. Seidel, P.M. Dijkman, W.A. Lea, G. van den Bogaart, M. Jerabek-Willemsen, A. Lazic, J.S. Joseph, P. Srinivasan, P. Baaske, A. Simeonov, I. Katritch, F.A. Melo, J.E. Ladbury, G. Schreiber, A. Watts, D. Braun, S. Duhr, Microscale thermophoresis quantifies biomolecular interactions under previously challenging conditions, Methods 59 (2013) 301–315, https://doi.org/10.1016/j.ymeth.2012.12.005.

[26] H. Kim, S.B. Robinson, K.G. Csaky, Investigating the movement of intravitreal human serum albumin nanoparticles in the vitreous and retina, Pharm. Res. 26 (2009) 329–337, https://doi.org/10.1007/s11095-008-9745-6.

[27] I. Melgar-Asensio, I. Kandela, F. Aird, S.R. Darjatmoko, C. de los Rios, C.M. Sorenson, D.M. Albert, N. Sheibani, J. Henkin, Extended intravitreal rabbit eye residence of nanoparticles conjugated with cationic arginine peptides for intraocular drug delivery: in vivo imaging, Investig. Ophthalmol. Vis. Sci. 59 (2018) 4071–4081, https://doi.org/10.1167/iovs.18-24087.

[28] A.V. Noulas, A.D. Theocharis, E. Feretis, N. Papageorgakopoulou, N.K. Karamanos, D.A. Theocharis, Pig vitreous gel: macromolecular composition with particular reference to hyaluronan-binding proteoglycans, Biochimie 84 (2002) 295–302, https://doi.org/10.1016/S0300-9084(02)01389-5.

[29] S. Shafaie, V. Hutter, M.B. Brown, M.T. Cook, D.Y.S. Chau, Diffusion through the ex vivo vitreal body – bovine, porcine, and ovine models are poor surrogates for the human vitreous, Int. J. Pharm. 550 (2018) 207–215, https://doi.org/10.1016/j.ijpharm.2018.07.070.

[30] Y. Liu, M. Grimm, W. tao Dai, M. chun Hou, Z.X. Xiao, Y. Cao, CB-Dock: a web server for cavity detection-guided protein–ligand blind docking, Acta Pharmacol. Sin. 41 (2020) 138–144, https://doi.org/10.1038/s41401-019-0228-6.

[31] E.F. Pettersen, T.D. Goddard, C.C. Huang, G.S. Couch, D.M. Greenblatt, E.C. Meng, T.E. Ferrin, UCSF Chimera – a visualization system for exploratory research and analysis, J. Comput. Chem. 25 (2004) 1605–1612.

[32] T. Mosmann, Rapid colorimetric assay for cellular growth and survival: application to proliferation and cytotoxicity assays, J. Immunol. Methods 65 (1983) 55–63, https://doi.org/10.1016/0022-1759(83)90303-4.

[33] F. Kayazawa, K. Miyake, Ocular fluorophotometry in patients with essential hypertension, Arch. Ophthalmol. 102 (1984) 1169–1170, https://doi.org/10.1001/archopht.1984.01040030947020.

[34] P.J. Missel, Simulating intravitreal injections in anatomically accurate models for rabbit, monkey, and human eyes, Pharm. Res. 29 (2012) 3251–3272.

[35] D.M. Maurice, S. Mishima, Ocular pharmacology, in: M. Sears (Ed.), Handb. Exp. Pharmacol, Springer-Verlag, Berlin-Heidelberg, 1984, pp. 16–119.

[36] F. Johnson, D. Maurice, A simple method of measuring aqueous humor flow with intravitreal fluoresceinated dextrans, Exp. Eye Res. 39 (1984) 791–805.

[37] C.B. Toris, Aqueous humor dynamics I: measurement methods and animal studies, Curr. Top. Membr. 62 (2008) 193–229.

[38] L.Z. Bito, E.V. Salvador, Intraocular fluid dynamics. III. The site and mechanism of prostaglandin transfer across the blood intraocular fluid barriers, Exp. Eye Res. 14 (1972) 233–241.

[39] I. Ekladious, Y.L. Colson, M.W. Grinstaff, Polymer–drug conjugate therapeutics: advances, insights and prospects, Nat. Rev. Drug Discov. 18 (2019) 273–294, https://doi.org/10.1038/s41573-018-0005-0.

[40] N. Larson, H. Ghandehari, Polymeric conjugates for drug delivery, Chem. Mater. 24 (2012) 840–853, https://doi.org/10.1021/cm2031569.

[41] Q. Feng, R. Tong, Anticancer nanoparticulate polymer-drug conjugate, Bioeng. Transl. Med. 1 (2016) 277–296, https://doi.org/10.1002/btm2.10033.

[42] R.S. Hunter, A.M. Lobo, Dexamethasone intravitreal implantfor the treatment of noninfectious uveitis, Clin. Ophthalmol. 5 (2011) 1612–1621, https://doi.org/10.2147/opth.s17419.

[43] B.D. Kuppermann, M. Goldstein, R.K. Maturi, A. Pollack, M. Singer, A. Tufail, D. Weinberger, X.-Y. Li, C.-C. Liu, J. Lou, S.M. Whitcup, Dexamethasone intravitreal implant as adjunctive therapy to ranibizumab in neovascular age-related macular degeneration: a multicenter randomized controlled trial, Ophthalmologica 234 (2015) 40–54, https://doi.org/10.1159/000381865.

[44] H.W. Kwak, D.J. D'Amico, Evaluation of the retinal toxicity and pharmacokinetics of dexamethasone after Intravitreal injection, Arch. Ophthalmol. 110 (1992) 259, https://doi.org/10.1001/archopht.1992.01080140115038.

[45] R. Bhagat, J. Zhang, S. Farooq, X.Y. Li, Comparison of the release profile and pharmacokinetics of intact and fragmented dexamethasone intravitreal implants in rabbit eyes, J. Ocul. Pharmacol. Ther. 30 (2014) 854–858, https://doi.org/10.1089/jop.2014.0082.

[46] H. Li, W. Liu, C.M. Sorenson, N. Sheibani, D.M. Albert, T. Senanayake, S. Vinogradov, J. Henkin, H.F. Zhang, Sustaining intravitreal residence with L-arginine peptide-conjugated nanocarriers, Investig. Ophthalmol. Vis. Sci. 58 (2017) 5142–5150, https://doi.org/10.1167/iovs.17-22160.

[47] K. Papangkorn, J.W. Higuchi, B. Brar, W.I. Higuchi, Ocular drug distribution and safety of a noninvasive ocular drug delivery system of dexamethasone sodium phosphate in rabbit, J. Ocul. Pharmacol. Ther. 34 (2018) 325–334, https://doi.org/10.1089/jop.2017.0093.

[48] J.J. Coffey, F.J. Bullock, P.T. Schoenemann, Numerical solution of nonlinear pharmacokinetic equations: effects of plasma protein binding on drug distribution and elimination, J. Pharm. Sci. 60 (1971) 1623–1628, https://doi.org/10.1002/jps.2600601106.

[49] J.J. Coffey, Effects of protein binding of drugs on areas under plasma concentration—time curves, J. Pharm. Sci. 61 (1972) 138–139, https://doi.org/10.1002/jps.2600610134.

[50] S.A. Boruchoff, A.M. Woodin, Viscosity and composition of solutions derived from rabbit vitreous humour, Br. J. Ophthalmol. 40 (1956) 113–118, https://doi.org/10.1136/bjo.40.2.113.

[51] E.A. Balazs, Functional anatomy of the vitreous, Duane's found, Clin. Ophthalmol. 1 (1993) 1–16.

[52] B. Matter, A. Ghaffari, D. Bourne, Y. Wang, S. Choi, U.B. Kompella, Dexamethasone degradation in aqueous medium and implications for correction of in vitro release from sustained release delivery systems, AAPS PharmSciTech 20 (2019) 1–11, https://doi.org/10.1208/s12249-019-1508-7.

[53] C. Larcher, H. Recheis, R. Sgonc, W. Göttinger, H.P. Huemer, E.U. Irschick, Influence of viral infection on expression of cell surface antigens in human retinal pigment epithelial cells, Graefes Arch. Clin. Exp. Ophthalmol. 235 (1997) 709–716.

[54] A.C. Bird, Therapeutic targets in age-related macular disease, J. Clin. Invest. 120

(2010) 3033–3041.
[55] I. Bhutto, G. Lutty, Understanding age-related macular degeneration (AMD): relationships between the photoreceptor/retinal pigment epithelium/Bruch's membrane/choriocapillaris complex, Mol. Asp. Med. 33 (2012) 295–317.
[56] J. Itkonen, A. Annala, S. Tavakoli, B. Arango-Gonzalez, M. Ueffing, E. Toropainen, M. Ruponen, M.G. Casteleijn, A. Urtti, Characterization, stability, and in vivo efficacy studies of recombinant human CNTF and its permeation into the neural retina in ex vivo organotypic retinal explant culture models, Pharmaceutics 12 (2020) 1–31, https://doi.org/10.3390/pharmaceutics12070611.

# Publication IV

International Journal of Pharmaceutics 621 (2022) 121800

Contents lists available at ScienceDirect

International Journal of Pharmaceutics

journal homepage: www.elsevier.com/locate/ijpharm

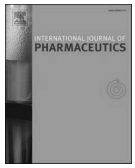

# Imaging, quantitation and kinetic modelling of intravitreal nanomaterials

Amir Sadeghi [a,*], Marika Ruponen [a], Jooseppi Puranen [a], Shoupeng Cao [c], Roxane Ridolfo [c], Shirin Tavakoli [b], Elisa Toropainen [a], Tatu Lajunen [a,b,e], Veli-Pekka Ranta [a], Jan van Hest [c], Arto Urtti [a,b,d]

[a] School of Pharmacy, University of Eastern Finland, Yliopistonranta 1 C, 70211 Kuopio, Finland
[b] Drug Research Program, Faculty of Pharmacy, University of Helsinki, Viikinkaari 5 E, 00790 Helsinki, Finland
[c] Bio-Organic Chemistry, Institute for Complex Molecular Systems, Eindhoven University of Technology, P.O. Box 513 (STO 3.31), 5600 MB Eindhoven, the Netherlands
[d] Laboratory of Biohybrid Technologies, Institute of Chemistry, St. Petersburg State University, Peterhof, 198504 St. Petersburg, Russia
[e] Laboratory of Pharmaceutical Technology, Department of Pharmaceutical Science, Tokyo University of Pharmacy & Life Sciences, 1432-1 Hachioji, Tokyo 192-0392, Japan

ARTICLE INFO

*Keywords:*
Liposome
Polymeric micelle
Intravitreal
Drug delivery
Pharmacokinetics
Retina
Modelling

ABSTRACT

In this study, the intravitreal pharmacokinetics of nanomaterials were investigated *in vivo* in rats and rabbits. Impact of particle size and shape (spherical, longitudinal) on ocular particle distribution and elimination was investigated with fundus camera, optical coherence tomography and ocular fluorophotometry. Differently sized particles showed prolonged ocular retention and remarkable differences in vitreal elimination, but size dependence was consistent, suggesting that other features have influence on their vitreal kinetics. We also demonstrate that liposomes are eliminated from the rabbit vitreous mainly via the anterior route. Simulation of drug concentrations after injection of intravitreal particles shows the importance of synchronized particle retention and drug release rate for efficient drug delivery. In conclusion, we provide kinetic insights in intravitreally administered nanoparticles to improve retinal drug delivery.

## 1. Introduction

Current retinal drug treatments are practised as repeated intravitreal injections. The number of intravitreal injections has increased dramatically, particularly after launching of the vascular endothelial growth factor (VEGF) inhibitors (bevacizumab, ranibizumab, aflibercept, brolucizumab) in the treatment of the neovascular form of age-related macular degeneration (Nicholson and Schachat, 2010). New technologies allowing longer intravitreal injection intervals and/or effective delivery to the retinal cells are needed.

Intravitreally injected drugs are capable of permeating into the retina for an extracellular (e.g. anti-VEGF compounds) or intracellular (e.g. corticosteroids) action. However, soluble drugs are eliminated from the vitreous rapidly as vitreal half-lives of small molecule drugs and antibodies are in the range of hours (Kidron et al., 2012) and days (Bakri et al., 2007), respectively. Vitreal drug retention can be prolonged with controlled release implants to months or even years (Del Amo and Urtti, 2008; Yang et al., 2015). For example, Iluvien is a non-degradable implant that release fluocinolone acetonide for up to 3 years in the vitreous. Ozurdex is biodegradable implant which release dexamethasone for up to 3 months (Chang-Lin et al., 2011; Sanford, 2013; Syed, 2017). However, the implant materials are not compatible with many drugs, they must be implanted with a 22-gauge needle, and they are not suitable for retinal drug targeting of nucleic acid based drugs (Lee et al., 2010). The implants release drug in free form into the vitreal cavity. The nucleic acid based drugs (RNA, DNA) are not able to enter the cells in free form. In those cases, some viral or non-viral vector system is needed for intracellular delivery.

Nanoparticles may avoid some problems that are associated with the implants. They can be delivered with small needles (31–32 G) and designed in versatile ways (e.g. particle size, surface charge, drug release, tissue targeting). Their surface may be functionalized with ligands for cell specific delivery of compounds with intracellular actions in the retina (Huang et al., 2018). Application of intravitreal nanoparticles started in the 1980s with drug loaded liposomes (Barza et al., 1985; Tremblay et al., 1985). Later, polymeric nanoparticles were tested as intravitreal delivery systems of drugs (Blazaki et al., 2020; Delrish et al., 2021; Mezei and Meisner, 1993; Zhou et al., 2021; Zimmer et al.,

* Corresponding author.
*E-mail address:* amir.sadeghi@uef.fi (A. Sadeghi).

https://doi.org/10.1016/j.ijpharm.2022.121800
Received 1 February 2022; Received in revised form 15 April 2022; Accepted 30 April 2022
Available online 6 May 2022

1994) and nucleic acid based therapeutics (siRNA, DNA) (Bochot and Fattal, 2012; del Pozo-Rodríguez et al., 2013; Huang and Chau, 2019). In preclinical studies, prolonged ocular retention and drug activity have been achieved with liposomes (Bochot and Fattal, 2012) and polymeric nanoparticles (Huang and Chau, 2019), but many pharmacokinetic aspects remain obscure. Currently no intravitreal nanoparticles are in clinical use, but some microparticles have been used in clinical trials (e.g. GrayBug AMD trials with sunitinib maleate microspheres; ClinicalTrials.gov Identifier: NCT03953079).

Systematic development of intravitreal nanoparticles benefits from improved pharmacokinetic understanding. Usually drug cargo, not liposomes, has been monitored in the eye, revealing modest (a few fold) (Alghadyan et al., 1988; Gupta et al., 2000) or substantial (even 30 fold) (Assil et al., 1991; Bourlaist et al., 1996) prolongation of vitreal drug retention. For example, vitreal retention of amikacin increased 1.8 fold with liposomes (Zeng et al., 1993), but vitreal half life of 5-fluorouridine monophosphate in rabbits increased from 4.5 h to 124 h with liposomes. Furthermore, *in vivo* fluorophotometry revealed long half-lives of intravitreal polymersomes (11.4–32.7 days) and polymeric micelles (4.3–9.5 days) in the rabbit vitreous. Fundus imaging showed accumulation of the polymersomes at the optic nerve head region (Junnuthula et al., 2021). However, impact of nanoparticle size and shape on vitreal elimination rate and route has not been quantitated. The *in vivo* distribution of nanoparticles within the vitreous has not been investigated even though it has been suggested that molecular distribution in the vitreous is not even (Araie and Maurice, 1991; Cunha-Vaz and Maurice, 1967). As only released drug is active, the interplay between ocular particle retention and drug release should be understood.

In this study, intravitreal distribution and elimination of fluorescently labelled liposomes, polymeric micelles and polymersomes were investigated in rats and rabbits. Nanoparticles with different sizes (40–1000 nm) and shapes (spherical, longitudinal) were investigated. For analyses, we used powerful non-invasive techniques, such as fundus camera, optical coherence tomography (OCT) and ocular fluorophotometry. Finally, kinetic simulation models were constructed yield insights on the interplay of particle residence and drug release in the eye.

## 2. Materials and methods

### 2.1. Commercial materials

Viscotears (hydrogel containing Carbomer 2 mg/g of weight) was obtained from Novartis (Finland). Ketamine was the product of Pfizer (Ketalar® 50 mg/ml, Pfizer Oy Animal Health, Finland) and medetomidine was obtained from Orion Pharma (Domitor® vet 1 mg/ml, Orion Pharma, Finland). Tropicamide (Oftan Tropicamid 5 mg/ml), obucaine (Oftan Obucain 4 mg/ml) and phenylephrine (Oftan Metaoksedrin 100 mg/ml) were obtained from Santen Pharmaceutical Co., Ltd. (Finland). Isoflurane was product of Chanelle Pharma (UK). Following lipids and mini-extruder were obtained from Avanti Polar Lipids, Inc. (USA): 1,2-distearoyl-*sn*-glycero-3-phosphocholine (DSPC), 1,2-dioleoyl-*sn*-glycero-3-phosphocholine (DOPC), 1,2-dioleoyl-*sn*-glycero-3-phosphoethanolamine-N-(carboxyfluorescein) (ammonium salt), 1,2-distearoyl-*sn*-glycero-3-phosphoethanolamine-N-[methoxy (polyethylene glycol)-2000] (DSPE-PEG), 1,2-distearoyl-*sn*-glycero-3-phosphoglycerol (DSPG). Nucleopore polycarbonate membranes (diameter 19 mm; 30, 50, 100 and 400 nm pore size) were supplied from Whatman Int. Ltd. (UK). Dulbecco's phosphate buffer saline (PBS) was purchased from Gibco® (USA).

### 2.2. Preparation of nanomaterials

*Synthesis and labelling of block-co-polymers.* The block-co-polymers were synthesized based on previously published protocols (Van Oppen et al., 2018) (Ridolfo et al., 2020). The details of synthesis and labelling the polymers are mentioned in supplementary materials (section A).

*Preparation of micelles.* The micelles were prepared according to a modified literature procedure (Ridolfo et al., 2020). First, $PEG_{22}$-b-$PTMC_{42}$ was dissolved in oligo (ethylene glycol) (OEG, $M_w = 350$ Da) at 50 wt% using mild heating (50 °C) and manual mixing used to ensure homogeneity. A 10 μl aliquot of these viscous liquids was composed of 50% copolymer and 50% OEG by weight. Thereafter, 10 μl of this viscous liquid was added to the bottom of a 5 mL glass vial and stirred at 280 rpm. The resulting liquid film was then hydrated using 1 mL of PBS with stirring for up to 1 h.

*Preparation of elongated nanoworms.* The procedure of nanoworms formation were reported in our publication (Ridolfo et al., 2020). First, $PEG_{22}$-b-$PTMC_{42}$ and $PEG_{22}$-b-P($TMC_{40}$-g-$CL_{10}$) were individually dissolved in oligo (ethylene glycol) (OEG, $M_w = 350$ Da) at 50 wt% using mild heating (50 °C) and manual mixing used to ensure homogeneity. A 10 μl aliquot of these viscous liquids was composed of 50% copolymer and 50% OEG by weight. The resulting stocks of either polymer (i.e., $PEG_{22}$-b-$PTMC_{42}$ and $PEG_{22}$-b-P($TMC_{40}$-g-$CL_{10}$) in OEG) were then combined at the desired ratio (e.g., 1:3.). Thereafter, 10 μl of this viscous liquid was added to the bottom of a 5 mL glass vial and stirred at 280 rpm. The resulting liquid film was then hydrated using 1 mL of PBS with stirring for up to 1 h.

*Preparation of liposomes.* Liposomes were prepared according to the previously reported method with a minor modification in the lipid compositions (Kari et al., 2020; Tavakoli et al., 2020, 2021). Briefly, DSPC, DOPC, DSPG and DSPE-PEG were mixed at a molar ratio of 75:10:10:5, respectively. The lipid mixtures (10 μmol) in chloroform were placed in a rotary evaporator to form a thin lipid film. Herein, the chloroform was evaporated at 55 °C under the nitrogen flow while the pressure was gradually reduced to below 100 mbar. Next, the thin lipid layer was hydrated by 1 mL of PBS buffer at 55 °C followed by sequential extrusion (11 times at 55 °C) through polycarbonate filter membranes to obtain the desired particle sizes. The liposomal formulation was then immediately cooled down and stored at 4 °C. PE-CF (1 mol %) was applied to label the liposomes by adding to the lipid mixture prior to film formation.

*Analysis of particle size.* Hydrodynamic diameters of liposomes and polymeric nanoparticles were measured with dynamic light scattering (DLS; Malvern Zetasizer APS automated plate sampler (Malvern Instruments Ltd., Malvern, United Kingdom). The experiments were run at room temperature with DLS automatically adjusting the measurement parameters for individual samples. Formulations were diluted 1:10 in PBS buffer before the measurements. The results were reported as size distributions (by particle number) and polydispersity indices (PDI).

### 2.3. In vivo methods

*Endotoxin test.* Prior to *in vivo* experiments the nanomaterials were tested for their endotoxin levels. Gel clot LAL assay kit (Lonza. CH-4002 Basel Switzerland) was used according to manufacturer's instructions. Shortly, the endotoxin standards were prepared at six concentrations (0.03, 0.06, 0.125, 0.25, 0.5 and 1.0 EU/mL) and the injectable materials were diluted (1:2, 1:8 and 1:64) in endotoxin free water. Standards, blank and samples (100 μl) were transferred to reaction tubes as duplicates, and LAL-reagent was added (100 μl) to each tube. The tube was mixed carefully and incubated at + 37 °C for 60 min. After incubation the tube was inverted 180°. Formation of a gel was a sign for the presence of endotoxin.

*Animals.* Lister hooded outbred male rats (average age 2–3 months; weight of 0.3–0.4 kg) and albino rabbits (average age of 6 months; weight of 3.0–3.5 kg) were used for the experiments. The animals were handled in accordance with ARVO statement for the use of animals in ophthalmic research. The animal experiments were carried out at the University of Eastern Finland under permit from National Project Authorization Board (ESAVI/27769/2020) and according to the EU directive 2010/63/EU.

Four rats were used for liposome testing. One rat was used per

formulation and both eyes were injected. For the polymeric micelles (spheres, worms), one rat (both eyes injected) per formulation was used. Three rabbits (both eyes injected) were used for intravitreal injections of liposomes (mean diameter of ≈50 nm). The information on the animal experiments has been compiled in Table 1.

*Intravitreal injections.* Intravitreal injections were given under isoflurane anaesthesia to rats, as described earlier (Sadeghi et al., 2021). Before injection, the pupil was dilated using 10 μl of phenylephrine and tropicamide eye drops. Topical medetomidine (10 μl) was used to prevent eye movements during anaesthesia and topical obucaine (one drop each eye) was used for ocular local anaesthesia just before the intravitreal injections. The needle (34 G) was inserted through the sclera (about 1 mm from the limbus) into the vitreous with the aid of ophthalmoscopic operating microscope. Both eyes in each animal were injected using 3 μl volume per eye. After injection, a topical hydrogel (Viscotears) was applied to prevent corneal dryness. After injection the eyes were checked with optical coherence tomography (OCT) and fundus camera (Phoenix MICRON™ MICRON IV/OCT, USA) for any possible damage of the lens and retina. Damaged eyes were excluded from the study.

Rabbits were anaesthetized with subcutaneous injection of ketamine (25 mg/kg) and medetomidine (0.5 mg/kg). The pupil was dilated with topical 5 mg/ml tropicamide solution. Ocular surface was anestesized with topical oxybuprocaine hydrochloride (4 mg/ml) just before the intravitreal injection. The intravitreal injections (40 μl per eye) were performed to the superior-temporal quadrant (4.5 mm behind the surgical limbus) using a 31 G needle and a 100 μl Hamilton syringe perpendicularly to the scleral surface. After the injections, topical hydrogel (Viscotear) was applied to prevent corneal dryness. Both eyes of each animal were injected.

*Ocular measurements and observations.* OCT, fundus imaging and fluorophotometry studies were performed under isoflurane anaesthesia in the rats. Before each measurement, the pupil of the rat was dilated using 10 μl of topical phenylephrine and tropicamide solutions. Fluorophotometry was performed using a Fluorotron Master fluorophotometer (Ocumetrics, Mountain View, USA). The fundus imaging was performed using both full color and green fluorescence filter (excitation: Semrock FF01-469/35; emission: Semrock BLP01-488R).

For fluorophotometric measurement in rabbits, the animals were lightly sedated by subcutaneously injected medetomidine (0.5 mg/kg). The pupil was dilated with tropicamide eye drops 20 min before the measurements. After measurement, sedation was discontinued with subcutaneously injected atipamezole (1 mg/kg). Technical details of fluorophotometric measurements have been described previously (Bhattacharya et al., 2020; Sadeghi et al., 2021). The average fluorescence signal in the vitreous was calculated by averaging the signals in the axial region of the eye between 3 mm anteriorly from the retina and the posterior edge of the lens. For aqueous humour values, the average values of the signals in the middle of this compartment were used. The data were calculated using the program of Fluorotron. Liposome and polymeric nanoparticle solutions were diluted in phosphate buffer (pH 7.4) to generate calibration curves for fluorophotometric quantitation (Lorget et al., 2016).

**Table 1**
Number of animals and intravitreal doses for each formulation.

| Nanoparticle type | Mean diameter (nm) | Species | Number of eyes | Dose of lipid or polymer per eye |
|---|---|---|---|---|
| Liposome | ≈ 50 | Rat | 2 | 0.6 nmol [a] |
| Liposome | ≈ 100 | Rat | 2 | 0.6 nmol [a] |
| Liposome | ≈ 250 | Rat | 2 | 0.6 nmol [a] |
| Liposome | >1000 | Rat | 2 | 0.6 nmol [a] |
| Micelle | ≈ 40 | Rat | 2 | 30 μg [b] |
| Worm | ≈ 90 | Rat | 2 | 30 μg [b] |
| Liposome | ≈ 50 | Rabbit | 6 | 8 nmol [a] |

[a] The dose is based on the amount of fluorescent lipids in the injected volume into the vitreous. [b] The dose is based on the total mass of nanoparticles in the solution.

### 2.4. Pharmacokinetic analyses and simulations

Curve fitting of the data and determination of pharmacokinetic parameters were performed with PKsolver software (Zhang et al., 2010). The data were fitted using a one-compartment model with first-order elimination. Non-linear weighting (1/(observed concentration)$^2$) was used to optimize fitting of the terminal time points.

Three types of kinetic simulations were performed in this study. Kinetic simulations of liposomes in rabbit eyes were performed based on the experimental parameters (vitreal clearance and volume of distribution) from fluorophotometry (Fig. 1A). The role of anterior elimination from the vitreous cavity was assessed. Clearance of liposomes from the anterior chamber was considered to be equal with aqueous humour outflow. Figure S10 in the supplement shows the model structure. The parameters are shown in Table S1 (supplement).

Dexamethasone was used as a model drug in the simulations, since it is used in clinical eye treatment (Adán et al., 2013; Boyer et al., 2014). Pharmacokinetics of intravitreal dexamethasone solution was simulated and simulations with optimized model matched the published experimental data (half-life 3.5 h) (Figure S11) (Kwak and D'Amico, 1992).

Concentrations of released dexamethasone in the vitreous and aqueous humour were simulated following virtual injection of drug loaded liposomes into the vitreous. Three first-order release rates were used in the simulations and the release rate constant was assumed to be equal in the vitreous and aqueous humour (Table S1). Fig. 1B shows a schematic presentation of the model. Details are included in the supplement (Fig. S12, Table S1).

STELLA® software (v. 8.1.1) (ISEE systems, USA) and fourth order Runge–Kutta algorithm were used for the simulations.

## 3. Results

### 3.1. Physico-chemical characterization of liposomes and polymeric nanoparticles

The liposomes had different sizes as expected based on the extrusion protocols (Table 2). In the case of liposomes with diameter above 1000 nm, the samples were prepared without extrusion, resulting in higher polydispersity index. All formulations were endotoxin negative (limit 0.03 EU/ml for 1/64 dilution).

### 3.2. Ocular distribution of intravitreally injected nanoparticles in rats

Ocular distribution of liposomes and polymeric nanoparticles was studied after intravitreal injections to rats. As nanoparticles were fluorescently labelled and scatter light their detection is possible both with fundus camera and OCT, respectively (Shakirova et al., 2020). The OCT signals overlapped with the fluorescent signals in the fundus images thereby revealing localization of the nanoparticles (Figure S1-S6). The OCT signals were usually more visible in the anterior vitreous than in the posterior part. Two rat eyes were injected and both eyes showed qualitatively similar results. The signal level was highest always in the vicinity of injection site, particularly in the case of the polymeric micelles that retained in the vitreous for more than two months. Even though the tests were done in small number of rat eyes, the qualitative results seem to be consistent.

*Liposomes.* Overall, vitreal retention of small liposomes (50, 100 and 250 nm) was shorter than that of large liposomes (>1000 nm) (Fig. 2). Liposomes with diameters of ≈100 nm and ≈250 nm disappeared from the vitreous during 10 days post-injection, but smaller liposomes (≈50 nm) retained in the vitreous for at least 10 days. Large liposomes (>1000 nm) showed long retention times (>20 days) in the rat eyes

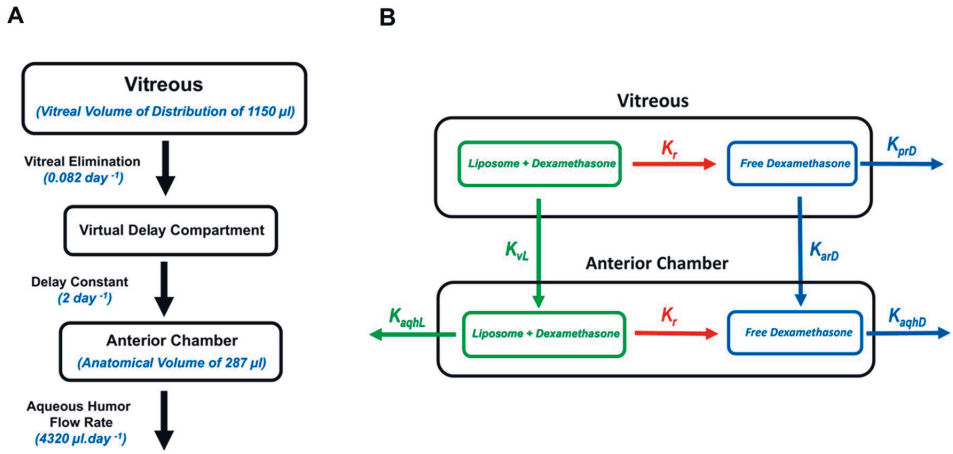


**Fig. 1.** Schematic diagram of the simulation models for rabbit eye. A) Model for liposome kinetics after intravitreal injection. A delay constant was adjusted to match the experimental values for $C_{max}$ in the aqueous humour. Concept of delay compartment was introduced previously by Hutton-Smith et al. (2017). B) Model for kinetic simulation of dexamethasone loaded intravitreal liposomes. $K_r$ is the first-order rate constant of drug release from liposomes. $K_{vL}$ and $K_{arD}$ describe distribution rate constants of liposomes and dexamethasone from vitreous to the aqueous humour, respectively. $K_{aqhL}$ and $K_{aqhD}$ are rate constants for liposome and dexamethasone elimination from aqueous humour, respectively. Transition delay compartments for liposomes and released dexamethasone from vitreous to aqueous humour were used to correctly simulate the lag time of material entrance to aqueous humour. Details of the models are presented in the supplement (Table S1, Figures S10-S12).

**Table 2**
Features of the formulations. The reported sizes of the nanoparticles are based on DLS method. The shape of the particles was not considered in this size measurement. The width and length of the particles (tubes and worms) based on cryo-TEM is>1 µm and the width is about 100 to 50 nm (Ridolfo et al., 2021). Vitreal retention times in rat eyes after intravitreal injections are based on qualitative observation in fundus imaging.

| Nanoparticle type | Mean diameter (nm) | Polydispersity index | Shape | Retention time in the vitreous (days) |
|---|---|---|---|---|
| Liposome | 48.6 ± 3.9 | 0.148 | Spherical | >10 |
| Liposome | 94. 6 ± 5.7 | 0.054 | Spherical | >4 |
| Liposome | 231.7 ± 44.8 | 0.029 | Spherical | >4 |
| Liposome | 1160.9 ± 234.1 | 0.494 | Spherical | >20 |
| Micelle | 37.5 ± 0.3 | 0.061 | Spherical | >65 |
| Micelle | 91.8 ± 1.2 | 0.294 | Worm shape | >65 |

(Fig. 2). Interestingly, the elimination of liposomes from the vitreous takes places before they reach homogenous distribution within the vitreous. Due to the non-homogeneous distribution of liposomes in the rat vitreous, reliable fluorophotometric measurements were not possible.

OCT was used to investigate retinal microstructure after liposome injections. No signs of inflammation or swelling in the retina was seen during 20 days after liposome injections (Fig S7).

*Polymeric nanoparticles.* Spherical and worm-like polymeric micelles retained in the rat vitreous, close to the injection site, for more than 65 days after intravitreal injection (Fig. 3). Based on the co-localized fundus camera and OCT images (Fig. S5-S6), the fluorescence signals represent intact particles, not detached labels. The OCT images show normal retina and vitreous without signs of inflammation (Fig. S8). These formulations were endotoxin negative.

The retention times of nanoparticles in the rat vitreous are summarized in Table 2.

### 3.3. Kinetics of intravitreal liposomes in the rabbit eye

Quantitative pharmacokinetics of intravitreally injected small liposomes (mean diameter ≈50 nm) were studied in rabbits with fluorophotometry. The fluorescence signals of liposomes in the vitreous showed concentration gradients along the eye axis, higher concentrations residing mostly in the posterior part of the vitreal cavity (Fig. 4). Such profiles became more prevalent at later time points, such as four weeks post-injection, but in some cases high signals were seen in the posterior border of the lens (Fig. 4). Also fundus images of the rabbit eyes, one month after the injections, are shown in Fig. 4. The accumulation of liposomes near the head of optic nerve is visible (Fig. 4A4-4F4) and in line with liposome concentrations in the posterior part of the vitreous (Fig. 4).

Fluorescence signals in the vitreous and aqueous humour declined over time when liposomes were eliminated from the eye (Fig. 5). For kinetic calculations, we used vitreal fluorescence levels at six days and onwards, when liposomes had distributed in the vitreous from the injection site. In the case of aqueous humour, fluorescence signals at one day and onwards were used in the kinetic analyses. The average elimination half-life of vitreal liposomes was 8.4 days, the apparent volume of distribution ≈ 1 mL and their average clearance from the vitreous was 82 µl/day (Table 3). The average concentration of liposomes in the aqueous humour was about 25 times lower than in the vitreous (Fig. 5). Elimination of liposomes from both compartments was parallel and showed similar slope of decline (Fig. 5).

### 3.4. Pharmacokinetic simulations

*Elimination of intravitreally injected liposomes.* Kinetic simulations were performed to elucidate the elimination routes of the intravitreal liposomes. It was assumed that the liposomes eliminate anteriorly and clearance from the anterior chamber equals aqueous humour outflow. With such assumptions, the simulated liposome concentrations in the anterior chamber matched the experimental values from fluorophotometry, thereby supporting the anterior elimination of liposomes (Fig. 6A). The concentration ratio of aqueous humour/vitreous ($C_a/C_v$) at pseudo steady-state was ≈ 0.026, while the experimental value was

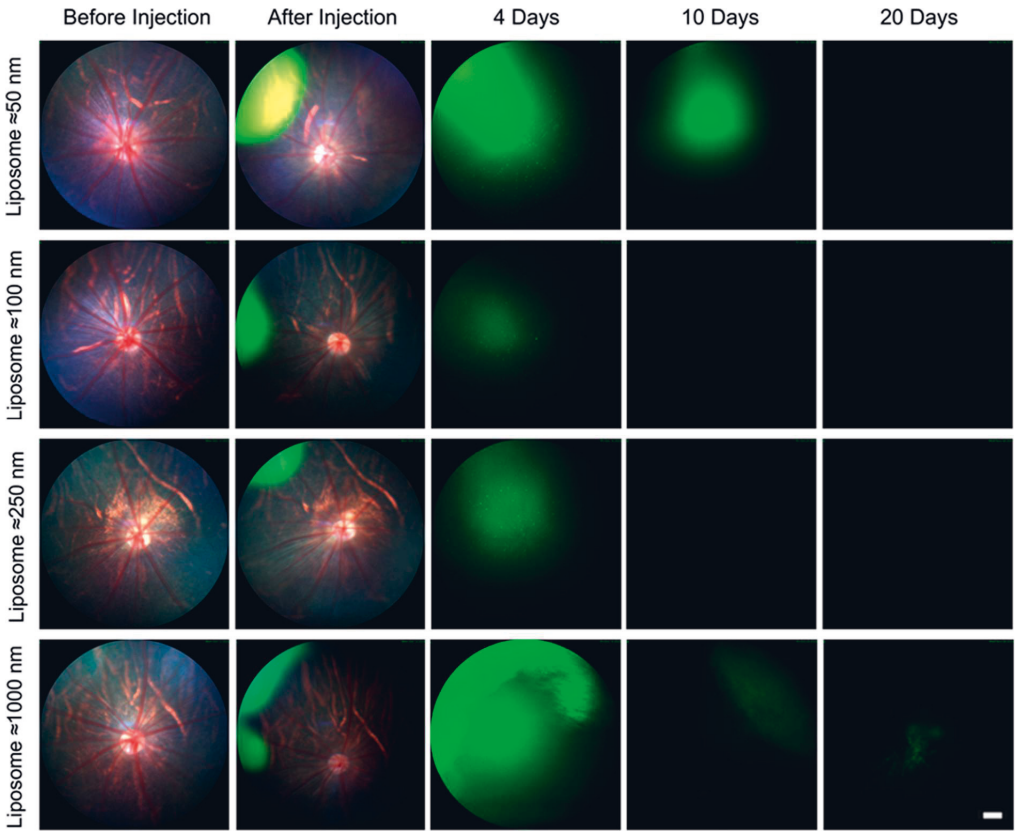


**Fig. 2.** Intravitreal distribution of differently sized liposomes in rats. Each row shows fundus images from the same eye before injection, immediately after injection and 4, 10 and 20 days post-injection. From day 4 onwards imaging was performed with green fluorescence filter. The combination of these fundus images with OCT are shown in supplement (Fig. S1-S4). The length of scale bar is 200 μm.

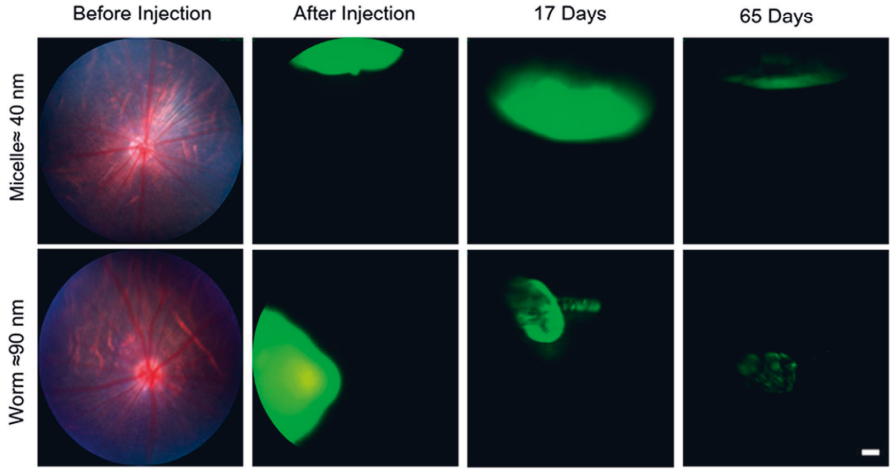


**Fig. 3.** Distribution of intravitreally injected polymeric micelles (spherical micelles ≈ 40 nm and worm shaped micelles ≈90 nm) in the rat vitreous. The fundus images are shown at different times post-injection. Combinations of fundus and OCT images are shown in the supplement (Fig. S5-S6). The scale bar is 200 μm. At day 17 and onwards imaging was performed with green fluorescence filter.

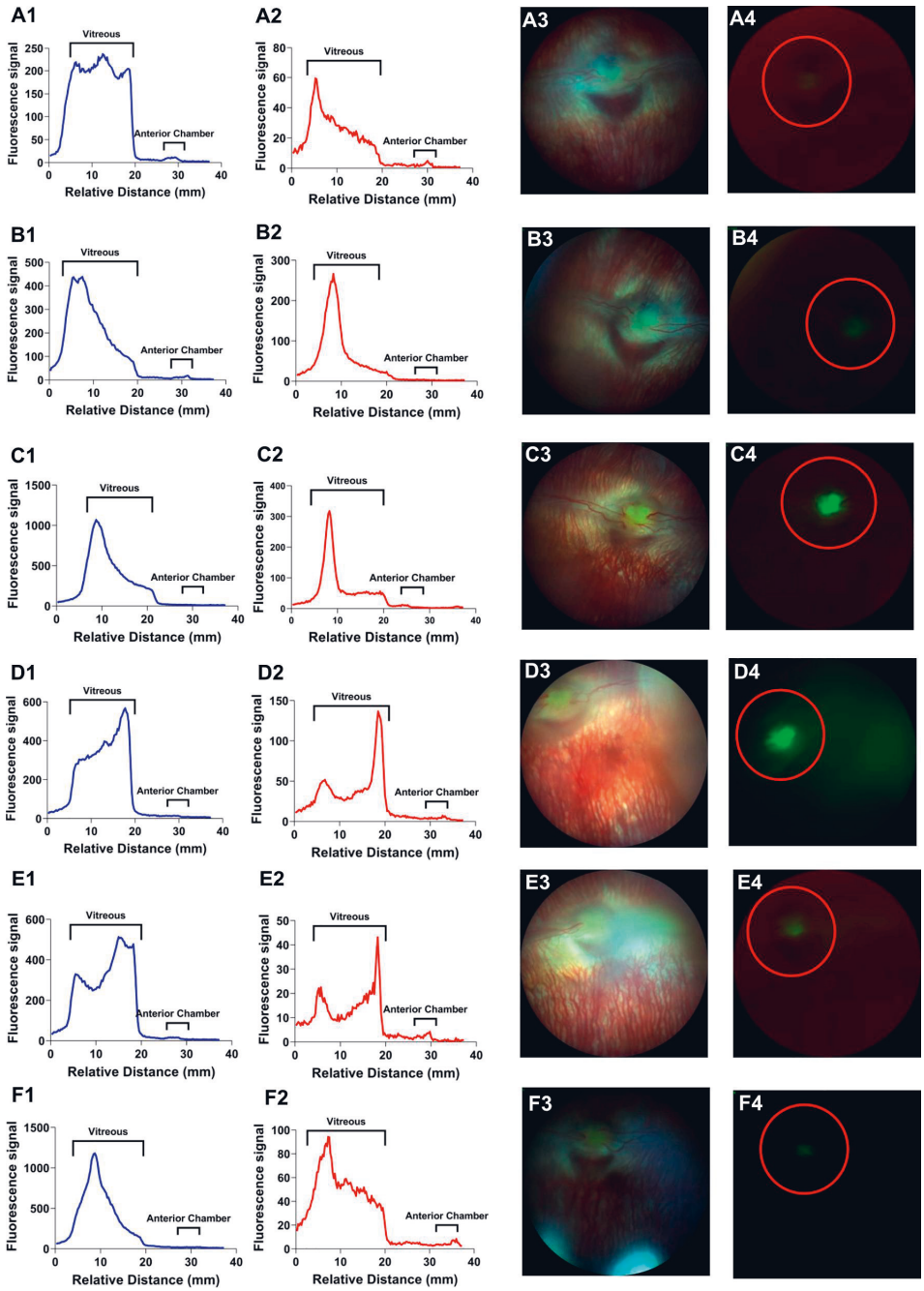


**Fig. 4.** Fluorophotometric scans and fundus images of six rabbit eyes after intravitreal injections of fluorescently labelled liposomes (diameter ≈50 nm). A1 is the fluorophotometric scan at one week and A2 is the scan of the same eye at four weeks post-injection. A3 and A4 are the full colour and green fluorescence fundus images of the eyes one month after injections, respectively. The panel B to F represent the other five eyes in the same order as row A. The red circles show accumulation of fluorescence at the optic nerve head region. The lengths of scale bars for fundus images are 200 μm. (For interpretation of the references to color in this figure legend, the reader is referred to the web version of this article.)

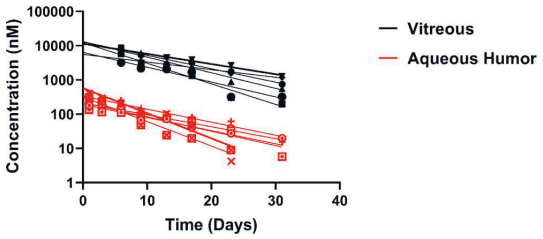


**Fig. 5.** Kinetic profiles of intravitreally injected liposomes in rabbit vitreous. Each symbol shows the values in a single eye at different time points. Black and red symbols show the concentrations in the vitreous and aqueous humour, respectively. The lines represent the best fits to the data based on one compartment model with first-order elimination process. The coefficients of determination ($R^2 = 0.79–0.91$) were similar for the curve fits both vitreal and aqueous humour data. (For interpretation of the references to color in this figure legend, the reader is referred to the web version of this article.)

$0.040 \pm 0.014$. The $C_a/C_v$ ratio in Maurice plot (Fig. 6B) is based on the anterior route of elimination (Maurice and Mishima, 1984). Maurice plot supports anterior elimination of liposomes, because the liposome data lies next to the theoretical line of anterior elimination (Fig. 6B).

### 3.5. Simulations on dexamethasone release from intravitreally injected liposomes

Simulations were performed to predict the concentrations of free dexamethasone in the vitreous and aqueous humour after intravitreal injection of drug loaded liposomes. In these simulations, liposome kinetics obeyed the experimental parameter values (Table 3), different hypothetical dexamethasone release rates were simulated (half-times of release 1 day, 1 week and 1 month), and pharmacokinetics of free dexamethasone was based on its known ocular pharmacokinetics (Table S1). A realistic dexamethasone loading of 10 mol% in the liposomes was used in the model (Kallinteri et al., 2002; Tsotas et al., 2007). Transit compartment was used to delay material movement from the vitreous into the aqueous humour (Fig. 1). This enabled us to reproduce the experimental $T_{max}$ for liposomes and free dexamethasone in the aqueous humour (Fig. 1A, 6 A and S12).

After a single injection of 80 nmol of dexamethasone solution to the rabbit vitreous, the simulated drug concentration remained at effective levels (>1 nM, limit of effectiveness) (Chang-Lin et al., 2011; Nauck et al., 1998) for ≈ 56 h (Fig. 7A). The expected duration of action was extended to 12, 42 and 50 days when the half-life of drug release from the liposomes was assumed to be 1 day, one week, and one month, respectively (Fig. 7B-7D). The simulated percentage of drug release within the eye was 94% for the fastest release rate (release $T_{1/2}$ of 1 day) but declined at slower release rates to 57% (release $T_{1/2}$ of 1 week) and 23% (release $T_{1/2}$ of 1 month). These simulations demonstrate the need to synchronize ocular retention and drug release from nanoparticles. In Fig. 8 the correlation of exposure period and ocular bioavailability (i.e. release within the eye) for different release half-lives are shown. Obviously, by increasing the release half-life the expected duration of action will increase but it will reach a plateau level at long release half-lives. This means that the design of efficient long-acting liposomes must involve synchronization of prolonged particle retention and drug release.

## 4. Discussion

*Vitreal retention of nanomaterials.* In this study, we demonstrate long intravitreal retention of at least 10 days and up to 65 days for small liposomes (≈ 50 nm) and polymeric micelles (spherical ≈ 40 nm; longitudinal ≈ 90 nm), respectively, in the rat eyes. Large liposomes of about one micron remained for at least 20 days in the rat eyes. The data suggest that small nanoparticles (<100 nm) and large ones (>1 μm) are preferred for prolonged vitreal retention. Based on previous studies polymeric nanoparticles and PEG-coated liposomes retain their original particle size upon storage (Abdelmohsen et al., 2016; Lajunen et al., 2016; Ridolfo et al., 2020), but the relationship between particle size and vitreal retention *in vivo* is complex due to the confounding variables, such as charge interactions, particle disintegration/aggregation and interactions with vitreal components (Bochot and Fattal, 2012; Huang and Chau, 2019; Pitkänen et al., 2003). It should be noted that the rat data herein, even though consistent, is qualitative and based on two injected eyes for each formulation. In previous reports, similar (Sakurai et al., 2001) and opposite (Kim et al., 2020) trends have been presented for the relationship between particle size and vitreal retention.

Vitreal retention of 50 nm liposomes was longer in rabbits (>30 days) than in rats (>10 days). Likewise, the half-lives of intravitreal soluble molecules are much shorter in mice (Schmitt et al., 2019) and rats (Sadeghi et al., 2021) than in rabbits (del Amo et al., 2017). The diffusional path in the rabbit vitreous is longer than in the rat eyes, thereby prolonging liposome elimination (Tavakoli et al., 2021). It is important to realize that required drug doses and liposomal retention times will change upon rat-to-rabbit and rat-to-human translation.

The literature on vitreal retention of intravitreally injected nanoparticle formulated drugs shows wide range of values in the rat and rabbit eyes: half-lives of 0.25–78 days (Alghadyan et al., 1988; Claro et al., 2009; Kim et al., 2020; Mezei and Meisner, 1993; Peyman et al., 1987; Sakurai et al., 2001; Zeng et al., 1993). This reflects differences in particle chemistry, size, charge, shape and other confounding factors. In this study, the chemistry of liposomes and polymeric micelles particles was not changed, but the sizes and shapes of the particles were modified in controlled way. Use of covalently bound fluorescent labels in the polymeric micelles and liposomes allowed reliable monitoring of the intravitreal nanomaterials. Colocalization of the fluorescence (fundus imaging) and the particles (OCT) confirmed that the labeling of the particles remained intact (Figure S1-S6, supplementary materials). This colocalization approach was previously introduced for the analysis of phosphorescence labeled liposomes in the rat vitreous (Shakirova et al., 2020). Injection volume was kept constant, eliminating potential differences due to pressure changes in the eye. Impact of injection on the intraocular pressure in rat eyes is unknown, but in human eyes the pressure rise lasts usually less than one hour post-injection (Lee et al., 2016), which is insignificant in comparison to the overall elimination time of biologicals and nanomaterials from the vitreous (Del Amo et al., 2017; Fig. 6A). In rabbits, 10-fold change in intravitreal injection volume (10 μl vs 100 μl) had minimal impact on the elimination kinetics of FITC-dextrans in rabbit eyes (Maurice, 1997).

Porcine vitreous was shown to limit modestly diffusion of anionic

**Table 3**
Kinetic parameters for intravitreally injected liposomes (≈50 nm) in rabbit eyes. Dose of 8 nmol (resp. fluorescent lipids) was injected per eye. Means ± S.D. (n = 6) are presented.

| Apparent volume of distribution (μl) | Vitreal elimination half-life (day) | Elimination half-life from aqueous humour (day) | Vitreal $C_{max}$ (nM) | Vitreal clearance (μl/day) | $C_a/C_v$ ratio [a] | Vitreal $AUC_{0\text{-}inf}$ (nM.day) |
|---|---|---|---|---|---|---|
| 954 ± 478 | 8.42 ± 3.8 | 6.66 ± 1.99 | 9817 ± 3538 | 82.33 ± 32.63 | 0.040 ± 0.014 | 108538 ± 36410 |

[a] $C_a$ and $C_v$ stand for lipid concentrations in aqueous humour and vitreous, respectively.

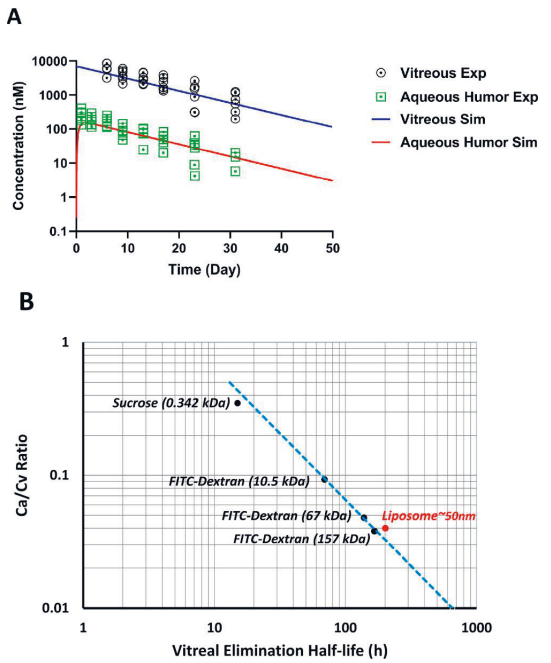


**Fig. 6.** Pharmacokinetics of intravitreally injected liposomes. A) Simulation of intravitreally injected liposome kinetics (lines) and experimental data (symbols). Only anterior route of elimination is assumed to be operative in the simulations. B) Maurice plot of aqueous humour/vitreous concentration ratio ($C_a/C_v$) against elimination half-life in the vitreous. The blue line shows $C_a/C_v$ values for sole anterior elimination from the rabbit vitreous. The sources of the data: sucrose (Bito and Salvador, 1972), FITC-dextrans (Johnson and Maurice, 1984) and liposomes (this study). (For interpretation of the references to color in this figure legend, the reader is referred to the web version of this article.)

and neutral liposomes (size range from <50 nm to >200 nm), whereas cationic liposomes had 1–2 orders of magnitude slower diffusion (Tavakoli et al., 2021). Small particles (≈50 nm) may also permeate to the retina across the inner limiting membrane (ILM), but 100 nm particles and bigger did not permeate to the *ex vivo* bovine retina (Tavakoli et al., 2020). Long vitreal retention of small sized liposomes and polymeric micelles will further improve chances of retinal permeation as they are capable of diffusing both in the vitreous and ILM (Lee et al., 2017; Tavakoli et al., 2020, 2021). Such formulations may be optimized for retinal drug targeting. On the other hand, very large liposomes are bigger than the mesh size of the vitreous (≈550 nm) (Peeters et al., 2005; Xu et al., 2013), explaining the long retention of large liposomes (>1000 nm) in this study (Fig. 2). Such particles are retained over prolonged periods at the injection site, therefore being potentially suitable for controlled drug release to the vitreous, but not for particle mediated delivery into the retina. Potentially misleading and easier retinal permeation of particles has been seen in the rodent eyes with thinner and leaky ILM (Lee et al., 2017; Tavakoli et al., 2021).

Interestingly, the longitudinal shape of the polymeric micelles did not seem to affect their retention in the rat vitreous, even though diffusivity of longitudinal particles in the vitreous is several times faster than their spherical counterparts with similar size (Ridolfo et al., 2021). Thus, faster elimination of the longitudinal particles from the rat vitreous might be expected. Similar kinetics is proposed based on qualitative imaging (Fig. 2), but quantitative studies are needed to firmly prove the size independent elimination of polymeric micelles. Interestingly, longitudinal particles are also able to cross the ILM into the retina (Ridolfo et al., 2021).

*Spatial distribution of nanomaterials in the vitreous cavity.* In vivo fluorophotometry showed interesting spatial distribution of liposomes within the vitreous: in most cases higher concentrations in the posterior than in the anterior vitreous and localization to the optic nerve head (Fig. 4). This may be due to anterior elimination of liposomes and convective flow (Araie and Maurice, 1991; Smith et al., 2020). Anterior elimination of FITC-dextrans generated such concentration gradients in the vitreous (Araie et al., 1991). Smith et al (2020) suggest that a fraction of aqueous humor may flow to the vitreous, eliminating via transretinal route. The flow may also contribute to the higher levels of liposomes in the posterior vitreous and at optic nerve head in rats (Fig. 4) and rabbits (Junnuthula et al., 2021). Optic nerve accumulation may be useful for therapeutic targeting to the optic nerve (e.g. in glaucoma) (DeBusk and Moster, 2018; Lavik et al., 2011), but it may constitute also a risk of toxicity. It has been claimed that optic nerve accumulation is less significant in monkeys and humans than in the rabbits (Hayreh, 1964), but this point has not been proven experimentally in humans.

*Anterior elimination route of intravitreal nanomaterials.* Although anterior elimination of intravitreal liposomes has been suggested previously (Barza et al., 1987), this study presents the first quantitative proof for the anterior elimination in rabbits. In computational model, the measured vitreal clearance of injected liposomes was assumed to represent only anterior elimination and clearance from the anterior chamber was set equal with aqueous humour outflow. The simulated liposome concentrations in the aqueous humor and vitreous showed perfect match with the experimental values, indicating that the intravitreal liposomes are eliminated via anterior route, and excluding previously proposed (Camelo et al., 2007) posterior or conjunctival elimination routes. In fact, posterior elimination pathway is significant only for small soluble molecules, that are capable of permeating across the retinal pigment epithelium and endothelia of retinal capillaries to the blood circulation (Del Amo et al., 2015).

Diffusion in the vitreous has been shown to be a critical factor in the anterior elimination of intravitreal biologicals (Hutton-Smith et al., 2016; Rimpelä et al., 2018). Accordingly, elimination of protein drugs from rabbit vitreous depends on compound diffusivity in the vitreous (Hutton-Smith et al., 2016). Therefore, it is logical that the liposomes with larger diameter (>1 μm) than the vitreal mesh size (≈ 0.55 μm) diffuse slowly (Del Amo et al., 2017) and show prolonged retention in the vitreous. Surprisingly, the small liposomes (≈ 50 nm) seem to retain longer in rat vitreous than the particles with intermediate size (≈ 100 nm and ≈ 200 nm), even though their diffusivities in the porcine vitreous were similar (Tavakoli et al., 2021). Polymeric micelles showed even longer retention (>65 days) in rat eyes, yet they have similar diffusivity in porcine ex vivo model (Ridolfo et al. 2021). Size exclusion phenomena in rat eye might explain these data: the smallest particles (a could enter denser vitreal compartments where larger particles do not enter, leading to prolonged retention. This theory is analogous with size exclusion chromatography, but needs to be experimentally proven. In the case of polymeric micelles, chemical interactions with vitreal components might contribute to the extended vitreal retention, but they should be investigated in more detail. Convection is another confounding factor (Tavakoli et al. 2021), but its impact on nanoparticle kinetics in the rat and rabbit eye has not been quantitated.

*Interplay of particle retention and drug release.* Unfortunately, to the best of our knowledge, there are no published studies that report free drug concentrations in the vitreous after intravitreal nanoparticle injections. Furthermore, no publications report simultaneous residence of both particle material and drug in the vitreous. Most publications show only levels of total drug in the vitreous (Alghadyan et al., 1988; Assil et al., 1991; Bourlaist et al., 1996; Gupta et al., 2000), even though only the released drug is pharmacologically active and required for proper extrapolation from pharmacokinetics to pharmacodynamics.

Interplay of hypothetical drug (dexamethasone as example) release

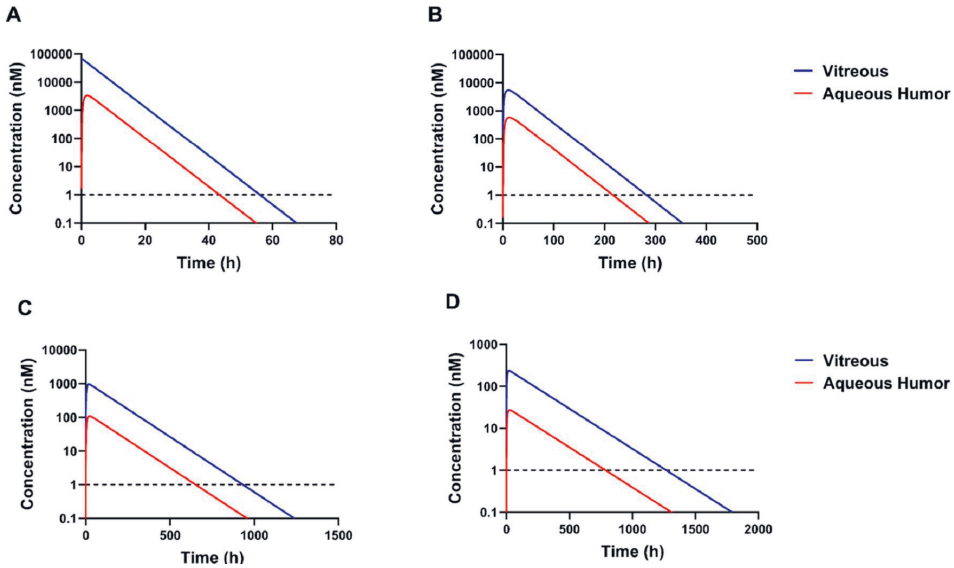


**Fig. 7.** Simulated concentrations of free dexamethasone in the vitreous and aqueous humour of rabbits after intravitreal injections. A) Injection of dexamethasone solution. B-D) Injection of dexamethasone liposomes. Drug release was assumed to obey the first-order kinetics at release half-lives of one day (B), one week (C) and one month (D). Simulated dexamethasone dose was 80 nmol per injection. The dotted line shows the minimum effective concentration of dexamethasone (1 nM) for inhibiting the vascular endothelial growth factor gene expression (Chang-Lin et al., 2011; Nauck et al., 1998).

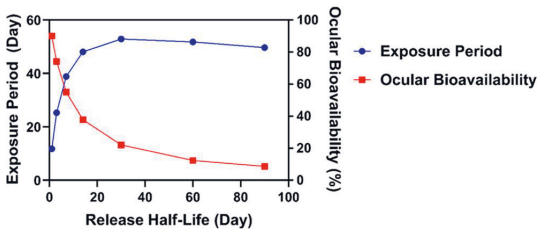


**Fig. 8.** Relationship between ocular drug bioavailability (percentage of dexamethasone release in the vitreous and aqueous humour) and drug release rate (half-life of release) from intravitreally injected liposomes. The simulation was performed using liposome kinetic parameters from Table 3. Also, effective exposure period of free dexamethasone in the vitreous is shown as a function of drug release rate. The exposure period is defined as the time period when free dexamethasone concentration in the vitreous remains above 1 nM.

rate and experimentally proven ocular residence of liposomes in rabbit eyes was explored computationally. Optimized intravitreal drug delivery requires synchronization of the drug release rate and vitreal retention of the nanoparticles (Fig. 8). Too slow drug release results in elimination of a major part of the drug dose in encapsulated form, resulting in low ocular bioavailability of free drug. On the contrary, too fast drug release results in short-lived drug response and non-productive residence of empty nanoparticles in the eye. The simulation models presented herein are valuable tools for drug development, since experimental drug release rates *in vitro*, known or predicted (Del Amo et al., 2015) clearance of free drug, and retention of the particles (estimated or determined) can be easily incorporated to the model as parameters. The model can be applied to optimize drug loading and release rate from nanomaterials. This will augment development of intravitreal formulations with desired target product profiles.

## 5. Conclusions

Pharmacokinetics of intravitreally injected liposomes and polymeric micelles were studied in rat and rabbit eyes. With fluorophotometry and OCT/fundus imaging we demonstrate prolonged vitreal retention and uneven vitreal distribution of small liposomes and polymeric micelles. In rabbits, *in vivo* fluorophotometry revealed higher liposome levels near the retina and optic nerve than in the anterior part of the vitreous. Liposomes were eliminated from the eyes anteriorly via aqueous humour outflow. Computational integration of drug release kinetics with the experimental data on liposome residence in the eye provides a tool for assessing the potential benefits of intravitreal drug releasing particles.

## CRediT authorship contribution statement

**Amir Sadeghi:** Investigation, Writing – original draft, Methodology. **Marika Ruponen:** Supervision, Conceptualization, Writing – review & editing. **Jooseppi Puranen:** Investigation. **Shoupeng Cao:** Investigation. **Roxane Ridolfo:** Investigation. **Shirin Tavakoli:** Investigation. **Elisa Toropainen:** Investigation, Supervision. **Tatu Lajunen:** Supervision, Conceptualization. **Veli-Pekka Ranta:** Supervision, Conceptualization. **Jan van Hest:** Supervision, Conceptualization, Writing – review & editing. **Arto Urtti:** Supervision, Conceptualization, Writing – review & editing.

## Declaration of Competing Interest

The authors declare that they have no known competing financial interests or personal relationships that could have appeared to influence the work reported in this paper.

## Acknowledgements

This study was supported by funding from European Union MCSA-ITN (OcuTher project, H2020-MSCA-ITN-2016, 722717) to AU and JH, Sigrid Juselius Foundation to AU. Phospholipid Research Center

(TLA-2019-068/1-1) to ST. Academy of Finland (330656), Eye Foundations' Postdoc Pool Finland and Instrumentarium Science Foundation to TL. Russian Government Mega Grant (14.W03.031.0025, Biohybrid technology for modern biomedicine) to AU.

## Appendix A. Supplementary data

Supplementary data to this article can be found online at https://doi.org/10.1016/j.ijpharm.2022.121800.

## References


Abdelmohsen, L.K.E.A., Williams, D.S., Pille, J., Ozel, S.G., Rikken, R.S.M., Wilson, D.A., van Hest, J.C.M., 2016. Formation of well-defined, functional nanotubes via osmotically induced shape transformation of biodegradable polymersomes. J. Am. Chem. Soc. 138 (30), 9353–9356.

Adán, A., Pelegrín, L., Rey, A., Llorenç, V., Mesquida, M., Molins, B., Ríos, J., Keller, J., 2013. Dexamethasone intravitreal implant for treatment of uveitic persistent cystoid macular edema in vitrectomized patients. Retina 33, 1435–1440.

Alghadyan, A.A., Peyman, G.A., Khoobehi, B., Milner, S., Liu, K.-R., 1988. Liposome-bound cyclosporine: clearance after intravitreal injection. Int. Ophthalmol. 12 (2), 109–112.

Araie, M., Maurice, D.M., 1991. The loss of fluorescein, fluorescein glucuronide and fluorescein isothiocyanate dextran from the vitreous by the anterior and retinal pathways. Exp. Eye Res. 52 (1), 27–39.

Assil, K.K., Hartzer, M., Weinreb, R.N., Nehorayan, M., Ward, T., Blumenkranz, M., 1991. Liposome suppression of proliferative vitreoretinopathy. Rabbit model using antimetabolite encapsulated liposomes. Invest. Ophthalmol. Vis. Sci. 32, 2891–2897.

Bakri, S.J., Snyder, M.R., Reid, J.M., Pulido, J.S., Ezzat, M.K., Singh, R.J., 2007. Pharmacokinetics of Intravitreal Ranibizumab (Lucentis). Ophthalmology 114 (12), 2179–2182.

Barza, M., Baum, J., Tremblay, C., Szoka, F., D'Amico, D.J., 1985. Ocular toxicity of intravitreally injected liposomal amphotericin B in rhesus monkeys. Am. J. Ophthalmol. 100 (2), 259–263.

Barza, M., Stuart, M., Szoka, F., 1987. Effect of size and lipid composition on the pharmacokinetics of intravitreal liposomes. Invest. Ophthalmol. Vis. Sci. 28, 893–900.

Bhattacharya, M., Sadeghi, A., Sarkhel, S., Hagström, M., Bahrpeyma, S., Toropainen, E., Auriola, S., Urtti, A., 2020. Release of functional dexamethasone by intracellular enzymes: A modular peptide-based strategy for ocular drug delivery. J. Control. Release 327, 584–594.

**Bito, L.Z., Salvador, E.V., 1972. Intraocular fluid dynamics. III. The site and mechanism of prostaglandin transfer across the blood intraocular fluid barriers. Exp. Eye Res. 14 (3), 233–241.** https://doi.org/10.1016/0014-4835(72)90008-5.

**Blazaki, S., Pachis, K., Tzatzarakis, M., Tsilimbaris, M., Antimisiaris, S.G., 2020. Novel Liposome Aggregate Platform (LAP) system for sustained retention of drugs in the posterior ocular segment following intravitreal injection. Int. J. Pharm. 576, 118987.** https://doi.org/10.1016/j.ijpharm.2019.118987.

**Bochot, A., Fattal, E., 2012. Liposomes for intravitreal drug delivery: a state of the art. J. Control. Release 161 (2), 628–634.** https://doi.org/10.1016/j.jconrel.2012.01.019.

Bourlaist, C.L., Chevanne, F., Ropert, P., Bretagne, G., Acar, L., Zia, H., Sado, P.A., Needham, T., Leverge, R., 1996. Release kinetics of liposome-encapsulated ganciclovir after intravitreal injection in rabbits. J. Microencapsul. 13 (4), 473–480.

Boyer, D.S., Yoon, Y.H., Belfort, R., Bandello, F., Maturi, R.K., Augustin, A.J., Li, X.-Y., Cui, H., Hashad, Y., Whitcup, S.M., 2014. Three-year, randomized, sham-controlled trial of dexamethasone intravitreal implant in patients with diabetic macular edema. Ophthalmology 121 (10), 1904–1914.

Camelo, S., Lajavardi, L., Bochot, A., Goldenberg, B., Naud, M.C., Fattal, E., Behar-Cohen, F., de Kozak, Y., 2007. Ocular and systemic bio-distribution of rhodamine-conjugated liposomes loaded with VIP injected into the vitreous of Lewis rats. Mol. Vis. 13, 2263.

**Chang-Lin, J.-E., Attar, M., Acheampong, A.A., Robinson, M.R., Whitcup, S.M., Kuppermann, B.D., Welty, D., 2011. Pharmacokinetics and pharmacodynamics of a sustained-release dexamethasone intravitreal implant. Invest. Ophthalmol. Vis. Sci. 52, 80–86.** https://doi.org/10.1167/iovs.10-5285.

**Claro, C., Ruiz, R., Cordero, E., Pastor, M.T., López-Cortés, L.F., Jiménez-Castellanos, M. R., Lucero, M.J., 2009. Determination and pharmacokinetic profile of liposomal foscarnet in rabbit ocular tissues after intravitreal administration. Exp. Eye Res. 88 (3), 528–534.** https://doi.org/10.1016/j.exer.2008.11.015.

Cunha-Vaz, J.G., Maurice, D.M., 1967. The active transport of fluorescein by the retinal vessels and the retina. J. Physiol. 191, 467–486.

DeBusk, A., Moster, M.I., 2018. Gene therapy in optic nerve disease. Curr. Opin. Ophthalmol. 29, 234–238.

**del Amo, E.M., Rimpelä, A.-K.-K., Heikkinen, E., Kari, O.K., Ramsay, E., Lajunen, T., Schmitt, M., Pelkonen, L., Bhattacharya, M., Richardson, D., Subrizi, A., Turunen, T., Reinisalo, M., Itkonen, J., Toropainen, E., Casteleijn, M., Kidron, H., Antopolsky, M., Vellonen, K.-S.-S., Ruponen, M., Urtti, A., 2017. Pharmacokinetic aspects of retinal drug delivery. Prog. Retin. Eye Res. 57, 134–185.** https://doi.org/10.1016/j.preteyeres.2016.12.001.

Del Amo, E., Urtti, A., 2008. Current and future ophthalmic drug delivery systems: a shift to the posterior segment. Drug Discov. Today 13 (3–4), 135–143.

**Del Amo, E.M., Vellonen, K.S., Kidron, H., Urtti, A., 2015. Intravitreal clearance and volume of distribution of compounds in rabbits: In silico prediction and pharmacokinetic simulations for drug development. Eur. J. Pharm. Biopharm. 95, 215–226.** https://doi.org/10.1016/j.ejpb.2015.01.003.

del Pozo-Rodríguez, A., Delgado, D., Gascón, A.R., Solinís, M.Á., 2013. Lipid nanoparticles as drug/gene delivery systems to the retina. J. Ocul. Pharmacol. Ther. 29 (2), 173–188.

**Delrish, E., Jabbarvand, M., Ghassemi, F., Amoli, F.A., Atyabi, F., Lashay, A., Soleimani, M., Aghajanpour, L., Dinarvand, R., 2021. Efficacy of topotecan nanoparticles for intravitreal chemotherapy of retinoblastoma. Exp. Eye Res. 204, 108423.** https://doi.org/10.1016/j.exer.2020.108423.

Gupta, S.K., Velpandian, T., Dhingra, N., Jaiswal, J., 2000. Intravitreal pharmacokinetics of plain and liposome-entrapped fluconazole in rabbit eyes. J. Ocul. Pharmacol. Ther. 16 (6), 511–518.

Hayreh, S.S., 1964. Pathogenesis of oedema of the optic disc (papilloedema): a preliminary report. Br. J. Ophthalmol. 48 (10), 522–543.

**Huang, D., Chen, Y., Green, C.R., Rupenthal, I.D., 2018. Hyaluronic acid coated albumin nanoparticles for targeted peptide delivery in the treatment of retinal ischaemia. Biomaterials 168, 10–23.** https://doi.org/10.1016/j.biomaterials.2018.03.034.

**Huang, X., Chau, Y., 2019. Intravitreal nanoparticles for retinal delivery. Drug Discov. Today. 24 (8), 1510–1523.** https://doi.org/10.1016/j.drudis.2019.05.005.

Hutton-Smith, L.A., Gaffney, E.A., Byrne, H.M., Maini, P.K., Gadkar, K., Mazer, N.A., 2017. Ocular pharmacokinetics of therapeutic antibodies given by intravitreal injection: estimation of retinal permeabilities using a 3-compartment semi-mechanistic model. Mol. Pharm. 14 (8), 2690–2696.

**Hutton-Smith, L.A., Gaffney, E.A., Byrne, H.M., Maini, P.K., Schwab, D., Mazer, N.A., Ga, E.A., Byrne, H.M., Maini, P.K., Schwab, D., Mazer, N.A., 2016. A mechanistic model of the intravitreal pharmacokinetics of large molecules and the pharmacodynamic suppression of ocular vascular endothelial growth factor levels by ranibizumab in patients with neovascular age-related macular degeneration. Mol. Pharm. 13, 2941–2950.** https://doi.org/10.1021/acs.molpharmaceut.5b00849.

Johnson, F., Maurice, D., 1984. A simple method of measuring aqueous humor flow with intravitreal fluoresceinated dextrans. Exp. Eye Res. 39 (6), 791–805.

**Junnuthula, V., Sadeghi Boroujeni, A., Cao, S., Tavakoli, S., Ridolfo, R., Toropainen, E., Ruponen, M., van Hest, J.C.M., Urtti, A., 2021. Intravitreal Polymeric Nanocarriers with Long Ocular Retention and Targeted Delivery to the Retina and Optic Nerve Head Region. Pharmaceutics 13 (4), 445.** https://doi.org/10.3390/pharmaceutics13040445.

Kallinteri, P., Antimisiaris, S.G., Karnabatidis, D., Kalogeropoulou, C., Tsota, I., Siablis, D., 2002. Dexamethasone incorporating liposomes: an in vitro study of their applicability as a slow releasing delivery system of dexamethasone from covered metallic stents. Biomaterials 23 (24), 4819–4826.

**Kari, O.K., Tavakoli, S., Parkkila, P., Baan, S., Savolainen, R., Ruoslahti, T., Johansson, N. G., Ndika, J., Alenius, H., Viitala, T., Urtti, A., Lajunen, T., 2020. Light-Activated Liposomes Coated with Hyaluronic Acid as a Potential Drug Delivery System. Pharmaceutics 12 (8), 763.** https://doi.org/10.3390/pharmaceutics12080763.

Kidron, H., del Amo, E.M., Vellonen, K.-S., Urtti, A., 2012. Prediction of the Vitreal Half-Life of Small Molecular Drug-Like Compounds. Pharm Res 29 (12), 3302–3311.

**Kim, H.M., Ha, S., Hong, H.K., Hwang, Y., Kim, P., Yang, E., Chung, J.Y., Park, S., Park, Y.J., Park, K.H., Kim, H., Woo, S.J., 2020. Intraocular distribution and kinetics of intravitreally injected antibodies and nanoparticles in rabbit eyes. Transl. Vis. Sci. Technol. 9 (6), 20.** https://doi.org/10.1167/tvst.9.6.20.

**Kwak, H.W., D'Amico, D.J., 1992. Evaluation of the Retinal Toxicity and Pharmacokinetics of Dexamethasone After Intravitreal Injection. Arch. Ophthalmol. 110, 259.** https://doi.org/10.1001/archopht.1992.01080140115038.

**Lajunen, T., Kontturi, L.-S., Viitala, L., Manna, M., Cramariuc, O., Róg, T., Bunker, A., Laaksonen, T., Viitala, T., Murtomäki, L., Urtti, A., 2016. Indocyanine Green-Loaded Liposomes for Light-Triggered Drug Release. Indocyanine Green-Loaded Liposomes for Light-Triggered Drug Release. 13 (6), 2095–2107.** https://doi.org/10.1021/acs.molpharmaceut.6b0020710.1021/acs.molpharmaceut.6b00207.s00110.1021/acs.molpharmaceut.6b00207.s002.

Lavik, E., Kuehn, M.H., Kwon, Y.H., 2011. Novel drug delivery systems for glaucoma. Eye 25 (5), 578–586.

Lee, J., Goh, U., Lee, H.-J., Kim, J., Jeong, M., Park, J.-H., 2017. Effective retinal penetration of lipophilic and lipid-conjugated hydrophilic agents delivered by engineered liposomes. Mol. Pharm. 14 (2), 423–430.

**Lee, S.S., Hughes, P., Ross, A.D., Robinson, M.R., 2010. Biodegradable implants for sustained drug release in the eye. Pharm. Res. 27 (10), 2043–2053.** https://doi.org/10.1007/s11095-010-0159-x.

Lee, W.J., Park, H., Choi, J.H., Lee, H.J., Moon, S.W., Kang, J.H., Kim, Y.G., 2016. Short-term changes of intraocular pressure and ocular perfusion pressure after intravitreal injection of bevacizumab or ranibizumab. BMC Ophthalmology 16, 69.

**Lorget, F., Parenteau, A., Carrier, M., Lambert, D., Gueorguieva, A., Schuetz, C., Bantseev, V., Thackaberry, E., 2016. Characterization of the pH and temperature in the rabbit, pig, and monkey eye: key parameters for the development of long-acting delivery ocular strategies. Mol. Pharm. 13 (9), 2891–2896.** https://doi.org/10.1021/acs.molpharmaceut.5b00731.

Maurice, D.M., 1997. The regurgitation of large vitreous injections. J. Ocul. Pharmacol. Ther. 13 (5), 461–463.

Maurice, D.M., Mishima, S., 1984. Ocular pharmacokinetics. Pharmacology of the Eye. Springer 19–116.

Mezei, M., Meisner, D., 1993. Liposomes and nanoparticles as ocular drug delivery systems. Biopharm. Ocul. Drug Deliv. 91–101.

Nauck, M., Karakiulakis, G., Perruchoud, A.P., Papakonstantinou, E., Roth, M., 1998. Corticosteroids inhibit the expression of the vascular endothelial growth factor gene in human vascular smooth muscle cells. Eur. J. Pharmacol. 341 (2-3), 309–315.

Nicholson, B.P., Schachat, A.P., 2010. A review of clinical trials of anti-VEGF agents for diabetic retinopathy. Graefe's Arch. Clin. Exp. Ophthalmol. 248 (7), 915–930.

Peeters, L., Sanders, N.N., Braeckmans, K., Boussery, K., Voorde, J.V., De, S., De, S.C., Demeester, J., Van De Voorde, J., De Smedt, S.C., Demeester, J., 2005. Vitreous: A barrier to nonviral ocular gene therapy. Investig. Ophthalmol. Vis. Sci. 46, 3553–3561. https://doi.org/10.1167/iovs.05-0165.

Peyman, G.A., Khoobehi, B., Tawakol, M., Schulman, J.A., Mortada, H.A., Alkan, H., Fiscella, R., 1987. Intravitreal injection of liposome-encapsulated ganciclovir in a rabbit model. Retina 7 (4), 227–229.

Pitkänen, L., Ruponen, M., Nieminen, J., Urtti, A., 2003. Vitreous is a barrier in nonviral gene transfer by cationic lipids and polymers. Pharm. Res. 20, 576–583.

Ridolfo, R., Arends, J.J., van Hest, J.C.M., Williams, D.S., 2020. Wormlike Nanovector with Enhanced Drug Loading Using Blends of Biodegradable Block Copolymers. Biomacromolecules 21 (6), 2199–2207.

Ridolfo, R., Tavakoli, S., Junnuthula, V., Williams, D.S., Urtti, A., van Hest, J.C.M., 2021. Exploring the impact of morphology on the properties of biodegradable nanoparticles and their diffusion in complex biological medium. Biomacromolecules 22 (1), 126–133. https://doi.org/10.1021/acs.biomac.0c00726.

Rimpelä, A., Kiiski, I., Deng, F., Kidron, H., Urtti, A., 2018. Pharmacokinetic Simulations of Intravitreal Biologicals: Aspects of Drug Delivery to the Posterior and Anterior Segments. Pharmaceutics 11, 9. https://doi.org/10.3390/pharmaceutics11010009.

Sadeghi, A., Puranen, J., Ruponen, M., Valtari, A., Subrizi, A., Ranta, V.-P., Toropainen, E., Urtti, A., 2021. Pharmacokinetics of intravitreal macromolecules: scaling between rats and rabbits. Eur. J. Pharm. Sci. 159, 105720. https://doi.org/10.1016/j.ejps.2021.105720.

Sakurai, E., Ozeki, H., Kunou, N., Ogura, Y., 2001. Effect of particle size of polymeric nanospheres on intravitreal kinetics. Ophthalmic Res. 33 (1), 31–36.

Sanford, M., 2013. Fluocinolone acetonide intravitreal implant (Iluvien®). Drugs 73 (2), 187–193.

Schmitt, M., Hippeläinen, E., Raviña, M., Arango-Gonzalez, B., Antopolsky, M., Vellonen, K.-S., Airaksinen, A.J., Urtti, A., 2019. Intravitreal Pharmacokinetics in Mice: SPECT/CT Imaging and Scaling to Rabbits and Humans. Mol. Pharm. 16 (10), 4399–4404.

Shakirova, J.R., Sadeghi, A., Koblova, A.A., Chelushkin, P.S., Toropainen, E., Tavakoli, S., Kontturi, L.-S., Lajunen, T., Tunik, S.P., Urtti, A., 2020. Design and synthesis of lipid-mimetic cationic iridium complexes and their liposomal formulation for in vitro and in vivo application in luminescent bioimaging. RSC Adv. 10 (24), 14431–14440.

Smith, D.W., Lee, C.-J., Gardiner, B.S., 2020. No flow through the vitreous humor: How strong is the evidence? Progress in Retinal and Eye Research 78, 100845. https://doi.org/10.1016/j.preteyeres.2020.100845.

Syed, Y.Y., 2017. Fluocinolone acetonide intravitreal implant 0.19 mg (ILUVIEN®): a review in diabetic macular edema. Drugs 77, 575–583.

Tavakoli, S., Kari, O.K., Turunen, T., Lajunen, T., Schmitt, M., Lehtinen, J., Tasaka, F., Parkkila, P., Ndika, J., Viitala, T., Alenius, H., Urtti, A., Subrizi, A., 2021. Diffusion and Protein Corona Formation of Lipid-Based Nanoparticles in the Vitreous Humor: Profiling and Pharmacokinetic Considerations. Mol. Pharm. 18 (2), 699–713.

Tavakoli, S., Peynshaert, K., Lajunen, T., Devoldere, J., del Amo, E.M., Ruponen, M., De Smedt, S.C., Remaut, K., Urtti, A., 2020. Ocular barriers to retinal delivery of intravitreal liposomes: Impact of vitreoretinal interface. J. Control. Release. 328, 952–961.

Tremblay, C., Barza, M., Szoka, F., Lahav, M., Baum, J., 1985. Reduced toxicity of liposome-associated amphotericin B injected intravitreally in rabbits. Invest. Ophthalmol. Vis. Sci. 26, 711–718.

Tsotas, V.-A., Mourtas, S., Antimisiaris, S.G., 2007. Dexamethasone incorporating liposomes: effect of lipid composition on drug trapping efficiency and vesicle stability. Drug Deliv. 14 (7), 441–445.

van Oppen, L.M.P.E., Abdelmohsen, L.K.E.A., van Emst-de Vries, S.E., Welzen, P.L.W., Wilson, D.A., Smeitink, J.A.M., Koopman, W.J.H., Brock, R., Willems, P.H.G.M., Williams, D.S., van Hest, J.C.M., 2018. Biodegradable synthetic organelles demonstrate ROS shielding in human-complex-I-deficient fibroblasts. ACS Cent. Sci. 4 (7), 917–928.

Xu, Q., Boylan, N.J., Suk, J.S., Wang, Y.-Y., Nance, E.A., Yang, J.-C., McDonnell, P.J., Cone, R.A., Duh, E.J., Hanes, J., 2013. Nanoparticle diffusion in, and microrheology of, the bovine vitreous ex vivo. J. Control. Release 167 (1), 76–84.

Yang, Y., Bailey, C., Loewenstein, A., Massin, P., 2015. Intravitreal corticosteroids in diabetic macular edema: pharmacokinetic considerations. Retina 35 (12), 2440–2449.

Zeng, S., Hu, C., Wei, H., Lu, Y., Zhang, Y., Yang, J., Yun, G., Zou, W., Song, B., 1993. Intravitreal pharmacokinetics of liposome-encapsulated amikacin in a rabbit model. Ophthalmology 100 (11), 1640–1644. https://doi.org/10.1016/S0161-6420(93)31423-5.

Zhang, Y., Huo, M., Zhou, J., Xie, S., 2010. PKSolver: An add-in program for pharmacokinetic and pharmacodynamic data analysis in Microsoft Excel. Comput. Methods Programs Biomed. 99 (3), 306–314.

Zhou, X., Lv, J., Li, G., Qian, T., Jiang, H., Xu, J., Cheng, Y., Hong, J., 2021. Rescue the retina after the ischemic injury by polymer-mediated intracellular superoxide dismutase delivery. Biomaterials 268, 120600. https://doi.org/10.1016/j.biomaterials.2020.120600.

Zimmer, A.K., Maincent, P., Thouvenot, P., Kreuter, J., 1994. Hydrocortisone delivery to healthy and inflamed eyes using a micellar polysorbate 80 solution or albumin nanoparticles. Int. J. Pharm. 110 (3), 211–222.

# Publication V

*pharmaceutics*

MDPI

*Article*

# Pharmacokinetics of Pullulan–Dexamethasone Conjugates in Retinal Drug Delivery

**Eva Kicková [1,†], Amir Sadeghi [2,†], Jooseppi Puranen [2], Shirin Tavakoli [3], Merve Sen [4], Veli-Pekka Ranta [2], Blanca Arango-Gonzalez [4], Sylvia Bolz [4], Marius Ueffing [4], Stefano Salmaso [1], Paolo Caliceti [1], Elisa Toropainen [2], Marika Ruponen [2] and Arto Urtti [2,3,5,*]**

1 Department of Pharmaceutical and Pharmacological Sciences, University of Padova, Via F. Marzolo 5, 35131 Padova, Italy; eva.kickova@yahoo.com (E.K.); stefano.salmaso@unipd.it (S.S.); paolo.caliceti@unipd.it (P.C.)
2 School of Pharmacy, Faculty of Health Sciences, University of Eastern Finland, Yliopistonranta 1C, 70211 Kuopio, Finland; amir.sadeghi@uef.fi (A.S.); jooseppi.puranen@uef.fi (J.P.); veli-pekka.ranta@uef.fi (V.-P.R.); elisa.toropainen@uef.fi (E.T.); marika.ruponen@uef.fi (M.R.)
3 Drug Research Program, Faculty of Pharmacy, University of Helsinki, Viikinkaari 5E, 00710 Helsinki, Finland; shirin.tavakoli@helsinki.fi
4 Centre for Ophthalmology, Institute for Ophthalmic Research, University of Tübingen, Elfriede-Aulhorn-Str. 7, D-72076 Tübingen, Germany; merve.sen@uni-tuebingen.de (M.S.); blanca.arango-gonzalez@klinikum.uni-tuebingen.de (B.A.-G.); sylvia.bolz@uni-tuebingen.de (S.B.); mue@klinikum.uni-tuebingen.de (M.U.)
5 Institute of Chemistry, St. Petersburg State University, Petergof, Universitetskii pr. 26, 198504 St. Petersburg, Russia
* Correspondence: arto.urtti@uef.fi
† Eva Kicková and Amir Sadeghi have equal contribution to the first authorship.

**Abstract:** The treatment of retinal diseases by intravitreal injections requires frequent administration unless drug delivery systems with long retention and controlled release are used. In this work, we focused on pullulan (≈67 kDa) conjugates of dexamethasone as therapeutic systems for intravitreal administration. The pullulan–dexamethasone conjugates self-assemble into negatively charged nanoparticles (average size 326 ± 29 nm). Intravitreal injections of pullulan and pullulan–dexamethasone were safe in mouse, rat and rabbit eyes. Fluorescently labeled pullulan particles showed prolonged retention in the vitreous and they were almost completely eliminated via aqueous humor outflow. Pullulan conjugates also distributed to the retina via Müller glial cells when tested in ex vivo retina explants and in vivo. Pharmacokinetic simulations showed that pullulan–dexamethasone conjugates may release free and active dexamethasone in the vitreous humor for over 16 days, even though a large fraction of dexamethasone may be eliminated from the eye as bound pullulan–dexamethasone. We conclude that pullulan based drug conjugates are promising intravitreal drug delivery systems as they may reduce injection frequency and deliver drugs into the retinal cells.

**Keywords:** pullulan; dexamethasone; conjugate; retinal drug delivery; ocular fluorophotometry; optical coherence tomography; pharmacokinetics



**Citation:** Kicková, E.; Sadeghi, A.; Puranen, J.; Tavakoli, S.; Sen, M.; Ranta, V.-P.; Arango-Gonzalez, B.; Bolz, S.; Ueffing, M.; Salmaso, S.; et al. Pharmacokinetics of Pullulan–Dexamethasone Conjugates in Retinal Drug Delivery. *Pharmaceutics* **2022**, *14*, 12. https://doi.org/10.3390/pharmaceutics14010012

Academic Editor: Ken-ichi Hosoya

Received: 22 November 2021
Accepted: 17 December 2021
Published: 21 December 2021



## 1. Introduction

Intravitreal injection is the most important mode of drug administration in the treatment of retinal diseases. In particular, anti-inflammatory drugs (e.g., corticosteroids) [1–3] and anti-neovascular inhibitors of vascular endothelial growth factor (VEGF) (antibodies, Fab-fragments, soluble receptors and aptamers) are widely used in clinics [4–8]. In general, intravitreal injections are safe, but frequent injections may result in reduced patient compliance and some rare, but serious, adverse effects (e.g., infection and retinal detachment) [5,9]. Implants with prolonged ocular residence and controlled release have been developed to prolong injection intervals of dexamethasone (e.g., Ozurdex) [1,3,9]. On the other hand, delivery systems for trafficking therapeutics to the retinal cells (e.g., intracellularly acting

peptides, proteins and nucleic acids) are needed. Therefore, nanoparticles and peptide conjugates have been recently investigated for retinal delivery of dexamethasone and nucleic acids [10–12].

Modified polysaccharides are promising candidates for the development of ocular drug delivery systems [13]. For example, pullulan [14], dextran [15], hyaluronic acid [16] and chitosan [17] have been investigated in this respect. Many polysaccharides can be chemically functionalized for optimized drug delivery [13,18] and they can be formulated as macroscopic implants [19,20], gels [21] and nanosized formulations [22]. In most studies, drugs have been physically encapsulated into the polysaccharide formulations, such as polymeric micelles or nanoparticles [13,23–25], whereas chemical covalent conjugation technologies have not been applied for ocular in vivo drug delivery with polysaccharides. Recently, the chemical conjugation through hydrazone bond was used to generate peptide-dexamethasone and pullulan–dexamethasone conjugates that were investigated in vitro [10,26]. In contrast to the ocular field, polymeric drug conjugates have been widely investigated to provide site-specificity and extended drug release in some other medical indications [27–32].

We have been investigating drug carriers based on pullulan, a fungal extracellular polysaccharide produced by *Aureobasidium pullulans* [33,34]. Inexpensive and conveniently modified pullulan is considered to be a biocompatible polymer. Previously, pullulan has been used as a backbone in the synthesis of bioconjugates for drug delivery to the liver and pancreas [14,27,33,35–37]. Conjugation of hydrophobic drugs to pullulan results in self-assembled colloids with drug molecules oriented to the core of the nanoparticles [27,28,33,35,36].

In this study, we investigated dexamethasone conjugates of pullulan that were obtained with recently published synthetic procedures [26]. Dexamethasone was conjugated to pullulan through a hydrazone bond that is expected to control drug release under the acidic intracellular compartments (endosomes or lysosomes). We investigated ocular safety, retinal distribution and ocular pharmacokinetics of fluorescently labelled pullulan–dexamethasone after intravitreal injections into mouse, rat and rabbit eyes. Retinal distribution of the conjugates was also investigated using ex vivo retinas of mice and cows.

## 2. Materials and Methods

Pullulan (67 kDa) was purchased from Hayashibara Biochemical Laboratories, Okayama, Japan. Dexamethasone (DEX) was purchased from Sigma/Merck KgaA, Darmstadt, Germany. Cyanine3 (Cy3) and bodipy (BDP) were purchased from Lumiprobe GmbH, Hannover, Germany.

### *2.1. Synthesis of Pullulan Conjugates*

Cy3-pullulan-DEX and Cy3-pullulan have recently been prepared and characterized by Kicková et al. [26]. Similar synthetic strategy was applied to prepare versions with green fluorescent label starting from pullulan-DEX, namely BDP-pullulan-DEX and BDP-pullulan (Supporting Information, SI-1). The chemical identity of the conjugates (Figure 1) was confirmed by the NMR spectroscopy (SI-1 and in Kicková et al. [26]).

Stock samples of pullulan-DEX, Cy3-pullulan-DEX, BDP-pullulan-DEX, Cy3-pullulan and BDP-pullulan were generated by dispersing them in mQ water or phosphate buffered saline.

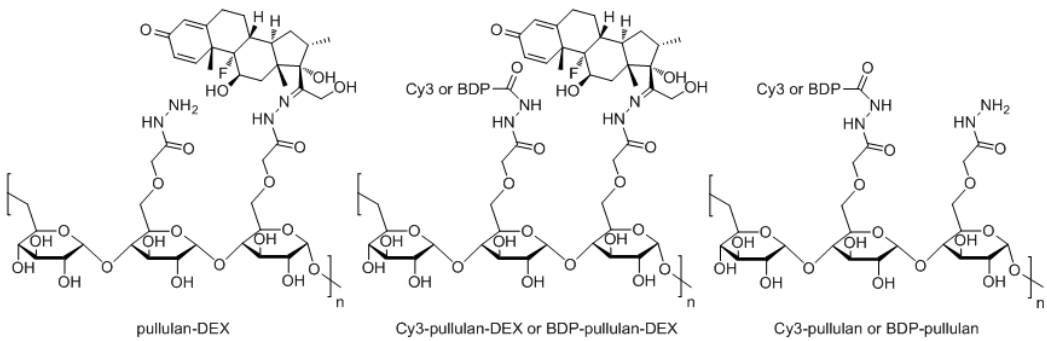


**Figure 1.** Chemical structures of fluorescently labelled pullulan conjugates. Synthetic details can be found in a recent publication [26] and in Supporting Information SI-1.

### *2.2. Size and Zeta Potential*

Aqueous dispersions of pullulan-DEX, Cy3-pullulan-DEX and BDP-pullulan-DEX were analyzed by dynamic light scattering (DLS) using the Zetasizer Nano ZS (Malvern Instrument Ltd., Malvern, Worcestershire, UK). Zeta potentials were analyzed from 1 mg/mL polymer dispersions in 1 mM phosphate buffer (pH 7.4) at room temperature. All analyses were performed in triplicate.

### *2.3. Endotoxin Tests*

The endotoxins in the pullulan conjugate dispersions were determined using Limulus Amebocyte Lysate gel-clot endotoxin assessment kit (Bioscience Lonza, Basel, Switzerland) according to the manufacturer's instructions. The stock solutions (5 mg/mL) of BDP-pullulan-DEX and BDP-pullulan were prepared in sterile PBS at pH 7.4. These dispersions were further diluted 1:1, 1:2 and 1:4 (*v*/*v*) with sterile endotoxin-free water as duplicates. The conjugate samples, endotoxin standards (1.0, 0.5, 0.25, 0.125, 0.06 and 0.03 EU/mL) and endotoxin-free water were transferred to reaction tubes (100 µL/tube) and reconstituted with Limulus Amebocyte Lysate reagent (100 µL) in each tube. After one-hour incubation at 37 °C each tube was inverted 180 degrees. Formation of firm gel was considered as an indication of endotoxin positivity.

### *2.4. Ex Vivo Retinal Studies*

#### 2.4.1. Ex Vivo Mouse Retinal Organ Culture

Six day old (PN6) wild-type mice (C57BL/6) were used in this study. The mice were housed and bred under standard white cyclic lighting with free access to food and water. All mouse procedures were approved by the Tübingen University committee on animal protection (Mitteilung nach §4 Abs. 3 TierSchG Nr. AK 03/20 M) and performed in compliance with the Association for Research in Vision and Ophthalmology ARVO Statement.

The preparation of organotypic retinal culture and maintenance of the retinal explants were performed according to published protocols [38–41] (for more details see SI-2). The tissues were randomly assigned to the following treatment groups: Cy3-pullulan (1.7 mg/mL), Cy3-pullulan-DEX (0.7, 1.4, and 1.9 mg/mL) and untreated control. The treatments were carefully applied on the top of the retinal tissues (on the ganglion cell layer) using volumes of 15 µL. Six retinal tissues were used for each group. The complete medium (1 mL) under the retina was changed every 48 h and maintained in a humidified atmosphere of 5% $CO_2$ at 37 °C for six days.

The dying cells in the retinal explants were monitored using TUNEL assay with in situ cell death detection kit based on conjugated fluorescein isothiocyanate [42]. The percentage of positive cells was derived by dividing the number of positive cells by the total number of

outer nuclear layer (ONL) or inner nuclear layer (INL) cells. One-way ANOVA method and Tukey's multiple comparisons test were selected for the statistical analyses, **** $p < 0.0001$.

#### 2.4.2. Ex Vivo Bovine Vitreo-Retinal Organ Culture

Fresh bovine eyes were obtained from a local slaughterhouse (HKScan Finland Oy, Outokumpu, Turku, Finland). The eyes were transported in carbon dioxide-independent medium at 4 °C (GIBCO, Thermo Fisher Scientific, Dreieich, Germany), cleaned from the connective tissues and dipped shortly into 20% ($v/v$) ethanol/water solution. The eyes were kept in carbon dioxide-independent medium at room temperature followed by 10 min incubation at 37 °C prior to dissection.

Vitreo-retinal explants were prepared as reported by Tavakoli et al. [43,44]. The vitreo-retinal explant with intact inner limiting membrane (1–2 $cm^2$) was placed onto a Transwell® membrane (75 mm, 0.4 µm pore, Corning Incorporated, Kennebunk, ME, USA) and the supplemented Neurobasal®-A medium (GIBCO, Thermo Fisher Scientific, Dreieich, Germany) was added under the membrane. BDP-pullulan-DEX (5 mg/mL) was carefully injected (100 µL) in the vitreous of the vitreo-retinal explant. Injections were performed horizontally to prevent retinal damage and avoid crossing the inner limiting membrane. The vitreo-retinal explant was maintained in a humidified atmosphere containing 5% $CO_2$ at 37 °C.

After incubation for 24 h, 20 cryosections of the vitreo-retinal explant were generated. Immunohistochemistry and imaging were performed according to the previously published methods [43,44]. Rabbit anti-collagen IV antibody (Abcam plc., Cambridge, UK) was used for labelling the inner limiting membrane. Hoechst (Thermo Fisher Scientific Inc./Invitrogen™, Carlsbad, CA, USA) stain was used to label the nuclei and Alexa Fluor 568-labelled goat anti-rabbit secondary antibody (Thermo Fisher Scientific Inc./Invitrogen™, Carlsbad, CA, USA) was used to label inner limiting membrane. The images were obtained by confocal microscope (Leica TCS SP8, Leica Microsystems GmbH, Wetzlar, Germany) using 20× (HC PL APO) and 93× (HC PL APO) objectives.

### *2.5. In Vivo Animal Studies*

Four months old male pigmented rats (HsdOla/LH), twelve-months old female albino New Zealand White rabbits and two-months old male pigmented mice (C57BL/6J) were used in these studies. The animals were housed under standard white cyclic lighting with free access to food and water. All experiments were designed and conducted in accordance with the guidelines of the ARVO Statement for the Use of Animals in Ophthalmic and Vision Research. All procedures were approved by the Finnish National Animal Experiment Broad (ELLA, Regional State Administrative Agency for Southern Finland), performed under project license (ESAVI-2020-027769) and in compliance with 3Rs principle (replacement, reduction and refinement) monitored by animal-welfare body of University of Eastern Finland Lab Animal Center (UEF LAC).

#### 2.5.1. Safety Studies in Mice

Mice were anesthetized with intraperitoneal injection of 60 mg/kg ketamine (Ketaminol®, 50 mg/mL; Pfizer Oy Animal Health, Espoo, Finland) and 0.4 mg/kg medetomidine (Domitor®, 1 mg/mL; Orion Pharma, Espoo, Finland). The mouse pupils were dilated with topically applied 0.5% tropicamide (Oftan® Tropicamid, 5 mg/mL; Santen Pharmaceutical Co., Ltd., Tampere, Finland). Under full anaesthesia, volumes of 1 µL of Cy3-pullulan (5 mg/mL) or Cy3-pullulan-DEX (5 mg/mL) in PBS (pH 7.4) were injected intravitreally into mice using Hamilton microinjector (Hamilton Co., Reno, NV, USA). A topical eye drop (Viscotears®, Alcon, Finland) was applied after intravitreal injections to prevent dryness of the cornea. Quality of intravitreal injections was confirmed by optical coherence tomography (OCT) and fundus camera (Phoenix MICRON™, Berkeley, CA, USA).

After 24 h the mice were sacrificed, the eyes were removed and incubated in a 4% PFA solution for 2 h. The eyes were stored in 1% PFA solution until further processing of

organotypic retinal cultures. The following procedures were performed according to published protocols [38–42] and method described in SI-2.

#### 2.5.2. Ocular Retention and Safety Studies in Rats

Anesthesia was induced in a box using an inhalation system run at 450–500 mL/min air flow and ≈4% of isoflurane purchased from Chanelle Pharma (London, UK). The anesthesia was maintained by 200–250 mL/min air flow containing ≈2% isoflurane. The eye muscles were relaxed with topical instillation of medetomidine. The pupil was dilated by topical instillation of tropicamide and phenylephrine (Oftan® Metaoksedrin, 100 mg/mL; Santen Pharmaceutical Co., Ltd., Tampere, Finland) few minutes before each measurement. The baseline autofluorescence in fluorophotometry (Ocumetrics, Inc., Mountain View, CA, USA) and fundus/OCT images of each eye were captured before intravitreal injections. Local ocular surface anesthesia was induced shortly before intravitreal injections by topical instillation of oxybuprocaine (Oftan® Obucain, 4 mg/mL; Santen Pharmaceutical Co., Ltd., Tampere, Finland).

The injected solutions were prepared in isotonic PBS buffer in a sterile condition. Intravitreal injections of BDP-pullulan (3 µL, 5 mg/mL) and BDP-pullulan-DEX (3 µL, 10 mg/mL) in PBS (pH 7.4) were performed with a Hamilton syringe (Hamilton Co., Reno, NV, USA) equipped with a 34 G needle. BDP-pullulan with 2.2% GPU (glucose per unit, repetition unit in the pullulan chain) modification by BDP (corresponding to 6% $w/w$) and BDP-pullulan-DEX with 1.1% GPU modification by BDP (corresponding to 3% $w/w$) and 5.2% GPU modification by DEX (corresponding to 10% $w/w$) were used in these experiments. Immediately after the intravitreal injections the eyes were topically covered with carbomer hydrogel (Viscotears®, 2 mg/g; Dr. Winzer Pharma, Berlin, Germany) to prevent corneal drying. Fundus and OCT images were obtained to check the quality of injections. The procedures of anesthesia, topical drop, muscle relaxant and pupillary dilatant applications were used in all measurements.

#### 2.5.3. Fluorophotometric Studies with Rabbits

The rabbits were anesthetized by s.c. injection of 0.5 mg/kg medetomidine and ketamine (25 mg/kg; Ketaminol®, 50 mg/mL; Pfizer Oy Animal Health, Espoo, Finland). The pupils were dilated by using topical tropicamide eye drop. The baseline autofluorescence for each eye was measured before intravitreal injection. Oxybuprocaine was instilled topically as local anesthetic a few minutes before the intravitreal injections.

The intravitreal injection (50 µL) of BDP-pullulan-DEX (10 mg/mL) solution in PBS (pH 7.4) was performed with 31 G needle inserted about 4 mm from the limbus transsclerally into the vitreous. Immediately after intravitreal injections, the eyes were topically covered with carbomer hydrogel to prevent corneal dryness.

The experimental measurements were performed under light sedation at various time points post-injection. Medetomidine (0.4 mg/kg) was used as a sedative by s.c. injection and topical tropicamide was used to dilate pupils a few minutes before each measurement. Atipamezole (0.2 mL/kg; Antisedan®, 5 mg/mL; Orion Pharma, Espoo, Finland) was used as an antagonist to reverse the sedation by s.c. injection.

The post-injection fluorescence signals were measured from the vitreous and aqueous humor. Autofluorescence was subtracted and the resulting values were converted to BDP-pullulan and BDP-pullulan-DEX concentrations with calibration standards (see SI-3, Figures S2 and S3). The concentrations were used to determine pharmacokinetic parameters (clearance, volume of distribution and half-life) with PKSolver software [45]. One compartment model with first-order elimination rate was used for curve fitting. The nonlinear weighting [1/(observed concentration)$^2$] method was used to improve the quality of fitting for terminal time points. More details on in vivo fluorophotometry and pharmacokinetic analyses can be found in our earlier publications [10,15].

2.5.4. Pharmacokinetic Simulations

Pharmacokinetic simulations were performed to estimate the elimination routes of polymer conjugate. The experimental values for the vitreal clearance and volume of distribution were used to build the model. The simulated in vivo release rate of dexamethasone was assumed to be similar with the release rate in vitro [26] (SI-4, Figure S4). The simulations for the concentrations of free dexamethasone in the vitreous and aqueous humor were performed for the rat, rabbit and human eyes. The schematic representation of the model is shown in Figure 2. The details are shown in SI-4, Table S1 and Figure S5. For numerical simulations, STELLA® software version. 8.1.1 (isee systems, Lebanon, NH, USA) was used with fourth order Runge–Kutta algorithm.

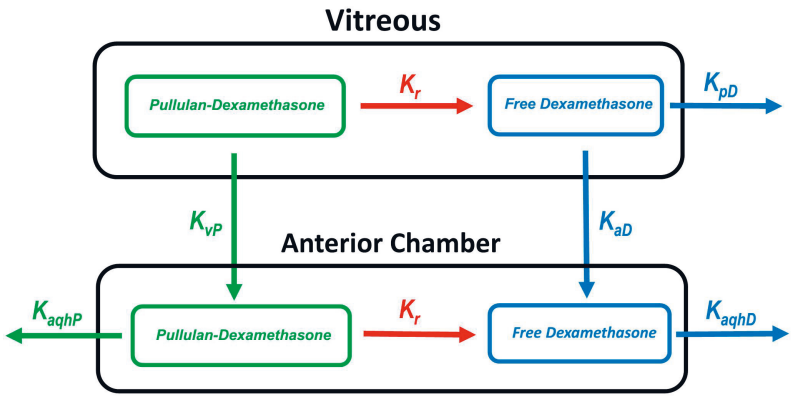


**Figure 2.** Scheme of the kinetic simulation model. The following parameters were used: $K_r$ (first-order release rate constant); $K_{pD}$ (elimination rate constant of free dexamethasone posteriorly from the vitreous); $K_{aD}$ (distribution rate constant of free dexamethasone from the vitreous to the anterior chamber); $K_{vP}$ (distribution rate constant of pullulan–dexamethasone from the vitreous to the anterior chamber); $K_{aqhP}$ (elimination rate constant of pullulan–dexamethasone from the anterior chamber) and $K_{aqhD}$ (elimination constant of dexamethasone from the anterior chamber). For detailed parameter values, see Supporting Information SI-4.

## 3. Results

### *3.1. Synthesis and Characterization of Pullulan Conjugates*

Pullulan is a water-soluble polysaccharide but conjugation of pullulan with dexamethasone (DEX) as a hydrophobic molecule results in an amphiphilic derivative that undergoes self-assembly to nanoparticles. The self-assembled particles of Cy3-pullulan-DEX and BDP-pullulan-DEX were smaller than pullulan-DEX particles and all nanoparticles had negative zeta potentials (Table 1).

**Table 1.** Intensity based mean sizes (±SD), polydispersity indices (PDI) and zeta potentials of the pullulan conjugate nanoparticles. The measurements were performed by dynamic light scattering.

| Sample | Mean Size ± SD (nm) | PDI | Zeta Potential (mV) |
|---|---|---|---|
| pullulan-DEX | 461 ± 30 | 0.39 ± 0.04 | −38.1 ± 0.5 |
| Cy3-pullulan-DEX | 299 ± 42 | 0.22 ± 0.11 | −20.3 ± 3.0 |
| BDP-pullulan-DEX | 219 ± 15 | 0.25 ± 0.07 | −40.9 ± 1.1 |

The endotoxin level of formulations was measured. All tested concentrations (2.5, 1.25 and 0.63 mg/mL) of fluorescently labelled BDP-pullulan-DEX showed endotoxin levels below 0.03 mEU/µL. Thus, endotoxin levels in the formulations used for in vivo administration are at acceptable levels below 0.2 EU per injection [46,47].

### 3.2. Intravitreal Kinetics of Pullulan Conjugates

Intravitreally administered BDP-pullulan and BDP-pullulan-DEX were monitored by fluorophotometry, fundus camera and OCT in rats. Vitreal elimination of pullulan formulations followed first-order elimination kinetics and the average vitreal half-life of both formulations was about 17 h in the rat eyes (Figure 3, Table 2). Fundus images showed that the formulations retained for about 3–5 days in the rat vitreous (Figure 4). The apparent volumes of distribution of pullulan conjugates (range of 42–84 μL) were close to the anatomical volume of rat vitreous (≈50 μL), whereas the vitreal clearance values (range of 1.8–3.5 μL/h) were lower than the average of aqueous humor flow rate in rats (21 μL/h) [48].

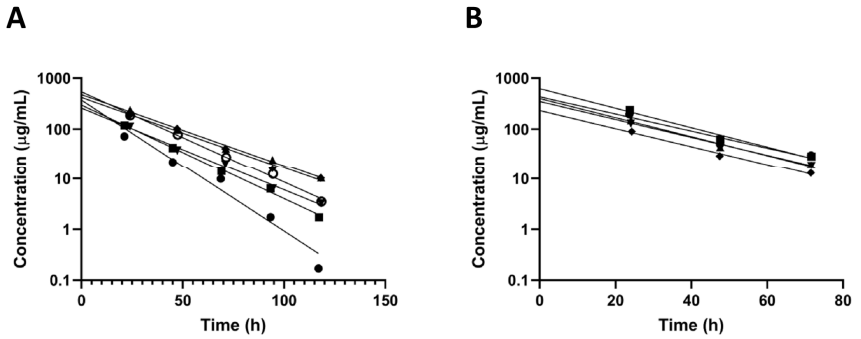


**Figure 3.** Concentrations of fluorescently labelled (**A**) BDP-pullulan ($n$ = 6 eyes) and (**B**) BDP-pullulan-DEX ($n$ = 5 eyes) in the vitreous of rats. One compartment model with first-order elimination rate constant was used for curve fitting (lines). The derived kinetic parameters are shown in Table 2. Each line represents the measurement from individual rat eye.

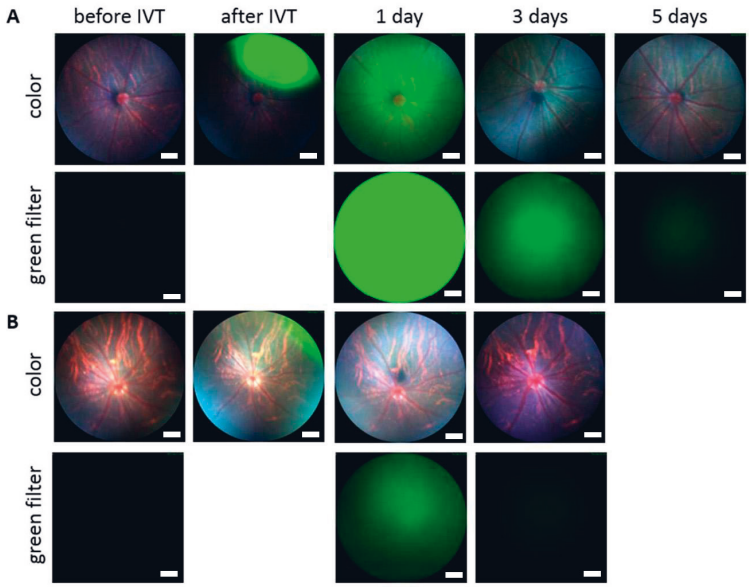


**Figure 4.** Full color and green fluorescent fundus images of rat eyes before and after intravitreal injection (IVT) of (**A**) BDP-pullulan and (**B**) BDP-pullulan-DEX. After one day, the labeled compounds distribute homogeneously in the vitreous. The length of scale bar is 200 μm.

**Table 2.** Kinetic parameters of intravitreally injected fluorescently labelled: BDP-pullulan ($n$ = 6 rat eyes) and BDP-pullulan-DEX ($n$ = 5 rat eyes; $n$ = 6 rabbit eyes) derived from fluorophotometric measurements.

| Material | Dose (μg) | Species | $C_0$ (μg/mL) | $t_{1/2}$ (h) | $V_d$ (μL) | CL (μL/h) |
|---|---|---|---|---|---|---|
| BDP-pullulan | 15 | rats | 386.4 ± 110.2 | 17.4 ± 3.9 | 42 ± 12 | 1.8 ± 0.7 |
| BDP-pullulan-DEX | 30 | rats | 393.7 ± 134.1 | 16.7 ± 0.8 | 84 ± 30 | 3.5 ± 1.2 |
| BDP-pullulan-DEX * | 500 | rabbits | 539.3 ± 43.1 | 60.3 ± 4.9 | 932 ± 72 | 11 ± 0.4 |

* The elimination half-life in rabbit aqueous humor was 87.5 ± 7.3 h.

BDP-pullulan-DEX concentrations in aqueous humor and vitreous were evaluated in rabbits by in vivo fluorophotometry. The vitreal half-life in rabbits (≈60 h) was longer than in the rats (≈17 h) and the elimination kinetics showed minimal inter-subject variability (Figure 5, Table 2). The average volume of distribution (932 μL) was close to the anatomical volume of vitreous humor in rabbits (≈1.5 mL) (Table 2). Moreover, in rabbits, the vitreal clearance (11 μL/h) was lower than the average of aqueous humor flow rate in normal albino rabbits (180 μL/h). The concentrations of BDP-pullulan-DEX in the aqueous humor were consistently about one order of magnitude lower than in the vitreous (Figure 5).

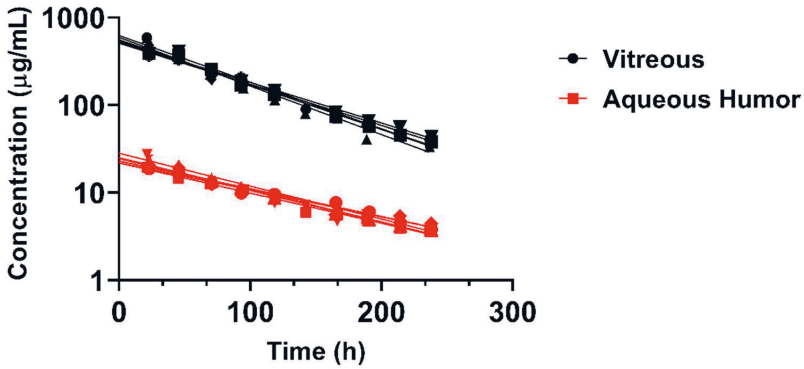


**Figure 5.** Concentrations of fluorescently labelled BDP-pullulan-DEX in the vitreous and aqueous humor of six rabbit eyes. Each line was fitted for the experimental data of one eye at different time points. One compartment model with first-order elimination rate constant was used for curve fitting.

### *3.3. Pharmacokinetic Simulations*

A kinetic model (Figure 2) was used to simulate the concentrations of pullulan-DEX in the vitreous and aqueous humor. The simulated results matched the experimental results from rat and rabbit vitreous, when the model assumes that all elimination takes place anteriorly (Figure 6A,B). For rabbit eye, the simulated concentrations in the aqueous humor were remarkably close to experimental values, supporting the dominant role of anterior route for nanoparticle elimination from the vitreous. The experimental values for aqueous humor could not be measured accurately with fluorophotometry in the rat eyes. In order to scale the kinetics of the formulation from preclinical animals to human, the vitreal kinetics of pullulan conjugate were simulated in humans (Figure 6C). It is evident that the retention of pullulan conjugates is longer in the human eyes than in the rabbit eyes. Retention in the rabbit eyes is much longer than in the rat eyes (Figure 6A,B).

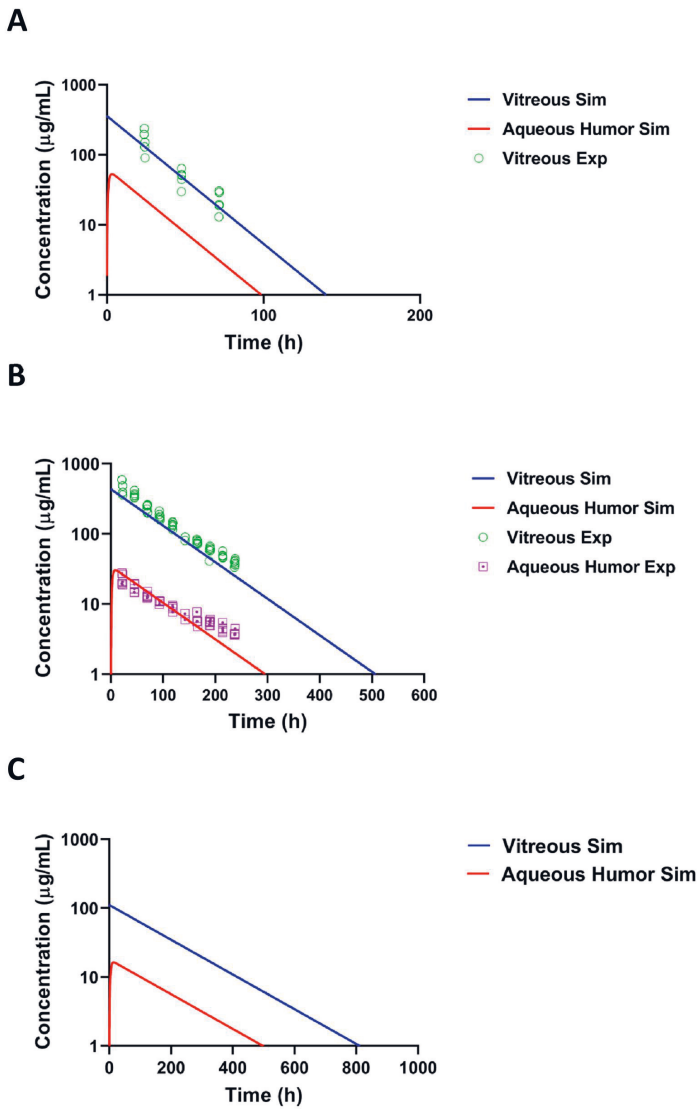


**Figure 6.** Simulated and experimental concentrations of BDP-pullulan-DEX in (**A**) rat, (**B**) rabbit and (**C**) human. The blue and red line shows the simulated concentration in vitreous and aqueous humor, respectively. The experimental concentrations in the vitreous and aqueous humor are indicated in the graphs.

The route of BDP labelled pullulan dexamethasone conjugate elimination in the rabbit eyes was further explored with Maurice plot that shows the relationship between $C_a/C_v$ and vitreal half-life (Figure 7) [49]. Location of pullulan conjugate in this plot, next to the straight line of compounds with anterior elimination route, supports the notion that the conjugate is mainly eliminated via anterior route. The plot is based on the equation $C_a/C_v = V_v\ k_v/nf$, where $C_a$ is the concentration in the aqueous humor, $C_v$ is the concentration in the vitreous humor, $V_v$ is the volume of distribution in the vitreal compartment (unit: µL), $k_v$ is the first order elimination rate constant (i.e., $k_v = \ln 2/t_{1/2}$) (unit: $h^{-1}$), f is the outflow rate of aqueous humor (unit: µL/min) and *n* is the coefficient that indicates the

fraction of anterior drug elimination after intravitreal injection. The average experimental $C_a/C_v$ ratio is 0.072 ± 0.021. Using a literature value of f (3 µL/min) and experimental values for $V_v$ (932 µL) and $t_{1/2}$ (60.3 h), we obtained *n* value of 0.827 or 82.7% elimination via anterior route. At average rabbit $V_v$ from the literature (1150 µL) [50], we obtained *n* value of 1.02 suggesting complete (≈100%) anterior elimination. Calculation based on both Vv (932 and 1150 µL) reveal anterior route as the main elimination pathway for pullulan conjugate. In Figure 7, three volumes of distribution (932, 1150 and 1700 µL) were used to derive the lines, indicating anterior chamber as the only elimination route.

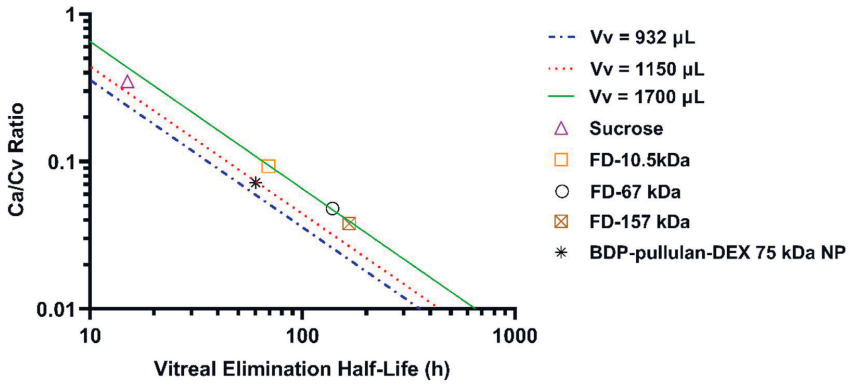


**Figure 7.** Maurice plot of intravitreally administered compounds in the rabbit eyes. The plot shows anteriorly eliminating compounds based on literature data: sucrose (0.342 kDa) [51], FITC-dextran (FD-10.5, FD-67 and FD-157 kDa) [52,53]. The green, red and blue line are derived from Maurice equation by assuming 932, 1150 and 1700 µL as vitreal volume of distribution. Location of BDP-pullulan-DEX NP (~75 kDa) data at close vicinity of the straight lines indicates anterior route of elimination in the rabbit eyes as the main elimination pathway.

Concentrations of free dexamethasone were simulated based on the pullulan conjugate retention in the eye and the published [26] release rate of dexamethasone from dexamethasone-pullulan conjugates. The simulated levels of free dexamethasone after intravitreal injection of BDP-pullulan-DEX in rats and rabbits are presented in Figure 8A,B. The simulated dexamethasone concentrations in the vitreous remain above the minimal active concentration 1 nM (or 0.394 ng/mL) [54] for 3.6, 16.5 and 25.5 days in the rats, rabbits and humans, respectively (Figure 8A–C). The simulations also reveal that only a small fraction of injected dexamethasone in the conjugate is released during the residence time of the polymeric conjugate in the eye (Table 3). Interestingly, the concentrations in the vitreous and aqueous humor differ more in the rabbits and humans than in the rats.

**Table 3.** Pharmacokinetic parameters of dexamethasone derived from simulations of intravitreally injected BDP-pullulan-DEX to rat, rabbit and human eyes. The dose of dexamethasone was 3, 50 and 50 µg per eye for rats, rabbits and humans, respectively.

| Parameter | Unit | Rat | Rabbit | Human |
|---|---|---|---|---|
| $C_{max\ Vitreous}$ | ng·mL$^{-1}$ | 14 | 58 | 24 |
| $T_{max\ Vitreous}$ | h | 5 | 15 | 24 |
| $C_{max\ Aqueous\ Humor}$ | ng·mL$^{-1}$ | 5 | 5 | 6 |
| $T_{max\ Aqueous\ Humor}$ | h | 5 | 15 | 24 |
| Aqueous humor/vitreous concentration ratio [a] | | 0.35 | 0.086 | 0.23 |
| Duration above minimal effective concentration | day | 3.6 | 16.5 | 25.5 |
| Dose of BDP-pullulan-DEX per eye | µg | 30 | 500 | 500 |
| Percent of the released DEX in the vitreous | % | 0.8 | 2.5 | 4.7 |
| Percent of the released DEX in the aqueous humor | % | 0.028 | 0.05 | 0.04 |

[a] Averaged at pseudo-steady state phase.

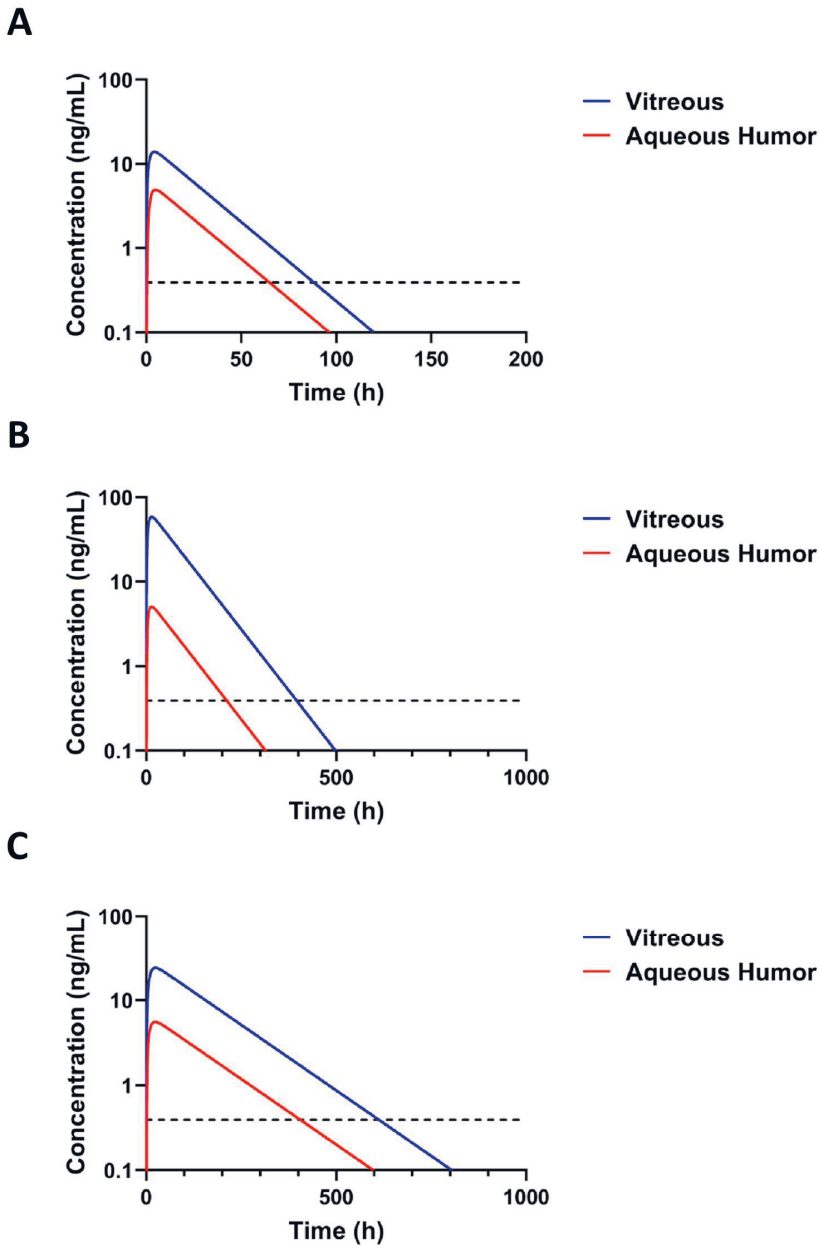


**Figure 8.** Simulation of released dexamethasone concentration in the vitreous and in the aqueous humor after intravitreal injection of BDP-pullulan-DEX in rat (**A**), rabbit (**B**) and human (**C**). The simulated doses of BDP-pullulan-DEX were 30, 500 and 500 μg per eye for rats, rabbits and humans, corresponding to DEX doses of 3, 50 and 50 μg per eye for rats, rabbits and humans, respectively. The dotted line (- - -) shows the minimum effective intravitreal concentration of dexamethasone for inhibiting the expression of VEGF, which is 1 nM (or 0.394 ng/mL) [54].

### *3.4. Safety Assessment of Pullulan-Based Formulations*

The safety of pullulan-based formulations was investigated ex vivo in mouse retinal explants and in vivo treated animals.

#### 3.4.1. Safety on Ex Vivo Mouse Retinal Explants

Ex vivo mouse retinal explants were treated with Cy3-pullulan (1.7 mg/mL) or Cy3-pullulan-DEX (0.7, 1.4 and 1.9 mg/mL) and untreated explants were used as controls. All three Cy3-pullulan-DEX concentrations significantly reduced the percentage of TUNEL positive cells in both the inner nuclear layer (INL) and the outer nuclear layer (ONL), indicating a reduction in the cell death in both layers (Figure 9A,B). This is due to the neuroprotective effect of DEX in ex vivo mouse retinal explants [55]. Treatment with Cy3-pullulan alone did not increase TUNEL labelled cells, indicating that the polymer had no toxic effects. The number of INL and ONL cell rows did not change (Figure 9C,D).

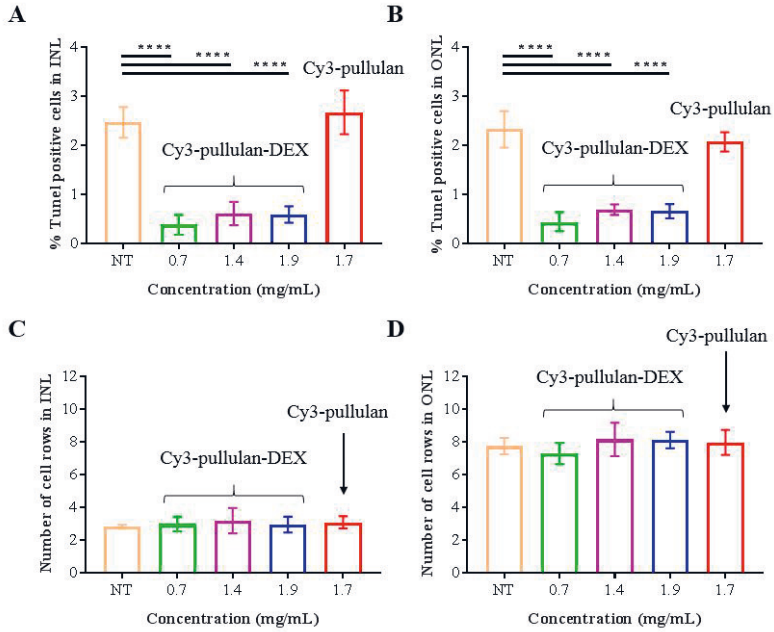


**Figure 9.** Ex vivo retinal explants of mice were treated with 15 µL of fluorescently labelled Cy3-pullulan-DEX (0.7, 1.4 and 1.9 mg/mL) and Cy3-pullulan (1.7 mg/mL). Untreated retina (NT) was used as control explant. TUNEL-positive nuclei in (**A**) the inner nuclear cell layer (INL), and (**B**) the outer nuclear cell layer (ONL) were counted and plotted as percentage of all nuclei in the INL and ONL areas. The number of cell rows in (**C**) INL and (**D**) ONL are also presented. Bars indicate standard deviations of means. One-way ANOVA **** $p < 0.0001$.

To evaluate any inflammatory response due to the conjugates, we visualized the microglial cell shape and distribution using Iba-1 antibody, an inflammatory marker for microglia. The microglial cells were observed in ganglion cell layer (GCL) and INL in all groups, but no microglial migration to the ONL was seen (Figure 10). The conjugates (Cy3-pullulan, Cy3-pullulan-DEX) were found in all monitored layers, mostly in GCL and INL, and partially in ONL. The inflammatory response of microglia was not activated, and the conjugates are well tolerated in the ex vivo retinas.

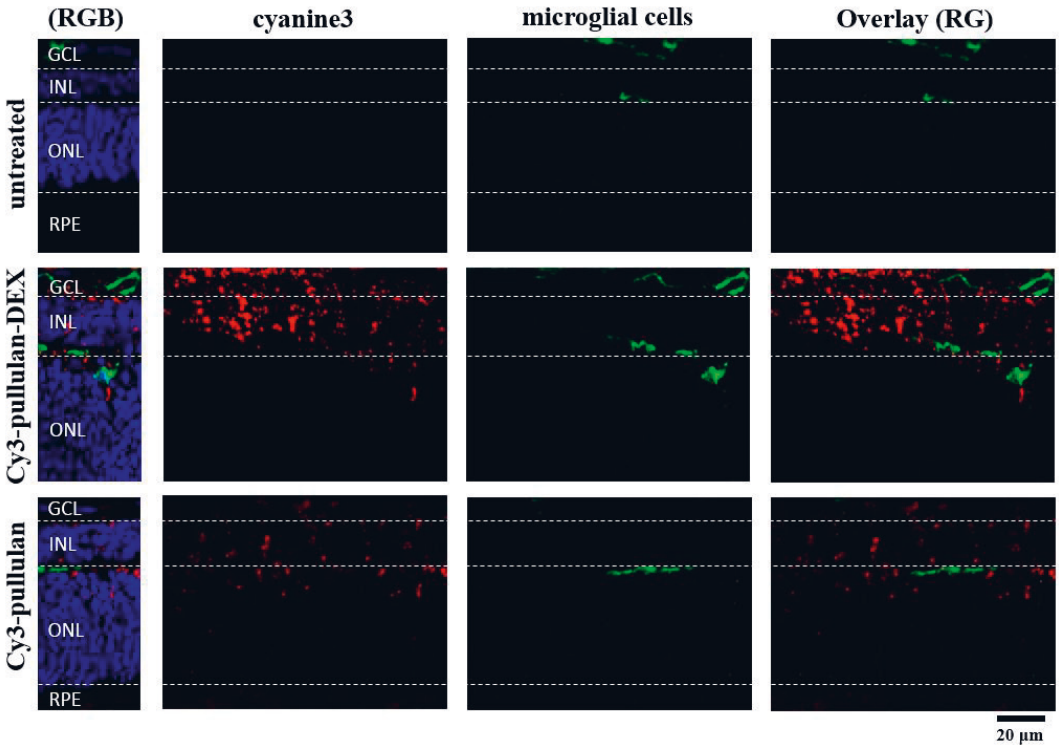


**Figure 10.** Microglial cells in sections of the ex vivo mouse retina labelled with an antibody against Iba-1 (green). Untreated retina, retina treated with Cy3-pullulan-DEX (15 µL, 1.9 mg/mL) and Cy3-pullulan (15 µL, 1.7 mg/mL) are shown. Cy3 fluorescence is shown as red. Nuclei were stained with DAPI (blue). RG: overlay of red and green channels for microglial cell, nanoparticle or conjugate colocalization. RGB: overlay of red, green and blue channels. Bar size: 20 µm.

#### 3.4.2. In Vivo Safety in Mice

In vivo safety of intravitreally injected pullulan formulations was evaluated in mice. Healthy status of the vitreous, retina and optic nerve were confirmed by fundus and OCT images 24 h after administration of fluorescently labelled Cy3-pullulan and Cy3-pullulan-DEX (SI-5, Figure S6). The animals were sacrificed, and the eyes were prepared for the TUNEL assay analysis that showed normal ONL and INL and no activation of cell death (SI-5, Figure S7).

#### 3.4.3. In Vivo Safety in Rats

In vivo safety of intravitreally injected pullulan formulations was evaluated in rats. Healthy status of the vitreous, retina, and optic nerve was confirmed by fundus and OCT images after exposure to BDP-pullulan and BDP-pullulan-DEX the following 3–5 days (Figure 11). Two weeks after intravitreal injections to the rat eyes, no visible alterations were seen (i.e., no conjunctival bleeding, cataracts, retinal detachment, swelling, clouding, changes in retinal morphology, cell debris or aggregation in the vitreous). No visual disturbance was detected since the vitreal clarity was confirmed by fundus imaging.

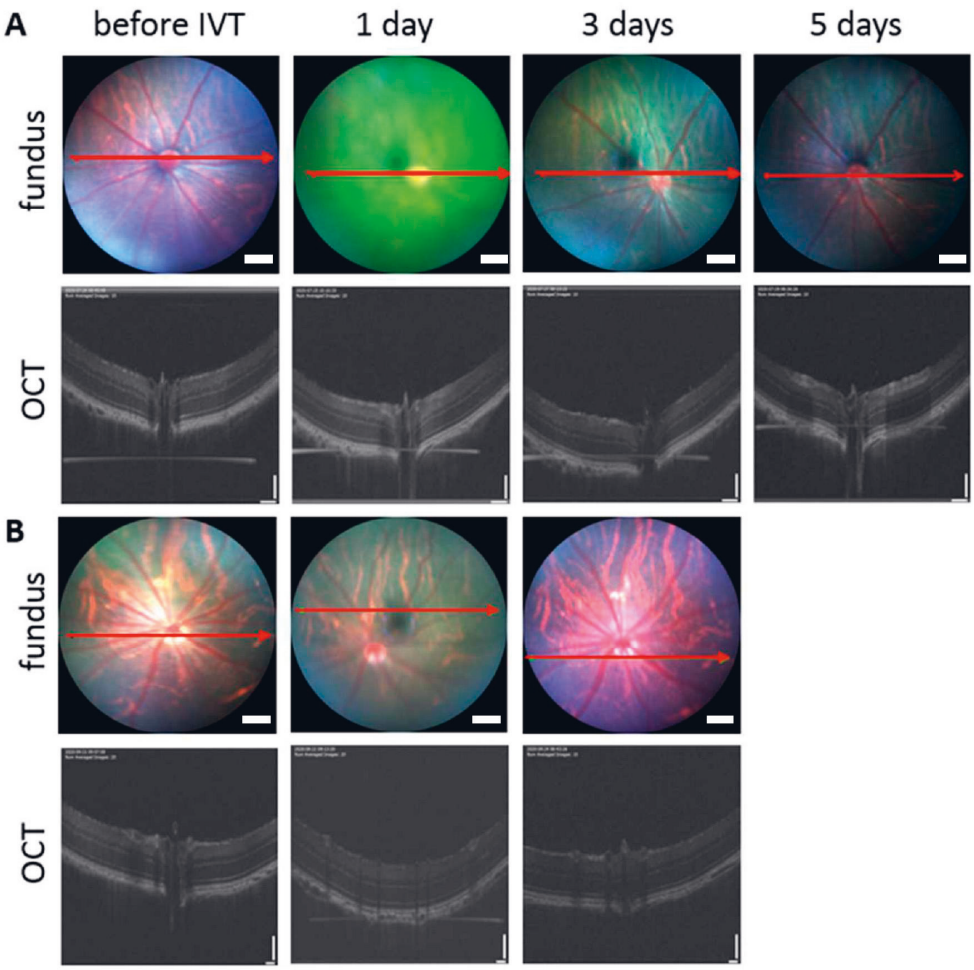


**Figure 11.** Fundus and optical coherence tomography (OCT) images of rat vitreous and retina. The figures are before and after intravitreal injections (1, 3 and 5 days) of BDP-pullulan (**A**) and BDP-pullulan-DEX (**B**). The length of scale bar for fundus images are 200 μm. In the case of OCT, vertical and horizontal scale bars in OCT are 110 and 130 μm, respectively.

### *3.5. Retinal Penetration and Distribution*

#### 3.5.1. Ex Vivo Studies

Distribution of pullulan-based formulations was studied in ex vivo mouse retinal explants (Figures 10 and 12). The conjugates, Cy3-pullulan and Cy3-pullulan-DEX, were present in GCL, INL and ONL layers. The formulations were visualized in radial sections (red punctas, Figures 10 and 12) through retinal layers overlapping with the Müller cells (Figure 12). Interestingly, the pullulan-based materials followed the route of Müller glial cells from the GCL to the distal part of the ONL, close to the retinal pigment epithelium (RPE) (Figure 12, 3D visualization in Supplementary Materials). Thus, this finding suggests that the pullulan-based conjugates may bypass the inner limiting membrane (ILM) via Müller cell phagocytosis in mouse retinal explants.

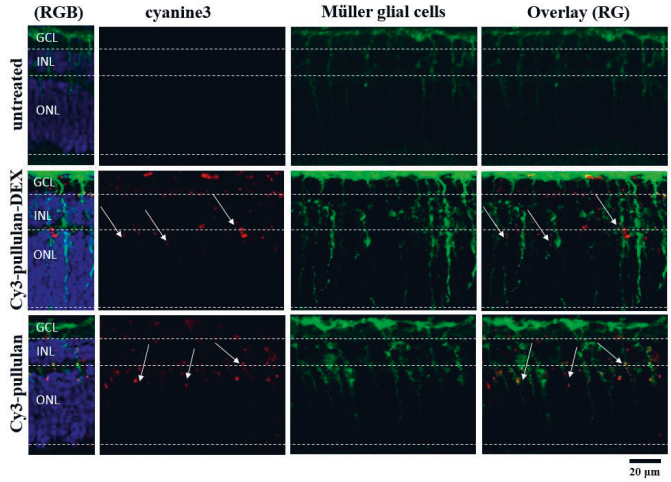


**Figure 12.** Müller glial cells in sections of the ex vivo mouse retina labelled with an antibody against glutamine synthetase (green). Untreated retina, retina treated with Cy3-pullulan-DEX (15 µL, 1.9 mg/mL) and Cy3-pullulan (15 µL, 1.7 mg/mL) are shown. Cy3 fluorescence is shown as red. Nuclei were stained with DAPI (blue). RG: overlay of red and green channels for Müller glial cell, nanoparticle or conjugate colocalization. RGB: overlay of red, green and blue channels. Bar size: 20 µm.

The retinal distribution of pullulan conjugates was also studied in ex vivo bovine retinal explants. In this tissue model, the nanoparticles were mainly localized at ILM. However, several sections showed a few signals (green punctas) from BDP-pullulan-DEX in GCL of the retina (Figure 13).

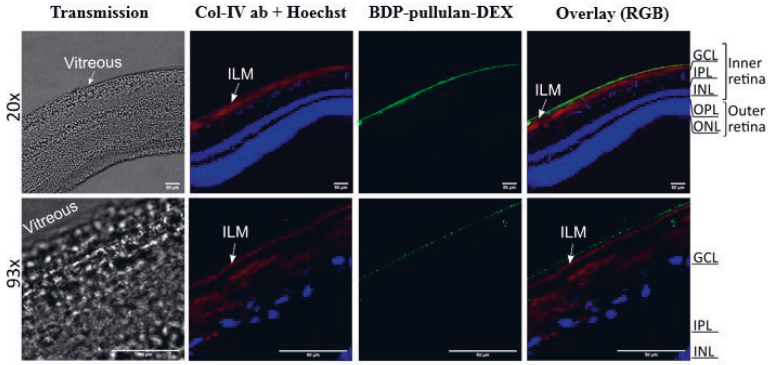


**Figure 13.** Retinal distribution of BDP-pullulan-DEX (100 µL, 5 mg/mL) in the vitreo-retinal ex vivo bovine explant 24 h after intravitreal injection. Representative confocal microscopy images of cryosections display the penetration of BDP-pullulan-DEX in the retinal layers (green). The inner limiting membrane (ILM) was labelled with rabbit anti-collagen type IV antibody (Col-IV ab, red). The vitreous can be seen as transparent layer in transmission imaging which is well aligned along the ILM while it appears in bright green color due to the high load of BDP-pullulan-DEX in merged channel mode. Nuclei are stained with Hoechst (blue). The white bar on the right bottom corner of each picture indicates the bar size: 50 µm. Abbreviations indicated in image: ganglion cell layer (GCL), inner plexiform layer (IPL), inner nuclear layer (INL), outer plexiform layer (OPL), outer nuclear layer (ONL), overlay of red/green/blue channels (RGB).

3.5.2. In Vivo Mouse Experiments

Two-months old mice were injected intravitreally with Cy3-pullulan-DEX. The results show localization of injected material across the retina, from inner to outer nuclear layers, mostly following Müller glial cells (Figure 14). This is in line with the ex vivo observations (Figure 12). Many particles accumulated in the cell bodies of Müller glial cells in the inner nuclear layer, but this was not seen in the other parts of the retina.

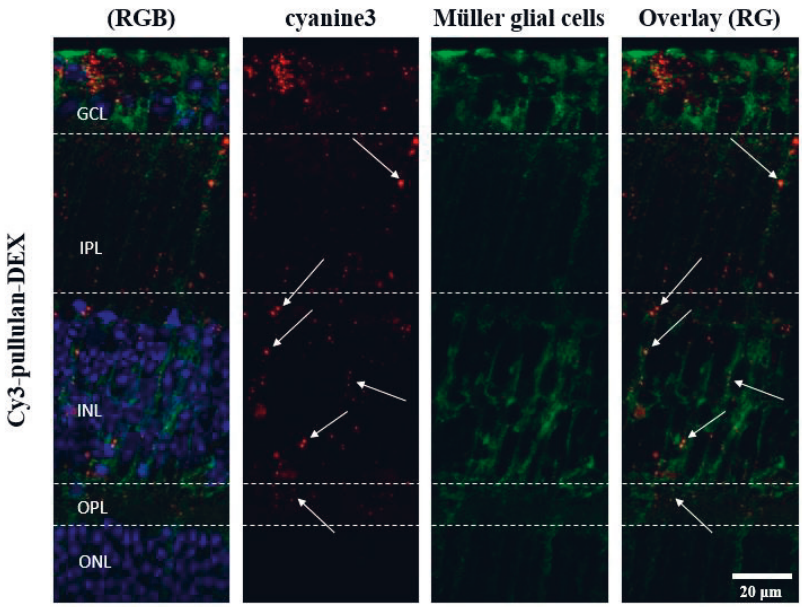


**Figure 14.** Images of retinal sections from two-months old mice after intravitreal injection (1 µL) of 5 mg/mL Cy3-pullulan-DEX (cyanine3, red). Müller glial cells were labelled with an antibody against glutamine synthetase (green). Nuclei were stained with DAPI (blue). RG: overlay of red and green channels for Müller glial cell and nanoparticle colocalization. RGB: overlay of red, green and blue channels. Bar size: 20 µm.

In adult mice, the presence of ILM in vivo and the penetration of pullulan material was detected as red dots in the Apotome microscopic images through GCL, INL and slightly in ONL layers (SI-5, Figures S8 and S9). The red fluorescently labelled pullulan samples were detected mostly in the GCL, inner plexiform layer (IPL) and INL layers and few dots were slightly visible in outer plexiform layer (OPL) and ONL (Figure 14).

## 4. Discussion

*Elimination kinetics.* The intravitreal pharmacokinetics and safety of pullulan–dexamethasone conjugates were investigated in detail. The results indicate that the conjugates are safe after intravitreal injections to the rodent eyes. Furthermore, they show prolonged retention in the rabbit eyes and retinal distribution via Müller glia cells in mouse eyes.

Non-modified pullulan behaves as a random coil of individual polymeric chains with diameters of few nanometers [13,33]. In this study, we used conjugates of pullulan with hydrophobic compound DEX and BDP. Pullulan conjugate with BDP was used since it allows direct and non-invasive monitoring of the particle kinetics after intravitreal injections. A roughly two-fold size difference was seen between pullulan-DEX and BDP-pullulan-DEX, but this should not cause kinetic differences since even several fold changes in liposome diameter (from <50 nm to >200 nm) did not change diffusivity in the vitreous [56]. These conjugates self-assemble to nanoparticles that showed similar retention times (half-

lives ≈2.5–6.0 days) in the rabbit vitreous as macromolecules (e.g., antibodies and FITC-dextrans) [15], but shorter than the retention of some polymeric micelles and polymersomes (half-lives ≈9–31 days) [12]. Based on particle size, longer half-lives would be expected for pullulan conjugates, but the pullulan conjugates are structurally different systems than polymeric micelles and polymersomes. Furthermore, pullulan conjugates showed even distribution in the rat vitreous already at one day after injection, suggesting fast diffusion of the pullulan conjugates in the rat vitreous. The reasons for the described kinetic profile of pullulan conjugates are not known, but could involve biological interactions or particle disassembly. Disassembly of the particles to individual polymer conjugates might explain the results, but particle exposure to homogenized vitreous did not indicate particle disassembly in our previous study [26]. In vivo studies of nanoparticle disassembly and other mechanisms in the vitreous are methodologically challenging and the molecular mechanisms of pullulan-DEX elimination remain open for the time being.

In order to elucidate the elimination route of pullulan conjugates from the vitreal cavity, we performed kinetic simulations by assuming that all polymer is eliminated to the anterior chamber at the experimental elimination rate from the vitreous and further eliminated from the anterior chamber at the rate of aqueous humor outflow. The simulated particle concentrations in the aqueous humor were close to the experimental values, indicating that practically all pullulan conjugates are eliminated from the vitreous via anterior route. Moreover, the Maurice plot ($C_v/C_a$ vs. vitreal half-life) derived estimates of anterior elimination suggested that the major fraction (at least 82.7%) of intravitreally injected pullulan conjugate is eliminated via anterior route [49]. An anterior elimination route has been shown earlier for soluble macromolecules (e.g., antibodies) [57,58], but we have shown here for the first time that this route dominates the vitreal elimination of nanoparticles.

According to the observed kinetics of pullulan-DEX in rats and rabbits, the vitreal elimination half-life was longer in the rabbits. This is in line with our previous data with FITC-dextrans in rats and rabbits [15]. The current data shows that similar species difference is seen also with nanoparticles. A bigger size of the rabbit eye explains the longer half-life in rabbits, since it takes longer time for material transfer from the vitreous to the anterior chamber [58]. In humans, the volume of vitreous is about three times (≈4.5 mL) bigger than in rabbits (≈1.5 mL) [59], leading to even longer retention. Possible effects of inflammation on the vitreal kinetics of pullulan conjugates are not known. Based on the literature it is not likely that clearance of released dexamethasone would change due to inflammation [60]. But infiltrated macrophages due to ocular inflammation [61] might take up the particles [62], leading to faster drug release in the lysosomal conditions in the cells.

*Interplay of polymer conjugate retention and drug release.* In this study, we used dexamethasone conjugate of pullulan, but did not measure concentrations of free pharmacologically active dexamethasone in the vitreous. We simulated free dexamethasone concentrations in the vitreous and aqueous humor before designing and performing labor intensive, expensive and analytically demanding in vivo studies to determine free and bound dexamethasone concentrations in the eye. Kinetic simulations were based on experimental kinetics of pullulan conjugates and in vitro release of dexamethasone from the conjugates [26]. For the first time in scientific literature, these simulations integrate the drug release rate and pharmacokinetics of particulate intravitreal drug delivery system. The results demonstrate that longer effective residence of dexamethasone in the rabbit vitreous (up to 16.5 days in rabbits and 25.5 days in humans) is clearly longer than the half-life of the delivery system (3.6 days) in the rabbit vitreous. This is possible because the residual nanoparticles still release dexamethasone that is active at small concentrations. At the threshold limit of dexamethasone activity (0.394 ng/mL) [54], the simulated amount of free drug in the eye is in the range of 1–4 ng in rabbit and human eyes. This is only less than 0.001% of the injected dexamethasone dose within the pullulan conjugate. Overall, this demonstrates the power of controlled release technology in intravitreal drug delivery and possibilities for further optimization.

The minimum effective dexamethasone concentration may be different at different pathological conditions. Here we chose 1 nM as the minimum therapeutic concentration [54]. This concentration of dexamethasone should inhibit expression of vascular endothelial growth factor in the human vascular smooth muscle cultured cells. The concentration of endogenous cortisol is 14 nM in the human vitreous [63]. Since the anti-inflammatory potency of dexamethasone is about 25 times higher than that of cortisol [64], dexamethasone should be anti-inflammatory at 1 nM concentration. After administration of dexamethasone implant (dose 700 μg) to the vitreous of rhesus monkeys, the levels of dexamethasone remained above 1 nM for 3 months, but the efficacy may be extended even at lower levels of dexamethasone [65]. Thus, efficacy of pullulan conjugates may extend beyond 25 days as reported here, and this technology may be further developed for more extended ocular retention.

Interestingly, our simulations on retention and release revealed that a major fraction of the conjugated dexamethasone dose will be eliminated from the eye as pullulan conjugate form (>99%), yet the drug action may be significantly prolonged. Ocular exposure to the released drug can be defined as intraocular bioavailability. Intraocular bioavailability of the released drug could be improved by increasing drug release rate (e.g., modification of chemical linker) and prolonging polymer-conjugate retention in the vitreous (e.g., increasing binding with vitreal components and molecular weight of polymer). The release and retention profiles of pullulan conjugated dexamethasone are very different from the intravitreal dexamethasone implants (e.g., Retisert). The implants release all the drug payload in the eye and thereafter a 'ghost matrix' remains in the eye. Interplay of delivery system retention, drug release and ocular pharmacokinetics has not been discussed in the literature. The presented simulation models provide useful tools for drug developers who optimize intravitreal drug delivery systems towards target product profiles.

*Retinal permeation.* The inner limiting membrane (ILM) is a mechanical and electrostatic barrier that limits access of nanoparticles into the retina. The ILM includes a negatively charged network of collagen and glycosaminoglycans [66]. Retinal delivery of materials with the molecular weights $\leq$ 100 kDa are not limited by ILM [67]. However, the electric charge of the materials can make a difference: FITC-dextrans of 20 kDa and 500 kDa permeated through ILM, but cationic poly-L-lysine (20 kDa) did not [68]. Recently, liposomes ($\approx$50 nm) with negative charge and PEG-coating were shown to permeate across bovine ILM that is considered a close model for human ILM [44]. However, larger liposomes of about 100 nm in diameter were not able to cross the ILM barrier in bovine retina. In this study, pullulan conjugates (particle size 200–400 nm) were permeating only to the ganglion cell layer of the bovine ex vivo retina, but not further into the retina. Ganglion cells are an important drug target, especially in the treatment of glaucomatous retinal degeneration [69]. Limited ILM permeation is also an obstacle in the field of retinal gene therapy with viral vectors and, for this reason, retinal gene therapy is performed using subretinal injections [70]. Better understanding of the ILM and other contributing factors will help in development of intravitreal treatments of retinal diseases. In various retinal disorders and upon ageing, ILM may become thinner and presents pores thereby become leakier to the nanoparticles [60].

Retinal permeation of pullulan was also investigated with organotypic mouse retinal explant that can be maintained as biologically active even for one month [71]. This model is useful in mechanistic pharmacological studies [1,2,72–75]. ILM in mouse retina is thinner and leakier than in the bigger eyes, potentially giving optimistic views on retinal permeation of particles [44]. However, this study showed qualitatively distinct retinal distribution: pullulan conjugates did not cross ILM, but they were taken up by the Müller cells that may not be as active in the isolated bovine retina. The pullulan–dexamethasone nanoparticles showed protective effects in the retina, suggesting drug release from the conjugates in the retina.

Delivery of pullulan conjugates to Müller cells can be explained on the location and properties of these cells. Müller cells are glial cells capable of phagocytosing cell bodies,

fragments of retinal cells and particles [76–78]. The cell bodies of Müller glia are located in the inner nuclear layer with its two stem processes extending in opposite directions and spanning the entire retina. Therefore, it is likely that intravitreal particles could be phagocytosed by Müller cells and carried into the inner retinal layers. In this study, the cultured retinal explants from wild-type mice were exposed to pullulan-based particles from the ganglion cell layer side on the retina. Colocalization with glutamine synthase antibody (Müller glia marker) confirmed particle localization in Müller cells and the particles were visualized in radial sections (red punctas, Figure 12) through all retinal layers in a linear distribution similar to the Müller cells extension (from the ganglion cell layer until reaching the distal part of the outer nuclear layer (Figure 12, and 3D visualization in Supplementary Materials). This indicates that the pullulan-based particles were phagocytized by the Müller cells, thereby overcoming the barrier of inner limiting membrane.

Müller glial cells are a major type of macroglial cells in the neural retina [79–83]. The close interactions that Müller cells have with other cells are crucial in the actions of antioxidants, neurotrophic factors and growth factors in the retina [80]. In this respect, Müller cells are an important cell target in retinal drug development and targeted localization of pullulan conjugates to the Müller cells opens possibilities to deliver drugs to these cells in a targeted manner. Furthermore, biocompatibility of the materials was confirmed in more detail in ex vivo studies with mouse organotypic retinal explants.

*Pullulan conjugates as potential intravitreal drug delivery systems*. The preclinical results showed that pullulan is a safe polymeric backbone for intravitreal drug delivery and capable of extending dexamethasone retention in the eye.

Previously, polymeric drug conjugates have been widely investigated as drug delivery systems for cancer treatment [84–86]. For ocular treatments, polymeric drug conjugates have been only sparsely studied [59,66,67]. In principle, polymeric conjugates provide major advantages: (1) large molecular size prevents elimination across blood–ocular barriers and slows diffusion to the anterior chamber, thereby prolonging drug residence in the eye; (2) covalent conjugation of drugs to the polymer backbone enables controlled drug release from soluble free polymer conjugates and self-assembled nanoparticles. Control of drug release is particularly significant because non-covalent drug loading to nanosystems results often in relatively fast drug release. Furthermore, covalent links allow generation of site-specific drug release in retina [10] or even in sub-cellular compartments [87].

Furthermore, OCT and fundus imaging showed no opacity in the vitreous after intravitreal pullulan conjugate injection, representing another advantage compared to implants, suspensions and microspheres [88]. Dexamethasone could be delivered as a water solution of polymeric conjugate without any visual disturbance. Further, the conjugated drug would not permeate to the lens, thereby decreasing the risk of corticosteroid cataract. Long-term exposure of dexamethasone may also cause higher intraocular pressure through increasing the stiffness of the trabecular meshwork [89]. Low dexamethasone dose (50 μg) and only partial release (<2.5 μg) from pullulan-DEX (50 μg) within the eye should reduce free drug exposure to the lens and trabecular meshwork to negligible levels as compared to the exposure after intravitreal administration of Ozurdex implant (700 μg) and dexamethasone suspension (50 μg). This factor may reduce the incidence of ocular adverse effects. The small needle size is another potential advantage of intravitreal polymeric conjugates. Compared to the 22 G Ozurdex needle the required needle size (31–32 G) for polymer conjugate is minimal thereby reducing the invasiveness of the treatment.

## 5. Conclusions

Delivery of intravitreally administered drugs may be improved with innovative drug delivery systems enabling more patient compliant administration, prolonged drug retention in the eye, controlled release and delivery to the retinal target cells. This research work demonstrates that dexamethasone conjugates of pullulan have such features. Pullulan–dexamethasone nanoparticles were safe in the preclinical animal models, distributed to the ganglion cells and Müller cells and showed prolonged ocular retention. Pharmacokinetic

models and simulations demonstrated important aspects in the interplay of ocular retention and drug release. These models will be useful tools in the field of ocular drug delivery system development. Overall, pullulan-based drug conjugates are a promising drug carrier platform for the intravitreal drug delivery.

**Supplementary Materials:** The following are available online at https://www.mdpi.com/article/10.3390/pharmaceutics14010012/s1. SI-1 and Scheme S1: Synthesis of pullulan-DEX conjugates; SI-2 and Figure S1: Ex vivo mouse retinal organ culture; SI-3 and Figures S2 and S3: Calibration curve for in vivo fluorophotometry measurements; SI-4, Figures S4 and S5 and Table S1: Pharmacokinetics simulations; SI-5 and Figures S6–S9: Safety on in vivo mice model; 3D visualization available online.

**Author Contributions:** E.K.: investigation, writing—original draft and methodology; A.S.: investigation, writing—original draft and methodology; J.P.: investigation and methodology; S.T.: investigation; M.S.: investigation; V.-P.R.: investigation, supervision and conceptualization; B.A.-G.: supervision, conceptualization, writing—review and editing; S.B.: investigation; M.U.: supervision and conceptualization; S.S.: supervision, conceptualization, writing—review and editing; P.C.: supervision, conceptualization, writing—review and editing, E.T.: supervision, investigation and methodology; M.R.: supervision, conceptualization, writing—review and editing; A.U.: supervision, conceptualization, writing—review and editing. All authors have read and agreed to the published version of the manuscript.

**Funding:** This project has received funding from the European Union's Horizon 2020 research and innovation programme under the Marie Skłodowska-Curie grant agreement No 722717. Arto Urtti was also supported by Russian Government Mega Grant (Agreement # 075-15-2021-637) and by Sigrid Juselius Foundation.

**Institutional Review Board Statement:** All procedures, used in ex vivo mouse model were approved by the Tübingen University committee on animal protection (Mitteilung nach §4 Abs. 3 TierSchG Nr. AK 03/20 M) and performed in compliance with the Association for Research in Vision and Ophthalmology ARVO Statement. All in vivo procedures were approved by the Finnish National Animal Experiment Broad (ELLA, Regional State Administrative Agency for Southern Finland), performed under project license (ESAVI-2020-027769).

**Informed Consent Statement:** Not applicable.

**Data Availability Statement:** Data are contained within the article and in Supplementary Materials. The additional data presented in this study are available on request from the authors.

**Conflicts of Interest:** The authors declare no conflict of interest.

## References

1. Dugel, P.U.; Bandello, F.; Loewenstein, A. Dexamethasone intravitreal implant in the treatment of diabetic macular edema. *Clin. Ophthalmol. (Auckland NZ)* **2015**, *9*, 1321. [CrossRef]
2. Abadia, B.; Calvo, P.; Ferreras, A.; Bartol, F.; Verdes, G.; Pablo, L. Clinical Applications of Dexamethasone for Aged Eyes. *Drugs Aging* **2016**, *33*, 639–646. [CrossRef] [PubMed]
3. Garweg, J.G.; Zandi, S. Retinal vein occlusion and the use of a dexamethasone intravitreal implant (Ozurdex®) in its treatment. *Graefe's Arch. Clin. Exp. Ophthalmol.* **2016**, *254*, 1257–1265. [CrossRef] [PubMed]
4. Cohen, S.Y.; Mimoun, G.; Oubraham, H.; Zourdani, A.; Malbrel, C.; Queré, S.; Schneider, V.; Group, L.S. Changes in visual acuity in patients with wet age-related macular degeneration treated with intravitreal ranibizumab in daily clinical practice: The LUMIERE study. *Retina* **2013**, *33*, 474–481. [CrossRef] [PubMed]
5. Holz, F.G.; Tadayoni, R.; Beatty, S.; Berger, A.; Cereda, M.G.; Cortez, R.; Hoyng, C.B.; Hykin, P.; Staurenghi, G.; Heldner, S. Multi-country real-life experience of anti-vascular endothelial growth factor therapy for wet age-related macular degeneration. *Br. J. Ophthalmol.* **2015**, *99*, 220–226. [CrossRef]
6. Krohne, T.I.M.U.; Eter, N.; Holz, F.G.; Meyer, C.H. Intraocular pharmacokinetics of bevacizumab after a single intravitreal injection in humans. *Am. J. Ophthalmol.* **2008**, *146*, 508–512. [CrossRef] [PubMed]
7. Mizutani, N.; Nabe, T.; Yoshino, S. Topical ocular treatment with monoclonal antibody Fab fragments targeting Japanese cedar pollen Cry j 1 inhibits Japanese cedar pollen-induced allergic conjunctivitis in mice. *Eur. J. Pharmacol.* **2017**, *798*, 105–112. [CrossRef]
8. Thiel, M.A.; Coster, D.J.; Standfield, S.D.; Brereton, H.M.; Mavrangelos, C.; Zola, H.; Taylor, S.; Yusim, A.; Williams, K.A. Penetration of engineered antibody fragments into the eye. *Clin. Exp. Immunol.* **2002**, *128*, 67–74. [CrossRef] [PubMed]

9. Sborgia, G.; Niro, A.; D'Oria, F.; Galeone, A.; Sborgia, L.; Boscia, F.; Sborgia, A.; Alessio, G. Surgical Management of Complications after Dexamethasone Implant. *Case Rep. Ophthalmol. Med.* **2020**, *2020*, 4837689. [CrossRef]
10. Bhattacharya, M.; Sadeghi, A.; Sarkhel, S.; Hagström, M.; Bahrpeyma, S.; Toropainen, E.; Auriola, S.; Urtti, A. Release of functional dexamethasone by intracellular enzymes: A modular peptide-based strategy for ocular drug delivery. *J. Control. Release* **2020**, *327*, 584–594. [CrossRef]
11. Pretto, C.; Tang, M.; Chen, M.; Xu, H.; Subrizi, A.; Urtti, A.; van Hest, J.C.M. Cowpea Chlorotic Mottle Virus-Like Particles as Potential Platform for Antisense Oligonucleotide Delivery in Posterior Segment Ocular Diseases. *Macromol. Biosci.* **2021**, *21*, 2100095. [CrossRef]
12. Junnuthula, V.; Sadeghi Boroujeni, A.; Cao, S.; Tavakoli, S.; Ridolfo, R.; Toropainen, E.; Ruponen, M.; van Hest, J.; Urtti, A. Intravitreal Polymeric Nanocarriers with Long Ocular Retention and Targeted Delivery to the Retina and Optic Nerve Head Region. *Pharmaceutics* **2021**, *13*, 445. [CrossRef]
13. Dubashynskaya, N.; Poshina, D.; Raik, S.; Urtti, A.; Skorik, Y.A. Polysaccharides in ocular drug delivery. *Pharmaceutics* **2020**, *12*, 22. [CrossRef] [PubMed]
14. Balasso, A.; Subrizi, A.; Salmaso, S.; Mastrotto, F.; Garofalo, M.; Tang, M.; Chen, M.; Xu, H.; Urtti, A.; Caliceti, P. Screening of chemical linkers for development of pullulan bioconjugates for intravitreal ocular applications. *Eur. J. Pharm. Sci.* **2021**, *161*, 105785. [CrossRef]
15. Sadeghi, A.; Puranen, J.; Ruponen, M.; Valtari, A.; Subrizi, A.; Ranta, V.-P.; Toropainen, E.; Urtti, A. Pharmacokinetics of intravitreal macromolecules: Scaling between rats and rabbits. *Eur. J. Pharm. Sci.* **2021**, *159*, 105720. [CrossRef]
16. Giri, T. Nanoarchitectured Polysaccharide-Based Drug Carrier for Ocular. In *Nanoarchitectonics for Smart Delivery and Drug Targeting*; Elsevier Science: Amsterdam, The Netherlands, 2016; Volume 119.
17. Irimia, T.; Ghica, M.V.; Popa, L.; Anuţa, V.; Arsene, A.-L.; Dinu-Pîrvu, C.-E. Strategies for improving ocular drug bioavailability and corneal wound healing with chitosan-based delivery systems. *Polymers* **2018**, *10*, 1221. [CrossRef]
18. Bernier, B. The production of polysaccharides by fungi active in the decomposition of wood and forest litter. *Can. J. Microbiol.* **1958**, *4*, 195–204. [CrossRef]
19. Thrimawithana, T.R.; Young, S.A.; Bunt, C.R.; Green, C.R.; Alany, R.G. In-vitro and in-vivo evaluation of carrageenan/methylcellulose polymeric systems for transscleral delivery of macromolecules. *Eur. J. Pharm. Sci.* **2011**, *44*, 399–409. [CrossRef] [PubMed]
20. Kim, Y.; Chun, C.; Chiang, B.; Wu, X.; Prausnitz, M.R. Ocular delivery of macromolecules. *J. Control. Release* **2014**, *190*, 172–181. [CrossRef]
21. Yu, Y.; Lau, L.C.M.; Lo, A.C.; Chau, Y. Injectable chemically crosslinked hydrogel for the controlled release of bevacizumab in vitreous: A 6-month in vivo study. *Transl. Vis. Sci. Technol.* **2015**, *4*, 5. [CrossRef]
22. Koo, H.; Moon, H.; Han, H.; Na, J.H.; Huh, M.S.; Park, J.H.; Woo, S.J.; Park, K.H.; Chan Kwon, I.; Kim, K.; et al. The movement of self-assembled amphiphilic polymeric nanoparticles in the vitreous and retina after intravitreal injection. *Biomaterials* **2012**, *33*, 3485–3493. [CrossRef]
23. Hassanzadeh, F.; Varshosaz, J.; Khodarahmi, G.A.; Rostami, M.; Hassanzadeh, F. Biotin-encoded pullulan-retinoic acid engineered nanomicelles: Preparation, optimization and in vitro cytotoxicity assessment in MCF-7 cells. *Indian J. Pharm. Sci.* **2016**, *78*, 557–565. [CrossRef]
24. Hassanzadeh, F.; Mahmoudi, E.; Varshosaz, J.; Khodarahmi, G.A.; Rostami, M.; Ghanadian, M.; Dana, N. Novel NGR anchored pullulan micelles for controlled and targeted delivery of doxorubicin to HeLa cancerous cells. *Iran. Polym. J.* **2018**, *27*, 263–274. [CrossRef]
25. Yuan, R.; Zheng, F.; Zhong, S.; Tao, X.; Zhang, Y.; Gao, F.; Yao, F.; Chen, J.; Chen, Y.; Shi, G. Self-assembled nanoparticles of glycyrrhetic acid-modified pullulan as a novel carrier of curcumin. *Molecules* **2014**, *19*, 13305–13318. [CrossRef] [PubMed]
26. Kicková, E.; Salmaso, S.; Mastrotto, F.; Caliceti, P.; Urtti, A. Pullulan Based Bioconjugates for Ocular Dexamethasone Delivery. *Pharmaceutics* **2021**, *13*, 791. [CrossRef]
27. Lu, D.; Wen, X.; Liang, J.; Gu, Z.; Zhang, X.; Fan, Y. A pH-sensitive nano drug delivery system derived from pullulan/doxorubicin conjugate. *J. Biomed. Mater. Res. Part B Appl. Biomater. Off. J. Soc. Biomater. Jpn. Soc. Biomater. Aust. Soc. Biomater. Korean Soc. Biomater.* **2009**, *89*, 177–183. [CrossRef]
28. Li, H.; Yu, C.; Zhang, J.; Li, Q.; Qiao, H.; Wang, Z.; Zeng, D. pH-sensitive pullulan-doxorubicin nanoparticles loaded with 1, 1, 2-trichlorotrifluoroethane as a novel synergist for high intensity focused ultrasound mediated tumor ablation. *Int. J. Pharm.* **2019**, *556*, 226–235. [CrossRef] [PubMed]
29. Howard, M.D.; Ponta, A.; Eckman, A.; Jay, M.; Bae, Y. Polymer micelles with hydrazone-ester dual linkers for tunable release of dexamethasone. *Pharm. Res.* **2011**, *28*, 2435–2446. [CrossRef] [PubMed]
30. Wang, D.; Miller, S.C.; Liu, X.-M.; Anderson, B.; Wang, X.S.; Goldring, S.R. Novel dexamethasone-HPMA copolymer conjugate and its potential application in treatment of rheumatoid arthritis. *Arthritis Res. Ther.* **2007**, *9*, R2. [CrossRef]
31. Liu, X.-M.; Quan, L.; Tian, J.; Laquer, F.C.; Ciborowski, P.; Wang, D. Syntheses of click PEG—Dexamethasone conjugates for the treatment of rheumatoid arthritis. *Biomacromolecules* **2010**, *11*, 2621–2628. [CrossRef]
32. Webber, M.J.; Matson, J.B.; Tamboli, V.K.; Stupp, S.I. Controlled release of dexamethasone from peptide nanofiber gels to modulate inflammatory response. *Biomaterials* **2012**, *33*, 6823–6832. [CrossRef]
33. Rekha, M.R.; Sharma, C.P. Pullulan as a promising biomaterial for biomedical applications: A perspective. *Trends Biomater Artif Organs* **2007**, *20*, 116–121.

34. Mulchandani, A.; Luong, J.H.T.; LeDuy, A. Biosynthesis of pullulan using immobilized *Aureobasidium pullulans* cells. *Biotechnol. Bioeng.* **1989**, *33*, 306–312. [CrossRef]
35. Akiyoshi, K.; Kobayashi, S.; Shichibe, S.; Mix, D.; Baudys, M.; Kim, S.W.; Sunamoto, J. Self-assembled hydrogel nanoparticle of cholesterol-bearing pullulan as a carrier of protein drugs: Complexation and stabilization of insulin. *J. Control. Release* **1998**, *54*, 313–320. [CrossRef]
36. Bonzi, G.; Salmaso, S.; Scomparin, A.; Eldar-Boock, A.; Satchi-Fainaro, R.; Caliceti, P. Novel pullulan bioconjugate for selective breast cancer bone metastases treatment. *Bioconjug. Chem.* **2015**, *26*, 489–501. [CrossRef] [PubMed]
37. Balasso, A.; Salmaso, S.; Pontisso, P.; Rosato, A.; Quarta, S.; Malfanti, A.; Mastrotto, F.; Caliceti, P. Re-programming pullulan for targeting and controlled release of doxorubicin to the hepatocellular carcinoma cells. *Eur. J. Pharm. Sci.* **2017**, *103*, 104–115. [CrossRef] [PubMed]
38. Osakada, F.; Ooto, S.; Akagi, T.; Mandai, M.; Akaike, A.; Takahashi, M. Wnt signaling promotes regeneration in the retina of adult mammals. *J. Neurosci.* **2007**, *27*, 4210–4219. [CrossRef]
39. Müller, B.; Wagner, F.; Lorenz, B.; Stieger, K. Organotypic cultures of adult mouse retina: Morphologic changes and gene expression. *Investig. Ophthalmol. Vis. Sci.* **2017**, *58*, 1930–1940. [CrossRef] [PubMed]
40. Arango-Gonzalez, B.; Szabó, A.; Pinzon-Duarte, G.; Lukáts, Á.; Guenther, E.; Kohler, K. In vivo and in vitro development of S-and M-cones in rat retina. *Investig. Ophthalmol. Vis. Sci.* **2010**, *51*, 5320–5327. [CrossRef]
41. Caffé, A.R.; Söderpalm, A.K.; Holmqvist, I.; van Veen, T. A combination of CNTF and BDNF rescues rd photoreceptors but changes rod differentiation in the presence of RPE in retinal explants. *Investig. Ophthalmol. Vis. Sci.* **2001**, *42*, 275–282.
42. Gavrieli, Y.; Sherman, Y.; Ben-Sasson, S.A. Identification of programmed cell death in situ via specific labeling of nuclear DNA fragmentation. *J. Cell Biol.* **1992**, *119*, 493–501. [CrossRef] [PubMed]
43. Peynshaert, K.; Devoldere, J.; Forster, V.; Picaud, S.; Vanhove, C.; De Smedt, S.C.; Remaut, K. Toward smart design of retinal drug carriers: A novel bovine retinal explant model to study the barrier role of the vitreoretinal interface. *Drug Deliv.* **2017**, *24*, 1384–1394. [CrossRef]
44. Tavakoli, S.; Peynshaert, K.; Lajunen, T.; Devoldere, J.; Del Amo, E.M.; Ruponen, M.; De Smedt, S.C.; Remaut, K.; Urtti, A. Ocular barriers to retinal delivery of intravitreal liposomes: Impact of vitreoretinal interface. *J. Control. Release* **2020**, *328*, 952–961. [CrossRef] [PubMed]
45. Zhang, Y.; Huo, M.; Zhou, J.; Xie, S. PKSolver: An add-in program for pharmacokinetic and pharmacodynamic data analysis in Microsoft Excel. *Comput. Methods Programs Biomed.* **2010**, *99*, 306–314. [CrossRef]
46. Bantseev, V.; Miller, P.E.; Bentley, E.; Schuetz, C.; Streit, T.M.; Christian, B.J.; Farman, C.; Booler, H.; Thackaberry, E.A. Determination of a no-observable effect level for endotoxin following a single intravitreal administration to dutch belted rabbits. *Investig. Ophthalmol. Vis. Sci.* **2017**, *58*, 1545–1552. [CrossRef]
47. Bantseev, V.; Miller, P.E.; Nork, T.M.; Rasmussen, C.A.; McKenzie, A.; Christian, B.J.; Booler, H.; Thackaberry, E.A. Determination of a no observable effect level for endotoxin following a single intravitreal administration to cynomolgus monkeys. *J. Ocul. Pharmacol. Ther.* **2019**, *35*, 245–253. [CrossRef] [PubMed]
48. Mermoud, A.; Baerveldt, G.; Minckler, D.S.; Prata, J.A. Aqueous humor dynamics in rats. *Graefe's Arch. Clin. Exp. Ophthalmol.* **1996**, *234*, S198–S203. [CrossRef] [PubMed]
49. Maurice, D.M.; Mishima, S.; Misidma, S. Ocular pharmacokinetics. In *Pharmacology of the Eye*; Springer: Berlin/Heidelberg, Germany, 1984; pp. 19–116.
50. Del Amo, E.M.; Vellonen, K.S.; Kidron, H.; Urtti, A. Intravitreal clearance and volume of distribution of compounds in rabbits: In silico prediction and pharmacokinetic simulations for drug development. *Eur. J. Pharm. Biopharm.* **2015**, *95*, 215–226. [CrossRef]
51. Bito, L.Z.; Salvador, E.V. Intraocular fluid dynamics. III. The site and mechanism of prostaglandin transfer across the blood intraocular fluid barriers. *Exp. Eye Res.* **1972**, *14*, 233–241. [CrossRef]
52. Johnson, F.; Maurice, D. A simple method of measuring aqueous humor flow with intravitreal fluoresceinated dextrans. *Exp. Eye Res.* **1984**, *39*, 791–805. [CrossRef]
53. Missel, P.J. Simulating intravitreal injections in anatomically accurate models for rabbit, monkey, and human eyes. *Pharm. Res.* **2012**, *29*, 3251–3272. [CrossRef] [PubMed]
54. Nauck, M.; Karakiulakis, G.; Perruchoud, A.P.; Papakonstantinou, E.; Roth, M. Corticosteroids inhibit the expression of the vascular endothelial growth factor gene in human vascular smooth muscle cells. *Eur. J. Pharmacol.* **1998**, *341*, 309–315. [CrossRef]
55. Siqueira, R.C.; Dos Santos, W.F.; Scott, I.U.; Messias, A.; Rosa, M.N.; Cunha, G.M.F.; da Silva Cunha, A., Jr.; Jorge, R. Neuroprotective effects of intravitreal triamcinolone acetonide and dexamethasone implant in rabbit retinas after pars plana vitrectomy and silicone oil injection. *Retina* **2015**, *35*, 364–370. [CrossRef]
56. Tavakoli, S.; Kari, O.K.; Turunen, T.; Lajunen, T.; Schmitt, M.; Lehtinen, J.; Tasaka, F.; Parkkila, P.; Ndika, J.; Viitala, T. Diffusion and Protein Corona Formation of Lipid-Based Nanoparticles in the Vitreous Humor: Profiling and Pharmacokinetic Considerations. *Mol. Pharm.* **2020**, *12*, 699–713. [CrossRef]
57. Rimpelä, A.; Kiiski, I.; Deng, F.; Kidron, H.; Urtti, A. Pharmacokinetic simulations of intravitreal biologicals: Aspects of drug delivery to the posterior and anterior segments. *Pharmaceutics* **2019**, *11*, 9. [CrossRef] [PubMed]

58. Hutton-Smith, L.A.; Gaffney, E.A.; Byrne, H.M.; Maini, P.K.; Schwab, D.; Mazer, N.A.; Ga, E.A.; Byrne, H.M.; Maini, P.K.; Schwab, D.; et al. A mechanistic model of the intravitreal pharmacokinetics of large molecules and the pharmacodynamic suppression of ocular vascular endothelial growth factor levels by ranibizumab in patients with neovascular age-related macular degeneration. *Mol. Pharm.* **2016**, *13*, 2941–2950. [CrossRef]
59. del Amo, E.M.; Urtti, A.; Eva, M.; Urtti, A.; del Amo, E.M.; Urtti, A.; Amo, E.M.; Urtti, A. Rabbit as an animal model for intravitreal pharmacokinetics: Clinical predictability and quality of the published data. *Exp. Eye Res.* **2015**, *137*, 111–124. [CrossRef]
60. del Amo, E.M.; Rimpelä, A.K.; Heikkinen, E.; Kari, O.K.; Ramsay, E.; Lajunen, T.; Schmitt, M.; Pelkonen, L.; Bhattacharya, M.; Richardson, D.; et al. Pharmacokinetic aspects of retinal drug delivery. *Prog. Retin. Eye Res.* **2017**, *57*, 134–185. [CrossRef]
61. McGahan, M.C.; Fleisher, L.N. Cellular response to intravitreal injection of endotoxin and xanthine oxidase in rabbits. *Graefe's Arch. Clin. Exp. Ophthalmol.* **1992**, *230*, 463–467. [CrossRef]
62. Gustafson, H.H.; Holt-Casper, D.; Grainger, D.W.; Ghandehari, H. Nanoparticle uptake: The phagocyte problem. *Nano Today* **2015**, *10*, 487–510. [CrossRef] [PubMed]
63. Weijtens, O.; Van der Sluijs, F.A.; Schoemaker, R.C.; Lentjes, E.; Cohen, A.F.; Romijn, F.; Van Meurs, J.C. Peribulbar corticosteroid injection: Vitreal and serum concentrations after dexamethasone disodium phosphate injection. *Am. J. Ophthalmol.* **1997**, *123*, 358–363. [CrossRef]
64. Brunton, L.L.; Hilal-Dandan, R.; Knollmann, B.C. *Goodman & Gilman's the Pharmacological Basis of Therapeutics*; McGraw-Hill Education: New York, NY, USA, 2018; ISBN 1259584739.
65. Chang-Lin, J.-E.; Attar, M.; Acheampong, A.A.; Robinson, M.R.; Whitcup, S.M.; Kuppermann, B.D.; Welty, D. Pharmacokinetics and pharmacodynamics of a sustained-release dexamethasone intravitreal implant. *Investig. Ophthalmol. Vis. Sci.* **2011**, *52*, 80–86. [CrossRef] [PubMed]
66. Halfter, W.; Dong, S.; Dong, A.; Eller, A.W.; Nischt, R. Origin and turnover of ECM proteins from the inner limiting membrane and vitreous body. *Eye* **2008**, *22*, 1207–1213. [CrossRef]
67. Jackson, T.L.; Antcliff, R.J.; Hillenkamp, J.; Marshall, J. Human retinal molecular weight exclusion limit and estimate of species variation. *Investig. Ophthalmol. Vis. Sci.* **2003**, *44*, 2141–2146. [CrossRef] [PubMed]
68. Pitkänen, L.; Pelkonen, J.; Ruponen, M.; Rönkkö, S.; Urtti, A. Neural retina limits the nonviral gene transfer to retinal pigment epithelium in an in vitro bovine eye model. *AAPS J.* **2004**, *6*, 72–80. [CrossRef]
69. Morgan, J.E. Retina ganglion cell degeneration in glaucoma: An opportunity missed? A review. *Clin. Experiment. Ophthalmol.* **2012**, *40*, 364–368. [CrossRef] [PubMed]
70. Prado, D.A.; Acosta-Acero, M.; Maldonado, R.S. Gene therapy beyond luxturna: A new horizon of the treatment for inherited retinal disease. *Curr. Opin. Ophthalmol.* **2020**, *31*, 147–154. [CrossRef]
71. Arango-Gonzalez, B.; Trifunović, D.; Sahaboglu, A.; Kranz, K.; Michalakis, S.; Farinelli, P.; Koch, S.; Koch, F.; Cottet, S.; Janssen-Bienhold, U. Identification of a common non-apoptotic cell death mechanism in hereditary retinal degeneration. *PLoS ONE* **2014**, *9*, e112142.
72. Kuppermann, B.D.; Blumenkranz, M.S.; Haller, J.A.; Williams, G.A.; Weinberg, D.V.; Chou, C.; Whitcup, S.M. Randomized controlled study of an intravitreous dexamethasone drug delivery system in patients with persistent macular edema. *Arch. Ophthalmol.* **2007**, *125*, 309–317. [CrossRef]
73. Rodríguez Villanueva, J.; Rodríguez Villanueva, L.; Guzmán Navarro, M. Pharmaceutical technology can turn a traditional drug, dexamethasone into a first-line ocular medicine. A global perspective and future trends. *Int. J. Pharm.* **2017**, *516*, 342–351. [CrossRef]
74. Bhagat, R.; Zhang, J.; Farooq, S.; Li, X. Comparison of the Release Profile and Pharmacokinetics of Intact and Fragmented Dexamethasone Intravitreal Implants in Rabbit Eyes. *J. Ocul. Pharmacol. Ther.* **2014**, *30*, 854–859. [CrossRef]
75. Pacella, F.; Ferraresi, A.F.; Turchetti, P.; Lenzi, T.; Giustolisi, R.; Bottone, A.; Fameli, V.; Romano, M.R.; Pacella, E. Intravitreal injection of Ozurdex® implant in patients with persistent diabetic macular edema, with six-month follow-up. *Ophthalmol. Eye Dis.* **2016**, *8*, OED-S38028. [CrossRef]
76. Nishizono, H.; Murata, Y.; Tanaka, M.; Soji, T.; Herbert, D.C. Evidence that Müller cells can phagocytize egg-lecithin-coated silicone particles. *Tissue Cell* **1993**, *25*, 305–310. [CrossRef]
77. Mano, T.; Puro, D.G. Phagocytosis by human retinal glial cells in culture. *Investig. Ophthalmol. Vis. Sci.* **1990**, *31*, 1047–1055.
78. Ryals, R.C.; Patel, S.; Acosta, C.; McKinney, M.; Pennesi, M.E.; Sahay, G. The effects of PEGylation on LNP based mRNA delivery to the eye. *PLoS ONE* **2020**, *15*, e0241006. [CrossRef]
79. Charlton-Perkins, M.; Almeida, A.D.; MacDonald, R.B.; Harris, W.A. Genetic control of cellular morphogenesis in Müller glia. *Glia* **2019**, *67*, 1401–1411. [CrossRef] [PubMed]
80. Coughlin, B.A.; Feenstra, D.J.; Mohr, S. Müller cells and diabetic retinopathy. *Vis. Res.* **2017**, *139*, 93–100. [CrossRef]
81. Williams, D.S.; Arikawa, K.; Paallysaho, T. Cytoskeletal components of the adherens junctions between the photoreceptors and the supportive Müller cells. *J. Comp. Neurol.* **1990**, *295*, 155–164. [CrossRef]
82. Uga, S.; Smelser, G.K. Comparative study of the fine structure of retinal Muller cells in various vertebrates. *Investig. Ophthalmol. Vis. Sci.* **1973**, *12*, 434–448.
83. Wang, J.; O'Sullivan, M.L.; Mukherjee, D.; Puñal, V.M.; Farsiu, S.; Kay, J.N. Anatomy and spatial organization of Müller glia in mouse retina. *J. Comp. Neurol.* **2017**, *525*, 1759–1777. [CrossRef]

84. Ulbrich, K.; Hola, K.; Subr, V.; Bakandritsos, A.; Tucek, J.; Zboril, R. Targeted drug delivery with polymers and magnetic nanoparticles: Covalent and noncovalent approaches, release control, and clinical studies. *Chem. Rev.* **2016**, *116*, 5338–5431. [CrossRef] [PubMed]
85. Lammers, T.; Kiessling, F.; Hennink, W.E.; Storm, G. Drug targeting to tumors: Principles, pitfalls and (pre-) clinical progress. *J. Control. Release* **2012**, *161*, 175–187. [CrossRef] [PubMed]
86. Kopeček, J. Smart and genetically engineered biomaterials and drug delivery systems. *Eur. J. Pharm. Sci.* **2003**, *20*, 1–16. [CrossRef]
87. Wang, S. pH-Responsive amphiphilic carboxylate polymers: Design and potential for endosomal escape. *Front. Chem.* **2021**, *9*, 145. [CrossRef]
88. Hou, H.; Wang, C.; Nan, K.; Freeman, W.R.; Sailor, M.J.; Cheng, L. Controlled release of dexamethasone from an intravitreal delivery system using porous silicon dioxide. *Investig. Ophthalmol. Vis. Sci.* **2016**, *57*, 557–566. [CrossRef] [PubMed]
89. Raghunathan, V.K.; Morgan, J.T.; Park, S.A.; Weber, D.; Phinney, B.S.; Murphy, C.J.; Russell, P. Dexamethasone stiffens trabecular meshwork, trabecular meshwork cells, and matrix. *Investig. Ophthalmol. Vis. Sci.* **2015**, *56*, 4447–4459. [CrossRef] [PubMed]

**AMIR SADEGHI BOROUJENI**

Pharmacokinetics is one of the main features to be assessed in the development of effective and safe therapeutics and drug delivery systems for treatment of retinal diseases. In this thesis we utilized non-invasive optical techniques to assess the vitreal pharmacokinetics of labeled compounds and nanomaterials in preclinical animal models. The provided kinetic insights into intravitreally injected compounds can be used in future for development of novel retinal drug delivery applications.

UNIVERSITY OF
EASTERN FINLAND

**uef.fi**

**PUBLICATIONS OF
THE UNIVERSITY OF EASTERN FINLAND**
Dissertations in Health Sciences

ISBN 978-952-61-4591-4
ISSN 1798-5706